Photocatalytic Thin Films

Their Characterisation and Antimicrobial Properties

A thesis presented to University College London in partial fulfilment of the requirements for the degree of Doctor of Philosophy

Kristopher Page

Supervised by

Professor Ivan P. Parkin
Materials Chemistry Centre, UCL Department of Chemistry

Professor Michael Wilson
Division of Microbial Diseases, UCL Eastman Dental Institute

2009

Declaration

I, Kristopher Page, confirm that the work presented in this thesis is my own. Where information has been derived from other sources, I confirm that this has been indicated in the thesis.

Abstract

This thesis is concerned with the synthesis and characterisation of TiO_2 based photocatalyst thin films and the assessment of their antimicrobial properties. When exposed to light of wavelength less than 380 nm TiO_2 films can demonstrate self-cleaning and self-disinfecting properties. This is due to photocatalytic processes occurring on the film surface resulting in film superhydrophilicity and reactive oxygen species (ROS) production. These ROS and radicals readily oxidise organic pollutants and microbes adherent to the material surface. Consequently, TiO_2 thin films are of great research interest as self-cleaning, antimicrobial coatings.

TiO_2 and doped TiO_2 materials were prepared by a simple sol-gel route from titanium n-butoxide as the principle precursor material. Film deposition was carried out using a dip-coating technique, with substrates withdrawn from the precursor sol at a fixed speed. Deposited films were calcined to produce crystalline thin films, with excellent adherence to the substrate (glass slides). Films were characterised using a number of analytical techniques including UV-visible spectroscopy, X-ray diffraction, scanning electron microscopy, atomic force microscopy, X-ray photoelectron spectroscopy and EXAFS/XANES.

Photocatalysis and film hydrophilicity were investigated using established methods. Stearic acid photodegradation, monitored by FT-IR was used to assess film photocatalysis, by monitoring the peak areas of the C-H stretching region. Relative film hydrophilicities were determined by measuring the contact angle of a sessile droplet of water.

Antimicrobial properties of the films were assessed with typical examples of Gram-positive and Gram-negative organisms. *Staphylococcus aureus* (NCTC 6571) and *Escherichia coli* (NCTC 10418) were selected. Films demonstrated microbicidal activity against both organisms under 365nm UV illumination, and under illumination by a typical hospital lamp (28W 2-D fluorescent). Microbial adhesion to various substrates was also examined, using a dip-blot method. Films produced in this study demonstrate excellent potential as durable surface coatings with significant antimicrobial activity against microbes of clinical importance.

Acknowledgements

I would like to thank Professor Parkin and Professor Wilson for being such enthusiastic and involved supervisors throughout the course of my PhD. It is a great motivation as a researcher when your supervisors are so engaged and interested in your work. Thank you both for the continual support, encouragement and advice. I could not have asked for two better people to have worked for. I also thank the UCL Department of Chemistry Horsell Studentship for awarding the funds for the research.

Many people have helped me out along the road to completing this work. My first thanks must go to my "three amigos", Stephen Potts, Paolo Melgari and Naima Narband – thank you for the laughs and banter and for sharing the PhD experience – we've all got through it together! I would also particularly like to thank Valérie Decraene – you managed to teach a Chemist how to do Microbiology. I hope I was able to teach you some Chemistry in return! I shall try to list everyone else who has assisted me here and I apologise in advance if I have inadvertently missed any one out. Everyone at UCL, Department of Chemistry, Materials Chemistry Centre, in particular: Christopher Blackman, Geoffrey Hyett, Ashti Rampaul, Robert Palgrave, Russell Binions, Charlie Dunnill, Andreas Kafizas, Sujata Kundu, Kevin Reeves (SEM, UCL Dept Archaeology) and Shelley Savin (EXAFS, University of Kent). Everyone at UCL Eastman Dental Institute, Division of Microbial Diseases, in particular: Derren Ready, Zoie Aiken, Sarah Tubby, Florent Chang-Pi-Hin, Linda Dekker, Wojciech Chrzanowski, Nicky Mordan and Aviva Petrie. Thank you everyone!

My final thanks must go to Mum, Dad and Nannie for their continued support and interest in what I've been doing for the past years. Thanks for putting up with me whilst I got this finished! I would like to dedicate this work to the members of my family who are sadly no longer with us, but who I'm sure would have loved to have seen the thesis – for Grandad, Great Nan and Nanna.

Contents

List of Figures

List of Tables

List of Schemes

List of Equations

List of Abbreviations

ACC	Aerobic colony count
AFM	Atomic Force Microscopy
CFU	Colony forming unit
CVC	Central venous catheter
CVD	Chemical vapour deposition
DLC	Diamond-like carbon
EDAX	Energy Dispersive Analysis of X-rays
EPR	Electron paramagnetic resonance
EPS	Extracellular polymeric substance
EXAFS	Extended X-ray Absorption Fine Structure
FTIR	Fourier transform infrared spectroscopy
HAI	Hospital-acquired Infection
IR	Infrared
ISC	Intersystem crossing
LAAA	Light activated antimicrobial agent
LPS	Lipopolysaccharide
MBC	Minimum bactericidal concentration (of an antimicrobial)
MIC	Minimum inhibitory concentration (of an antimicrobial)
MRSA	Methicillin resistant *Staphylococcus aureus*
P25	Evonik Industries (formerly Degussa) dispersed TiO_2 powder
PBS	Phosphate buffered saline
PCO	Photocatalytic Oxidation
PDT	Photodynamic therapy
PEG	Poly(ethylene glycol)
PEI	Polyethyleneimine

PISR	Photoinduced Surface Reorganisation
PSH	Photoinduced Superhydrophilicity
RODAC	Replicate Organism Detection and Counting
ROS	Reactive oxygen species
SAM	Self-assembled monolayer
SEM	Scanning Electron Microscopy
TBO	Toluidine blue-O
TEM	Transmission Electron Microscopy
TTIP	Titanium tetraisopropoxide
WDX	Wavelength Dispersive Analysis of X-rays
XANES	X-ray Absorption Near Edge Structure
XPS	X-ray Photoelectron Spectroscopy
XRD	X-ray Diffraction

Thesis Aim and Structure

Aim

The purpose of this work was to study the photocatalytic thin films of TiO_2, produced by a sol-gel route and to assess their potential as antimicrobial and antifouling surface coating treatments. The ultimate goal is to produce light-activated materials which exhibit antimicrobial and/or antifouling characteristics for use in combating the spread of nosocomial pathogens in a hospital environment.

Structure

Chapter 1 will consider inanimate surfaces as reservoirs of microbes, and their role in the spread of disease – particularly hospital-acquired infections (HAIs). Microbial adhesion to surfaces will be considered, alongside methods by which surfaces may be made anti-fouling or anti-adhesive. Finally, attention will be given to the production and function of antimicrobial surfaces – in particular those utilising light-activated antimicrobial agents (LAAAs). The desirability to use photocatalyst thin films as antimicrobial surfaces will be outlined. Chapter 2 documents the synthesis and the characterisation of a selection of TiO_2 and modified TiO_2 type materials. In Chapter 3 the antimicrobial testing methodology for the synthesised films is discussed, alongside the results obtained from these experiments. Experiments were carried out under ultraviolet and fluorescent lighting conditions and in the absence of lighting. This is then linked to Chapter 4, in which microbial adhesion to some test substrates is examined by a simple methodology. The final chapter draws some conclusions from the studies carried out in this work and considers additional work which may be carried out in further experiments in the future.

Chapter 1: Introduction

1.1 The Role of Surfaces in the Epidemiology of Hospital-Acquired Infections

For some time scientists and healthcare professionals have believed in the importance of surfaces as reservoirs of microbes implicated in a wide variety of hospital acquired infections (HAIs). Papers published as early as the 1960's[1] showed some initial evidence supporting the role of surfaces in the epidemiology of disease, but it was not until more recently that good quality evidence for this has become available.[2] It is perhaps the staphylococci, in particular methicillin-resistant *Staphylococcus aureus* (MRSA) that have received the greatest interest and indeed media attention. Various studies have examined microbial contamination and the survival of microbes in the hospital environment.

Infections caused by organisms such as MRSA are more common in hospital environments than elsewhere[3] and *S. aureus* is most commonly passed on by direct contact, usually by the hands of healthcare workers (nosocomial infection).[3-5] The spread of MRSA and other infectious agents can be controlled effectively through a rigorous hygiene regime. Simply washing ones hands is sufficient to help control the spread of MRSA,[3, 6] but washing of the hands is of little use if the hospital environment is heavily contaminated.[4]

It is quite logical to assume that surfaces may act as reservoirs of microbes which could in turn lead to the spread of infection upon being touched, either by healthcare workers, or indeed patients. Despite this however, there is currently little in the way of direct scientific evidence to link pathogens found on a particular surface with a specific manifestation of infection or disease.[4, 5, 7] The available evidence shows that i) common surfaces/articles within the hospital environment can become contaminated with pathogenic microbes and ii) hands (gloved or un-gloved) can become contaminated with these organisms after touching such a surface.

Studies have shown contamination of common hospital surfaces such as room door handles,[6] sterile packaging,[8] mops,[9] ward fabrics and plastics,[10] healthcare worker's pens[11] keyboards and taps,[12] stethoscopes[13] and telephones[14] by potentially harmful microbes. In addition to this, there is mounting indirect evidence of a link between contaminated surfaces and nosocomial infection.[7, 15, 16] Boyce *et al.*[15] found that contamination of the inanimate environment with MRSA occurred when either infected or colonised individuals were present in hospital rooms. More significantly, it was found that 65% of nursing staff that had directly treated an infected individual contaminated their gowns/uniforms with the microbe. MRSA contamination of gloves was also observed in 42% of personnel who had no direct contact with the patient, but had touched surfaces in infected patient's rooms. The studies of Boyce *et al.*[15] and Bhalla *et al.*[16] both clearly demonstrate how the hands (gloved or otherwise) of healthcare workers can become contaminated, presumably by touching surfaces in the immediate vicinity of an infected patient.

By combining our knowledge of pathogen survival on surfaces, and the evidence for transmission of pathogens from surfaces to hands, we can see the importance of the inanimate hospital environment as a microbial reservoir of nosocomial pathogens such as MRSA. It is not surprising for the link between surface contamination and nosocomial infections to have been demonstrated, particularly when MRSA, for example, can survive for up to 9 weeks if it dries on a surface, or 2 days when on a plastic laminate surface[5] and is stable in varying conditions of temperature, humidity, exposure to sunlight and desiccation.[17]

One area which is still under investigation is the determination of typical surface contamination levels, and quantification of a minimum infective dose at which a contaminated surface becomes a problem to health. There have been numerous studies of microbial contamination of surfaces in the hospital environment – what can be said about this is that there is great variation in colony forming units (cfu) recovered per unit area.

	Site	Microbial Load	Reference
Healthcare	Hospital ward surfaces	55 to 80% of sampled sites had >5 cfu/cm^2	White *et al.* 2007[18]
Healthcare	Hospital ward surfaces	2.5 to 40 cfu/cm^2; ward cleaning reduced this to < 2.5 cfu/cm^2	Griffith *et al.* 2000[19]
Healthcare	Hospital ward surface Ward floor	< 3 cfu/cm^2 < 5 cfu/cm^2	Rutala *et al.* 1983[20]
Healthcare	Stethoscope membrane	In > 54% of cases >5 cfu/cm^2; in 18% of cases >29 cfu/cm^2	Bernard *et al.* 1999[21]
Healthcare	Hospital kitchen surfaces	2 to 294 cfu/cm^2	Aycicek *et al.* 2006[22]
Healthcare	Nurse workstation Under ward bed	< 9 cfu/cm^2 < 25 cfu/cm^2	Hardy *et al.* 2007[23]
Food	Meat preparation surfaces	10^5 cfu/cm^2	Upmann *et al.* 1998[24]
Food	Vegetable preparation surfaces	> 10^5 cfu/cm^2	Kaneko *et al.* 1999[25]
Food	Abattoir surfaces	8 to 1.3 ×10^4 cfu/cm^2	Grosspietsch *et al.* 2006[26]
Food	Refrigerator surfaces	813 to 6 ×10^8 cfu/cm^2	Jackson *et al.* 2007[27]
Food	Food contact surfaces	630 to 1.8 ×10^9 cfu/cm^2	Gounadaki *et al.* 2008[28]

Table 1.1 Some typical microbial loads for healthcare and food industry related surfaces. Note: many of the above values have been derived from other measures, including $\log_{10}$ cfu/cm^2 and total aerobic colony count on RODAC/contact plates. Where conversions and derivations have been performed the cfu/cm^2 value is to the nearest whole cfu.

Currently there is no microbiological quality control standard for surface hygiene in general hospital ward areas – this is quite surprising and there is an obvious need for this to be developed. Surface hygiene standards have been proposed,[4] these are based on two standards 1) the monitoring of so-called "indicator organisms" and 2) the total aerobic colony count in a sampled area. The first standard concerns monitoring the clinical area for microbes of clinical importance, for example *S. aureus*, *Clostridium difficile*, and vancomycin-resistant enterococci (the "indicator organisms") – a surface contamination standard for these organisms is proposed at <1 cfu/cm^2.[4] The second standard concerns the total aerobic colony count (ACC) – this is a non-selective assay of the aerobic organisms harvested from a test area. Standards for the total ACC already exist for food processing plants in the US and Sweden, the threshold being <5 cfu/cm^2 and this threshold is suggested for hand contact surfaces in hospitals.[4] There is, however, no evidence regarding what level of surface contamination is hazardous, and the infective dose for MRSA varies from study to study and on a patient-to-patient basis.[2] In general, the number of cfu required to initiate an infection by MRSA lies in the very broad range of between 10 and several million.[2] It would be exceptionally challenging to design an experiment to assess the minimum infective dose from a known surface contamination – and to the best of the author's knowledge this has not been attempted. What is clear is that when it comes to the level of surface contamination, particularly in a healthcare environment, the lower the microbial load the better.

By considering the evidence regarding surfaces and the epidemiology of disease in the hospital environment we can propose a scheme to represent the situation in a typical hospital environment (Figure 1.1). Surface contamination may arise in a number of ways, but in particular we can see how it may be due to direct transfer (by touching) from an infected or colonised patient, or from a healthcare worker who is carrying the pathogen on their hands. Once a surface has become contaminated, a cyclical problem exists since this contamination can now be propagated to other surfaces and patients in the vicinity. Whilst appropriate hand washing by healthcare workers can control the further spread of the

microorganism,[6] it cannot eradicate the surface contamination, nor the potential direct transfer by the patient and the cycle will always remain. The efficacy of traditional cleaning methods to remove this contamination is questionable. A recent study of MRSA contamination in the hospital environment detected MRSA on 74% of swab samples prior to cleaning, and on 66% of swab samples after cleaning.[29] In order to fully tackle the situation, it is clear that a bioactive surface – which can either prevent microbial contamination altogether, or destroy adherent organisms, is required.

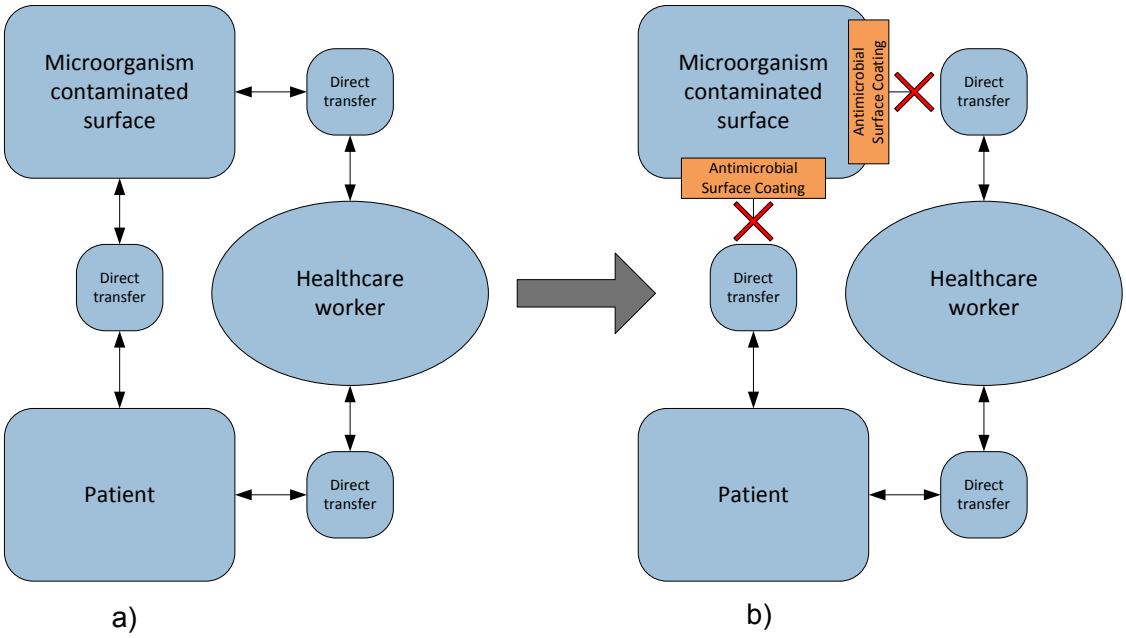

Figure 1.1 The role of surfaces and antimicrobial surface coatings in the epidemiology of HAIs – beating the "nosocomial infection loop"

The development of actively antimicrobial surface coatings can play an important role in tackling the problems highlighted by the cyclical nature of Figure 1.1a. Such a coating would be able to reduce microbial loads on a surface without outside intervention and hence would play a part in reinforcing the hygiene regime of a clinical environment. By removing the ability of a surface to act as a microbial reservoir it may be possible to break this "nosocomial infection loop" and we are left only with the problem of person-person transmission – which can be addressed

by appropriate hand washing and the use of alcohol hand rubs by healthcare workers.

1.2 Microbial Adhesion to Inanimate Surfaces

Microbes can be commonly found colonising surfaces in diverse environments, indeed it may be considered to be nature's default situation that microbes accumulate on surfaces, especially where there are sufficient nutrients and favourable conditions for growth.[30] These surface-attached microbes form what is termed a biofilm. Biofilms comprise microbial cells in a growth phase which is significantly distinct from that of planktonic cells.[31] Donlan and Costerton[32] define a biofilm as "a microbially derived sessile community... irreversibly attached to a substratum [and] embedded in a matrix of extracellular polymeric substances [EPS] that they have produced." There is one further point of definition, which sets the biofilm microbes apart from planktonic cells on a surface – biofilm cells display an altered phenotype in terms of growth rates and gene transcription, when compared to planktonic cells of the same organism.[32] This point of definition makes biofilm cells uniquely different from planktonic cells. The structure of biofilms makes them a tenacious problem in a variety of settings, particularly healthcare, where biofilm contamination of biomedical devices is a major event in the aetiology of HAIs.[32, 33] Biofilms are also a problem in the water supply, where supply pipe work can become constricted, corroded or contaminated by both benign and pathogenic microbes[30] and in oil extraction, where biofilm growth can initiate the degradation of the oil rig structure, as well as affecting the pipelines in a similar way to the water supply case.[30] It is the area of healthcare and the rise of biomedical device related infections that are perhaps presently of most interest and the implications of microbes adherent to surfaces in this arena will now be considered.

1.2.1 Reasons for Microbial Attachment to Surfaces

Surface-adhered microbes were first studied by Antonie van Leewenhoeck in 1683 who wrote to the Royal Society detailing his observation of microscopic "Animals" recovered from the "white matter as thick as wetted flower [*sic*]" found between his teeth.[34] This was the first observation of biofilm microbes. However,

microbiology quickly became interested in planktonic cells, the infections that they cause, for example; *Vibrio cholerae* (Cholera) and *Yersinia pestis* (Plague) and the culture of microbes in liquid media.[33] Surface-attached microbes were largely forgotten. Consequently biofilm research was very slow off the ground in comparison to that of free moving planktonic cells and biofilms have only been extensively studied for about 20-30 years. One of the key areas addressed was the question of why should a microorganism attach to a surface and form a biofilm. It is accepted that there are three reasons why forming a biofilm might be advantageous:

1) **Protection.** A biofilm affords protection to the microbes from which it is comprised. The EPS matrix, which is predominantly comprised of polysaccharides, holds the microbes in place and protects them from physical damage or from being swept away.[30, 35] Equally it may also afford protection from chemical damage because the toxic molecules of an antimicrobial compound applied to a biofilm can sometimes be prevented from acting because the EPS acts like an ion exchanger.[36] The EPS matrix has also been shown to take up microbicidal metal ions such as Cu^{n+} and Ag^{+}, preventing them from exerting their toxic effects upon the microbes of the biofilm. EPS has also been implicated in affording protection for the biofilm from other stresses such as UV irradiation, changes in pH, osmotic changes and desiccation.[35, 37]

2) **Nutrients and Growth**. The extracellular matrix holds the biofilm in a place which is advantageous to growth – this favourable site has the correct conditions for optimal growth, in terms of nutrients, moisture and environmental factors – hence, being part of the biofilm is beneficial to the survival of newly adhering microbes.[30] In addition to holding the organisms of the biofilm in one environmentally advantageous location, the biofilm structure allows nutrients to move through the biofilm. The biofilm structure consists of water channels, which provide a means by which nutrients can flow through the biofilm, between microcolonies – it has been likened to a primitive circulatory system.[35] This arrangement also leads to

the possibility of metabolic cooperation both between organisms making up the biofilm – a further advantage.[35]

3) **Genetic Exchange**. The biofilm allows the microbial cells to exist in close proximity to one another. This means that there is a greater opportunity for genetic exchange and the biofilm constituents may also benefit from quorum sensing (cell-to-cell communication *via* signalling molecules).[30, 35] As biofilms are considered to be the predominant mode of growth in nature, conjugation is considered to be the way in which genetic material is exchanged within, or between, microbial populations.[35] This transfer of genetic material between microbial populations in a biofilm has been demonstrated with the transfer of a conjugative transposon from a *Bacillus subtilus* donor to a *Streptococcus acidominimus* recipient in a model oral biofilm in a constant depth film fermentor (CDFF).[38] This is particularly interesting as it shows how antimicrobial resistance can be genetically propagated through a biofilm – a matter of great concern in biofilm related infection.

Perhaps one further explanation for why microbes should become surface-attached is that, as previously stated – the biofilm is the normal way microbes would grow in nature, rather than the bulk liquid culture that is the norm in the laboratory. Biofilm growth may be a manifestation of the "default" mode of microbial growth.

1.2.2 Microbial Attachment

A schematic diagram showing the steps in microbial attachment to a surface and subsequent biofilm formation is given in Figure 1.2. It is the initial step (labelled A) in the diagram, which is of greatest interest in the field of antimicrobial coatings and surfaces, because it is the initial point of microbial adhesion. If a surface can be designed and engineered such that this process is affected, microbial contamination of the surface may be attenuated.

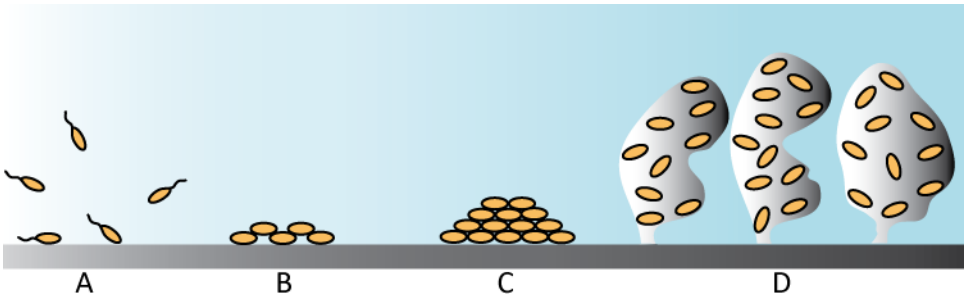

Figure 1.2 A schematic representation of the steps in the formation of a biofilm. A: planktonic cells initially attach to a surface reversibly (seconds timescale). B: microbes become irreversibly attached (seconds-minutes timescale). C: microcolony formation, microbial growth and EPS production (hours-days timescale). D: matured biofilm consisting of attached islands of microbes with water channels. Adapted from Costerton *et al*. and Biofilms Online (Montana State University USA).[33, 39]

The adsorption of microbes on to a surface is a complicated process, which is still under intense debate and study. On a basic level it is accepted that there is an interplay of various short range attractive/repulsive forces such as electrical charge, electrostatics and Van der Waal's forces, this has collectively been summarised in the Derjaguin, Landau, Verwey and Overbeck (DLVO) theory.[39, 40] A recent paper[41] has attempted to explain the adhesion of microbes to surfaces in physico-chemical terms and concludes that microbial attachment to a surface is governed by "macromolecular physics and chemistry in the interfacial environment". This can be linked to genetics because organisms with the ability to adapt their macromolecular structure can consequently adapt this physicochemical interaction, resulting in enhanced or reduced ability to adhere to a surface. These physicochemical interactions arise from the microbial cell surface structures, and the way that these interact with the substrate. Regardless of whether an organism is classified as Gram-positive or Gram-negative, most have a charged surface at neutral pH – due to ionisation of the macromolecules on the microbe surface. Surface charge can be quite significant because of the high surface area-volume ratio of prokaryotic cells.[42] The Gram classification (positive or negative) does not refer to microbial surface charge, but refers to whether a microbe retains a particular stain in microscopy (the Gram stain) and is a result of the two types of

cell wall structures shown in Figure 1.3 and Figure 1.4. (Note: diagrams not drawn to same scale).

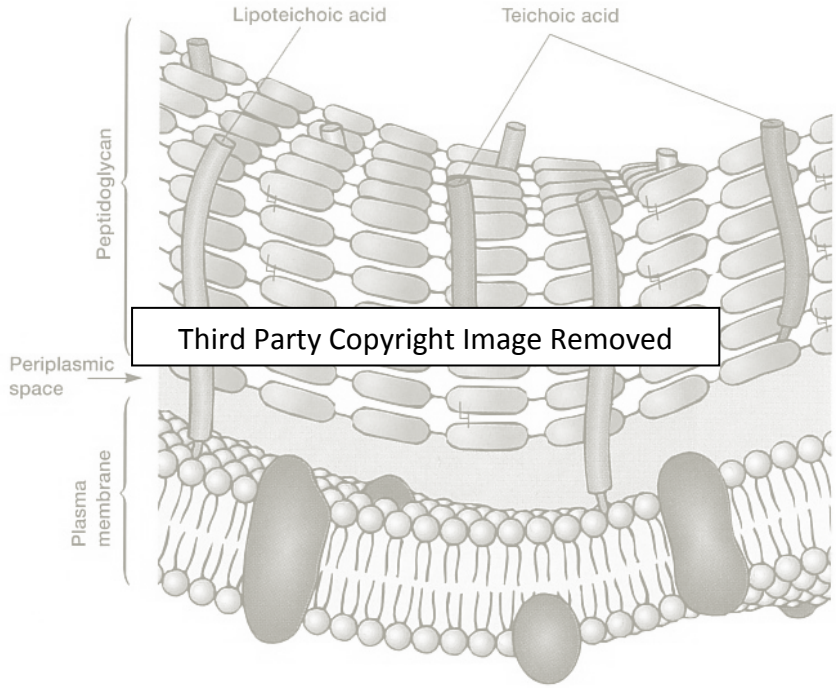

Figure 1.3 The Gram-positive cell wall, image from "Microbiology"[43]

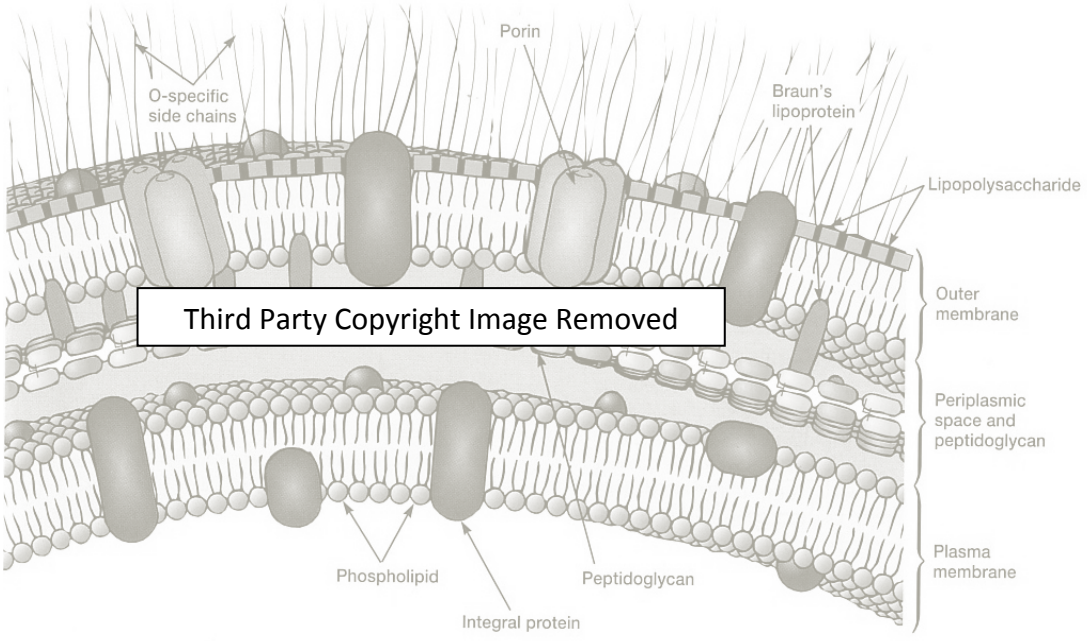

Figure 1.4 The Gram-negative cell wall, image from "Microbiology"[43]

The Gram-positive wall (Figure 1.3) consists mainly of a thick peptidoglycan shell (20-30 nm thick) outside of the plasma membrane, with other biopolymers such as

teichoic and teichuronic acids – the carboxylate groups of these compounds may be ionised to COO-, leaving a negative surface charge.[41, 42] The Gram-negative wall (Figure 1.4) consists of a lipid bilayer outermost, with a thin layer of peptidoglycan between it and the plasma membrane. The outer face of the lipid bilayer consists primarily of lipopolysaccharide (LPS)- and it is the macromolecular structure of the LPS that affects the physicochemistry of the cell surface.[42] The readily ionisable headgroups of the lipid bilayers leads to a net negative charge on the outside surface. The recent work of Geoghegan *et al.* [41] shows that the previously studied electrostatic, Van der Waal's and electrical charge issues are not the only physicochemical factors for microbial adhesion. They also showed the importance of polysaccharides, esters, carboxylic acids and carboxylates by FTIR measurements. What is clear is that the precise mechanism for the initial microbial attachment to a surface is still yet to be fully understood, but by studying the process we can look to design materials which prevent or reduce the initial interaction between microbe and substratum.

1.3 Antifouling and Anti-adhesive Coatings

One approach to microbial contamination of surfaces is to prepare a surface which microbes find it hard to become attached to. The strategy of this technique is to prevent microbial adhesion to the device or surface in the first place. As such this is a preventative strategy.

1.3.1 Poly(ethylene glycol) Coatings

One well established method for preventing the adhesion of microbes, proteins and mammalian cells to surfaces is to coat them with a layer of poly(ethylene glycol), or PEG. PEG modification of polyurethane surfaces was first shown to inhibit microbial adhesion in the late 1990's, with much research being carried out in this area subsequently.[44-47] The current methodology involves the deposition of a self-assembled monolayer (SAM) on a substratum (usually a gold surface), followed by functionalisation of the SAM to contain the required PEG functionality. PEG polymeric surfaces are antifouling because of firstly the hydrophilic interaction with the otherwise hydrophobic microbial cell envelope, which does not favour

microbial attachment to the surface. The second reason for the antifouling properties lies in the dynamic movement of the PEG chains tethered to the surface, coupled with their lack of binding sites – these factors making it more difficult for a microbe to become attached to the surface. PEG, and modified PEG surfaces have been shown to effectively inhibit the adhesion of microbes by up to a 3 log unit reduction in attached microbes (as well as a reduction in adherent proteins and mammalian cells). The principal drawback of this technology is that currently the deposition of a PEG surface requires 3 synthetic steps and can only be done to a surface during manufacture.[45]

1.3.2 Diamond-Like Carbon Films

Diamond-like carbon (DLC) films are comprised of metastable, amorphous carbon, with significant sp^3 character (a-C) comprising small quantities of hydrogen – hence the films are sometimes known as amorphous hydrogenated carbon (a-C:H).[48-50] First prepared by an ion-beam technique in the 1970s,[51] these materials are now more commonly produced in the laboratory by plasma assisted/plasma enhanced chemical vapour deposition (PA/PECVD).[49, 52] A plasma of atomic hydrogen is used, which prevents the deposition of sp^2 carbon in the form of graphite and allows deposition of sp^3 carbon in a diamond-like thin film.[49, 52] The hydrogen plasma is therefore the source of the hydrogen which becomes deposited, up to ca. 60%, within the a-C:H film.[48] Other deposition methods include sputtering, cathodic vacuum arc and pulsed laser.[48, 49]

DLC films exhibit many of the useful characteristics of bulk diamond, such as very low friction coefficients, high wear resistance, chemical inertness and optical transparency, but are significantly cheaper and more facile to manufacture than the bulk material.[48, 49, 53] The physical and mechanical properties of these films, especially in the study of their tribology meant that initial uses were as protective coatings at the interfaces between the magnetic storage platters and the read/write heads of hard disk drives.[48] However, researchers have subsequently realised many other uses, in particular that of DLC as a biocompatible surface coating for biomedical devices such as stents or replacement joints.[50, 53, 54] Liu *et al.*

reported that a DLC film can reduce the adhesion of *Pseudomonas aeruginosa* to a stainless steel substrate, and by doping the DLC with Si or N, this can be reduced even further.[53] DLC films may be doped with other atoms as well, so it is possible to manufacture a coating which has properties of both low microbial adhesion, and by doping in cytotoxic species such as Ag or Cu, antimicrobial properties too.[54] This represents a very interesting and new area of research, and doped DLC coatings may be very useful to prevent infections due to invasive biomedical devices such as venous and renal catheters, which are a major source of HAIs in the UK. HAIs are estimated to cost the NHS up to £1000 million per annum,[55] but the proportion of this cost resulting from catheter infection is undetermined.[56] In the USA, catheter related infections are estimated to cost $20,000 on healthcare costs alone, per patient.

1.3.3 Zwitterionic Polymer Biomimetic Surfaces

Recently it has been shown that polymers with zwitterionic head groups can be applied as surface coatings, which inhibit biofouling of the surface. Polymers which have received research interest are poly(phosphorylcholine) polymers,[57-59] poly(sulfobetaine) polymers[60] and poly(carboxybetaine) polymers.[60] The initial discovery was that these zwitterionic surfaces are biocompatible and non-thrombogenic. The biocompatibility results from the zwitterionic nature of the polymer headgroup (see Figure 1.5 for the phosphorylcholine headgroup) which mimics that found in the lipid bilayers of biological membranes. The logical connection was then made that increased biocompatibility of a surface would also lead to reduced microbial adhesion.

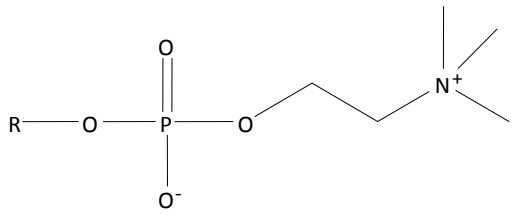

Figure 1.5 The phosphorylcholine polymer headgroup – a typical example of a zwitterionic polymer used in biomimetic surface coatings, which exhibit reduced microbial adhesion

Recent studies[58, 60] have shown that these zwitterionic surfaces prevent initial microbial adhesion, and that biofouling and biofilm formation is significantly arrested. These zwitterionic surfaces demonstrate promise for coating medical devices such as catheters, because their biomimetic nature firstly affords biocompatibility by reducing attachment of human cells to the device and secondly afford protection against microbial biofilm formation which can lead to device-related infections. This technology is relatively new but will no doubt receive further research interest in an attempt to reduce infections caused by indwelling biomedical devices.

1.3.4 Hydrophobic Easy Clean Surfaces

Water droplet contact angle is a measure of how easy it is for a microbe to colonise a surface.[61] The contact angle is the angle subtended by the water droplet on the surface. For self-cleaning surfaces either an exceptionally hydrophilic (less than 10°) or hydrophobic (>140°) surface is required, intermediate contact angles of 30-100° do not have easy clean features and are significantly easier for microbes to stick to and form a biofilm.[62] Very smooth surfaces are, in general, harder to colonise than rough surfaces – although rough surfaces are needed for very high contact angles. Nature uses exceptionally rough surfaces on some plant leaves to produce a self-cleaning surface known as the Lotus effect.[63] The Lotus effect is where water droplets on the surface of the plant leaves have exceptionally high contact angles, typically greater than 140° and these droplets roll and spin across the surface at very low tip angles (5° or less). The spinning action picks up dirt, dust, microbes and viruses from the leaf surface with remarkable effect. Lower contact angles encourage water droplets to slide across the surface, the sliding action is inefficient at removing the microbes. Man-made replicates of the Lotus effect are widespread, however these have yet to be adopted in the hospital environment.[64, 65]

1.4 Antimicrobial Coatings and Surface Technologies

There are a wide variety of antimicrobial coating technologies which are either currently available as marketed products, or which are in research stages. Some of

these technologies are organic antimicrobials, released from the product (for example Microban® which contains Triclosan (5-chloro-2-(2,4-dichlorophenoxy)-phenol) as the antimicrobial agent), whereas others rely on inorganic antimicrobials – most commonly the silver ion Ag^{+}. These techniques which utilise diffusible antimicrobials have the potential problem of inducing microbial resistance, because the products continually deliver active compounds to the environment. Increased exposure of microbes to these compounds will inevitably lead to increased occurrences of resistance to the treatments, though at present there are few organisms which display resistance to Ag or Cu.

1.4.1 Microbicide-Releasing Surfaces

One of the most heavily marketed and most widespread products for suppressing microbial growth is Microban®.[66] Microban® incorporates Triclosan (5-chloro-2-(2,4-dichlorophenoxy)phenol) – a broad spectrum phenolic antimicrobial into a surface, normally a polymer. It works more like a disinfectant, i.e. killing outside in, rather than an antibiotic, i.e. inside out. With a Microban® product, the antimicrobial leaches from the surface of the product to perform the antimicrobial function. This means that effectively they are non-permanent. Triclosan is found in many products such as hand wash soaps, toothpastes as well as on touch surfaces and items such as chopping boards and cling film. Microban® has been shown to suppress microbial growth within the domestic, especially kitchen, environments; however it is not widely used within hospitals. One of the first uses of Microban® as an antimicrobial in a UK hospital was at the John Radcliffe in Oxford at the end of 2006, where it was used as a coating on door handles.[67] There has also been significant concern about possible development of Triclosan resistance; furthermore some studies[68, 69] suggest that Triclosan can, under the action of UV-light, produce dioxins, which are extremely hazardous to man.

1.4.2 Silver and Silver-Containing Surfaces

Silver has long been known to be an antimicrobial, the Greeks and Romans used silver coins and vessels to make drinking water potable.[70] More recently in the 1900s 1% silver nitrate solution was commonly applied to the eyes of newborns to

prevent infections that lead to blindness.[70, 71] Ag^+ ions have a significant antimicrobial effect and have found uses in a number of commercial applications, documented in a recent review.[72] These include the silver sulphadiazine creams, successfully applied topically to burns patients. This cream consists of 1% silver sulphadiazine and 0.2% chlorhexidine digluconate[72] and is effective as a result of the synergistic action of these antimicrobials. Silver has also been successfully used in wound dressings and as an additive in catheters and other medical devices.[72] When it comes to available commercial coating products; AgION Technology's AgION™[73] and AcryMed's SilvaGard™[70] are two of the more well known. Both of these silver-containing products rely on the diffusion of Ag^+ ions from the substrate material and their subsequent action on adherent microbes as broad spectrum antimicrobials. To date, few organisms have developed resistance towards the silver ion as an antimicrobial. It is widely believed that the effectiveness of Ag^+ as an antimicrobial is due to its ability to bind with thiol (–SH) groups on proteins and enzymes – thereby inactivating them.[71] Despite the initial effectiveness of these existing antimicrobial coatings, they have one major drawback – they are non-permanent, relying on diffusible antimicrobials to which microbes can evolve resistance, however the concentration of Ag^+ required for action is actually very low and varies from study to study.

1.4.3 Copper and Copper Alloy surfaces

Like silver, copper has long been considered to be a hygienic material. It has been known since the 1980s that copper, along with other heavy metals such as cadmium and lead are toxic to microbes,[74] and it was suggested by at least one researcher that brass touch surfaces, such as doorknobs, be maintained in hospitals instead of the stainless steel replacements.[75] It was only more recently that copper and its alloys have been thoroughly investigated as antimicrobial surfaces. Keevil[76-80] has assessed the antimicrobial activities of copper and some of its alloys in comparison with stainless steel. Keevil's group have assessed a number of microbes of clinical importance, including MRSA,[77] *E. coli* O157,[76] *Listeria monocytogenes*,[78] *Clostridium difficile,*[80] and Influenza A virus.[79] In all experiments the copper surfaces clearly exerted an antimicrobial effect, as did the majority of

the copper alloys. Stainless steel was shown to be inert compared to the coppers. The studies with MRSA, *E. coli* O157 and *L. monocytogenes* were carried out on 1 cm^2 coupons of material, inoculated with 10^7 cfu of test organism. On pure copper substrates the inocula were reduced to a level at or below the experimental detection limit (100 cfu) within 90 minutes or less at 20-22 °C.[76-78] Vegetative cells and spores of *C. difficile* were also effectively killed by the copper coupons, with complete kill in 24 to 48 hours. Stainless steel coupons showed no change in microbial load, even after 1 week of exposure.[80]

The work of Keevil's group shows that, despite its association with hygiene, stainless steel surfaces may not be the best choice for areas where microbial surface contamination is an issue. Whilst it is an easy material to clean, stainless steel has no ability to reduce the microbial load on its surface. Despite its excellent antimicrobial response however, copper is not a suitable replacement for stainless steel in a hospital environment. This is because of its poor mechanical properties in comparison with stainless steel and its less than aesthetic appearance when exposed to the air. However, as Keevil has shown, the copper alloys also exhibit antimicrobial activity, albeit of smaller magnitude. These alloys have improved aesthetic and mechanical properties and may be more suited to real world applications. A clinical trial of copper and copper alloy fixtures and fittings is currently underway in Selly Oak Hospital, Birmingham, UK.[81] The results from this will allow an assessment of the real-world benefit of copper surfaces to combat nosocomial infections.

1.4.4 Bacteriophage Modified Surfaces

Bacteriophages are viruses which infect prokaryotic cells. Phages usually target individual species of microbes, bind to their surface, inject their genetic material and replicate within the microbial host. If the replication of the phage is by what is known as a "lytic" process the eventual result is the lysis of the host cell, and the release of more phages.[30, 82] The replication process is self-propagating until there is no more host organism available. As a result of this, lytic bacteriophages make interesting candidates for antimicrobial use. Phages were first used therapeutically

in 1919 by French bacteriologist Félix d'Herelle to treat severe dysentery in a Parisian children's hospital with great success.[82, 83] With the discovery in 1928 and rapid development of penicillin in the 1930s and 40s, bacteriophage therapy in the Western world was largely made redundant as pharmaceutical companies focussed on the large scale production of penicillin. However, phage therapy research and development continued in Eastern Europe, most notably in the former Soviet Union, where it is still widely used.[83] It is only more recently; from about 2001 onwards, that Western science has started to revisit the use of bacteriophages as a viable antimicrobial therapy, largely as a result of the growing problem of antimicrobial resistance. An article in *Science*[83] brought phage therapy back to the attention of the general scientific community. The article in *Science*[83] details the use of a phage-containing wound dressing, PhagoBioDerm (a wound dressing containing, amongst other ingredients, lytic bacteriophages for *Pseudomonas aeruginosa*, *E. coli*, *S. aureus*, *Streptococcus* spp. and *Proteus*). The dressing was used in the treatment of some skin infections which were not responding to conventional antimicrobial therapy. The papers which document these results fully[84, 85] acknowledge that the trials were not rigorously controlled and double blind, but it is clear from the results that the treatment does appear to work well, though adequate clinical trials are needed.

The concept of modifying a surface with bacteriophages in order to produce an antimicrobial surface is a very recent development. Curtin *et al.* demonstrated how this could be done successfully on a hydrogel coated silicone catheter model in 2006.[86] Indwelling catheters are a major route by which bloodstream HAIs can occur, and numerous methods are being developed to combat the formation of microbial biofilms on these devices, including some which have already been discussed, such as silver loading. In the work of Curtin *et al.*[86] the formation of a *Staphylococcus epidermidis* biofilm on catheters pre-treated with coagulase-negative staphylococcus phage 456 was monitored. It was shown that this modified surface, containing phage units, reduced biofilm formation significantly. With phage 456 and $MgCl_2$ or $CaCl_2$ supplements, a 4.47 log reduction in the mean viable count per cm^2 of substrate was recorded over 24 hours relative to a control

having 7.01 log cfu/cm^2. A 2.34 log reduction was recorded when the supplements were not used.

A phage-modified surface is certainly an interesting antimicrobial approach, in particular because organisms currently resistant to antibiotics do not show resistance towards phages. Equally, because it theoretically only needs one phage to infect a host cell for a cascade in phage production, it could be a very efficient way of disinfecting a surface without significantly deactivating the surface in the process. There are, however, a number of potential problems. The first is the inherent specificity of the phage for individual microbial species. Whilst this is excellent for a targeted *in vivo* therapy, it is less useful for a surface, where a number of different organisms, not necessarily just microbes, may be present. A combination of phages would have to be used to increase the spectrum of activity, but this may leave out potentially harmful organisms. One other area of concern is that of phage resistance – microbes can become resistant to a phage through mutations which change the susceptibility of the cell wall to the phage enzymes used to enable injection of genetic material.[30, 83] Whilst it is believed to be easier to deal with resistance to phages by selecting new phages from culture that maintain virulence[83] it is still a concern. Phage-treated surfaces or products would have to be constantly monitored and their formulation modified to remain efficacious – which will no doubt cause problems for regulatory approval.

1.4.5 Polycationic Antimicrobial Surfaces

Surfaces with cations deposited upon them, were shown to kill microbes upon contact in the 1980's.[87] More recently, surfaces treated with hydrophobic polycations were demonstrated to kill microbes in a similar manner upon contact with the treated surface by causing physical damage to the microbe's cell envelope.[88] The basic premise of these materials is to target microbes by taking into account two features of the microbial cell envelope – namely that they are hydrophobic and negatively charged. By depositing a coating consisting of hydrophobic polymer chains, interaction with the microbe cell envelope is favoured; however, the polymer chains will not tend to stand erect from the

surface to interact with an incident microbe, without some form of repulsive interaction between chains. To this end, a positively charged moiety is required – this keeps the hydrophobic chains separated and erect from the surface, and also electrostatically attracts microbes, due to the net negative charge on their surface. In effect, these materials attract a microbe towards the treated surface, resulting in the puncturing of the microbial cell envelope, and subsequent death of the cell. The most recent surface coatings of this type are polyethyleneimines (PEI's) and two examples are given in Figure 1.6. These types of surface have been shown to be effective against a variety of microbes, including *S. aureus* and some viruses.[88-91] Whilst these PEI coatings are described as being permanently microbicidal, their mechanical stability and longevity has not been described and it is still yet to be seen how well they might respond to the rigours of use and indeed cleaning in a clinical setting.

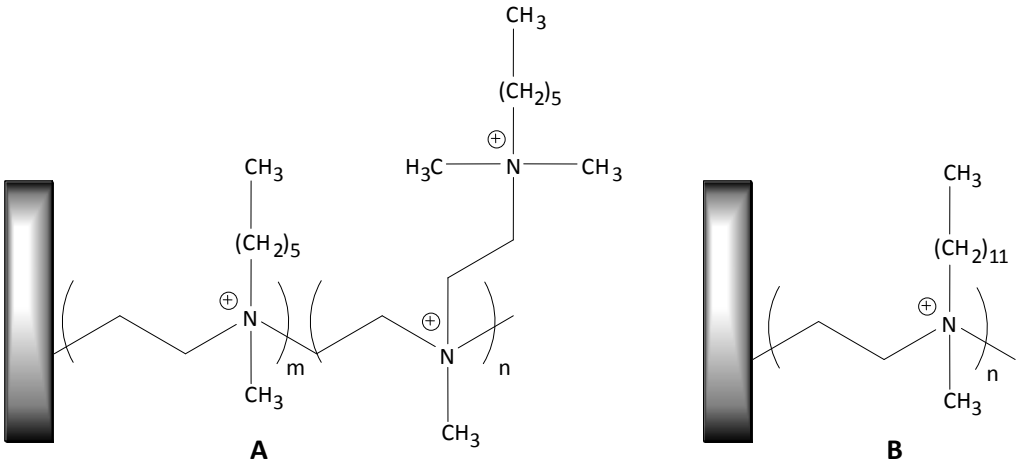

Figure 1.6 Polycationic PEI antimicrobials. Branched *N*-hexyl,*N*-methyl-polyethyleneimine (A) and *N*-dodecyl,*N*-methyl-polyethyleneimine (B).

1.4.6 Light-Activated Antimicrobial Agents (LAAAs)

An alternative method of disinfecting a surface is by the use of a coating which produces reactive radical species. Radical species, unlike the antimicrobials previously discussed, have no specific target within a microbe, that is to say they are completely non-selective microbicides.[92, 93] This has one very important implication – it avoids the potential problems of microbes developing resistance to

a microbicidal treatment, since there is no one site within a microbe upon which they act.[92] Resistance only develops when a specific target site is used by a microbicide.

There are two principal coating types which produce these reactive species and act as antimicrobial surfaces; 1) a coating comprised of a photosensitiser, immobilised in a coating and 2) a titanium dioxide based photocatalyst coating. These materials fall under the broad classification of light-activated antimicrobial agents (LAAAs).

1.4.6.1 Photosensitiser Antimicrobials

The use of a photosensitiser as an antimicrobial agent is a direct refinement of the technique of Photodynamic Therapy (PDT). PDT is a commonly used therapy to target and destroy cancerous tissues. PDT is a form of indirect phototherapy,[94] in which light is used as a means to activate the curative agent – the photosensitiser. The photosensitiser is most usually administered systemically, but is so designed as to accumulate preferentially in the region of cancerous growth. The tumour area, complete with accumulated photosensitiser is then illuminated with visible light, and the therapeutic process begins.

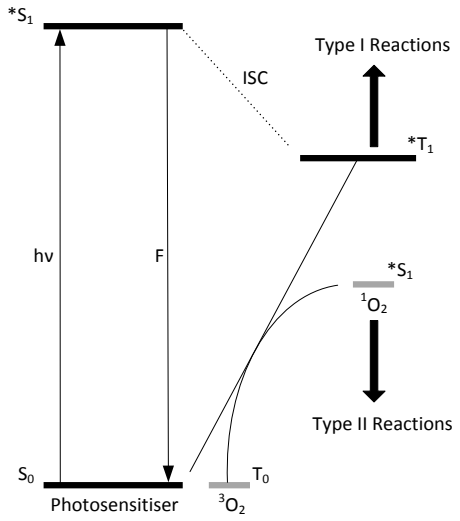

Figure 1.7 Jablonski diagram showing energetic transitions from a photoexcited photosensitiser molecule to molecular oxygen. (Legend: hv = incident visible light energy, F = fluorescence, ISC = intersystem crossing).

The mechanism of photoexcitation of the photosensitiser in PDT is shown in Figure 1.7. The photosensitiser, in a singlet ground state (S_0), is photoexcited to the first excited singlet state, electron spins paired ($^*S_1$) by visible light incident on the photosensitiser. This excited state can either relax to the ground state *via* fluorescence (F), or it may undergo an intersystem crossing (ISC) to a triplet excited state, electron spins unpaired ($^*T_1$). It is this triplet state which leads to the therapeutic effects of PDT, as there are two available pathways of reactions. The Type I reactions involve electron transfer and result in the production of radicals such as superoxide and the hydroxyl radical. The Type II reactions involve energy transfer from the triplet excited state, as it relaxes back to the ground state. Energy is typically transferred to ground state triplet oxygen, which is excited to a singlet state.[94] Principally, it is the production of singlet oxygen by the Type II process which is thought to act upon the cancerous cells, but the reactive oxygen species (ROS) produced by the Type I process are similarly destructive to cells.[94]

In PDT the photosensitiser is chosen such that it preferentially accumulates in the cancerous tissue, and such that its absorption is at a convenient wavelength for the surgical equipment. The first PDT agents were porphyrins and phthalocyanines but other chromophores, such as the phenothiazines (e.g. methylene blue and toluidine blue-O [TBO]) have been studied. A selection of photosensitisers studied for both cancer and antimicrobial PDT are shown in Figure 1.8.

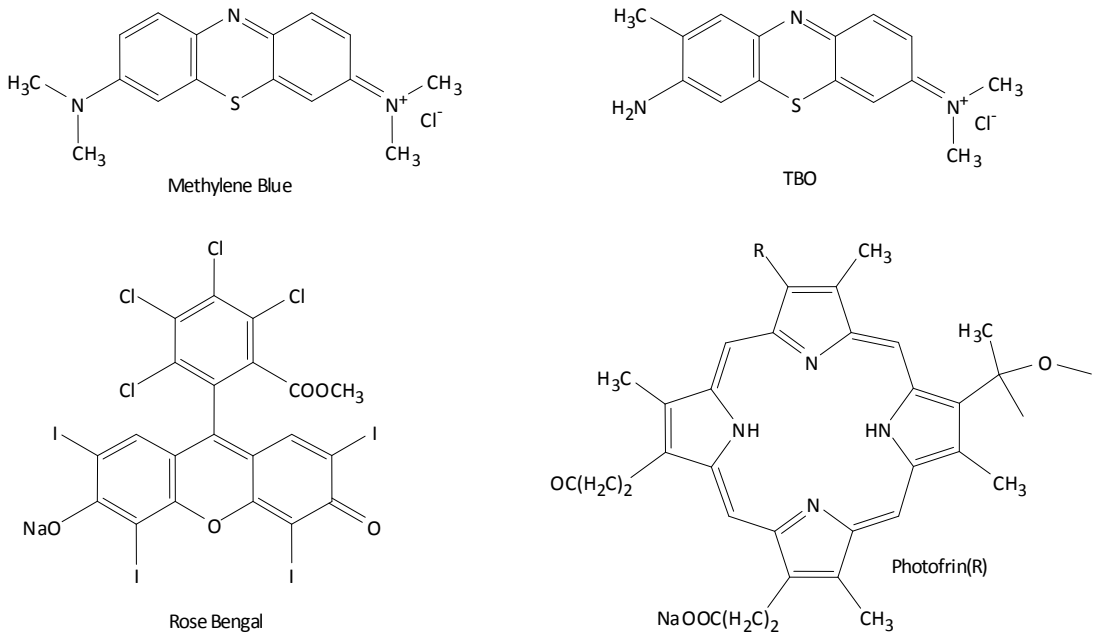

Figure 1.8 Some common photosensitisers employed in anticancer and antimicrobial PDT

The destructive power of the radicals produced by photosensitisers can be put to use in a microbicidal surface coating when the photosensitiser is immobilised within a polymer matrix and applied to a surface.[92] In the recent work of Wilson[92] and Decraene *et al.*[95-97] photosensitisers such as toluidine blue and rose bengal were immobilised in a cellulose acetate coating. It was shown that the photosensitisers did not leach from the cellulose acetate matrix and produced a microbicidal surface active under visible (white) light conditions. The coating materials were shown to be highly effective in the laboratory and clinical environments against a wide variety of microbes of clinical importance, such as *S. aureus*, *E. coli*, *C. difficile*, *Candida albicans* and *Pseudomonas aeruginosa*. The key benefits of this antimicrobial surface are that it can reduce microbial loads on a surface using visible light and avoids the problems of microbial resistance. In similar work by Perni *et al*.[98, 99] toluidine blue and toluidine blue/nanogold impregnated polymers demonstrated unprecedented levels of light-activated antimicrobial activity (greater than 10^5 cfu/ml with 1 minute of 634 nm red laser illumination). There is, however, a potential disadvantage to this technology, in that the ROS produced by the photosensitiser could, in the long term, degrade the polymer matrix containing the photosensitiser. This would result in possible degradation of the coating, loss of

photosensitiser from the matrix and eventual loss of microbicidal activity. As yet no extensive studies of this have been made, and it is something to be considered before this technology proceeds further.

1.4.6.2 Titanium Dioxide Antimicrobials

The efficacy of titanium dioxide (TiO_2) semiconductor particles as a means of disinfection was first realised in 1985 by Matsunaga and co-workers.[100] In this first study it was found that platinised TiO_2, when irradiated with ultra band gap UV radiation (wavelength less than approximately 387 nm); acted as an antimicrobial agent being 100% effective against 10^3 cfu/ml *Saccharomyces cerevisiae* and 10^3 cfu/ml *E. coli* after 2 hours UV illumination. Photodisinfection was rationalised as a result of photocatalytic processes taking place on the TiO_2 surface. Ever since this discovery, research into the efficacy of TiO_2 antimicrobials has centred on three areas of interest:

1. How TiO_2 acts as a photocatalyst.
2. How microbes are killed by the TiO_2 surface.
3. How the surface can be made more efficient at killing microbes.

The first two areas of interest have been extensively studied and the modes of action are very well understood, both in terms of how photocatalysis occurs and how this leads to the killing of microbes.

1.4.6.2.1 Industrial Preparation of Titanium Dioxide

Industrially, titanium dioxide is prepared from the mineral ores ilmenite ($FeTiO_3$) and rutile (TiO_2). Purified titanium dioxide is a white powder, generally obtained by chemical refinement of the mineral ores. The choice of refinement process is determined by the ore being refined. Low grade ilmenite is refined by the sulphate process and higher grade rutile, which does not dissolve in concentrated sulphuric acid, is refined by the chloride process. This is also the cheaper of the two refinement processes and is gaining in popularity. Both processes are summarised overleaf in Figure 1.9.

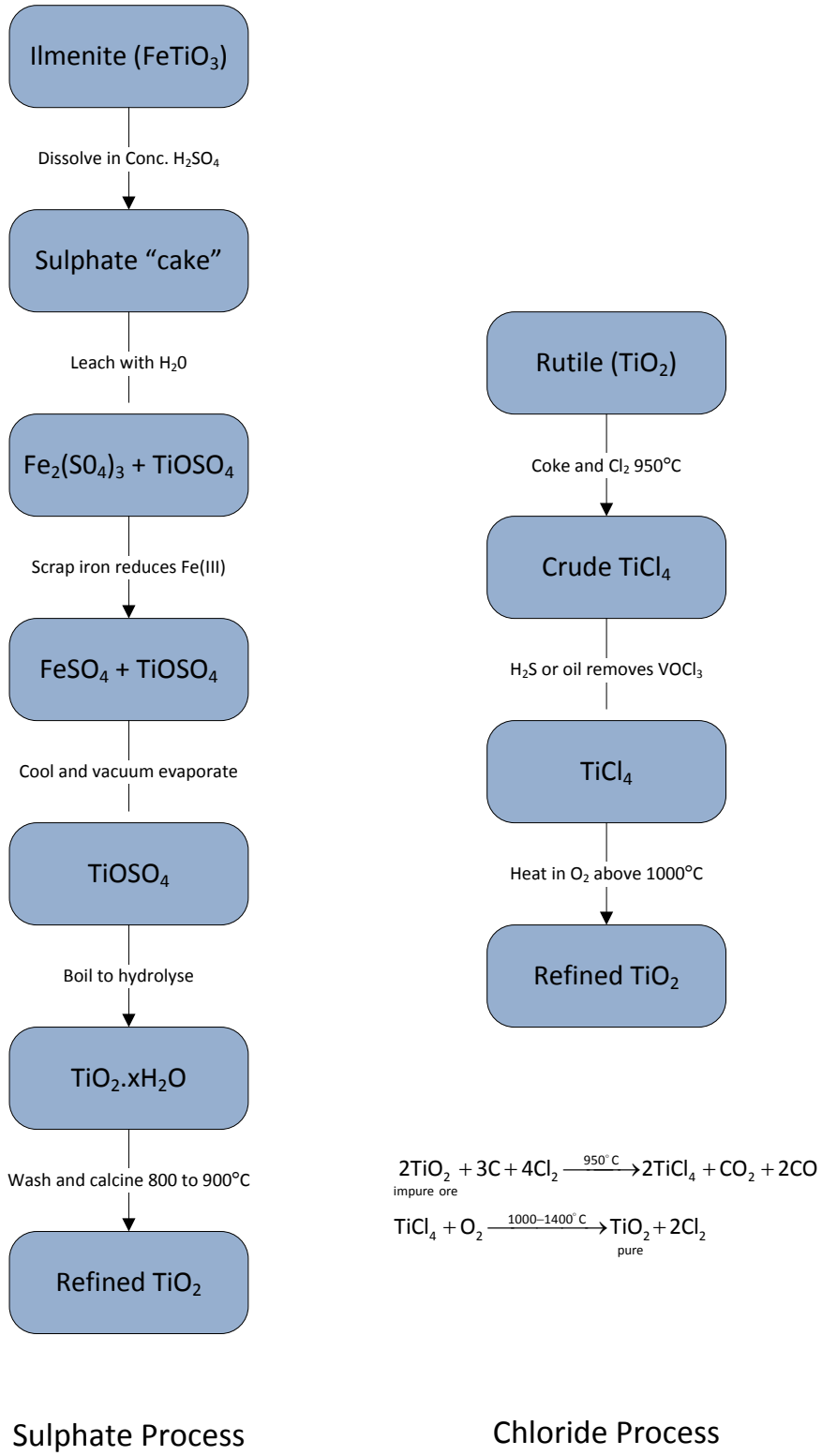

Figure 1.9 The sulphate and chloride process for the refinement of TiO_2 from its ores. Adapted from Greenwood, N.N. and A. Earnshaw, *Chemistry of the Elements*.[52]

The titanium dioxide formed after purification is one of two crystalline forms, anatase or rutile. Rutile is the most common of these forms as it can be produced

from anatase at high temperatures. When employed as a photocatalyst in antimicrobial research, TiO_2 has often been used in the "as manufactured" form. The so-called gold standard of preformed TiO_2 used in a considerable amount of antimicrobials research is Evonik Industries (formerly Degussa) P25.[101-108] P25 is produced by a flame hydrolysis route known as the AEROSIL® process. This process involves the introduction of vaporised $TiCl_4$ precursor in the presence of H_2 and O_2 into a flame reactor, resulting in the production of a TiO_2 aerosol *via* hydrolysis.[109, 110] This is shown in Scheme 1.1.

$$2H_2 + O_2 + TiCl_4 \xrightarrow{\text{Flame Hydrolysis}} TiO_2 + 4HCl$$

Scheme 1.1 The AEROSIL® process for production of TiO_2 *via* flame hydrolysis[109]

The very first demonstration of antimicrobial activity of TiO_2, by Matsunaga *et al*. was performed using P25 suspensions.[100, 111] P25 is a highly dispersed preparation consisting of both anatase and rutile titania in an 80:20 ratio, with a very high specific surface area of 50±15 m^2/g.[112, 113] Many researchers opt to make the TiO_2 materials themselves, often as thin films. The two most common deposition methods for this are Chemical Vapour Deposition (CVD) and Sol-Gel – these are discussed in the following section.

1.4.6.2.2 Chemical Vapour Deposition of Titanium Dioxide (CVD)

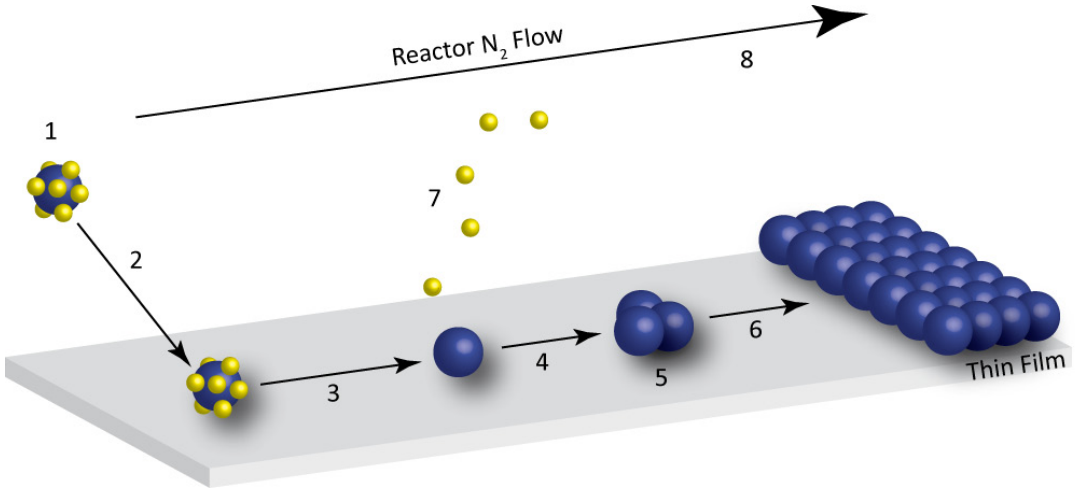

Figure 1.10 Schematic view of the CVD process – see text for legend numbering

Chemical Vapour Deposition (CVD) refers to a technique by which the deposition of a thin film of material occurs from reactants in the vapour phase onto a heated substrate. It is mentioned here for completeness in terms of synthetic technique, but it is not a focus of this study.

The principle steps in the CVD process, highlighted by number in Figure 1.10, are briefly described below:

1. Mass transport of precursor into the reactor chamber – precursor is in the gas phase along with N_2 carrier gas
2. Physisorption of the precursor onto the heated substrate
3. Surface reactions and precursor decomposition
4. Surface atom migration to a site of chemisorption
5. Nucleation
6. Growth of the film
7. Desorption of side-products into the carrier gas stream
8. Carrier gas flow to waste

CVD is used industrially for the deposition of TiO_2 thin films onto window glass to manufacture windows with self cleaning properties, such as Pilkington Activ^{TM}. In the laboratory these kinds of films might typically be deposited from titanium isopropoxide precursor, or a combination of $TiCl_4$ and ethyl acetate,[114] producing thin films of predominantly anatase. Indeed the industrial process, which is carried out on the float glass line, uses the $TiCl_4$ with ethyl acetate co-reactant route, producing a 25 nm thick homogenous coating of anatase TiO_2.

1.4.6.2.3 Sol-Gel Deposition of Titanium Dioxide

Sol-gel synthesis is a wet chemistry technique, and is the synthetic focus of this study. Sol-gel involves essentially the hydrolysis and polymerisation of a colloidal precursor solution (the sol) into a loosely formed matrix, called the gel. The gel has

then to be dried, allowing solvent evaporation; this leaves a mechanically weak and non-crystalline solid, known as a xerogel. To obtain the crystalline material the xerogel is calcined at high temperature, typically 450 to 500 °C, resulting in crystalline TiO_2. The technique is adapted to produce thin films of material rather than bulk solid by deposition of the sol onto a substrate, often by either spin coating or dip coating.

The sol-gel synthetic process for TiO_2 is most usually carried out with a titanium alkoxide as the titanium precursor solution. Perhaps one of the simplest routes uses titanium tetraisopropoxide (TTIP) in isopropanol, with a few drops of HCl to catalyse the reaction[115] or alternatively water can be used to hydrolyse the precursor. A typical sol-gel process for TiO_2 is outlined in Figure 1.11.

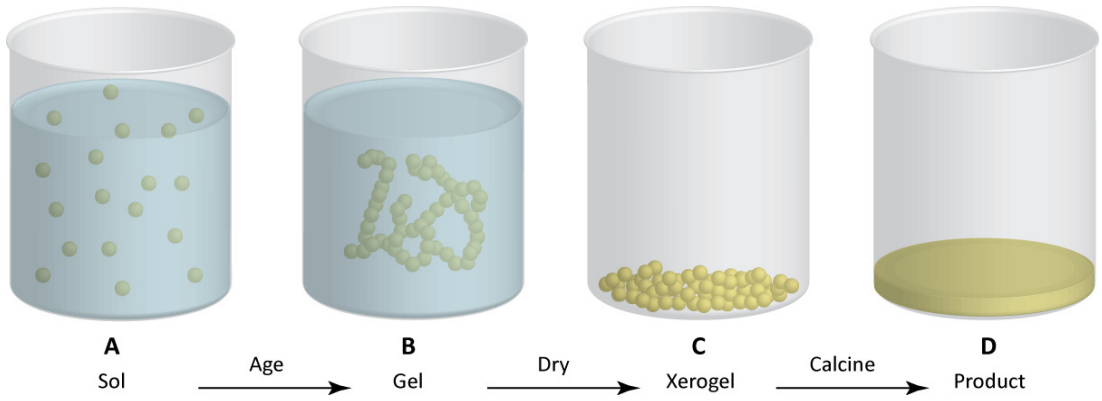

Figure 1.11 Schematic representation of the Sol-Gel process

1) **Preparation of the sol.** In this step (shown in Scheme 1.2) titanium alkoxide and alcohol are mixed together in appropriate proportions. Upon addition of the hydrating agent (water or acid) the hydrolysis process begins. Alkoxide groups are exchanged for hydroxide with elimination of the alcohol (Step A). The now hydrated precursor condensates with other precursor moieties, eliminating water (Step B). The network begins to grow and the colloidal sol is formed (Step C and Figure 1.11A).

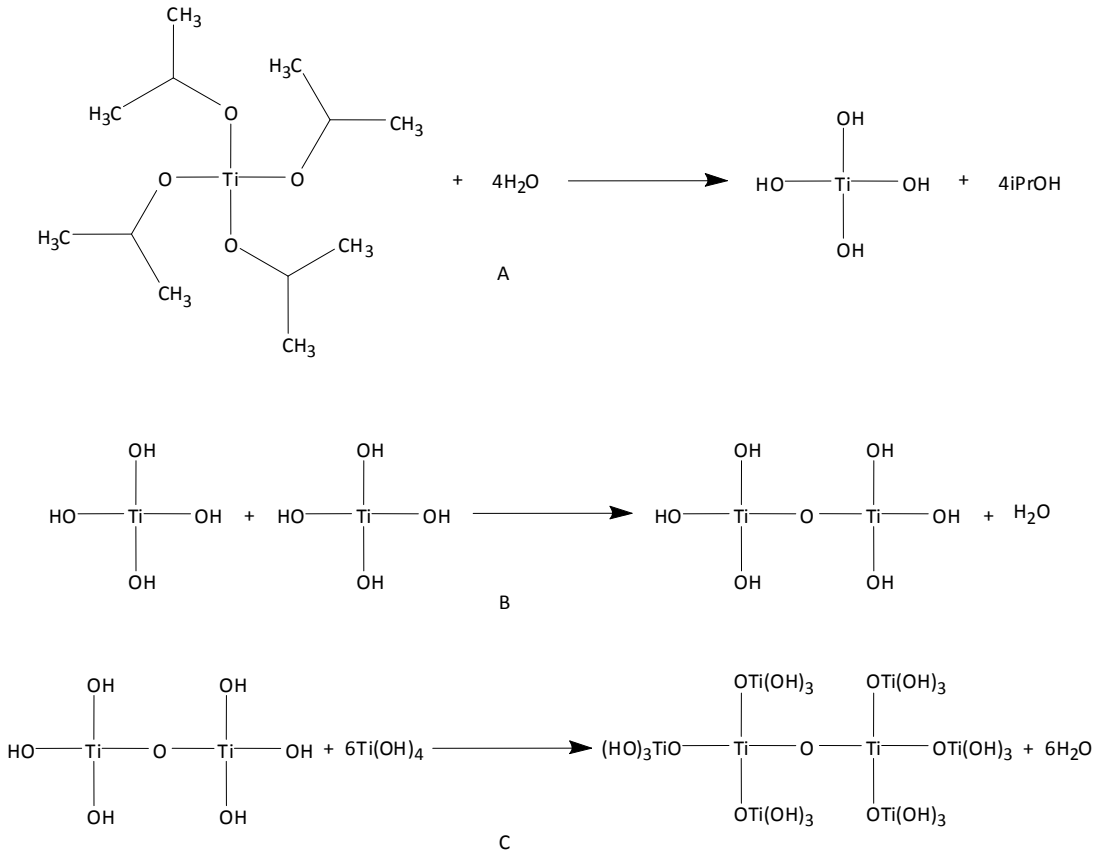

Scheme 1.2 Sol-gel synthesis of TiO_2

2) **Gelation and Aging.** In this step the condensed titania species continue to polymerise together, forming a loosely held together 3 dimensional network. As the network is allowed time to "age" the network densifies. At this stage the network contains solvent and the water and alcohol eliminated during reaction (Figure 1.11B).

3) **Drying.** The aged sol is allowed to dry and dehydrate. This removes most of the alcohol and water trapped in the matrix. The resulting material is known as the xerogel – literally dried gel from the Greek "xeros" meaning dry (Figure 1.11C).

4) **Calcination.** The xerogel has poor mechanical strength and is non-crystalline. In order to crystallise and densify the material, the xerogel is calcined at high temperature, usually around 500 °C to produce a dense and crystalline product (Figure 1.11C).

The above sol-gel process yields a solid powder, rather than a thin film. In order to create a thin film coating by sol-gel, the process is modified so that the aged sol is cast onto a suitable substrate. Casting onto a substrate may be carried out either by dropping the liquid sol onto a spinning substrate (spin coating), or by immersing a substrate in the sol, and removing at a constant vertical velocity (dip coating). In both cases casting as a thin film has the added benefit of accelerating further condensation of precursor and reducing the need for drying.[115] A precursor film is formed on the substrate almost immediately with minimal drying required. The coated substrates are then calcined to produce dense, crystalline thin films. This process is shown below in Figure 1.12.

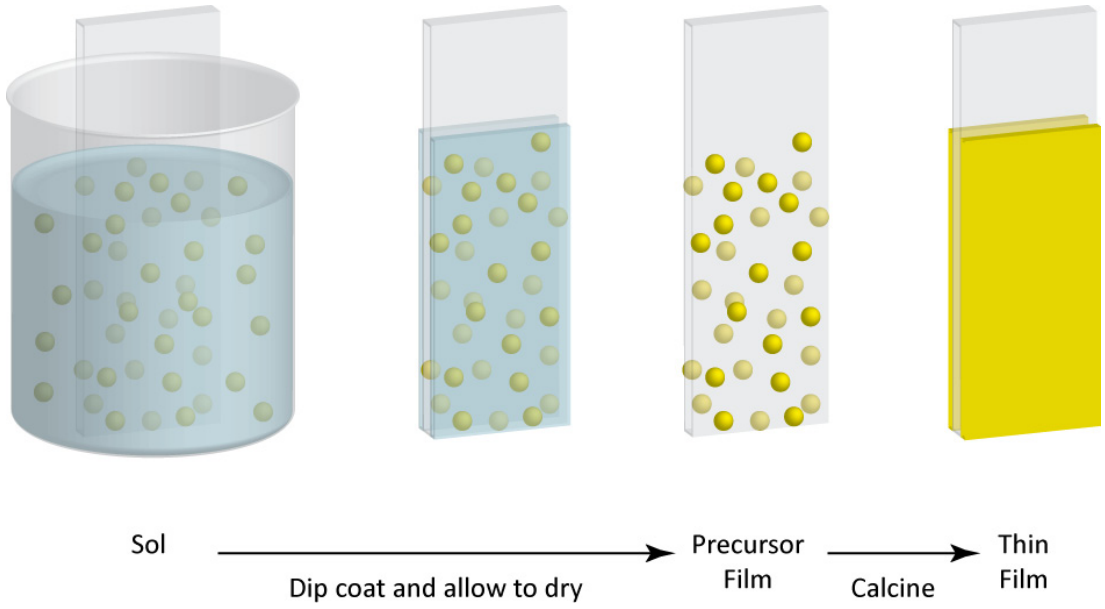

Figure 1.12 Schematic representation of the Sol-Gel preparation of a thin film by dip coating

1.4.6.2.4 Titanium Dioxide Photocatalysis

Titanium dioxide is well known to be a semiconductor. In the anatase form, it has a band gap energy (E_g) of 3.2 eV.[110] Irradiation of anatase TiO_2 with UV radiation greater than E_g causes promotion of an electron from the valence band, to the conduction band. This results in the formation of an electron-hole pair. This is a free electron (e^-) in the conduction band, and a hole (h^+) in the valence band.[93, 101, 110, 111] These reactive species then participate in oxidation and reduction processes either within the TiO_2 itself (electron and hole recombination), or with adsorbates at the surface. This is shown in Figure 1.13. This is the key mechanism of titanium

dioxide photocatalysis, since it produces reactive species at the catalyst surface. The principle reactive species is the hydroxyl radical, which is produced by redox reactions between photoexcited TiO_2 and adsorbed H_2O, molecular oxygen and from hydroxide groups on the catalyst surface.[93] Scheme 1.3 details the production of reactive species at the catalyst surface. The hydroxyl radicals produced by the redox processes at the TiO_2 surface are highly reactive and completely non-selective. These attributes make the radical species extremely potent biocides,[93] with the ability to oxidise most organic compounds at the catalyst surface.[101] Scheme 1.3 highlights a common misconception about photocatalysis, in that light energy is actually a reactant and is not the catalyst. It is more correct to say that TiO_2 acts as the catalyst in a photosensitised heterogeneous process.

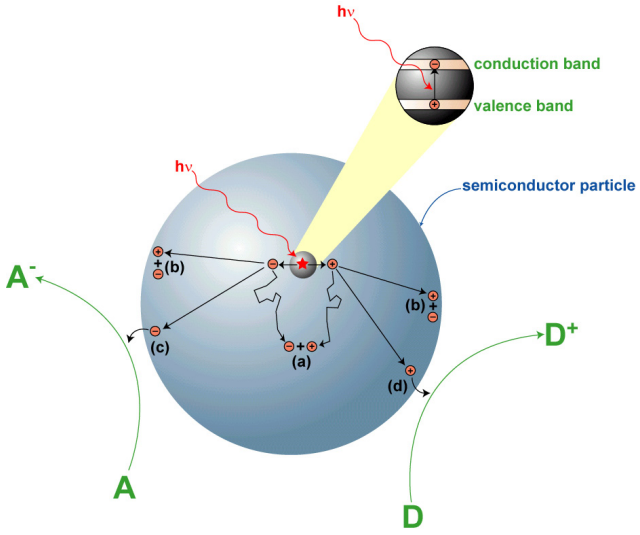

Figure 1.13 Photo-excitation processes in TiO_2, leading to redox behaviour. (a) Electron and hole recombination in the bulk, (b) Electron and hole recombination at the surface, (c) Adsorbate reduction at the surface and (d) Adsorbate oxidation at the surface. Image courtesy Prof. Ivan Parkin.

$$TiO_2 + h\nu \rightarrow e^- + h^+$$
$$h^+ + H_2O_{(ads)} \rightarrow HO^\bullet + H^+$$
$$h^+ + OH^-_{(surface)} \rightarrow HO^\bullet$$
$$e^- + O_2 \rightarrow O_2^{\bullet -}$$
$$2O_2^{\bullet -} + 2H_2O \rightarrow 2HO^\bullet + 2OH^- + O_2$$

Scheme 1.3 Reactive radical species generated by TiO_2 photocatalysis.[93]

1.4.6.2.4.1 Photodisinfection by TiO_2 Mediated Photocatalysis

Disinfection of a surface by photocatalysed reactions on TiO_2 is a popular possible alternative to using chemical disinfectants such as chlorine bleach because it avoids the use of chemicals for which there are currently concerns about possible toxicity and mutagenesis.[111, 116] Consequently, the development of an effective surface-activated disinfection system is highly attractive. Researchers are interested as to the mechanism by which titanium dioxide antimicrobial films cause cell death, and this has been a topic of debate since the first work on TiO_2 antimicrobials by Matsunaga *et al.*[100, 111] Recently the three competing theories were evaluated[117] and considered in the light of the latest evidence collected. The three theories so far considered are set out below:

1. Direct oxidation of coenzyme A (CoA), which inhibits cell respiration, ultimately leading to cell death. This was the original theory proposed by Matsunaga *et al*.

2. Cell wall decomposition and disorder in cell permeability observed by Transmission Electron Microscopy (TEM).

3. Cell wall damage followed by cytoplasmic membrane damage.

Huang *et al.*[117] considered the above in the light of evidence collected by probing *E. coli* with ortho-nitrophenol β-D-galactopyranoside (ONPG). An increase in cell wall permeability to ONPG, and leakage of large molecules from the interior of the cell was observed – reinforcing the third theory above. It was found that damage to the cell wall was non-lethal, whereas breach of the cytoplasmic membrane and leakage of the cytoplasm resulted in cell death. Further corroboratory evidence can be found for this in previous work by Watts *et al.*[116] comparing the efficacy of TiO_2 photodisinfection of viruses and microbes and by more recent Atomic Force Microscopy (AFM) studies of TiO_2 photodisinfection by Lu *et al.*[118] Watts *et al*.[116]showed that TiO_2 was four times more effective at killing poliovirus 1 than it was at killing common coliform microbes. The explanation for this lies in the fact that a virus has a much greater surface area to volume ratio than a bacterium, so

the rate of surface reactions between the TiO_2 generated hydroxyl radicals and the organic components of the virus is much greater than the equivalent process for a bacterium. Damage is therefore limited to the surface of the bacterium. The latest work in this area by Lu *et al.*[118] examined the effect of TiO_2 on *E. coli*, using AFM and measurement of K^+ ion leakage. AFM was able to demonstrate firstly the decomposition of the cell wall, followed by the destruction of the cell membrane. Cell death was due to leakage of the cytoplasm through the damaged membrane. This was confirmed by a notable increase in K^+ ion concentration leaking from the cells. K^+ ions are vital to microbial cells as they play a part in protein synthesis – so the detection of a leakage of K^+ ions clearly shows that the cell membrane is compromised by the action of TiO_2 under photocatalytic conditions.

1.4.6.2.4.2 Modifying the TiO_2 Surface to Increase Efficacy

Currently the predominant research area in titania photocatalysis is an exploration of ways in which the material composition can be altered in order to produce films which are either more photocatalytically active, are able to utilise visible light, or both. The effectiveness of the TiO_2 as a photocatalyst is principally dependent upon the rate of production of hydroxyl radicals at the surface of the semiconductor. However, this is in turn dependent upon the energy of the light illuminating the surface and the competition between electron-hole recombination and the redox processes occurring on the surface (see Figure 1.13). The ultimate research goal is to synthesise a durable, reusable coating which is more antimicrobially efficient, and which is able to effectively utilise visible light, rather than UV light.

In all research to date, the route taken to improve the efficacy of a titania surface is to introduce dopant materials in an attempt to modify the material properties. Often the dopants change the way in which the semiconductor behaves when light (UV or visible) is shone on it. Addition of dopant materials may have three effects:

1. More efficient harvesting of energy from absorbed photons, in effect enabling more energy to be absorbed.

2. Expansion of the wavelength range over which photons can be harvested, so that visible light energy can be used.

3. Maintain separation of charges in the semiconductor, thereby preventing electron-hole recombination and amplifying the photo-redox processes at the catalyst surface.[110]

Although much work has been carried out in the field of semiconductor photocatalysis, production of visible light-activated materials is a comparatively new discipline. Visible light-activated photocatalysis was reported by Asahi *et al.*[119] in 2001. In this work nitrogen-doped titanium oxide ($TiO_{2-x}N_x$) was studied by theoretical simulations, followed by the practical synthesis of the material by sputtering a TiO_2 target in a N_2/Ar atmosphere, followed by annealing in a N_2 atmosphere. The resulting yellowish transparent films demonstrated photocatalytic ability against methylene blue and acetaldehyde. Most interestingly, the UV-Visible spectra of the films show that the nitrogen doping results in a shift of the band edge into the visible light region. It was shown that substitutional doping of N narrowed the band gap due to the mixing of its *p* states with the 2*p* on O. The visible light absorbing intra-band gap states formed by this doping are close to the conduction band edge – this allows electronic coupling between the states and the conduction band electrons and prevents electron-hole recombination.[120] Calculations showed that S doping would have a similar effect, however, the larger ionic radius of S compared with N would make it difficult to incorporate into the TiO_2 crystal.[119] Other dopant materials (fluorine, carbon and phosphorus) were considered, but were deemed unsuitable because the intra band gap states are located in the centre of the band gap, a situation favouring electron-hole recombination.[119, 120]

Another method for narrowing the band gap is to dope the titania with another metal oxide, which has a narrower band gap. One such metal oxide dopant which has already received research interest is WO_3.[115] Tungsten oxide has a band gap of 2.8 eV (equivalent to a light wavelength of 442 nm), which makes the coating able to access the visible solar spectrum, and harvest visible light photons. Inclusion of

another metal oxide semiconductor, such as WO_3 also provides an enhancement in charge separation, by preventing the recombination of electrons and holes.[121] These combined effects allow the surface to be more photocatalytically active and more superhydrophilic than an anatase control. This effect was demonstrated in by Rampaul *et al.*[115] with a 2% loading of WO_3/TiO_2.

Coatings such as those described above may have the potential to be highly successful antimicrobial coatings due to the combined effects of narrower band gap, greater photocatalytic ability and surface superhydrophilicity. In effect they would be self-disinfecting (*via* photocatalysis) and anti-adhesive (due to surface superhydrophilicity) even under visible light because of the narrower band gap. Visible light-activated photocatalysts are likely to become the principal focus for semiconductor photocatalysis research because of the potential real world use and importance of these new materials. In the next chapter the new synthesis techniques for these TiO_2 and doped thin film materials developed in this work and their characterisation will be considered.

Chapter 2: Synthesis and Characterisation of TiO_2 and Composite TiO_2 Films Formed by Dip-Coating

2.1 Introduction

In Chapter 1 the basics of the synthetic methods for producing thin films of TiO_2 type materials reported in the literature were outlined. In this chapter the sol-gel synthesis routes and the deposition of the thin films made in this work will be described in more detail. In all of the syntheses, the principle is the same. This is the hydrolysis and subsequent polymerisation of the precursor material (a titanium alkoxide) into a matrix, which upon aging and dehydration, can be calcined into a crystalline powder, or deposited as a thin film. The technique for deposition of sol-gel thin films *via* dip coating will be discussed first, with the specific details for the sols for each material discussed separately in subsequent sections. Various characterisation methods were utilised for studying some film types. These techniques and any observations made by them relating to materials properties or composition will also be discussed in this chapter.

2.2 Experimental

2.2.1 Sol-Gel Film Deposition by Dip Coating

All thin films were deposited upon standard low iron microscope slides. For dip coating standard width (25 to 26 mm wide) glass microscope slides, the aged sols were transferred to a tall form narrow beaker of 50 cm^3 capacity. This ensured that almost all of the slide could be immersed in the sol. For larger samples such as double width (50 mm wide) microscope slides a larger beaker was required and the reagent amounts had to be doubled so that a sufficient amount of the substrate could be coated. Where substrate thickness allowed, a dip-coating apparatus was used to withdraw the substrate from the sol at a steady rate of 120 cm min^{-1} (see Figure 2.1 for

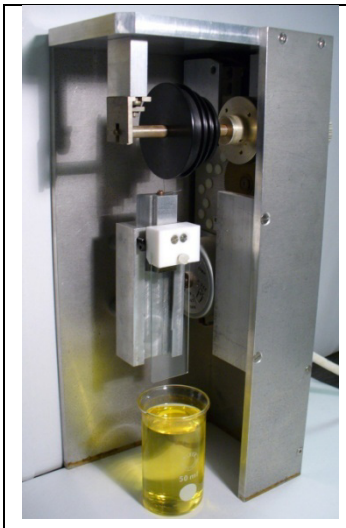

Figure 2.1 The dip-coater.

picture of dip-coating apparatus with Ag/TiO_2 sol in place). If more than one coat was required, the previous coat was allowed to dry before repeating the process. Previous research has shown that three to four coats was the optimum for photocatalytic activity.[115] As a result the maximum number of dip coats carried out was four coats. Films that had not been previously studied were made in a variety of thicknesses from one to four coats. The deposited xerogel films are not mechanically stable, and require calcination in order to properly adhere to the substrate and to become crystalline. Hence, all films were annealed in a furnace at 500 °C for one hour.

2.2.2 TiO_2 Sol Preparation

Reagents used: acetylacetone, butan-1-ol, titanium n-butoxide, distilled water, isopropanol, acetonitrile. Method adapted from Epifani et al.[122]

Acetylacetone (2.52 g, 0.025 mol) was dissolved in butan-1-ol (32 cm^3, 0.35 mol) forming a clear and colourless solution. To this solution titanium n-butoxide (17.016 g, 0.050 mol) was added. The solution became a pale straw yellow and remained clear and without precipitate. The solution was stirred vigorously for an hour, after which no changes could be observed. Distilled water (3.64 g, 0.20 mol) was dissolved in isopropanol (9.050 g, 0.15 mol) and added to the stirring titanium n-butoxide solution. The sol remained clear, but deepened in yellow colouration and was stirred for a further hour. Finally acetonitrile (1.66 g, 0.04 mol) was added to the solution, which was stirred for a final hour. The sol was allowed to age overnight before being used for dip-coating.

2.2.3 Ag_2O/TiO_2 Sol Preparation

Reagents used: acetylacetone, butan-1-ol, titanium n-butoxide, distilled water, isopropanol, acetonitrile, silver nitrate. Method adapted from Epifani et al.[122]

Titanium n-butoxide (17.016 g, 0.05 mol [viscous clear pale yellow liquid]) was chelated with a mixture of acetylacetone (2.503 g, 0.025 mol) in butan-1-ol (32 cm^3, 0.35 mol). A clear, straw yellow solution was produced, with no precipitation. The solution was covered and stirred for an hour. Distilled water (3.6 g, 0.2 mol) was

dissolved in propan-2-ol (9.015 g, 0.15 mol) and added to hydrolyse the titanium precursor. The solution remained a clear straw yellow colour, with no precipitate. The solution was stirred for a further hour. At this point the Ag doping level was chosen. Solutions were prepared with 5% Ag:Ti, 10% Ag:Ti and 20% Ag:Ti ratios. In each case silver nitrate was dissolved in acetonitrile and added to the pale yellow titanium solution, which was stirred for a final hour. After the final stirring, the resultant sol was a slightly deeper yellow in colour, but remained clear and without precipitate. Reagent amounts for each doping level are listed in Table 2.1. The resulting sol was left to age overnight, after which no changes in appearance occurred.

	Silver Nitrate	Acetonitrile
5% Ag Dopant	0.42 g, 0.0025 mol	0.82 g, 0.020 mol
10% Ag Dopant	0.85 g, 0.005 mol	1.64 g, 0.04 mol
20% Ag Dopant	1.70 g, 0.010 mol	3.28 g, 0.08 mol

Table 2.1 Table detailing the required quantities of both silver nitrate and acetonitrile required to achieve Ag to Ti ratios of 5, 10 and 20 % within the sol.

2.2.4 Preparation of Photo-deposited Ag on TiO_2

Materials used: silver nitrate, methanol, one-coat TiO_2 thin films as substrates (prepared as in section 2.2.2).

A solution of silver nitrate ($AgNO_3$) 5×10^{-3} mol/dm^3 was prepared in volumetric glassware, in methanol. This was then used as a second dip-coating solution, using the same dip coat apparatus, as described in section 2.2.1. The TiO_2 substrates were immersed in the $AgNO_3$ solution for a period of one minute, and then withdrawn from the solution by the dip-coater at a speed of 120 cm/min. The methanol evaporated from the slide very quickly and an imperceptible layer of $AgNO_3$ precursor was left behind. Glass blanks were treated in the same way, to act as controls. In both cases the appearance of the coated material was unchanged.

$AgNO_3$ coated TiO_2 and glass slides were then transferred to the 254 nm germicidal UV lamp and were illuminated for a period of 30 minutes. At the end of this illumination period, the samples were removed. At this point the treated TiO_2 films had become a pink colour, presumably due to photochemical deposition of silver on the titania surface and the treated glass blanks appearance was still unchanged. A second batch of $AgNO_3$ treated coatings was prepared, in exactly the same way as above and underwent a further annealing step at 500 °C for 1 hour after having been exposed to the 254 nm UV lamp for 30 minutes.

2.2.5 WO_3/TiO_2 Sol Preparation

Reagents used: acetylacetone, butan-1-ol, titanium n-butoxide, tungsten (V) ethoxide, distilled water, isopropanol, acetonitrile.

Titanium n-butoxide (17.016 g; 0.05 mol [viscous clear pale yellow liquid]) was chelated with a mixture of acetylacetone (2.50 g; 0.025 mol) in butan-1-ol (32 cm^3; 0.35 mol). To this solution tungsten (V) ethoxide (0.41 g; 0.001 mol) in acetylacetone (0.24 g; 0.002 mol) (amber-brown solution) was added. The solution was then covered with a watch glass and stirred for an hour. The appearance of the sol was unchanged by the addition of the tungsten precursor – it remained a pale straw yellow. Distilled water (3.60 g; 0.2 mol) was then dissolved in propan-2-ol (9.01 g; 0.15 mol) and added to hydrolyse the titanium precursor. Addition of the reagents in this step deepened the yellow colour of the sol. The darker yellow solution was then stirred for a further hour. Finally acetonitrile (1.64 g; 0.04 mol) was added and the solution stirred for another hour. The sol was then covered and left overnight to age, before being used to deposit coatings. After aging overnight the sol was unchanged in appearance.

2.3 Materials Characterisation Techniques

2.3.1 Appearance and Mechanical Properties

All samples produced in the study were initially examined and an assessment of their visual appearance and basic mechanical properties was made. Mechanical

property testing was not quantitative, since this could be an area of research in and of itself. Rather the tests carried out serve as indicators of comparative mechanical properties between materials under test. The following mechanical assessment tests[123-125] were carried out:

1. A wipe test using a gloved finger, - to see if any loose material was present on the surface of the coating
2. A Scotch® Tape test – this tests the adherence of the coating material to the substrate
3. A water dip test – to see if there is any loose surface material, and to see if it washes off easily
4. A scratch test, carried out with a sharp metal stylus and with a diamond tipped glass marker. This test examines the hardness/durability of the coating material.

2.3.2 Water Droplet Contact Angles

The water droplet contact angle is measure of the angle subtended from a tangent on the surface of the water droplet to the surface upon which it rests – this is marked θ_c in Figure 2.2.

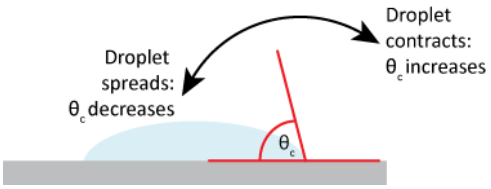

Figure 2.2 Schematic representation of the contact angle

A three dimensional representation of hydrophobic versus hydrophilic behaviour is given in Figure 2.3. If a surface is hydrophilic, the water droplet contact angle is low - the droplet spreads because the surface has an affinity for water. If the surface is hydrophobic, the water droplet contact angle is high – the droplet contracts because the surface doesn't have an affinity for water. As the photoinduced

hydrophilicity of a sample is observed, the droplet spreads, its diameter increases, and its contact angle decreases.

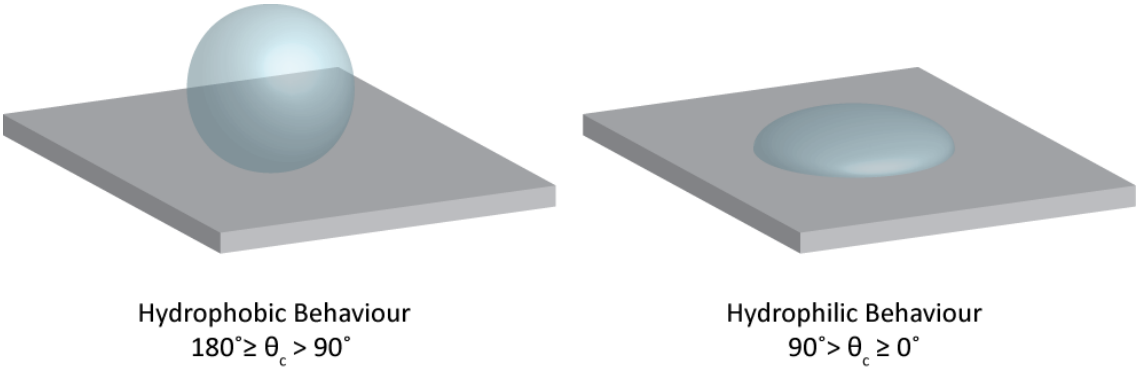

Figure 2.3 3D representation of hydrophobic and hydrophilic behaviour of a droplet of water

In order to assess the potential photoinduced superhydrophilicity of the candidate materials, the water droplet contact angles were measured. Fixed volumes of distilled water (typically 5 µl) were dropped onto the substrate surface from a graduated microsyringe, or from a micropipettor. The diameter of the droplet was then measured using a 20× measuring microscope (Peak Optics Model 2009 Shop Microscope) with graduated reticule in the eyepiece. Volume-diameter data was collected for the different samples before and after varying periods of UV 254 nm illumination. The volume-diameter data was then entered into a computer programme for the calculation of the contact angles. This is a quick and easy alternative to goniometer measurement and has been used successfully in other studies.[115, 126, 127]

2.3.3 Photocatalytic Activity

Photocatalytic activity was assessed by monitoring the photodegradation of a stearic acid overlayer by use of FTIR spectroscopy (Shimadzu 8400s and Perkin Elmer Spectrum RX 1). Prior to depositing a stearic acid layer, the films were firstly activated by 30 minutes exposure to UV radiation from a 254 nm germicidal lamp (Vilber Lourmat VL-208G – BDH/VWR Ltd). The IR spectrum of the stearic acid layer was then recorded over the range 3000 – 2700 cm^{-1} and the integrated area of the peaks between 2950 – 2875 and 2863 – 2830 cm^{-1} was calculated. The integrated area of these peaks is in effect a means of monitoring the concentration of stearic

acid. The stearic acid was applied by dip coating the samples in a 0.02 $moldm^{-3}$ solution of stearic acid in methanol.

2.3.4 UV-Visible and Optical Band Gap

UV-Visible spectra were recorded in the range 300 – 800 nm using a Thermo Helios alpha single beam instrument. Attention was paid to observing the anatase band edge. In addition to recording UV-visible spectra, an estimate of the optical band gap was made *via* extrapolation. This estimate is obtained by what is known as a Tauc plot.[128-130] This is the extrapolation of the linear portion on a plot of $(ahv)^{1/2}$ versus *hv*, where *a* is the absorbance coefficient of the film (a = -log T/T_0; T, sample optical transmission; T_0, substrate optical transmission) and hv the incident photon energy.

2.3.5 X-ray Diffraction (XRD)

Powder X-ray diffraction techniques can be used to analyse the composition of thin films because crystalline material diffracts X-rays in a material specific manner according to the Bragg condition, set out below.

$$n\lambda = 2d\sin\theta$$

Equation 2.1 Bragg's law of diffraction, where n is an integer, λ is the wavelength of incident X-rays, d is lattice spacing and θ the diffraction angle

Constructive interference between incident and diffracted X-rays only occurs over integer wavelengths and when the conditions set out in Equation 2.1 are met. Hence peaks in diffracted X-ray intensity are recorded only at diffraction angles which meet the Bragg condition. Different crystalline materials even if they share unit cell type, will have different lattice spacing, determined by atomic distances and so have distinct diffraction peaks. Unknown materials may therefore be indexed either by comparison against reference patterns of known compounds, or by calculating lattice parameters and unit cell sizes from the diffraction data. Hence, X-ray diffraction study of thin films is invaluable in determining their composition.

X-ray diffractograms were obtained for thin films using a Bruker AXS D8 Discover instrument equipped with a General Area Detection Diffraction System (GADDS) using glancing angles and a 0.5 mm collimator. The TiO_2 coating was examined with an angle of incidence of 5° over an angular range of 10-66° for a 15 minute period. The Ag/TiO_2 coating was examined with an angle of incidence of 1.5° over an angular range of 10-62.5° for a 30 minute period. Powders of a number of the materials were also examined in a conventional manner. The powders were obtained by drying the sol to a bulk xerogel. This was then lightly ground to a powder, which was fired under the same conditions as used for firing the films. The obtained diffraction patterns were compared against a database of diffraction patterns in order to identify where possible the crystalline compounds present in the coatings. An estimate for mean crystallite sizes was performed using the Scherrer equation.

2.3.6 Scanning Electron Microscopy (SEM)

The TiO_2 samples and Ag/TiO_2 thin films produced by the synthesis described in section 2.2.3 were examined by scanning electron microscopy (SEM), including both EDAX (energy dispersive analysis of X-rays) and WDX (wavelength dispersive analysis of X-rays) techniques. For imaging, samples were gold coated. For analysis, samples were carbon coated. SEM was also used to examine samples with microbes attached. The study with microbes is discussed in more detail in Chapter 4 and provides some context between the surface morphologies of some coatings and the way in which microbes respond to them.

2.3.7 X-ray Photoelectron Spectroscopy (XPS)

X-ray Photoelectron spectroscopy (XPS) is a surface spectroscopic technique allowing quantification of elements present in a thin film, along with identification of their oxidation state. XPS data is obtained by X-ray irradiation of a sample under high vacuum and collection of electrons ejected from the surface. Both the kinetic energy and number of ejected electrons is recorded. This information is used to determine a binding energy using Equation 2.2.

$$KE = hv - BE$$

Equation 2.2 The fundamental XPS equation, where KE is the kinetic energy of an ejected electron, hv is the incident x-ray photon energy and BE is the binding energy

A typical XPS experiment plots the number of electrons detected, versus the binding energy, as calculated from Equation 2.2. This produces an output which is characteristic of the electronic configuration of the element from which the ejected electron originated, with peaks in the number of detected electrons located at element specific binding energies. Hence XPS can be used to identify elements present in a thin film, and their oxidation state.

The samples produced by the synthesis outlined in section 2.2.3 were examined by XPS in collaboration with Robert Palgrave from the Department of Chemistry, UCL (now of Department of Chemistry, University of Oxford). XPS measurements were carried out on a VG ESCALAB 220i XL instrument using focussed (300 mm spot) monochromatic Al-Kα X-ray radiation at a pass energy of 20 eV. Scans were acquired with steps of 50 meV. A flood gun was used to control charging and the binding energies were referenced to surface elemental carbon at 284.6 eV. Depth profile analysis was undertaken using argon sputtering.

2.3.8 X-ray Absorption Near Edge Structure (XANES)

The samples produced by the synthesis outlined in section 2.2.3 were submitted to an X-ray Absorption Near Edge Structure (XANES) analysis in collaboration with Shelley Savin from the University of Kent. This was carried out in order to elucidate the form of Ag present within the films. The intention of the study was to utilise the XANES region of the EXAFS spectra as a "fingerprint". By comparing the XANES oscillations of various standards with those collected for the sample films it is possible to determine which form of Ag is present within the films. XANES measurement involves illumination of the sample with synchrotronic light in the X-ray region. The incident X-rays are absorbed by the atoms of the sample, resulting in the ejection of a core photoelectron. The principle is very similar to that of XPS (discussed in the previous section). The ejected photoelectron is emitted radially and interacts with local atoms. This interaction, which is dependent upon the local

environment and oxidation states, results in constructive and destructive interference patterns. These are manifested in the experimental output as the post edge oscillations in the spectra. Hence XANES can be successfully used as a fingerprint technique, and is especially suited to dilute samples, due to the brilliance of the synchrotronic light source.

Extended X-ray Absorption Fine Structure (EXAFS) spectra were collected on Station 9.3 at the Daresbury Synchrotron. The synchrotron electron energy at Daresbury is 2 GeV. The average ring current during measurements was 150 mA. Due to the small amount of Ag present within the films, analysis of one sample film by both transmission and fluorescence modes was fruitless – no Ag edge was detectable. To overcome this problem a number of sample films were sandwiched together in the beam, such that effectively 20 layers of sample were being examined, rather than two. Silver K-edge EXAFS spectra were recorded for these films in fluorescence mode – multiple scans were performed overnight to improve signal-noise ratio in the output. These were compared to standard powders of the silver oxides AgO and Ag_2O along with a reference of silver metal foil. The standards were measured in transmission mode, with the sample presented in a pellet of polyvinylpyrrolidine (PVP) diluent. The PVP was mixed with the standard powders and pressed into a pellet using a 13 mm pellet press (as used to prepare KBr discs for infrared spectroscopy). The amount of sample in the pellet was adjusted such that an absorption of $\mu d = 1$ was measured (μ is the absorption coefficient and d is the sample thickness). Spectra were collected out to $k = 16$ $Å^{-1}$(k is the wave vector associated with the photoelectron). Data collected from these measurements was processed using the Daresbury EXAFS programmes, EXCALIB and EXBACK.[131, 132]

2.4 Results and Discussion

2.4.1 Syntheses of TiO_2 and Doped TiO_2 Films

All materials were prepared by a sol gel technique, the syntheses for which are described in sections 2.2.2 to 2.2.5. In all cases the sol was prepared in advance, along with the substrates, which were cleaned thoroughly before use. Deposition

of the thin films was carried out by sol-gel dip coating, as described in section 2.2.1. During the annealing stage at 500 °C the furnace was open to the atmosphere. This is not a matter of concern, since the materials being made are all oxides in nature. The elevated temperature is also sufficient to burn off residual organics from the sol which were used to stabilise the nanoparticles. Indeed, if one periodically examines the samples after different annealing periods, they go through a phase where they appear blackened, as the organic materials are burnt off.

One of the most important materials to be produced for this study, were the undoped TiO_2 films, as these serve as a control for all of the doped materials later prepared. The TiO_2 control films were used in all of the characterisation, functional testing and antimicrobial testing phases as the "baseline" performance indicators for all other materials. The documented synthesis using titanium n-butoxide as the titanium source was the second route to be tried. Initially a similar approach, using titanium isopropoxide as the titanium source was employed, but more adherent films were obtained when the butoxide route was used instead.

The synthetic method for preparation of Ag_2O/TiO_2 thin films is very similar to that for the TiO_2 controls and is a modification of the procedure used by Epifani et al. [122] The principal modifications to the methodology being that the procedure was carried out in air and was modified for the inclusion of different Ag dopant amounts, as described in the experimental section. This synthetic route forms nanoparticulate Ag_2O *in situ*.

The preparation of the photo-deposited Ag on TiO_2 materials followed a very different synthetic method and were prepared in a two or three-step process, unlike the other TiO_2 based materials, which are made in a one-step process. The first step was the preparation of a standard TiO_2 thin film base-layer, as described in section 2.2.2. The second and third steps relate to the further functionalisation of the surface by application of $AgNO_3$ overlayer, UV irradiation and for some samples a further anneal. A one coat TiO_2 film was prepared in all cases as the base layer in this system. It is important to note that the first step was completed in its entirety before further functionalisation. That is to say that a fully annealed and cooled

sample was used as the base layer. Following the photo-deposition, some samples were annealed a second time. This was intended to attempt to fix any Ag within the TiO_2 matrix by diffusion of Ag into the matrix (Ag is mobile in the high temperature environment).

2.4.2 Appearance and Mechanical Properties

With the exception of the photodeposited Ag samples (which are covered separately below), all of the sol gel films were of very similar, indistinguishable appearance. All films were transparent and demonstrated a multicoloured appearance. This is a result of refringence effects due to the variable thickness of the coating. This can be seen in Figure 2.4, which shows a representative selection of Ag_2O/TiO_2 films.

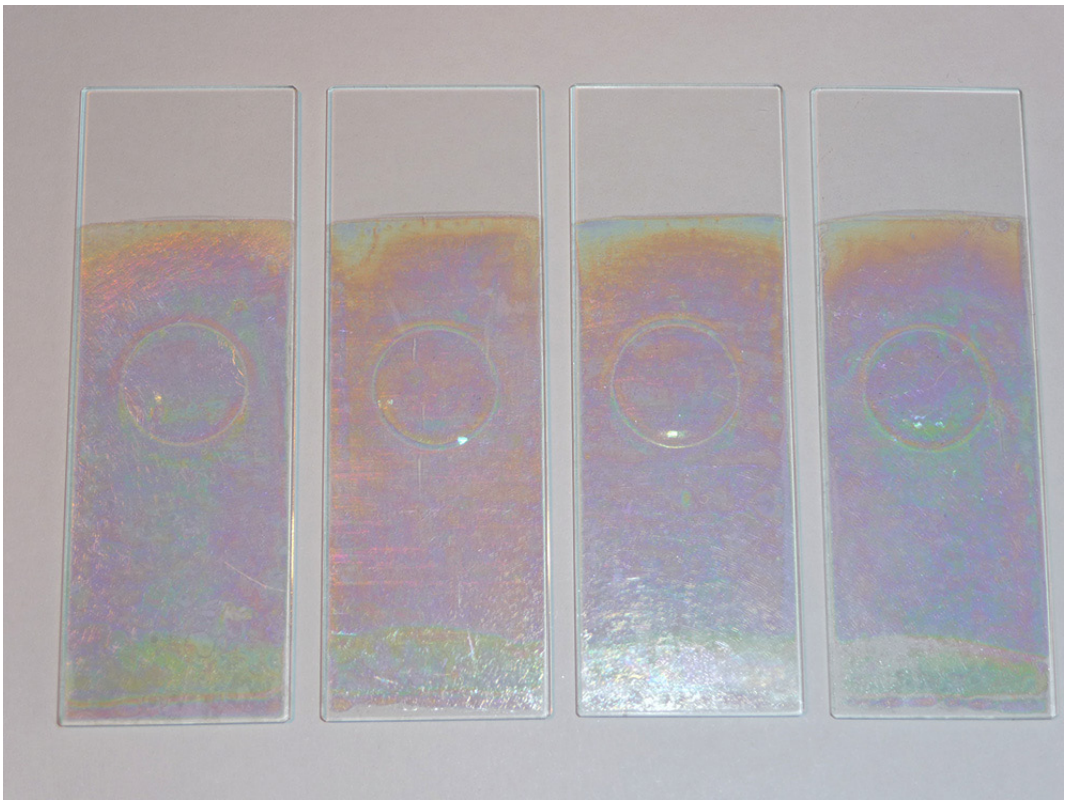

Figure 2.4 Photograph of some Ag_2O/TiO_2 films – note the multicoloured nature of the films due to refringence effects

Note in the figure the cavities on the substrate – this is where subsequent tests with microbial inocula were carried out (see Chapter 3 for details). The films were all typically rugged and survived all of the aforementioned mechanical tests.

Regardless of the coating type it was not possible to remove the coatings by rubbing with a gloved finger, by using Scotch tape, or by dipping the samples in water. The coatings were not damaged by a metal stylus, but could be scratched and removed using a diamond tipped glass marker.

The photodeposited Ag samples had changed in appearance most markedly in comparison to untreated TiO_2 films, whereas the Ag treated glass controls maintained the original appearance of the glass. The $AgNO_3$ on TiO_2 films had a pinkish to brown appearance in the area covered by the $AgNO_3$ precursor, but remained unchanged in any area not coated. The pink overlayer could not be rubbed from the surface by a gloved finger or removed by the Scotch® Tape test. It could however be damaged by a sufficiently sharp implement, such as a stylus or scalpel blade. The samples which had undergone a further annealing step lost the pink hue. The $AgNO_3$ on glass controls remained unchanged in their appearance despite a second anneal and continued to look similar to the samples in Figure 2.4.

A swab soaked in saline when applied to the pink overlayer surface turned slightly black, but there was no noticeable removal of any coating form the surface. This may presumably suggest removal of Ag from the surface onto the swab. However, the quantities were too small to easily analyse. It is probable that the loss of the pink colouration upon annealing is due to the loss of Ag from the surface, or perhaps its transformation to the oxide – a result of the combination of high temperature and availability of atmospheric oxygen in the furnace.

It is postulated that the photocatalytic processes occurring on the TiO_2 surface are providing electrons for the reduction of the Ag^+ to Ag metal, which is deposited as a nanoparticulate layer. The holes presumably participate in oxidative processes, perhaps involving the nitrate ion. The postulated formation of Ag by this method is described in Scheme 2.1.

$$\underset{\text{Substrate}}{TiO_2} + h\nu \rightarrow e^- + h^+$$

$$e^- + \underset{\text{Overlayer on } TiO_2}{AgNO_3} \rightarrow Ag_{metal} + NO_3^-$$

Scheme 2.1 Photo-deposition of Ag metal on a TiO_2 film *via* photocatalytic reduction.

Such a coating may offer a bi-functional approach to antimicrobial coating technology – in that it is a light activated antimicrobial material, which can also maintain an amount of antimicrobial activity in the absence of light *via* release of microbicidal Ag. There is a potential synergy between the photocatalyst and the Ag overlayer, in that it can maintain the presence of Ag on the surface by continually keeping the Ag in a reduced form. This could be one of the more interesting candidate antimicrobial compounds and will be examined in Chapter 3.

2.4.3 Water Droplet Contact Angles

One of the most interesting features of the photocatalytic materials is that they often demonstrate an effect known as photoinduced superhydrophilicity (PSH). This effect is the observation of an increase in the hydrophilicity of the photocatalyst surface upon illumination by ultraviolet light. A superhydrophilic surface such as this may have certain advantages for antimicrobial/antifouling applications.

There are two proposed explanations given in the literature for the mechanism underlying the PSH effect, and it currently remains an area of debate.[133, 134] The first explanation is that oxidative destruction of hydrophobic organic surface contaminants *via* photocatalytic oxidation (PCO) processes (as described in Section 1.4.6.2.4) yields an increase in surface hydrophilicity. The second is that the hydrophilicity results from water dissociatively adsorbed at the surface due to a photoinduced surface reorganisation (PISR) of the photocatalyst surface. The two mechanisms will be discussed below.

2.4.3.1 PSH by Photocatalytic Oxidation of Contaminants (PCO Mechanism)

The initially proposed mechanism[133, 135] for the PSH effect is also the most simple. The photocatalytic processes, as discussed in Chapter 1 produce electron/hole pairs, which move to the surface of the TiO_2 photocatalyst. These electron/hole pairs participate in redox reactions with adsorbates at the surface and produce reactive oxygen species and radicals, which oxidatively destroy organic contaminants at the surface. Organic contaminants are intrinsically hydrophobic in

nature because of the inability of water to hydrogen bond to them. Hence the removal of the hydrophobic organic contaminants will lead to a reduction in the hydrophobic character of the sample – i.e. it becomes hydrophilic, seemingly due to the UV irradiation of the sample.

2.4.3.2 PSH by Dissociative Adsorption of Water (PISR Mechanism)

The second explanation proposed by Wang *et al*.[136] for the PSH mechanism is more complicated. Like the PCO mechanism, the PISR process is said to begin with the migration of electron/hole pairs to the surface of the photocatalyst.[136-138] At this point the electrons reduce Ti^{4+} centres to Ti^{3+}, and the holes accumulate at bridging oxygen sites in the lattice, as shown in Scheme 2.2.

$$e^- + Ti^{4+} \longrightarrow Ti^{3+}$$
$$4h^+ + 2O_2^{2-} \longrightarrow O_2 \uparrow$$

Scheme 2.2 Action of electron/hole pairs at Ti and O centres[137]

With the loss of O_2 from the lattice and the reduction of the Ti^{4+} sites, oxygen vacancies are left at the lattice surface. These vacancies are filled by water, which dissociatively adsorbs. This results in a hydroxylated surface to which water may hydrogen bond, and hence creates a hydrophilic surface environment. This mechanism is summarised in Scheme 2.3, which is adapted from Fujishima.[137]

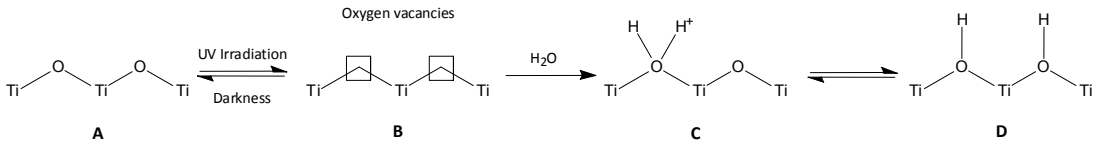

Scheme 2.3 Mechanism for PSH *via* dissociative adsorption of water

Whilst the second theory appears to be the more mechanistically rigorous, there is in fact much evidence in support of both mechanisms. Some studies, such as that of Takeuchi *et al*.[134] were unable to definitively side either way, and concluded that both processes occurred and the mechanism for PSH was synergistic. However, more recent works have found increasing support for the more simplistic PCO model. In a recent study[133] it was shown that both glass and titania surfaces could be rendered superhydrophilic *via* a number of techniques, including UVC/ozone,

aqua regia and heating above 500 °C. It was also shown that pristinely clean and hydrophilic samples of glass and titania became hydrophobic when left on a laboratory bench. Glass has no intrinsic photoactivity hence; the generation of oxygen vacancies and the PISR model have no applicability. The observation of superhydrophilicity must therefore be due to the removal of organic contaminants from the surface by the harsh treatments used. This therefore gives credibility to the PCO model for PSH in titania samples. What is clear is that a definitive answer has yet to be given, because both theories have convincing supporting evidence. Regardless of the mechanism by which it occurs, photoactivated titania surfaces demonstrate this useful self cleaning property of PSH and hence materials made in this study were tested for the effect.

The most popular way to measure the contact angle of a droplet is with a CCD imaging camera and goniometer; however this technique was not available. Instead the contact angle was calculated from drop volume and diameter parameters.

	UV 254 nm Irradiation Time		
	0 Hours	**0.5 Hours**	**1.0 Hours**
Microscope Slide	23	Not measured	28
Float Glass	57	Not measured	62
TiO_2	10	4	2
5% Ag/TiO_2	15	1	0
10% Ag/TiO_2	4	0	0
20% Ag/TiO_2	5	1	1
2% WO_3/TiO_2	3	1	1

Table 2.2 Water droplet contact angle data for a selection of thin films against control materials for different UV irradiation times

Water droplet contact angle data demonstrates that the photocatalyst materials all exhibit photoinduced superhydrophilicity. The glass control surfaces, the microscope slide and the float glass, do not demonstrate any reduction in contact angle upon UV irradiation. The small increases in contact angle most likely arising from experimental error – since an increase in contact angle for these materials has

no physical or chemical basis (aside from contamination of the surface with organic material – which is believed not to have occurred). The photocatalyst materials had "as made" contact angles of between 15 and 3 degrees, however, upon UV irradiation, the contact angles reduced markedly. In particular, the TiO_2 and films from a 5%Ag/TiO_2 sol reduced from 10 and 15 degrees respectively to 4 and 1 degrees. Whilst there is clearly some variability amongst the materials (possibly due to the limitations of the measuring technique) it is clear to see that PSH was demonstrated and that all materials achieved similar levels of PSH. The exception to this is the TiO_2 control, which did not reach the same level of hydrophilicity as the modified materials. In terms of PSH there is really nothing between the materials under test, and for antimicrobial/self cleaning applications, all would be appear to be appropriate. All of the contact angles are appreciably low, which may be due to the samples being particularly clean before testing. The photocatalytic activity and antimicrobial efficacy will be a more important indicator for their potential.

2.4.4 Photocatalysis

One of the most widely used methods for the observation of photocatalysis is to measure the destruction of an organic "contaminant" overlayer by the photocatalytic process. It is common to use an overlayer of stearic acid as this overlayer. The presence of the overlayer is monitored *via* the FT-IR absorbance of the CH stretch peaks of the stearic acid, between 2750 and 3000 cm^{-1}. As the stearic acid is destroyed by the photocatalyst, the magnitude of the CH stretching peaks diminishes. Figure 2.5, Figure 2.6 and Figure 2.7 show the FT-IR output in the CH stretch region for a TiO_2 control film, a film deposited from a 10%Ag/Ti sol (produced from the synthesis in Section 2.2.3) and a film deposited from a 2%W doped TiO_2 sol respectively.

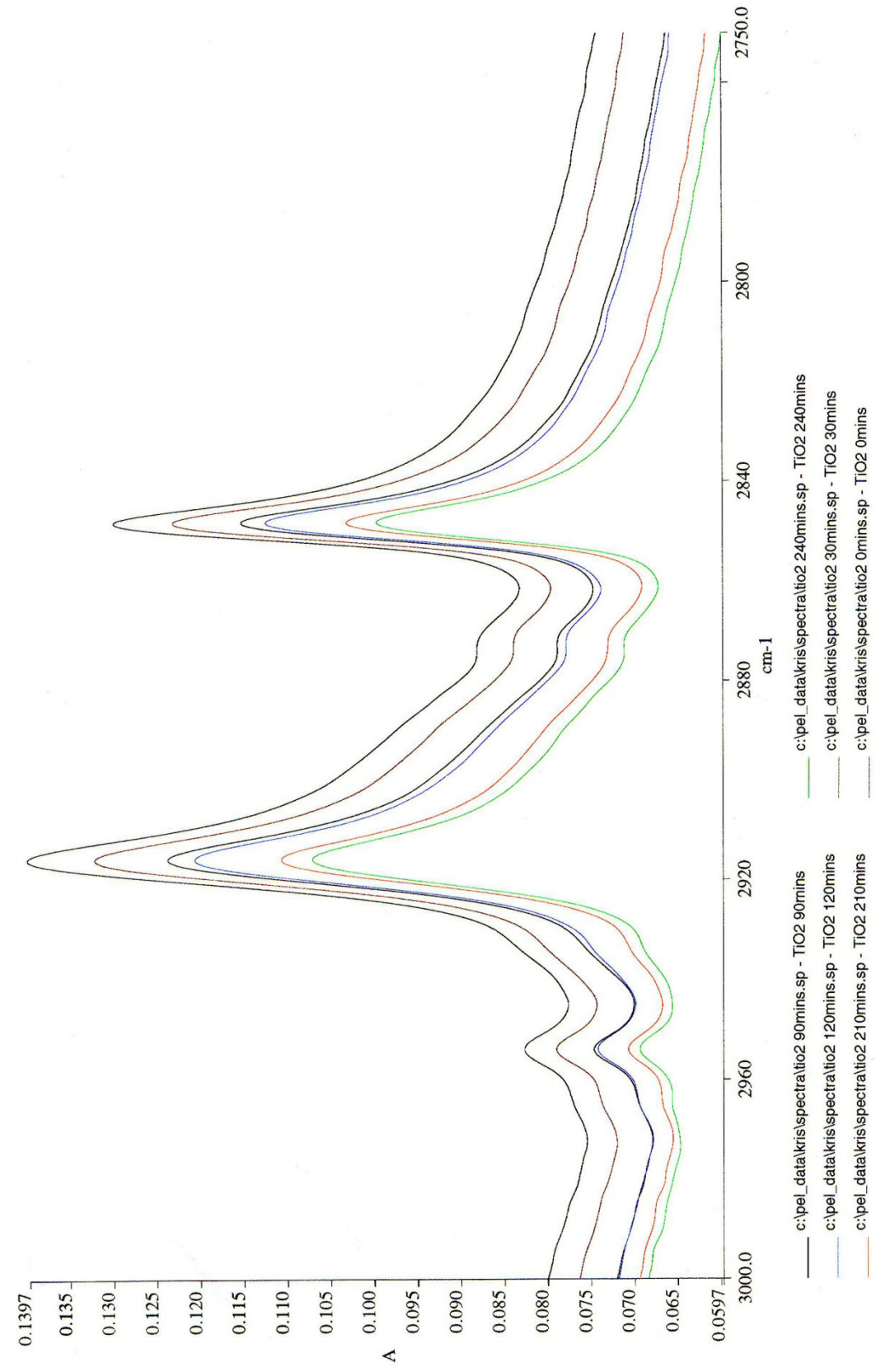

Figure 2.5 FT-IR spectrum for the CH stretch region of stearic acid overlayer on TiO_2 substrate after various periods of UV 254 nm irradiation. (Note: traces automatically offset in software)

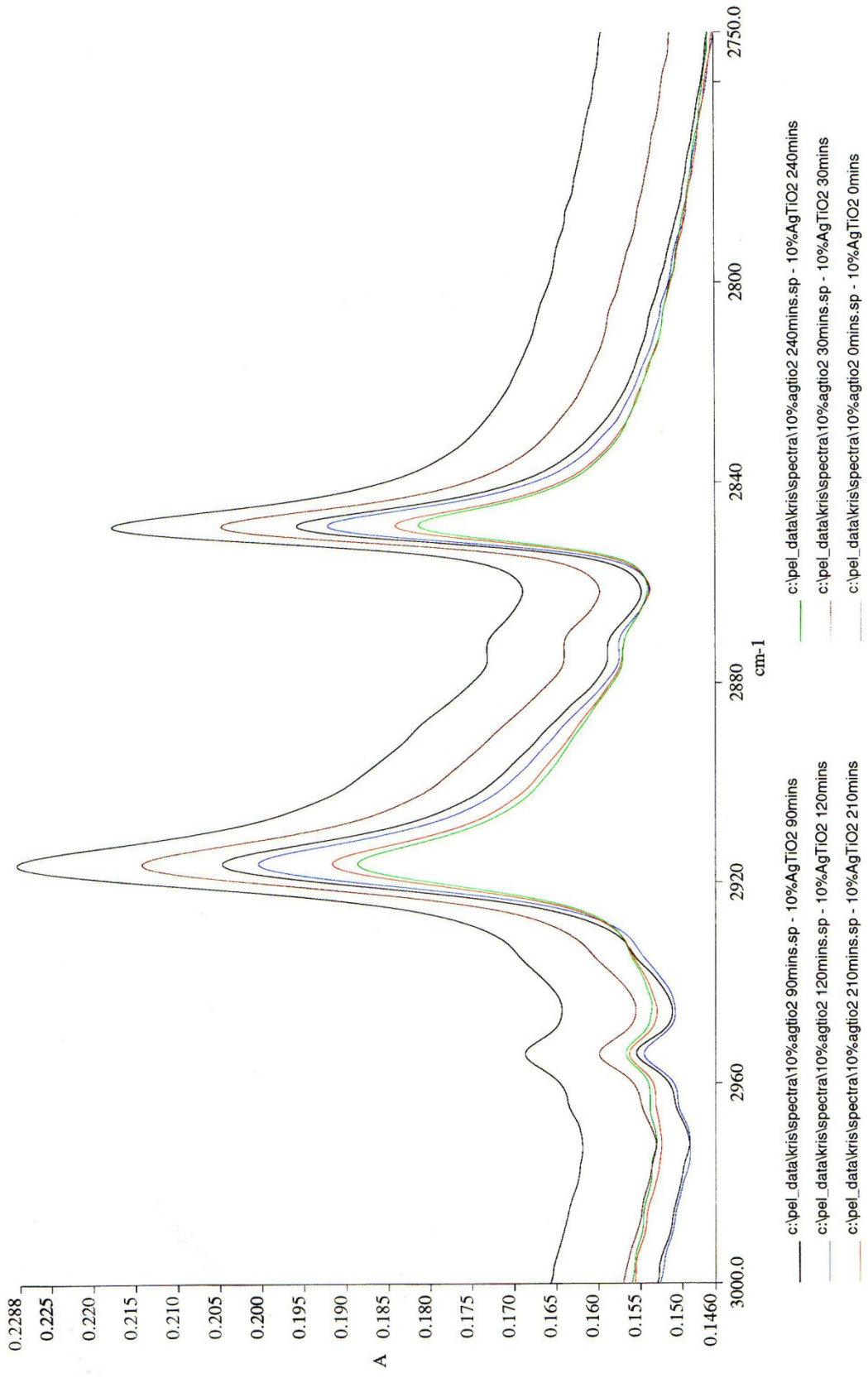

Figure 2.6 FT-IR spectrum for the CH stretch region of stearic acid overlayer on film deposited from 10%Ag/Ti sol, after various periods of UV 254 nm irradiation. (Note: traces automatically offset in software)

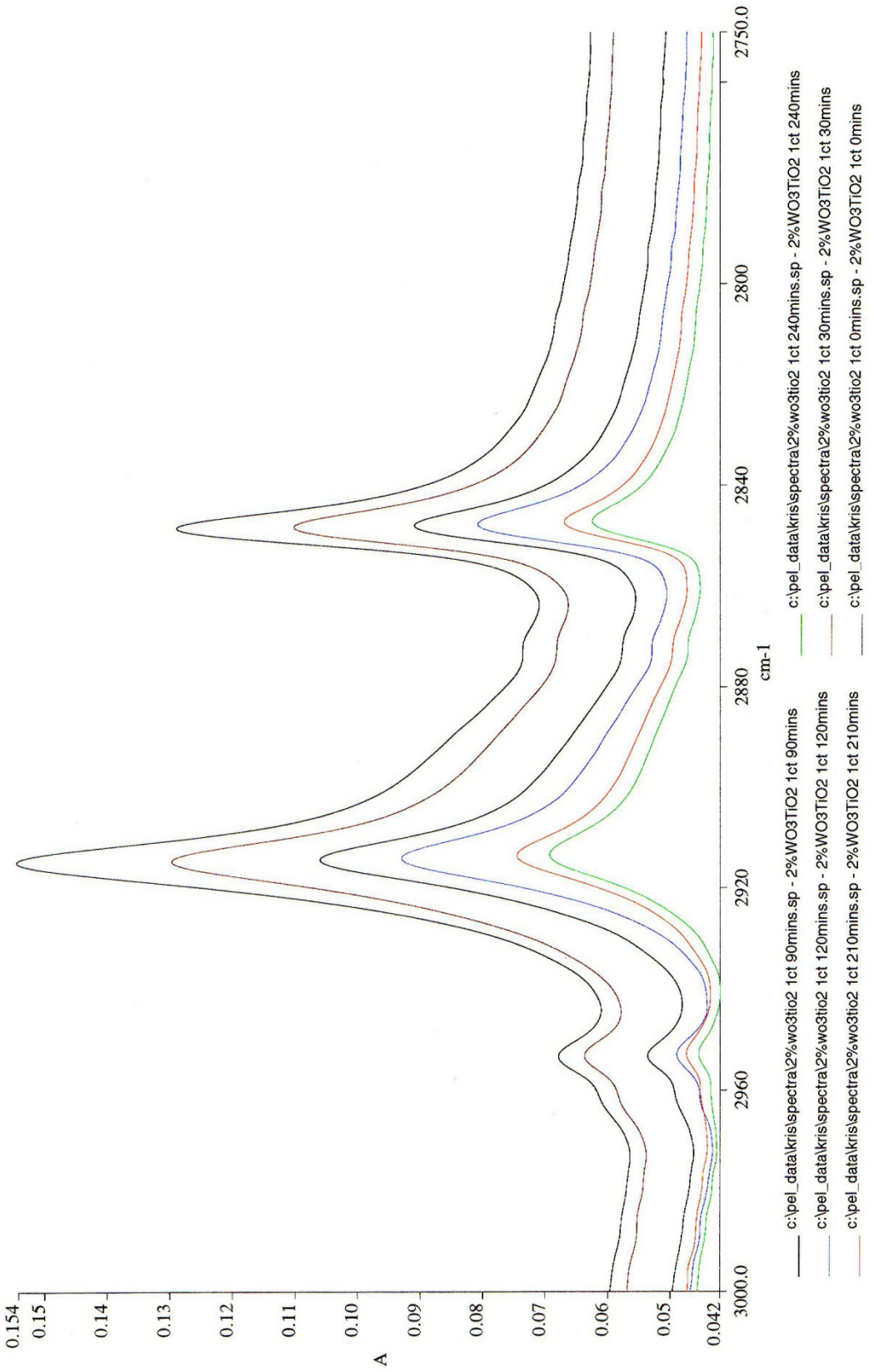

Figure 2.7 FT-IR spectrum for the CH stretch region of stearic acid overlayer on film deposited from 2%WO_3/TiO_2 sol, after various periods of UV 254 nm irradiation. (Note: traces automatically offset in software)

In all of the previous FT-IR spectra, it can be clearly seen that the magnitude of the CH stretching peaks is diminished with exposure to the photocatalyst over an irradiation period of 240 minutes. The absorbance diminishes towards the baseline of the spectrum in all cases. In order to bring some quantitative basis to the measurements it is possible to calculate the integrated area under the peaks, relative to the baseline. This gives an indication of the amount of stearic acid present in the overlayer and allows further calculations, such as rates of destruction to be made.

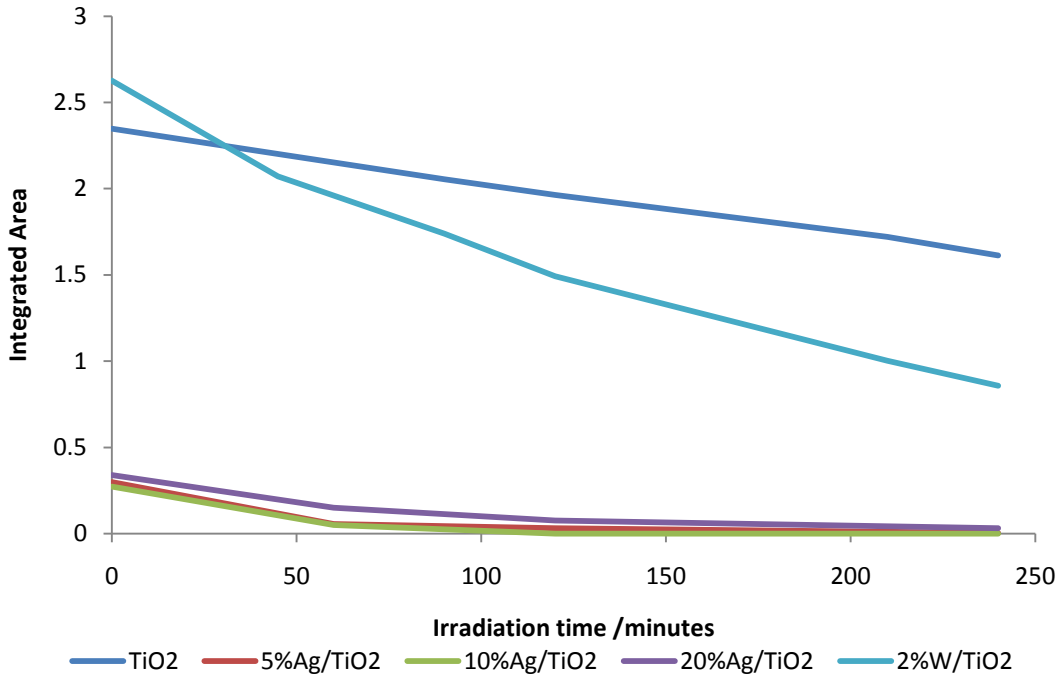

Figure 2.8 Comparison of stearic acid integrated peak area against UV 254 nm irradiation time.

By measuring the initial gradient of the traces in Figure 2.8 one can determine a value for the initial rate of destruction of stearic acid (R_i), in terms of integrated peak area units per unit time. It has been stated that the number of stearic acid molecules per cm^2 per unit of integrated area is 9.7×10^{15} molecules.[139] Using this conversion value, it is possible to calculate a meaningful initial rate of stearic acid destruction in terms of molecules per square cm per minute. The values obtained from this conversion are given Table 2.3.

Sample	Line gradient (×10^{-3} units integrated area)	Initial Rate (R_i) (×10^{12} molecules cm^{-2} min^{-1})
TiO_2	3.23	31.30
5%Ag/TiO_2	4.04	39.22
10%Ag/TiO_2	3.71	35.99
20%Ag/TiO_2	3.16	30.67
2%W/TiO_2	12.30	119.31

Table 2.3 Rates of photocatalysis for some candidate thin film samples

The values given in Table 2.3 are calculated from the data plotted in Figure 2.8. This data represents the best performing samples for each film type tested. The results for the doped films are of the same order of magnitude as those in the literature. A typical sol gel TiO_2 film of thickness around 40 nm might have an R_i value of approximately 73×10^{12} molecules cm^{-2} min^{-1} [140]. This literature value is greater than the majority of films produced here, which have an R_i of between approx 31×10^{12} molecules cm^{-2} min^{-1} and 39×10^{12} molecules cm^{-2} min^{-1}. There could be a number of reasons for this difference, including film thickness, relative crystallinity, and the anatase/rutile ratio of the samples under test, though there is likely no one single explanation for the lower R_i values for the films produced in this study. The W doped sample performed better than the other doped samples, but was still little better than the literature reports, having an R_i of approximately 119×10^{12} molecules cm^{-2} min^{-1}.

There is very little in the way of distinction both between the samples produced in this study, and between the samples and those in the literature, in terms of their photocatalytic activities. Hence all may be suitable candidates for photocatalytic antimicrobial surface materials. The photoactivity of the film deposited from a 10% Ag/Ti sol, coupled with having the most significant level of PSH (described in Section 2.3.2), makes the Ag_2O/TiO_2 material one of the more interesting candidates for a self cleaning, antimicrobial surface coating – which will be examined fully in Chapter 3 and Chapter 4.

2.4.5 Assessment of Hydroxyl Radical Production

As has been discussed in Chapter 1, the photocatalytic process is known to produce hydroxyl radicals, which are believed to be the active species for the destruction of organic contaminants and microbes. It was decided to attempt to design an experiment to assess the production of these radicals *via* a fluorescent chemical probe. In the literature a methodology using disodium terephthalate has been used successfully.[141-147] The technique relies upon the hydroxylation of the terephthalate ion. There is only one product isomer, 2-hydroxyterephthalate, which has a distinct fluorescence at 425 nm when irradiated by 315 nm light. This is summarised in Scheme 2.4.

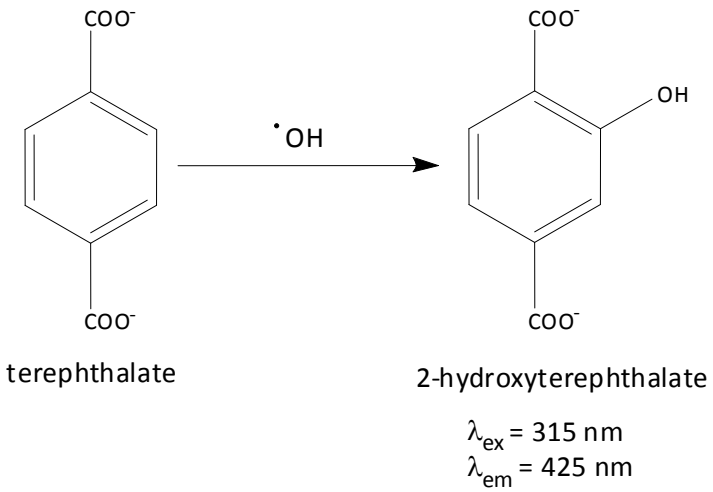

Scheme 2.4 Terephthalate assay for hydroxyl radicals

A 5×10^{-4} M solution of disodium terephthalate, prepared using 2×10^{-3} M $NaOH_{(aq)}$ solvent was used as the probe solution. P25 5mg in 10ml probe solution, along with TiO_2 and control films were irradiated for a period of 2hr 40 minutes by 254 nm germicidal lamp.

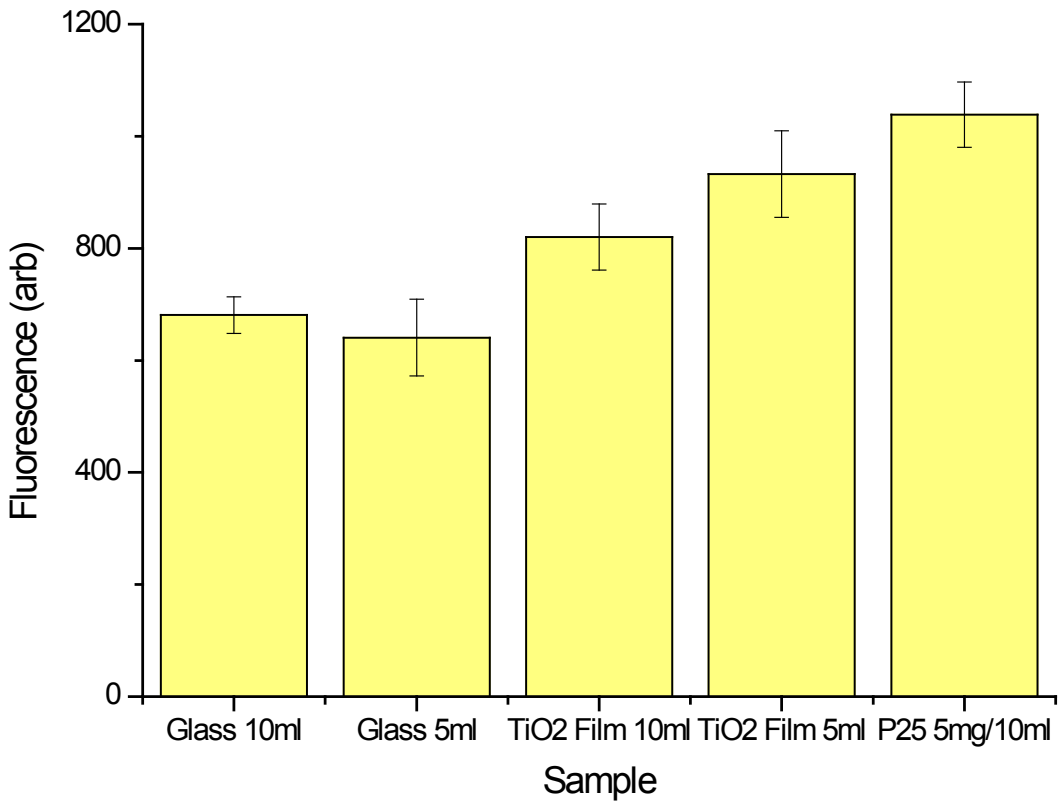

Figure 2.9 Hydroxyl radical production monitored by 2-hydroxyterephthalate fluorescence

Further experiments were attempted to refine the results but in the limited time available, no improvement could be made upon the data obtained above. The data does indeed suggest the production of hydroxyl radicals by both a TiO_2 thin film, and by the P25 powder. Detection of the hydroxylated product in greater quantity than for a glass control shows that photocatalytic production of hydroxyl radicals is occurring. However, this is far from conclusive evidence, and further tests will be required in future studies, either by refinement of this methodology, or by utilisation of a different technique, such as EPR – as used in other studies within the research group.[148]

2.4.6 UV Visible Spectroscopy and Optical Band Gaps

Since all materials synthesised ideally contain anatase TiO_2 the band edge in the 380 nm region – which is indicative of the O^{2-} to Ti^{4+} transition in anatase TiO_2 [115] is a key feature to be present within the UV-visible spectra. Also, a Tauc extrapolation to determine the optical band gap was performed. The literature band gap energy for anatase TiO_2 is 3.2 eV (wavelength equivalent to 387 nm), the band gap for

rutile is 3.0 eV [110]. For coatings containing anatase TiO_2, one expects the band gap to be in the region of 3.2 eV, though the addition of dopants could alter this, perhaps narrowing the gap. UV-visible and Tauc extrapolations are given in the following sections below.

2.4.6.1 TiO_2 Thin Film

Figure 2.10 and Figure 2.11 show the UV-visible and Tauc extrapolations respectively, for a candidate TiO_2 thin film.

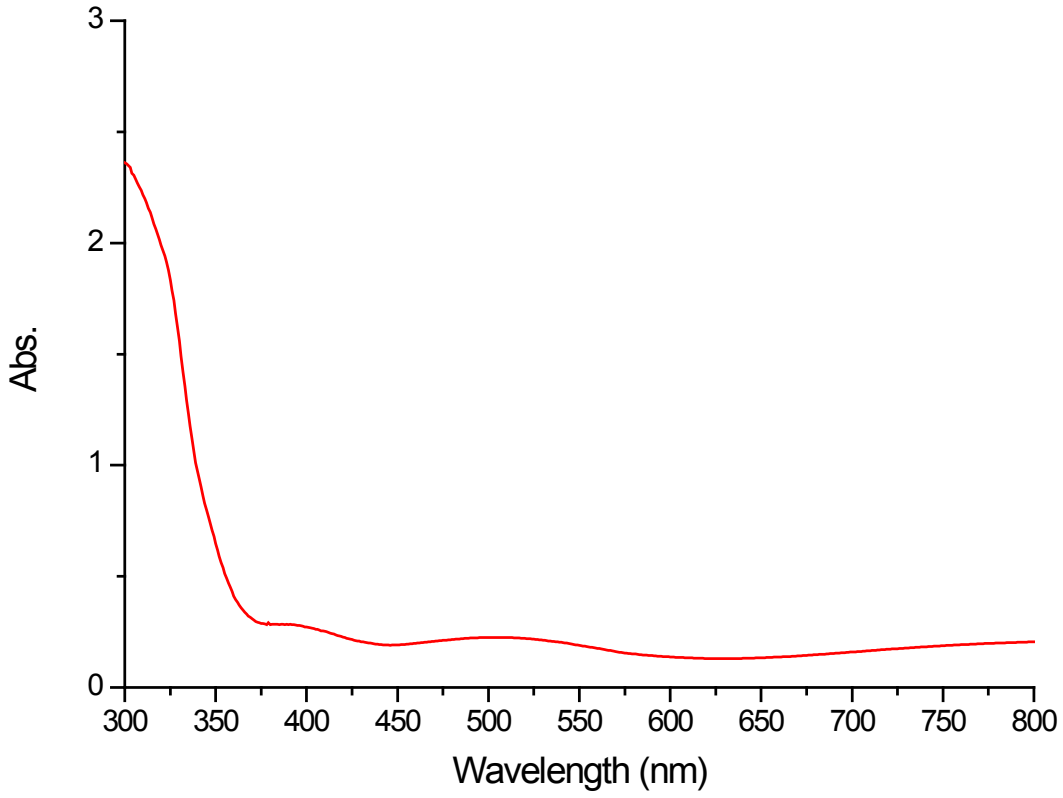

Figure 2.10 UV-Visible absorption spectrum of TiO_2 thin film

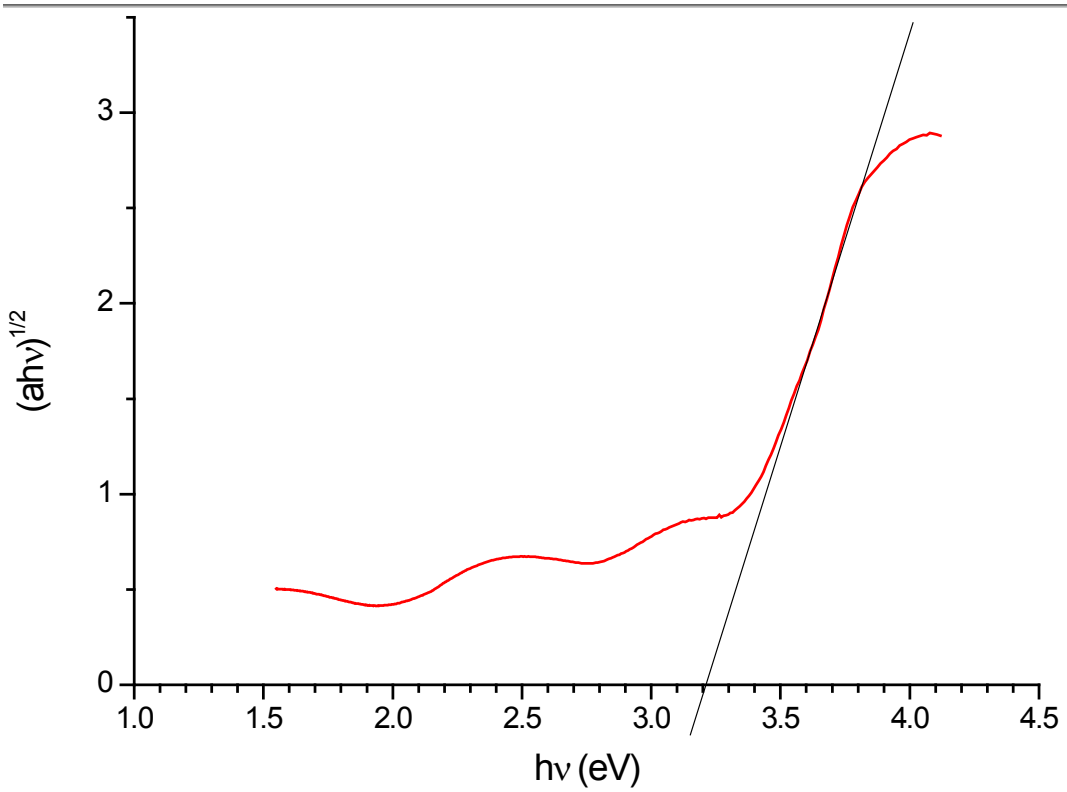

Figure 2.11 Tauc extrapolation for TiO_2 thin film

The characteristic anatase band edge in the 380 nm region is clearly present in the UV-visible spectrum. The Tauc extrapolation gives an optical band gap in the region of 3.2 eV – this is to be expected for anatase TiO_2.

2.4.6.2 5% Ag/TiO_2

Figure 2.12 and Figure 2.13 show the UV-visible and Tauc extrapolations respectively, for a candidate thin film produced from the synthesis outlined in Section 2.2.3 with an Ag dopant level in the starting sol of 5%.

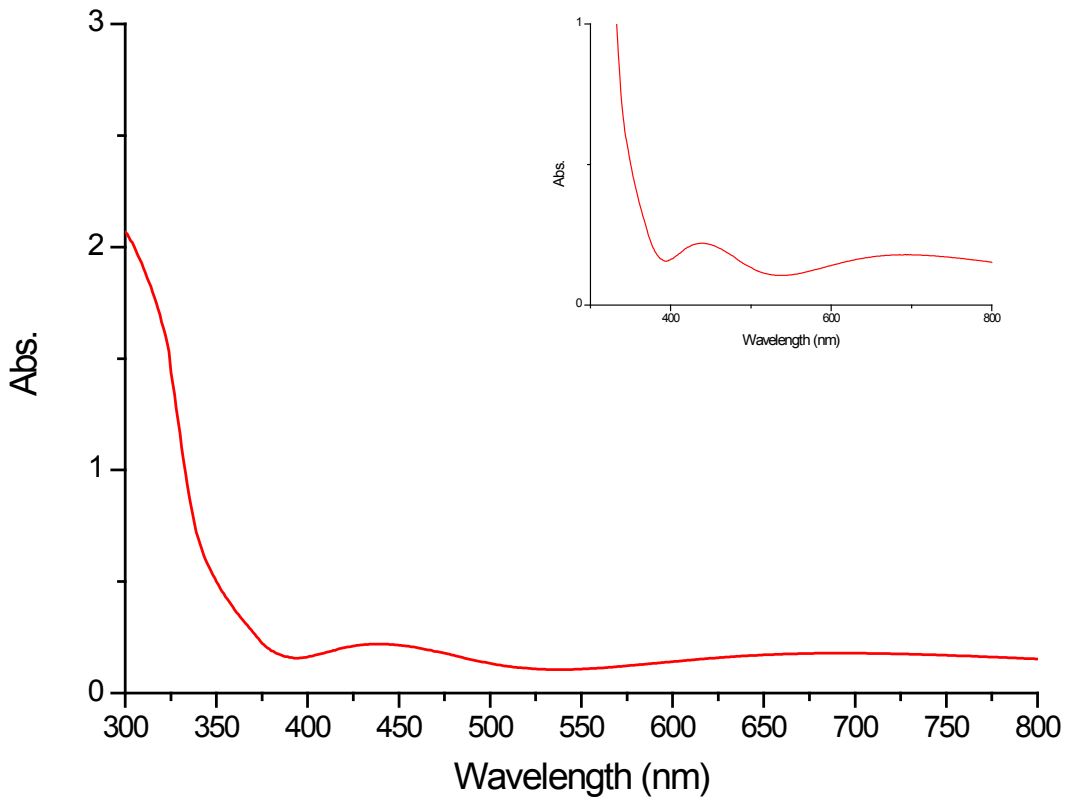

Figure 2.12 UV-Visible absorption spectrum for thin film deposited from 5%Ag:TiO_2 sol. Inset graph is rescaled to highlight absorbance peak at approx 440 nm.

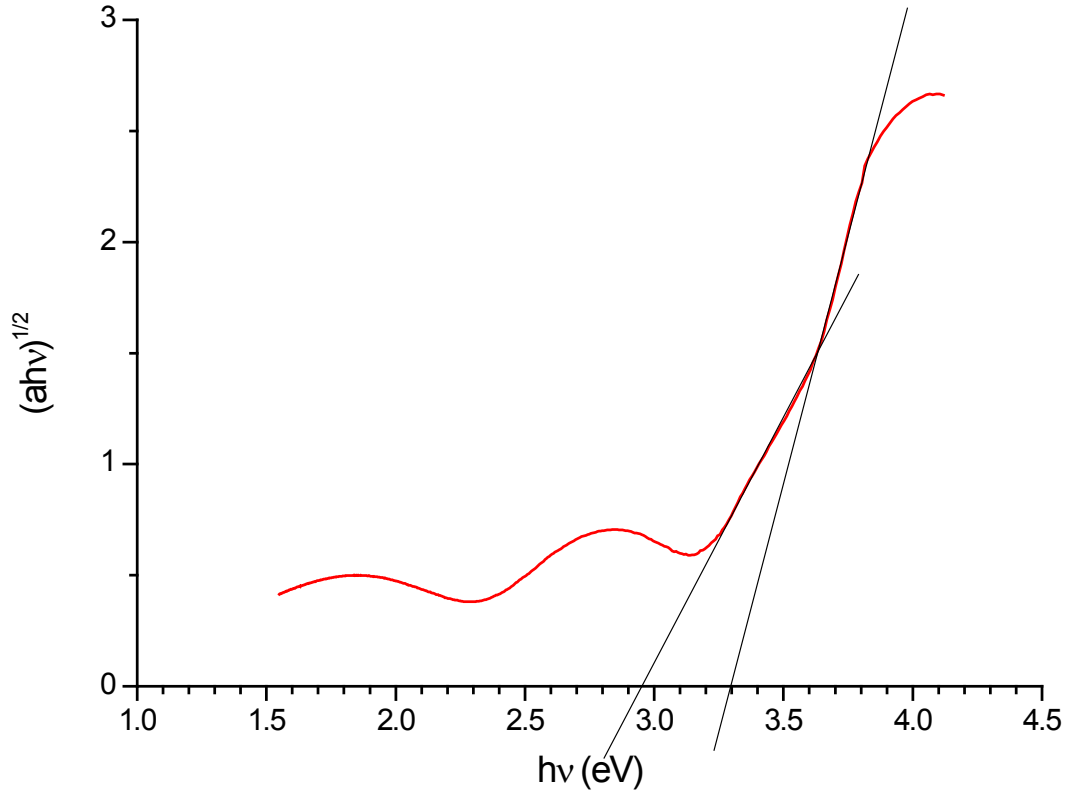

Figure 2.13 Tauc extrapolation for thin film deposited from 5%Ag:TiO_2 sol

The UV-visible spectrum demonstrates the characteristic anatase band edge at approximately 380 nm, along with a small absorbance peak (more easily seen in the inset spectrum) at approximately 440 nm. This is possibly indicative of the surface plasmon resonance band of nanoparticulate silver, which typically occurs in this region, but may also be attributed to Bragg type interference effects resulting from the wavelength of incident light being of the same order of magnitude as the film thickness. The Tauc extrapolation is somewhat ambiguous, as there are two distinct slopes to the graph. They correspond to optical band gaps of 2.95 and 3.3 eV respectively. This is more likely the result of interference effects rather than demonstrating the presence of a rutile/anatase mix. Indeed, as will be seen later, XRD shows exclusively anatase to be present in the film.

2.4.6.3 10%Ag/TiO_2

Figure 2.14 and Figure 2.15 show the UV-visible and Tauc extrapolations respectively, for a candidate thin film produced from the synthesis outlined in Section 2.2.3 with an Ag dopant level in the starting sol of 10%.

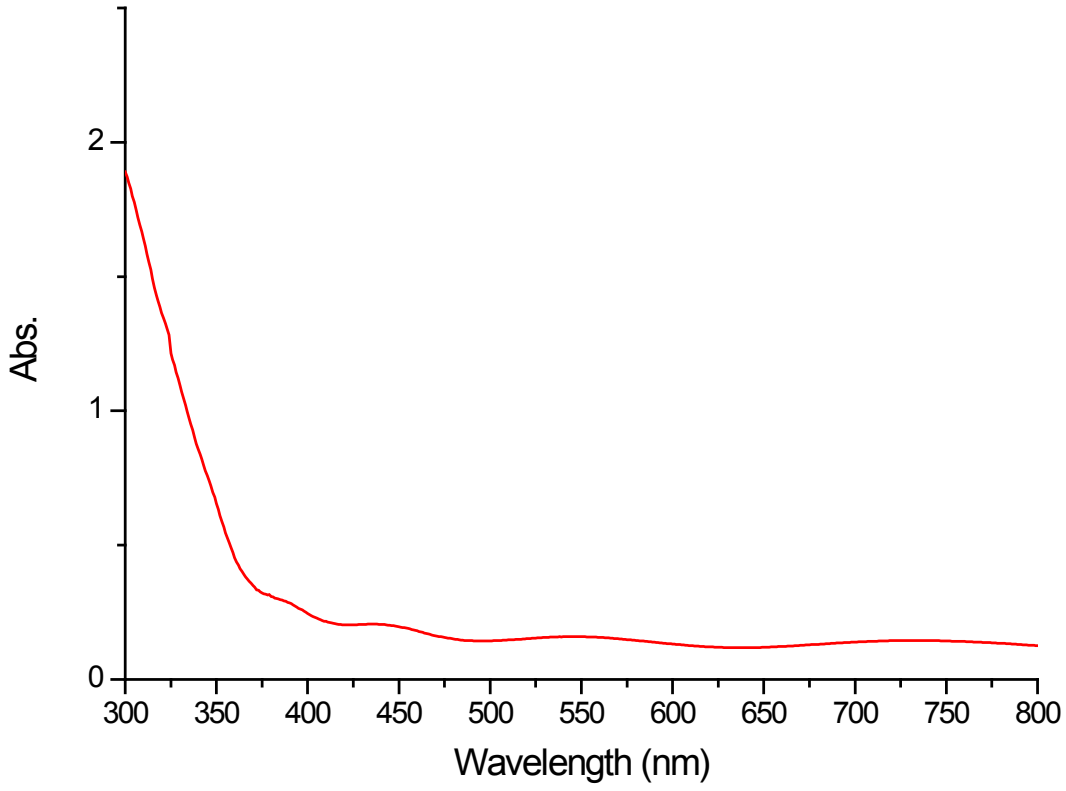

Figure 2.14 UV-Visible absorption spectrum for thin film deposited from 10%Ag:TiO_2 sol

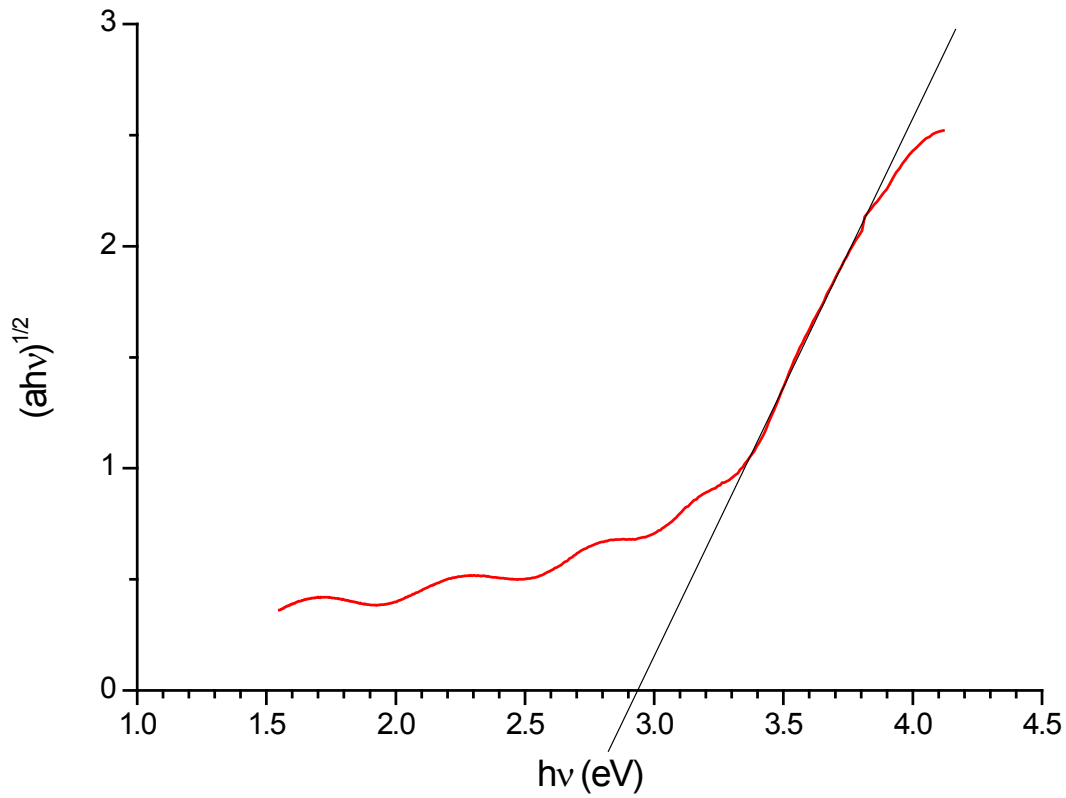

Figure 2.15 Tauc extrapolation for thin film deposited from 10%Ag:TiO_2 sol

The UV-visible and Tauc extrapolations for the sample from a 10% Ag/Ti sol are as expected. Unlike the sample deposited from a 5% Ag/Ti sol, there is no sign of an absorption peak indicative of silver nanoparticles in the 430 nm region. The Tauc extrapolation yields an optical band gap of approx 2.9 eV.

2.4.6.4 20%Ag/TiO_2

Figure 2.16 and Figure 2.17 show the UV-visible and Tauc extrapolations respectively, for a candidate thin film produced from the synthesis outlined in Section 2.2.3 with an Ag dopant level in the starting sol of 20%.

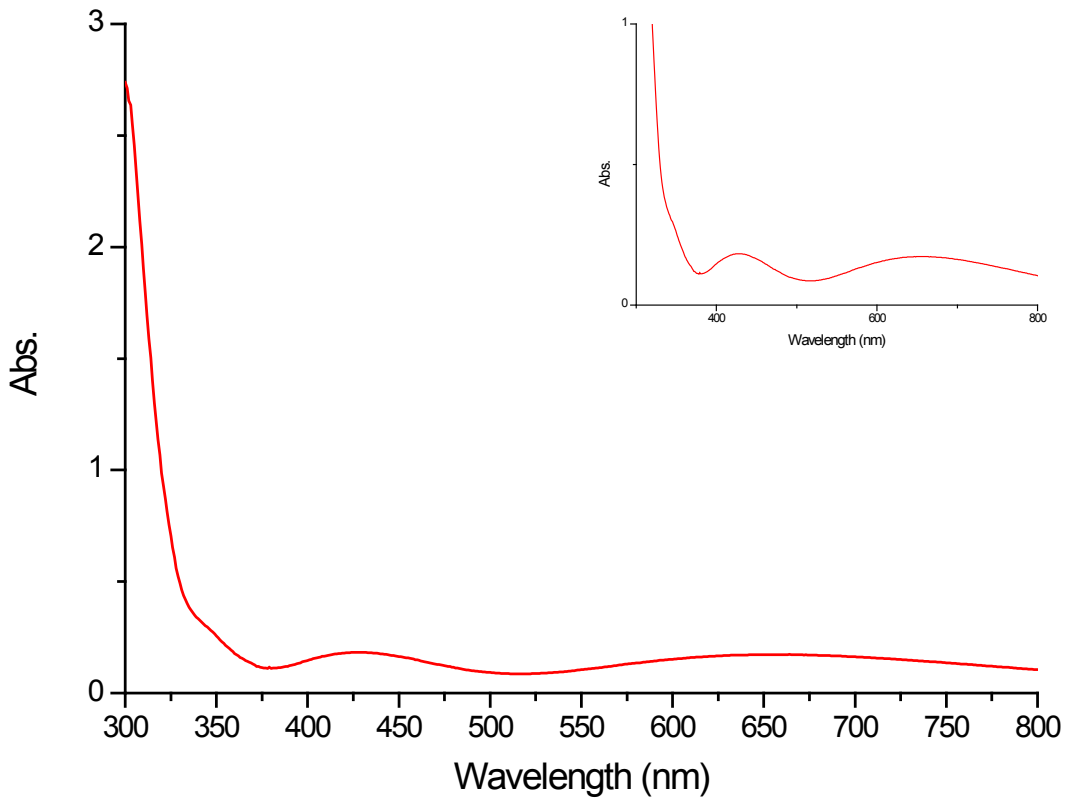

Figure 2.16 UV-Visible absorption spectrum for thin film deposited from 20%Ag:TiO_2 sol. Inset graph rescaled to highlight absorbance peak at approx 430 nm.

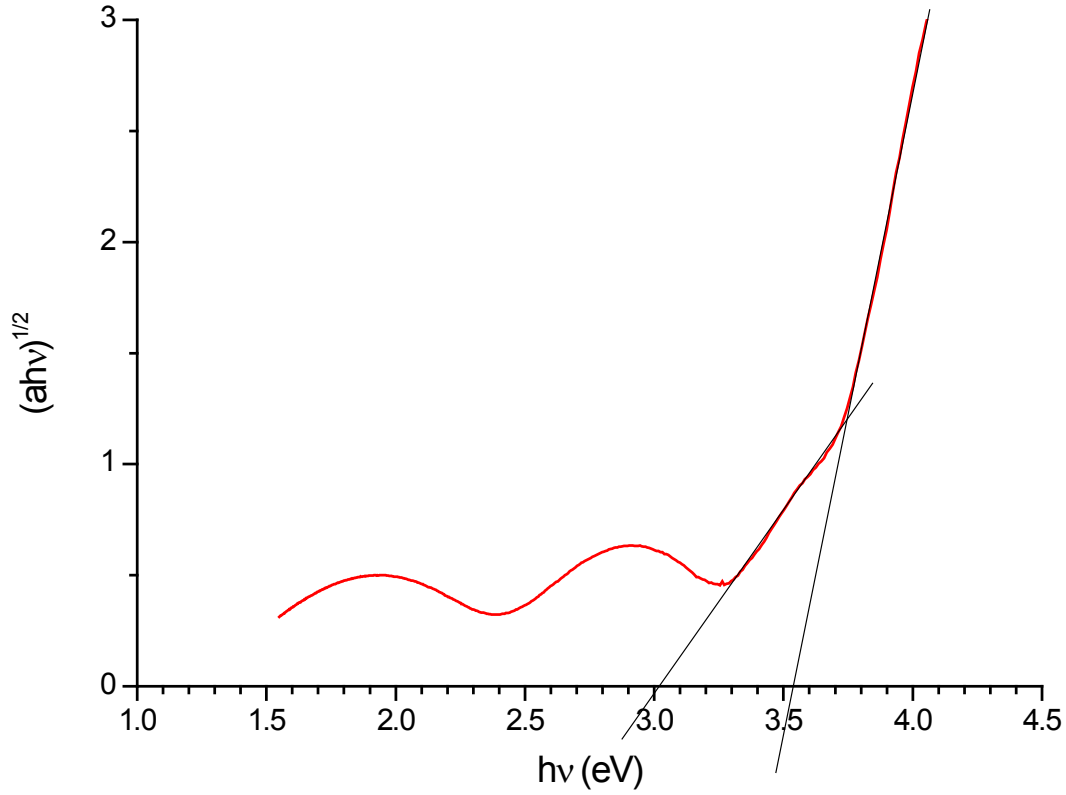

Figure 2.17 Tauc extrapolation for thin film deposited from 20%Ag:TiO_2 sol

The UV-visible spectrum has the characteristic band edge for anatase TiO_2 starting in the 380 nm region. Like the sample deposited from a 5% Ag/Ti sol, this spectrum also has a small absorbance peak in the same region. This one is located at approximately 430 nm. The Tauc extrapolation is also very similar to the one of the sample deposited from the 5% Ag/Ti sol, with two distinct straight line sections, which extrapolate to approximately 3.0 and 3.5 eV respectively. This, along with the absorbance peak may once again be due to interference effects resulting from the film thickness being of the same order of magnitude as the incident light.

2.4.6.5 2%WO_3/TiO_2

Figure 2.18 and Figure 2.19 show the UV-visible and Tauc extrapolations respectively, for a candidate thin film produced from the synthesis outlined in Section 2.2.5 with a W dopant level in the starting sol of 2%.

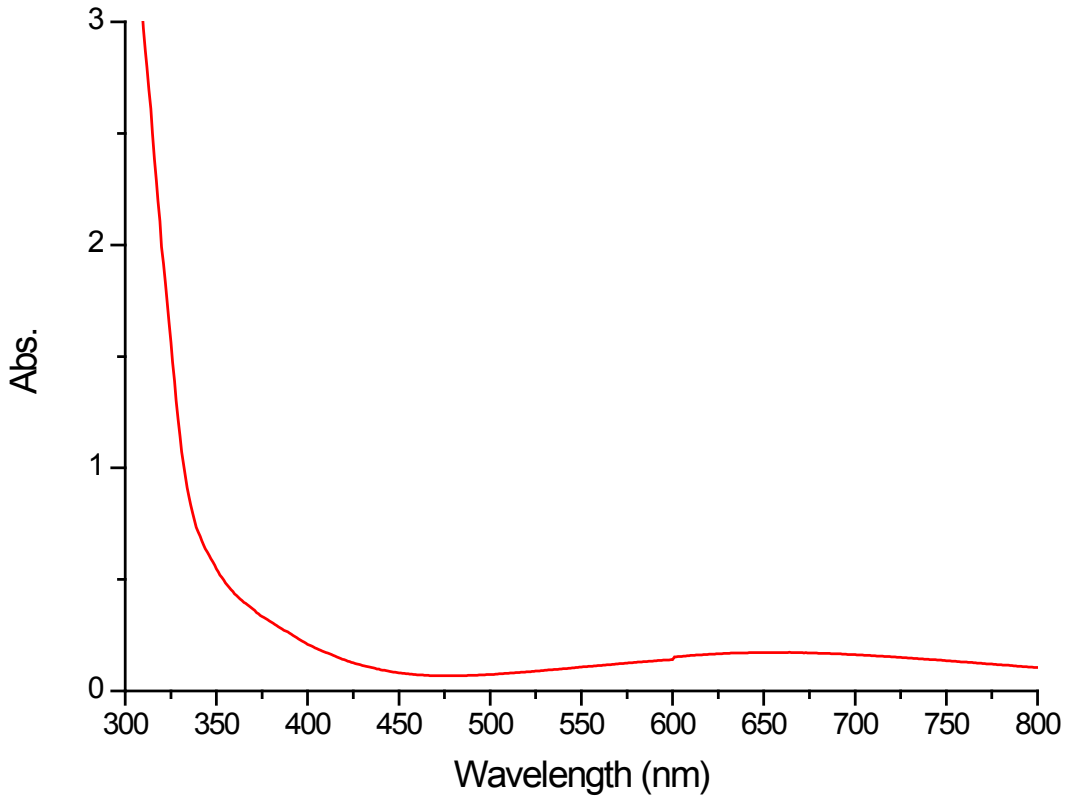

Figure 2.18 UV-Visible absorption spectrum for thin film deposited from 2%W:TiO_2 sol.

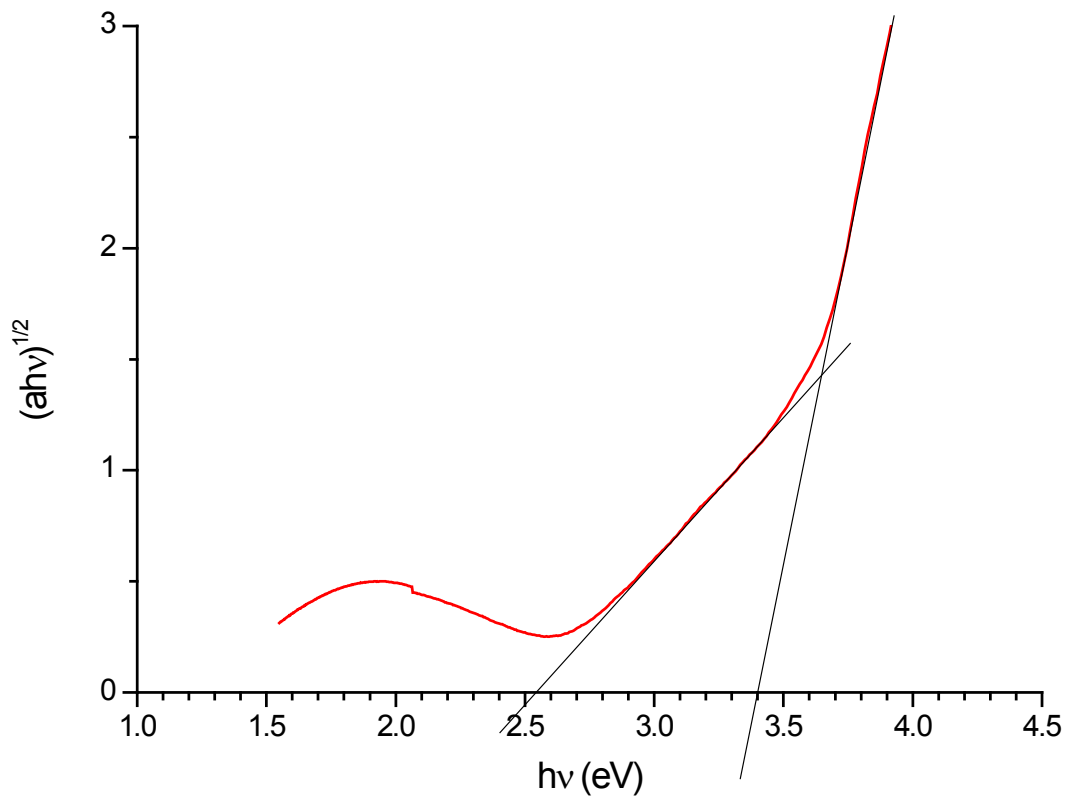

Figure 2.19 Tauc extrapolation for thin film deposited from 2%W:TiO_2 sol

The UV-visible of the W modified coating demonstrates the shifting of the band edge towards the visible. Instead of being in the 380 nm region for anatase TiO_2, the edge is located in the 450 nm region and the blue end of the spectrum. This is potentially useful for the harvesting of visible light photons and might produce a visible light activated photocatalyst. The Tauc extrapolation yields two straight line sections, of intercepts of approximately 2.5 eV and 3.4 eV. Whilst these do not correspond exactly, they are close to the literature values for WO_3 and anatase TiO_2, which are 2.7 and 3.2 eV respectively[110]. This suggests the inclusion of a separate phase of WO_3 within the TiO_2 matrix.

2.4.7 X-ray Diffraction

X-ray diffraction patterns were collected as described in 2.3.5 for a number of materials, both the thin films and the powders from dried and annealed sols. Thin films had to be examined by glancing angles because of the thin nature of the coatings. Despite using glancing angles the diffraction patterns all contain a large

amorphous peak from the underlying glass substrates. Powders were examined in a conventional manner resulting in superior quality diffraction patterns.

2.4.7.1 TiO_2 Thin Film and TiO_2 Annealed Powder

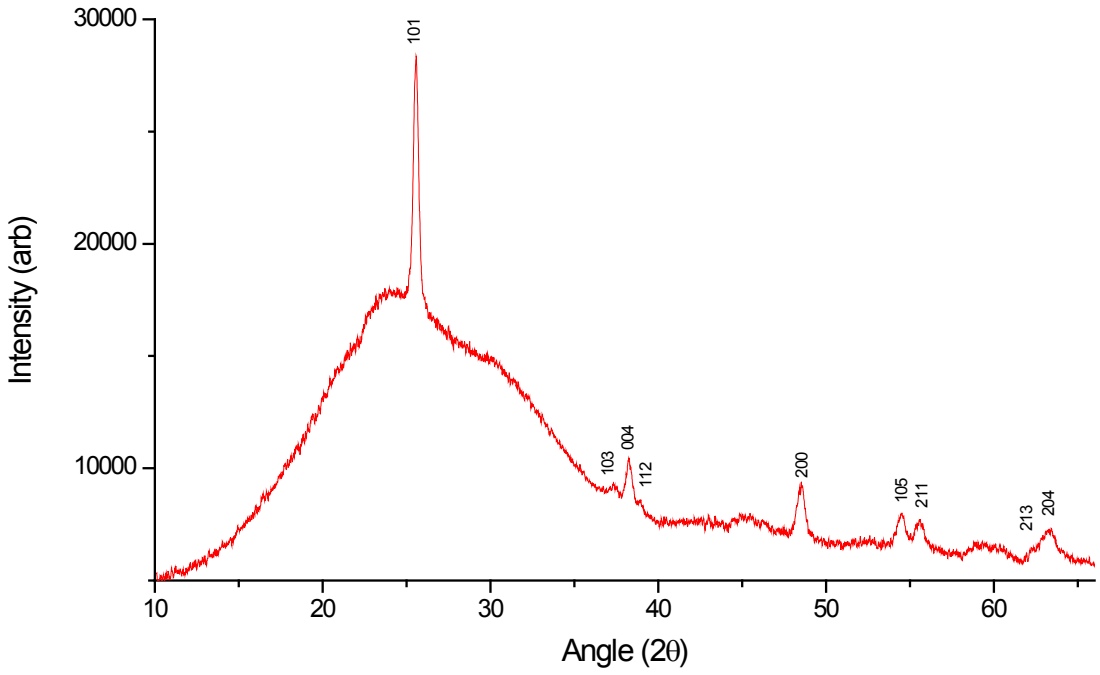

Figure 2.20 Glancing angle XRD for TiO_2 thin film coating – peak assignments confirm anatase TiO_2

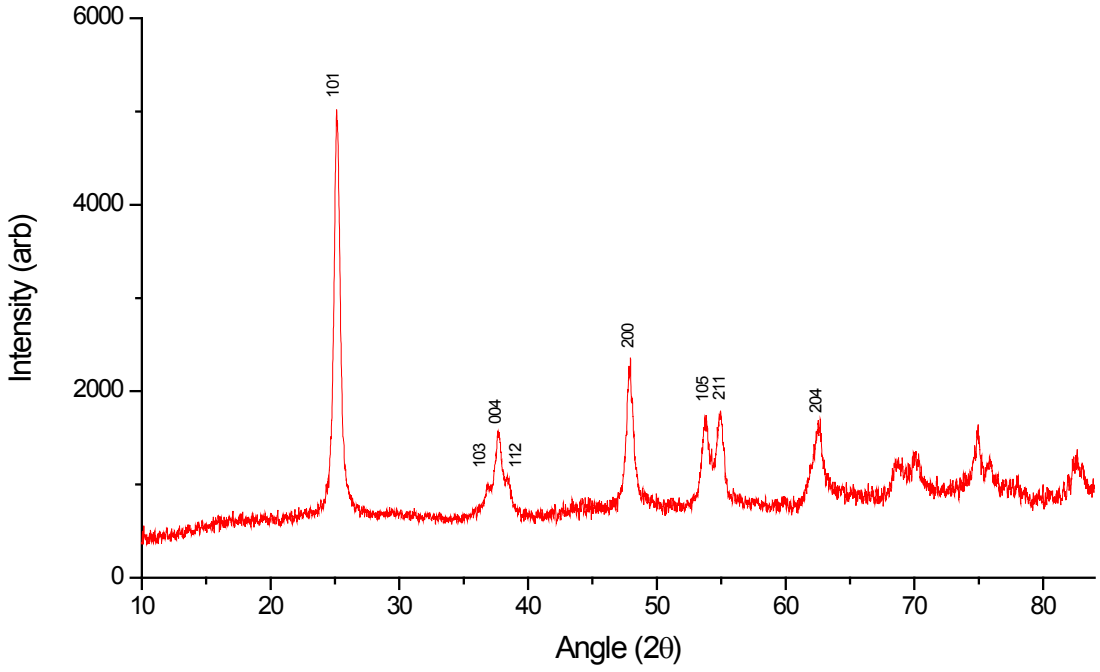

Figure 2.21 Powder XRD for annealed TiO_2 sol powder - peak assignments confirm anatase TiO_2

Figure 2.20 and Figure 2.21 show the thin film TiO_2 and powder TiO_2 diffraction patterns respectively. In both cases the diffraction patterns index as anatase TiO_2, with no indication of the rutile phase being present. This is in agreement with the observed anatase band edge and 3.2 eV optical band gap observed *via* UV-visible spectroscopy and Tauc extrapolation in Section 2.4.6.1.

2.4.7.2 10%Ag/TiO_2 Thin Film and Annealed Powder

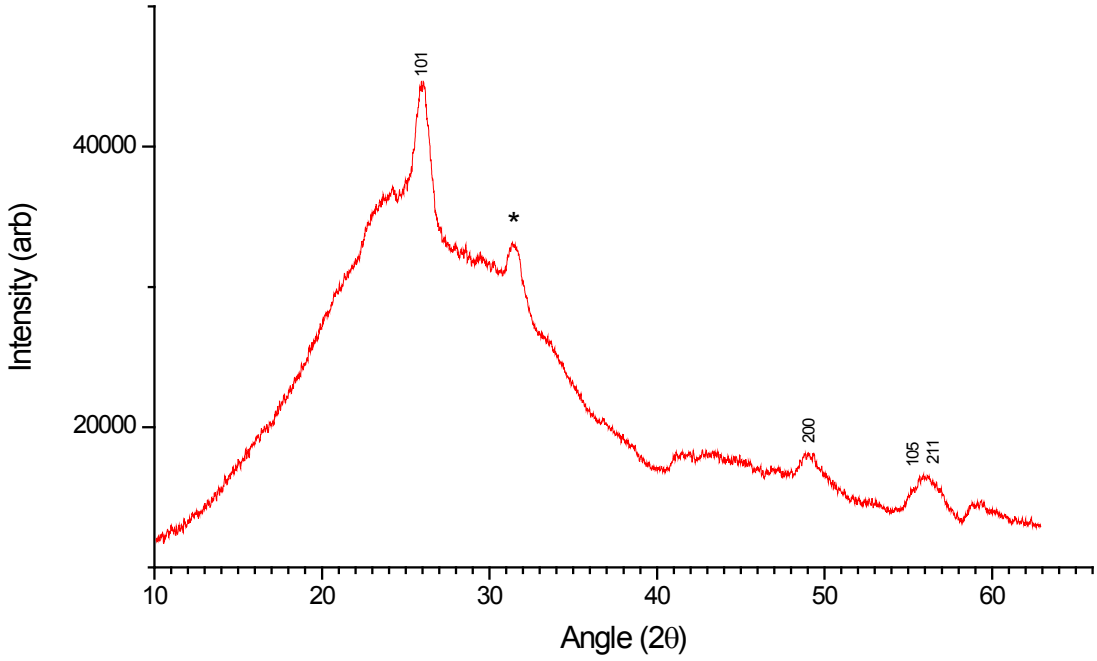

Figure 2.22 Glancing angle XRD of thin film from 10%Ag/Ti sol– peak assignments suggest anatase TiO_2

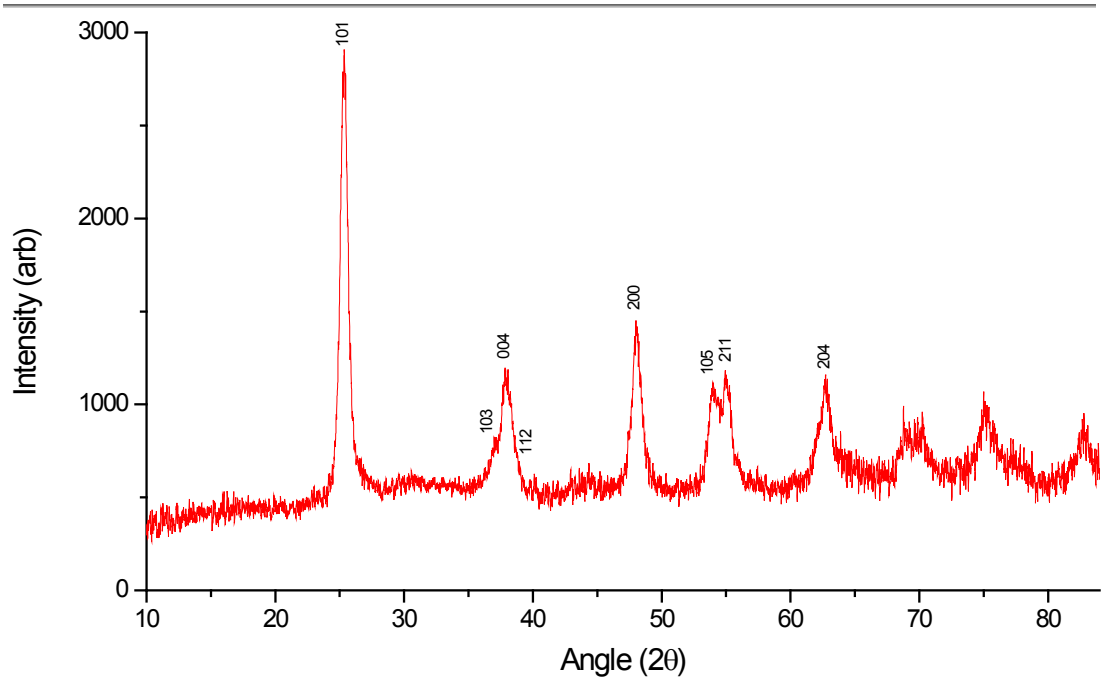

Figure 2.23 Powder XRD of 10%Ag/TiO_2 sol powder – peak assignments confirm anatase TiO_2

Figure 2.22 and Figure 2.23 show the thin film and powder diffraction patterns for one of the thin films deposited from a 10%Ag/Ti sol (synthesis described in Section 2.2.3). The thin film pattern has peaks which index as anatase TiO_2, along with one other peak at approximately 32 degrees. This unassigned peak could not be matched to any single compound in the XRD database, but did correspond with a number of Ag compounds including silver oxide. Interestingly, the powder pattern in Figure 2.23 does not manifest this peak, and indexes solely as anatase TiO_2.

2.4.7.3 20%Ag/TiO_2 Annealed Powder

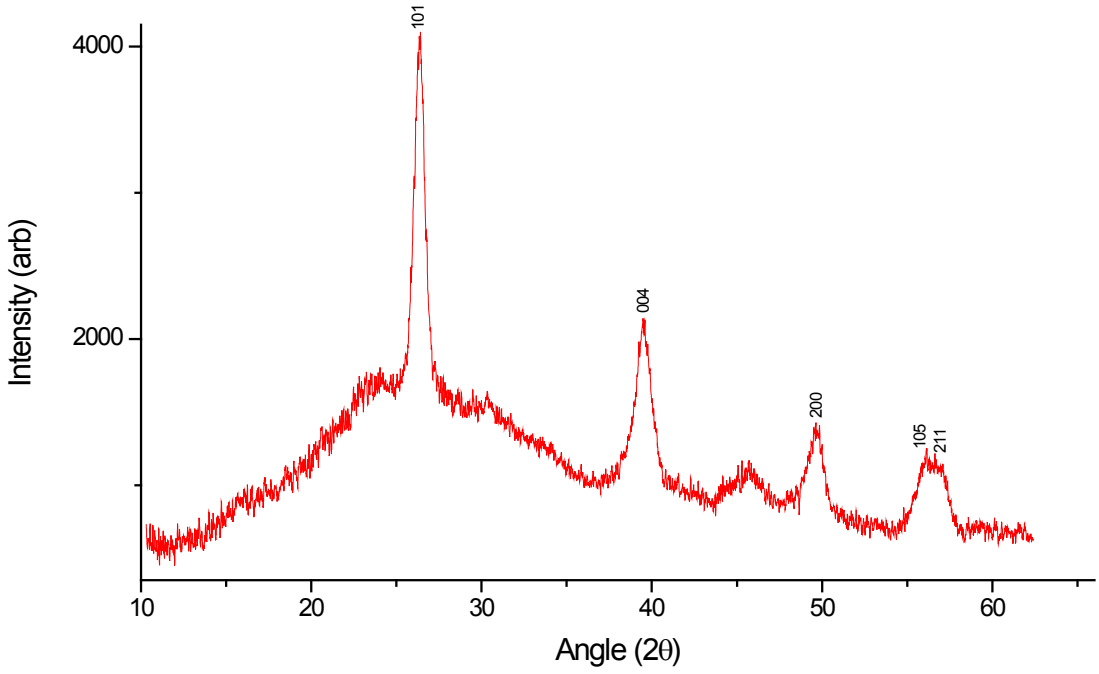

Figure 2.24 Powder XRD of 20%Ag/TiO_2 sol powder – peak assignments confirm anatase TiO_2

Figure 2.24 shows the powder XRD pattern for a powder derived from a 20%Ag/Ti sol (synthesis described in Section 2.2.3). The pattern has peaks which index as anatase TiO_2, along with some amorphous character not observed in any of the other powder patterns. In common with Figure 2.23 the possible Ag compound peak which was apparent in Figure 2.22 is absent.

2.4.7.4 Photodeposited Ag on TiO_2 Thin Film

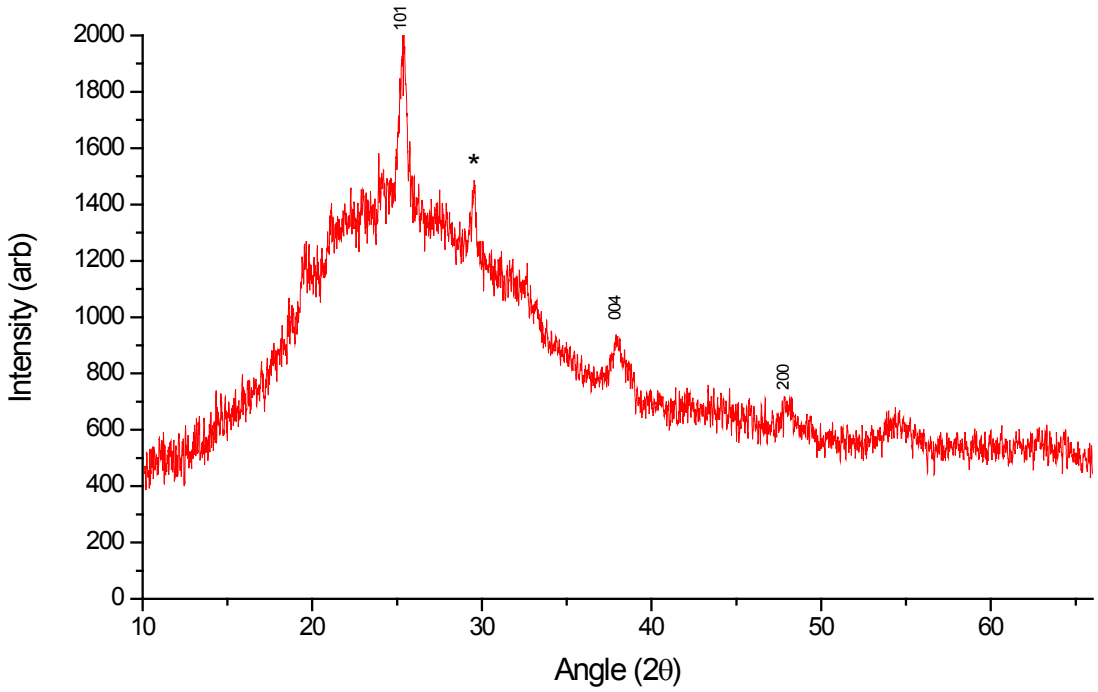

Figure 2.25 Glancing angle XRD of photodeposited Ag on TiO_2 thin film – peaks confirm anatase

Figure 2.25 shows the diffraction pattern for one of the photodeposited Ag on TiO_2 thin films. The peak assignments confirm the anatase phase of TiO_2 to be present. It can also be noted that the diffractogram is very similar to the thin film shown in Figure 2.22, and displays one unassigned peak, at approximately the same diffraction angle. When viewing in comparison to database reference patterns, this doesn't index as Noble Ag metal. In common with the pattern in Figure 2.22 the peak coincides with a number of Ag compounds, but cannot be definitively assigned.

2.4.7.5 W/TiO_2 Annealed Powder

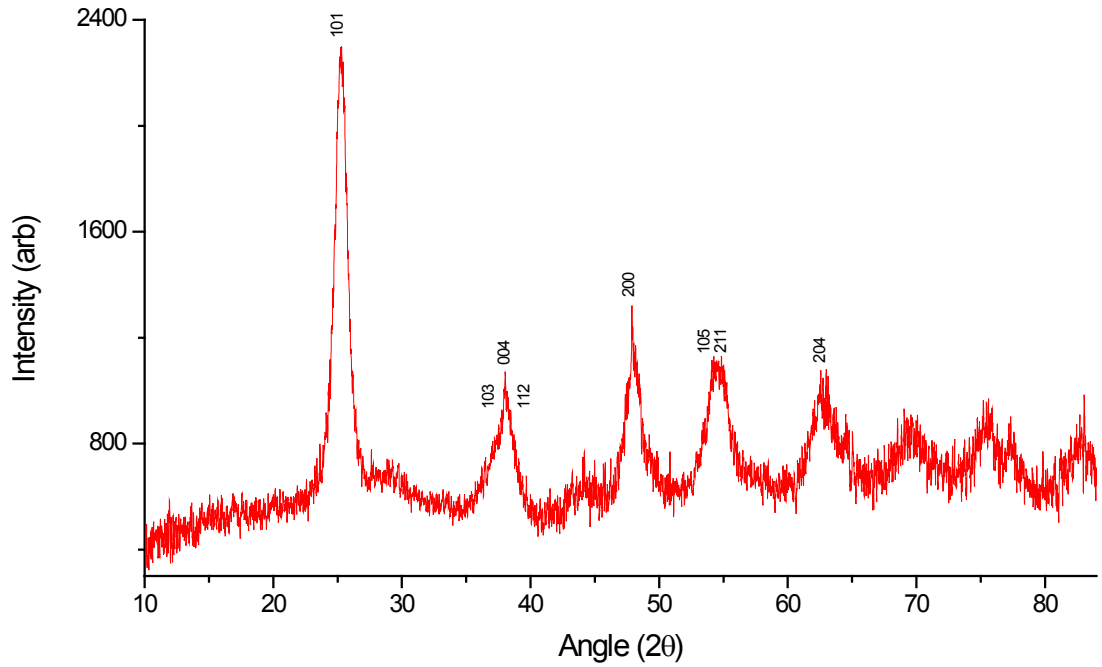

Figure 2.26 Powder XRD of W/TiO_2 annealed sol powder – peak assignments confirm anatase

Figure 2.26 shows the powder diffractogram from a W doped TiO_2 sol powder. The peaks can be indexed as anatase TiO_2, and there is no indication of any other crystalline phase or crystalline dopant material present. This may be due to lack of crystallinity or simply that any dopant WO_3 is present in too small a quantity to be satisfactorily resolved in the XRD.

2.4.7.6 Determination of Crystallite Sizes by the Scherrer Equation

The Scherrer equation allows determination of crystallite sizes from XRD peak broadening. A theoretical perfect single crystal diffraction pattern produces sharp peaks. Reducing the crystallite sizes from single crystal size results in peak broadening. The form of the Scherrer equation used in this study is given below:

$$t_{hkl} = \frac{c\lambda}{\beta_{hkl}\cos\theta_{hkl}}$$

Equation 2.3 The Scherrer Equation

In Equation 2.3, t_{hkl} is the crystallite size determined from a particular *hkl* reflection , c is the Scherrer constant, λ is the wavelength of the incident X-rays, β_{hkl} is the full

width half-maximum of a reflection from a specific crystal plane (*hkl*) and θ_{hkl} is the diffraction angle of the chosen *hkl* reflection. For the purposes of this study, c was set at 0.95 and the wavelength of incident X-rays was 0.154056 nm. It is important to note also that β is in terms of 2θ in radians and θ is in degrees, in terms of θ (i.e. value is diffraction angle/2).

The powder and thin film patterns shown in Figure 2.20 to Figure 2.26 were manipulated in OriginPro 8 (OriginLabs, Northampton MA, USA) to enable determination of the necessary parameters for the Scherrer equation. The most intense reflection, arising from the 101 crystal plane was analysed in all cases.

Sample	Crystallite Size /nm
TiO_2 Powder	16
WO_3/TiO_2 Powder	7
10% Ag_2O/TiO_2 Powder	12
20% Ag_2O/TiO_2 Powder	14
TiO_2 Thin Film	25
10% Ag_2O/TiO_2 Thin Film	10
Photo deposited Ag/TiO_2 Film	19

Table 2.4 Crystallite sizes to nearest nm determined by the Scherrer equation

The powder samples had a mean crystallite size of approximately 13 nm and the thin films had a mean crystallite size of approx 18 nm (all to nearest nm). The data shows that there is some variation in the crystallite sizes – most likely due to the limitations of utilising the Scherrer equation. The data shows that the powder crystallite sizes are smaller than the thin films – most likely due to the method by which the powder was prepared. The data also shows that within a sample type (film or powder) the crystallite sizes are of a similar magnitude.

Determining the crystallite size by the Scherrer equation serves as an indicator of trends in crystallite size, rather than an exact determination, because it does not consider instrumental peak broadening (therefore underestimating crystallite size) and gives a single value, for something which is actually a statistical distribution of sizes.[149] Despite these shortcomings it is a useful technique for observing trends in the samples and because the instrumental peak broadening introduces a systematic error, all samples will be underestimated in the same way. As a result, meaningful

comparisons can be made between samples, whilst not having to accept the calculated crystallite sizes as correct.

2.4.8 SEM/WDX

2.4.8.1 TiO_2 SEM

Figure 2.27, Figure 2.28 and Figure 2.29 show the SEM images obtained for a TiO_2 thin film at increasing levels of magnification from x1200 up to x400,000.

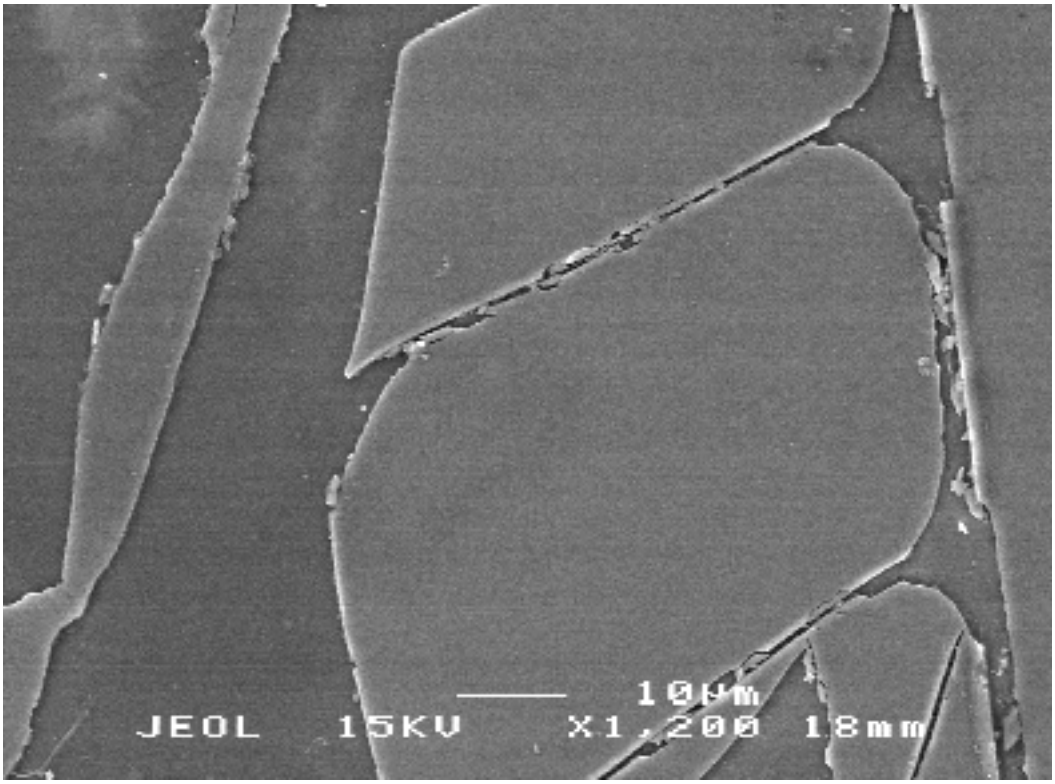

Figure 2.27 SEM image x1200 of TiO_2 thin film

Figure 2.27 shows a low magnification image at x1200. This shows shrink-cracking (a characteristic of sol gel films) and an interesting feature of platelets of the coating material, with the underlying glass substrate visible in the gaps between the plates. The fact that the coatings does not appear to uniformly cover the substrate may account for the relatively low photoactivity of the TiO_2 control samples compared with both the literature reports and the other samples examined in this study (see Section 2.4.4).

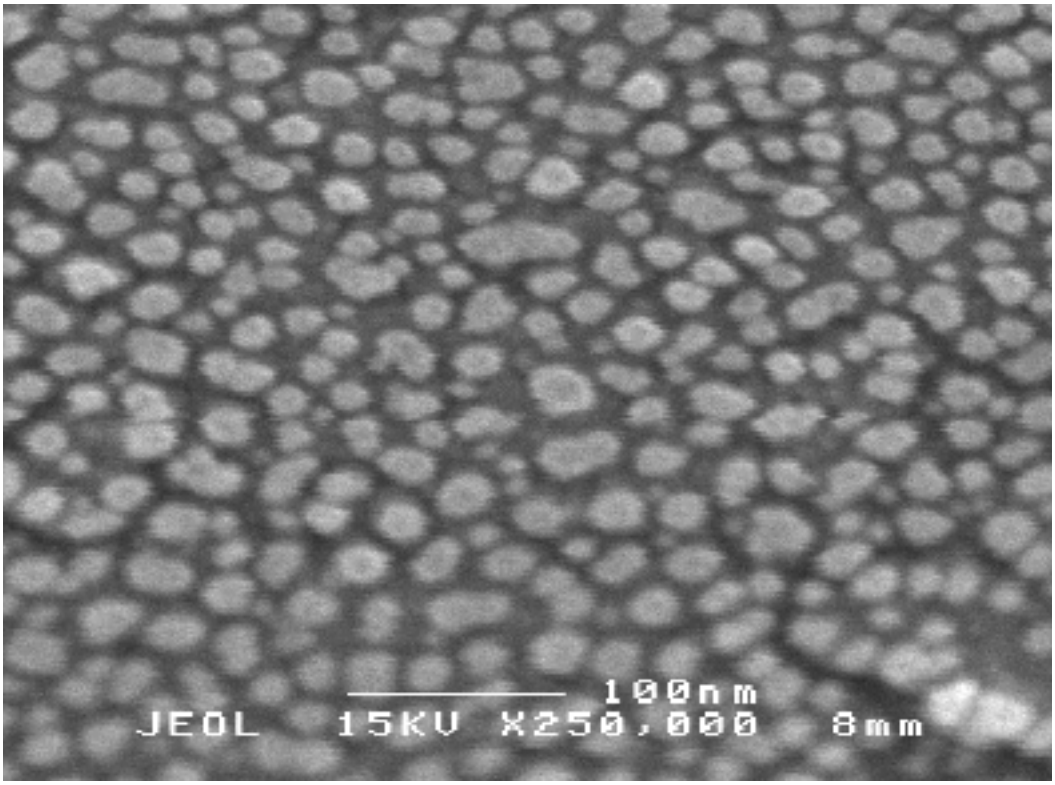

Figure 2.28 SEM image x250,000 of TiO_2 thin film

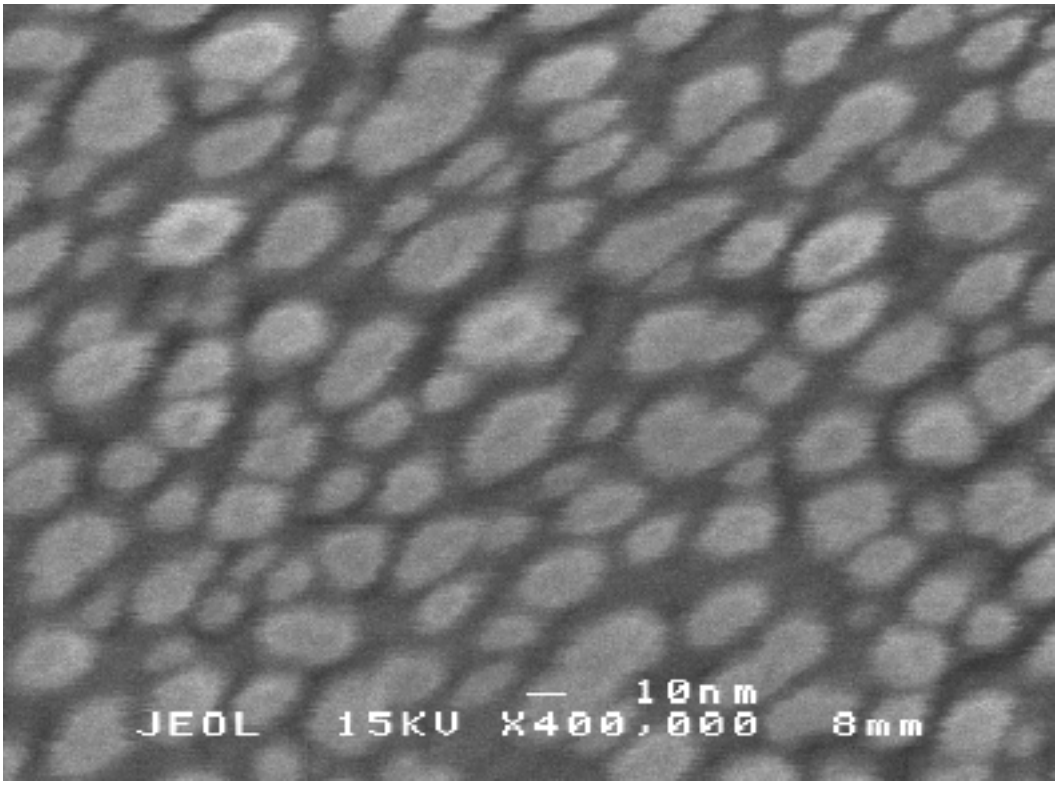

Figure 2.29 SEM image x400,000 of TiO_2 thin film

The higher magnification images in Figure 2.28 and Figure 2.29 demonstrate the nanocrystalline nature of the TiO_2 coating film. Individual particles, up to approximately 30 nm in size can be seen in the x400,000 image, shown in Figure 2.29. The observation of the particles and the determination of their size in this manner demonstrates the underestimation of the crystallite size by the Scherrer equation, as discussed in Section 2.4.7.6. The crystallite size *via* the Scherrer equation (mean 18 nm) is however of the same magnitude.

2.4.8.2 Ag/TiO_2 SEM

Figure 2.30 to Figure 2.33 shows SEM images of the Ag/TiO_2 thin films, produced from the synthesis outlined in Section 2.2.3 with a 10% dopant ratio in the starting sol. These are shown at various levels of magnification. Figure 2.32 and Figure 2.33 differ slightly in quality as they were captured during quantification study, rather than during an imaging run. Unfortunately it was not possible to obtain such high magnification images as were obtained for the TiO_2 sample.

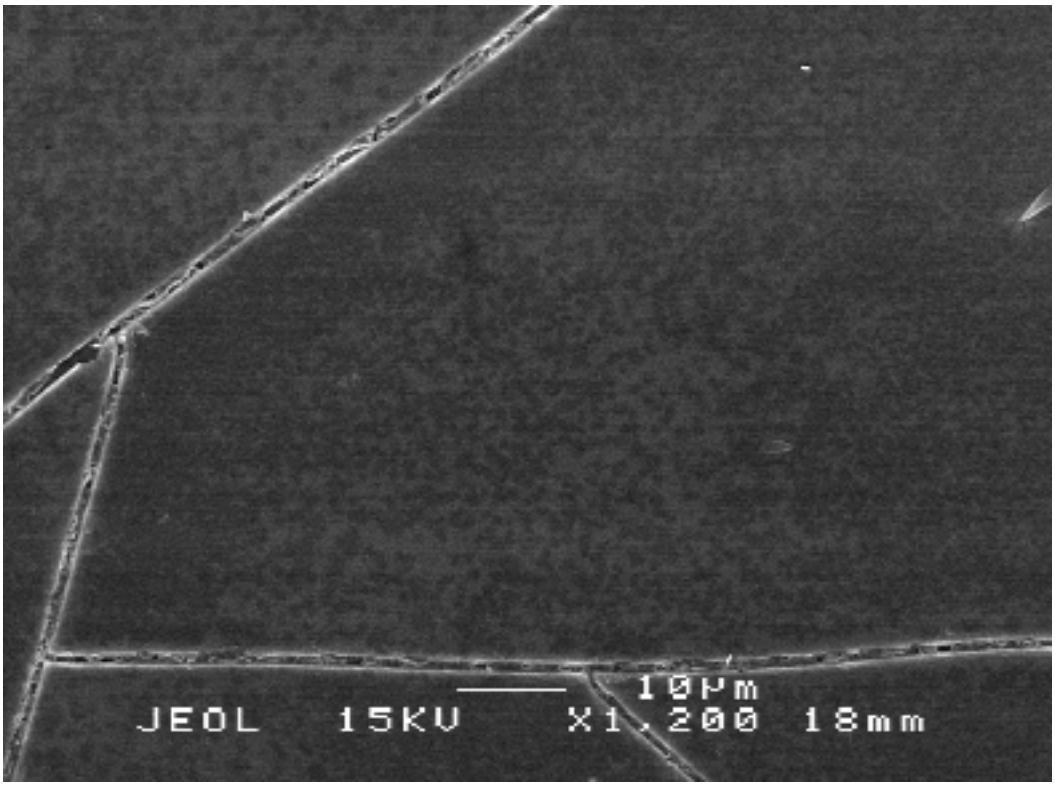

Figure 2.30 SEM x1200 of Ag/TiO_2 thin film

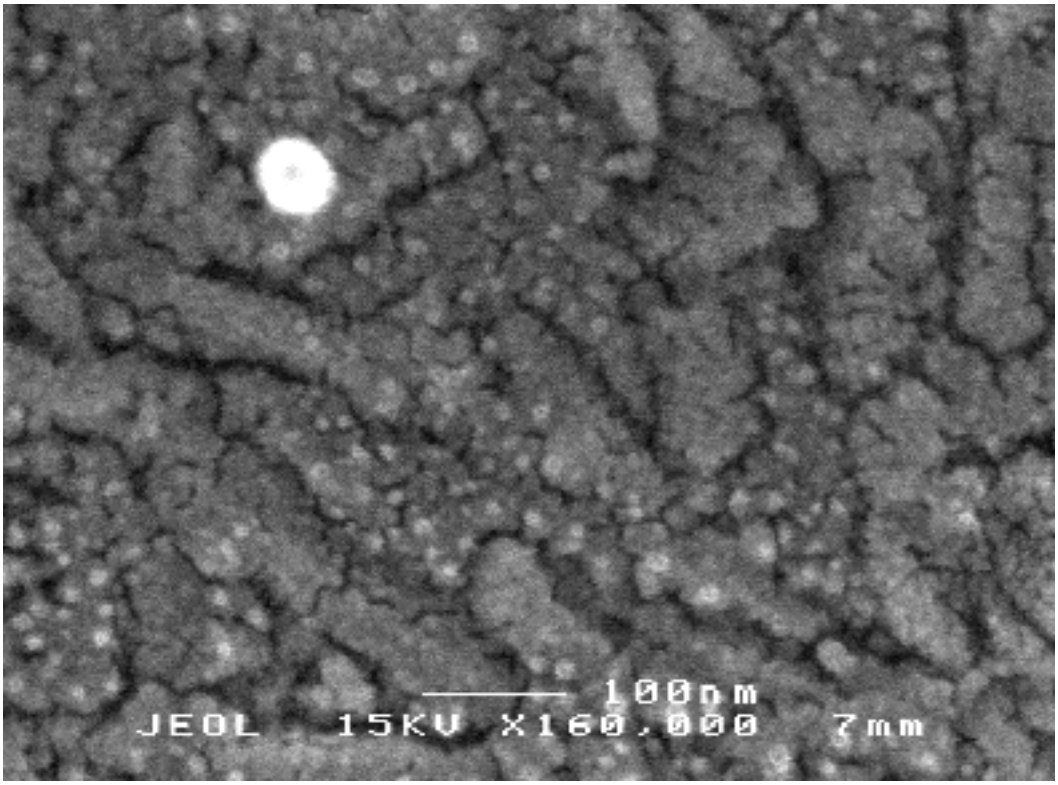

Figure 2.31 SEM x160,000 of Ag/TiO_2 coating

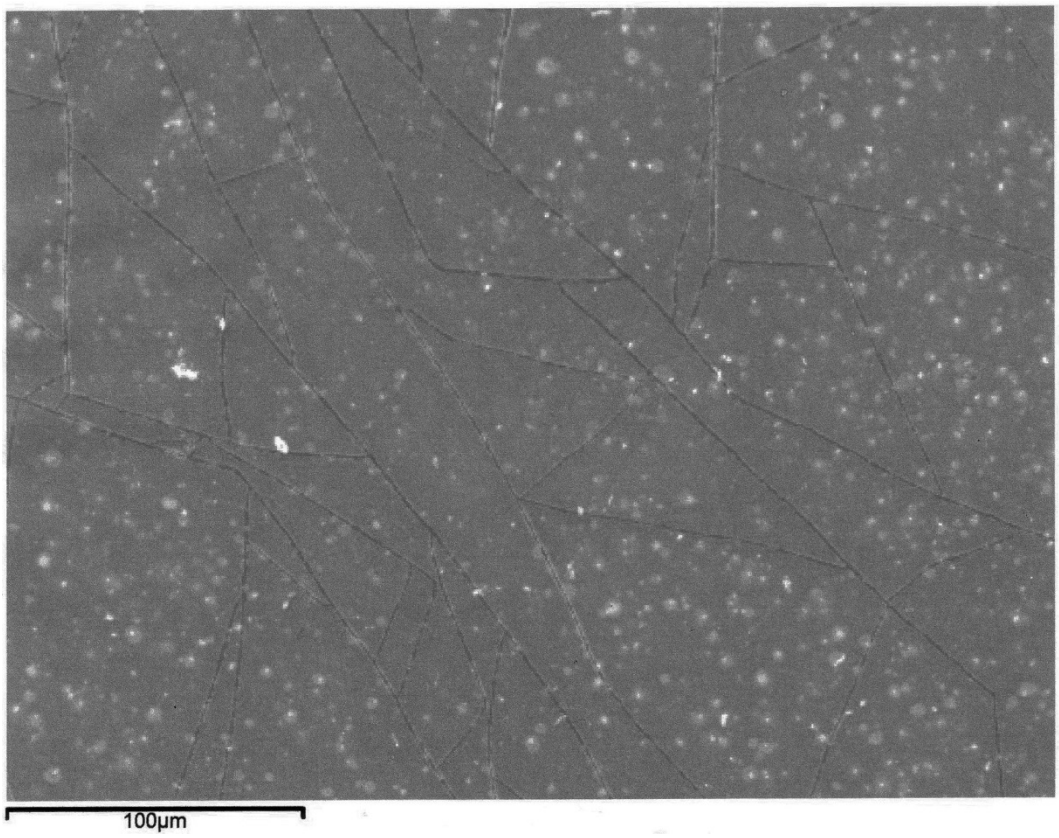

Figure 2.32 SEM of Ag/TiO_2 thin film

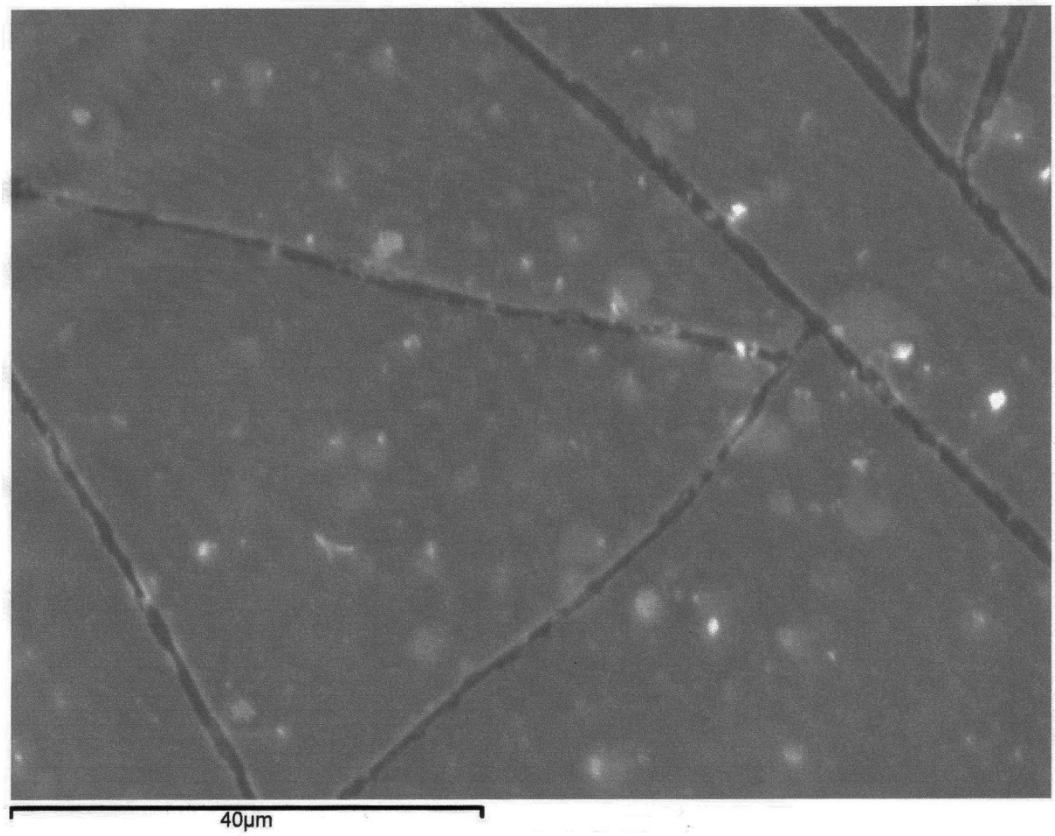

Figure 2.33 SEM of Ag/TiO_2 thin film

In common with the TiO_2 SEM images, there is significant shrink- cracking of the coatings – this seems typical of these sol gel dip coat derived materials. The principle difference is that there is much less breakthrough to the underlying substrate than was observed for the TiO_2 material. In effect this means more active, available surface area, and may therefore be a part of the explanation for the relative photoactivities between the TiO_2 control and the Ag/TiO_2 materials. Figure 2.32 and Figure 2.33 have a significant presence of high electron density artefacts over the surface – showing up as white spots in contrast to the background. These, spots, along with the larger one in Figure 2.31 are most likely particles of Ag, as this has a higher electron density than the TiO_2 matrix.

In addition to the top-down measurement, cross sectional SEM was performed, which showed the coating thickness to be approximately 150 nm for a 2 coat sample, and 300 nm for a 4 coat sample. An example thickness measurement SEM performed on a two coat thin film is given below in Figure 2.34.

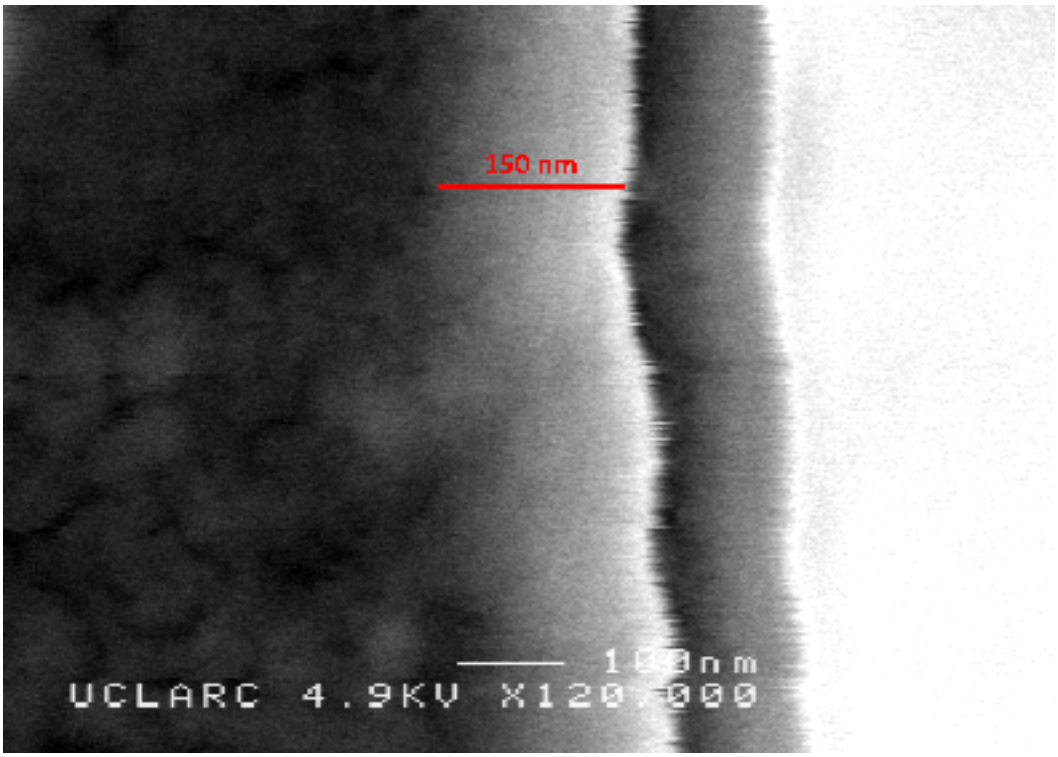

Figure 2.34 Edge on SEM measurement of two-coat film thickness

WDX analysis was variable across the sample and showed the presence of Ag, but only in very small amounts. The amount of Ag present was around 0.2 atomic percent, but was as high as 0.9 atomic percent in some places. This is much lower than the starting amount in the sols.

2.4.9 X-ray Photoelectron Spectroscopy

X-ray photoelectron spectroscopy (XPS) was undertaken on two sets of four coat Ag–TiO_2 films (from synthetic method in section 2.2.3), one on a set exposed to UV light and one on the films as made. Both films gave the same XPS profile. This profile is shown in Figure 2.35.

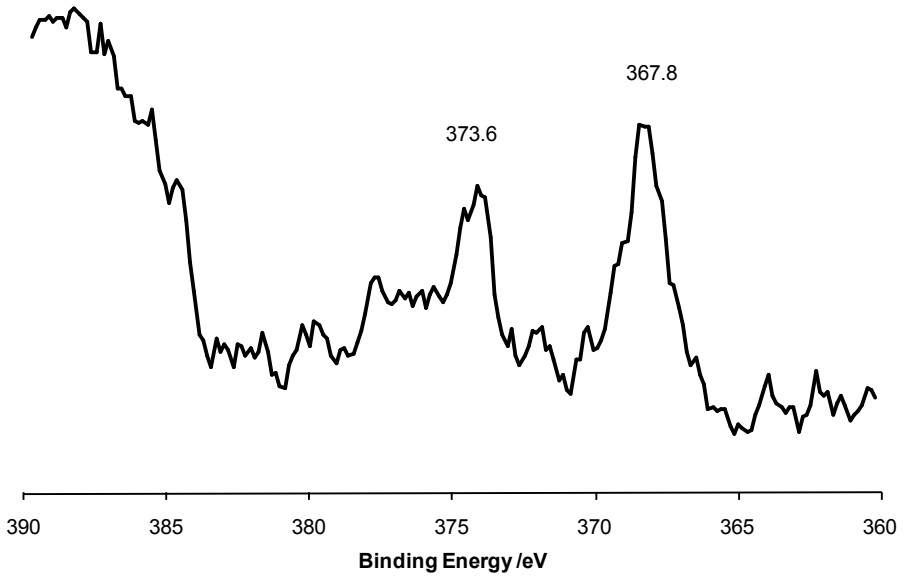

Figure 2.35 Silver XPS profile for a four coat Ag-TiO_2 film.

The titanium to oxygen atomic ratio was 1:2 – as expected for TiO_2, no other elements were detected other than carbon and silicon at a few atom percent. The percentage of the carbon decreased dramatically on depth profiling (Figure 2.36), indicating that it was residual carbon from within the XPS chamber.

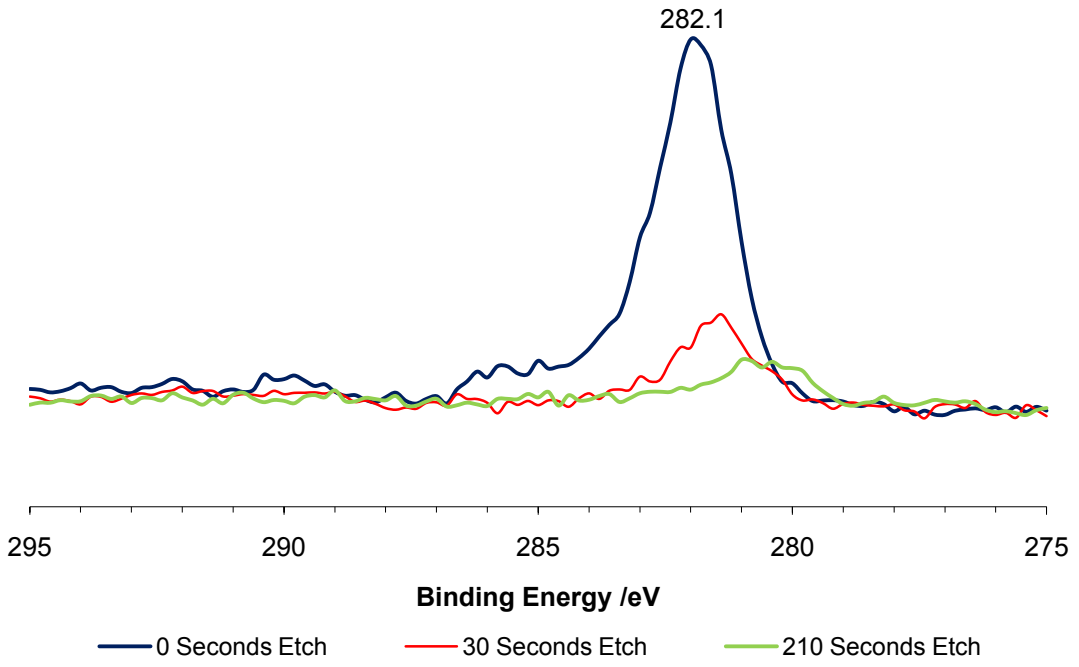

Figure 2.36 Carbon XPS profile for a four coat Ag-TiO_2 film with Ar sputter of 0, 30 and 210 seconds.

The Si abundance was constant with etching and probably a result of breakthrough to the underlying glass on regions where there was a small crack in the titania coating, notably it was only seen in one of the four samples analysed. Silver was detected both at the surface and throughout the film and its abundance was invariant with sputter depth, as can be seen in Figure 2.37.

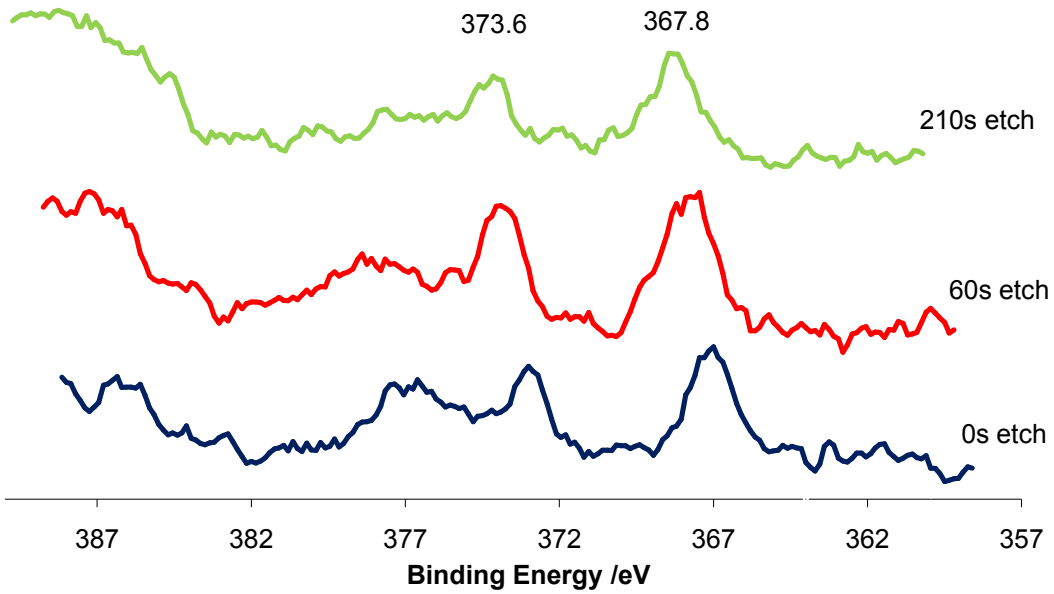

Figure 2.37 Ag XPS profile for a four coat Ag-TiO_2 film with Ar sputter of 0, 60 and 210 seconds - traces offset for clarity.

Binding energy /eV	Assignment
282.1	C 1s (residual C in XPS chamber)
367.8	Ag $3d_{5/2}$ in Ag_2O
373.6	Ag $3d_{3/2}$ in Ag_2O
458.6	Ti $2p_{3/2}$ in TiO_2
530.1	O 1s in TiO_2

Table 2.5 XPS spectral line assignments[150]

Silver was typically detected at below 1 atom%—significantly lower than that in the initial sol but comparable to that observed by WDX analysis (values ranged around

0.2 atom%, however accurate quantification was difficult at such low levels). The detection limit of the instrument is approximately 0.1 atom% and for quantification it is 0.2 atom%. XPS spectra were collected and referenced to elemental standards. The Ti $2p_{3/2}$ and O 1s binding energy shifts of 458.6 eV and 530.1 eV match exactly literature values for TiO_2[150]. In the sample exposed to UV light just prior to measurement there was a small shoulder to both the Ti and O peaks that correspond to Ti_2O_3. Interestingly the silver $3d_{5/2}$ XPS showed a single environment centred at 367.8 eV which gave a best match for Ag_2O (literature reports at 367.7–367.9 eV) rather than for silver metal 368.3 eV[150]. Hence the XPS is consistent with the silver being oxidised as Ag(I) rather than a metallic form in the thin films. Furthermore sputtering studies showed no change in the silver environment with sputter depth. This indicates that the silver is present as Ag_2O and not a Ag_2O coated Ag particle; as otherwise an asymmetry to the peak shape would have occurred.

2.4.10 X-ray Absorption Near-Edge Spectroscopy

The X-ray Absorption Near-Edge Spectroscopy (XANES) regions for the films studied compared with Ag, AgO and Ag_2O standards are given in Figure 2.38, Figure 2.39 and Figure 2.40 respectively. Particular attention should be paid to the post-edge oscillations resulting from ejected photoelectrons interacting with local atoms and undergoing constructive and destructive interference.

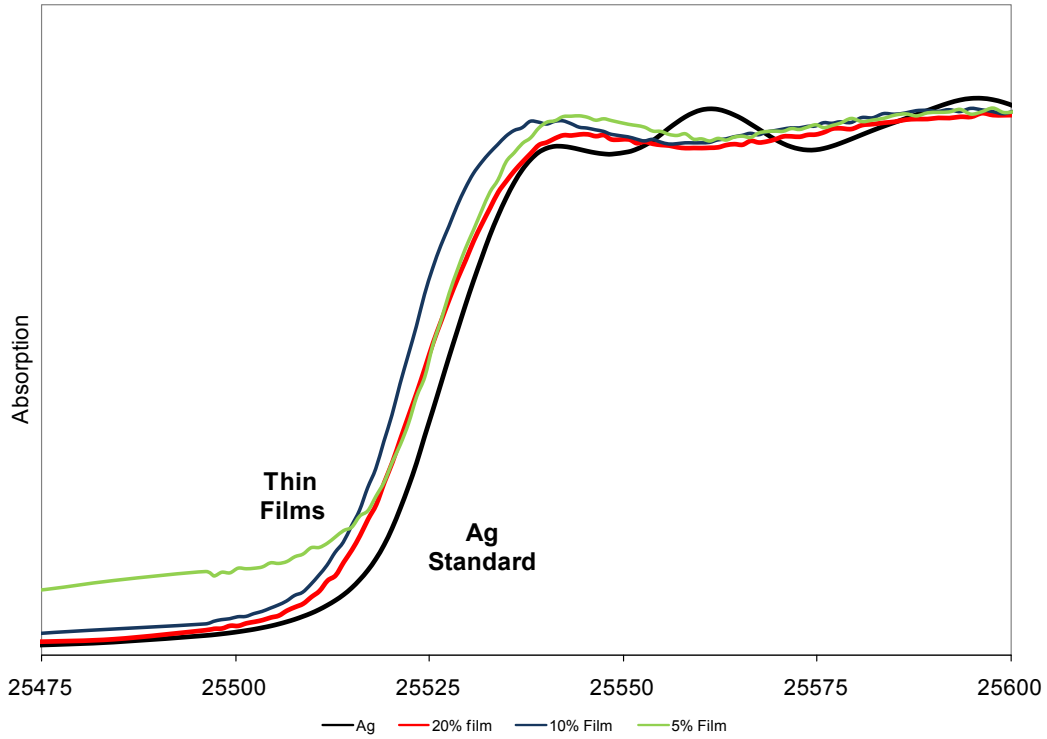

Figure 2.38 XANES region of the EXAFS spectra for thin films against Ag standard

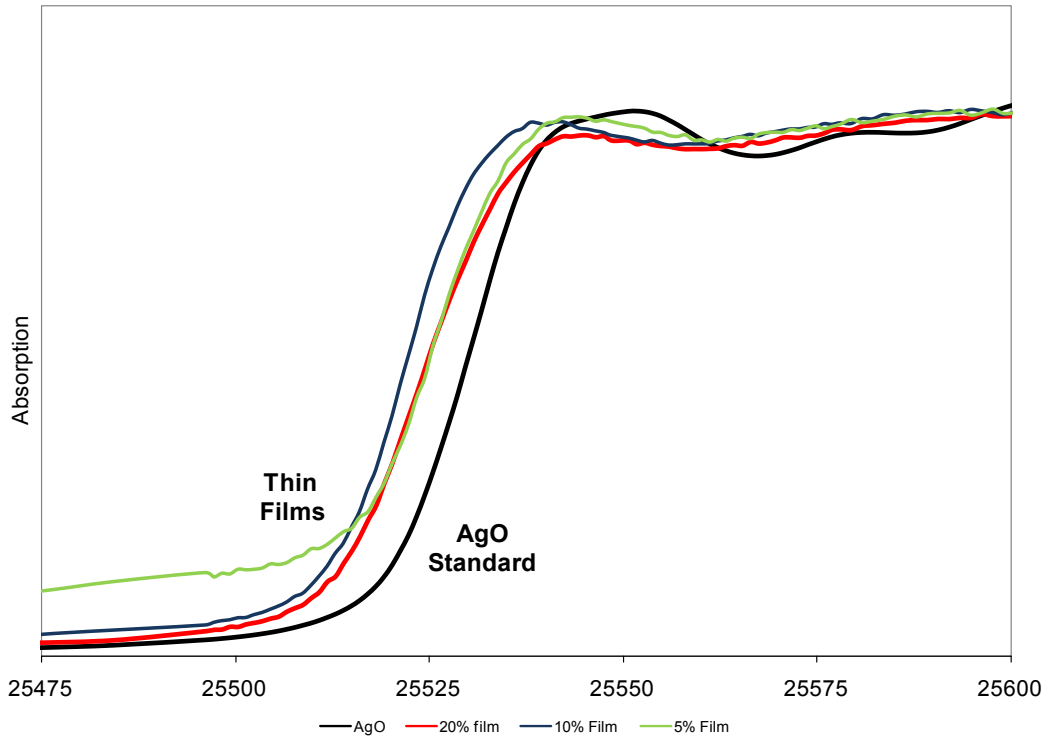

Figure 2.39 XANES region of EXAFS spectra for thin films against AgO standard

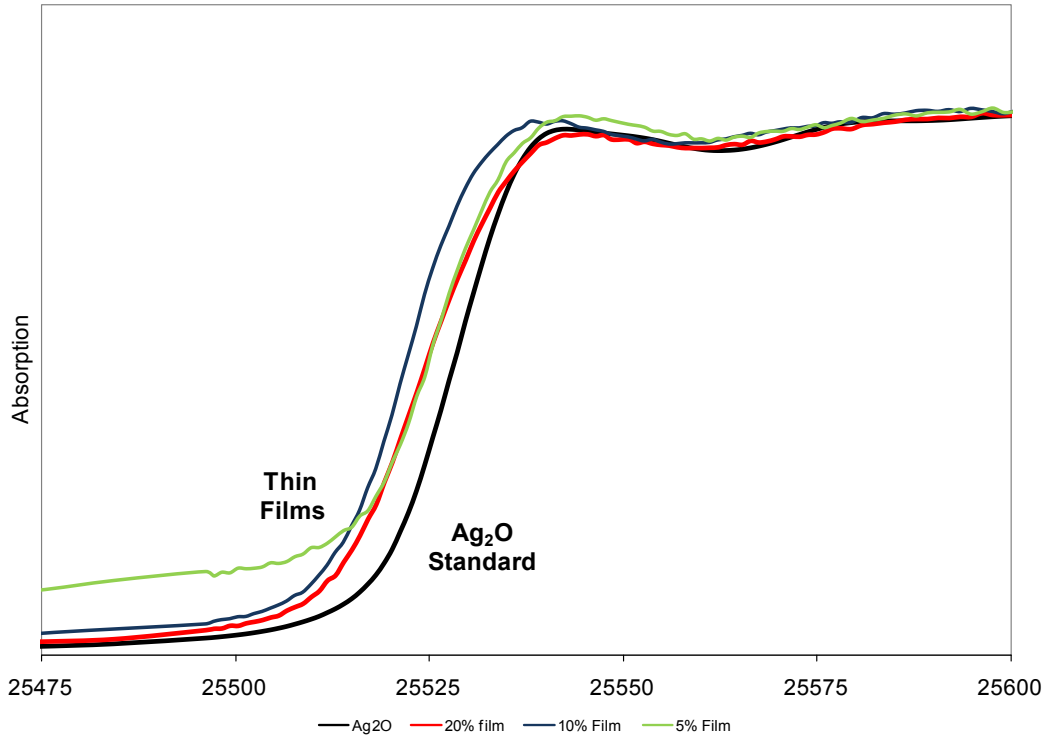

Figure 2.40 XANES region of EXAFS spectra for thin films against Ag_2O standard

By looking at the post-edge oscillations present within the XANES regions of the films and comparing them with the standards (as shown in Figure 2.38 to Figure 2.40), it is possible to elucidate the form of silver which is present within the thin films formed from the sol described in section 2.2.3. It is quite clear firstly that all three film types tested have very similar EXAFS spectra. The sample from a 5% Ag/Ti sol looks a little different in the pre-edge region from the others because normalisation of the energies was not carried out at the time of measurement, and hence the usual correction could not be applied. Nonetheless, in the post edge region, the oscillations in the spectra are well matched and near identical. This suggests that all three samples have silver present in the same oxidation state. Secondly, by now comparing the post-edge oscillations of the films with those of the controls, the oxidation state itself may be determined. It only takes a very quick glance at the spectra to see that the Ag and AgO traces are very different from those recorded by the films. In contrast, the Ag_2O trace matches the post-edge oscillations near-perfectly. It is therefore possible to say that these films contain silver in the form of Ag_2O – this is a new observation as in similar syntheses Ag has

been formed[122]. The different result observed here is probably due to the elevated temperatures of the anneal process being carried out in air, rather than in an inert atmosphere. Recent research[151] has shown that at elevated temperature in the presence of oxygen the most stable thermodynamic form for Ag is Ag_2O, so this might be offered as an explanation for the presence of the oxide rather than the metal for the annealed samples. Unfortunately it was not possible to examine all samples to this degree - the XANES measurements, despite yielding some of the most useful characterisation results, are very time consuming to make and require synchrotron beam time. This is undoubtedly an area to be examined in much greater detail in any future work as it will allow full, unambiguous materials characterisation - indeed study of the photodeposited Ag on TiO_2 would be interesting to study with XANES and should match the Ag metal standard.

2.5 Conclusions

Thin films of TiO_2 and doped TiO_2 materials were successfully prepared *via* a sol-gel dip coating technique. The thin films were rugged and well adhered to the glass substrates. Coatings could not be wiped off, rubbed off or washed from the surface with water. Coating materials were typically resistant to scratching by sharp metal stylus, but all could be damaged by a diamond tipped scribe. Save for the TiO_2 films with a photo deposited layer of Ag, films were indistinguishable in appearance. The photodeposited samples had a pinkish hue due to the deposited overlayer. The pink area produced a black precipitate on a saline soaked swab – perhaps indicative of low level removal of silver. This coating appears to offer bifunctionality in that it may be able to function as a light activated antimicrobial, as well as a microbicide release coating. This means it would be able to function both under conditions of illumination and conditions of darkness. This will be investigated further in the following chapter.

All of the materials were characterised by XRD as consisting of an anatase TiO_2 matrix. Analysis of the peak broadening by the Scherrer equation showed that all samples had similar crystallite sizes. SEM imaging showed the thin film coatings to be comprised of TiO_2 nanocrystallites up to 30 nm in size – this is in agreement with

the thin film crystallite sizes determined by the Scherrer equation. Coatings typically had optical band gaps in the region of 3.2 eV – determined by Tauc extrapolations. Some Tauc extrapolations suggested the presence of the rutile phase of TiO_2, but this could not be observed at all in the XRD. All thin films and bulk powders were exclusively anatase by XRD. The Tauc extrapolation for the W doped film suggested the presence of WO_3 *via* its optical band gap of 2.7 eV. Some of the Ag/TiO_2 films exhibited Ag surface plasmon resonance bands in the 430 nm region. However, characterisation of all dopants present proved very difficult. Where possible to detect them, dopant levels within the coatings and powders were considerably lower than in the sol from which they were deposited. Clearly the efficiency of the transfer of dopants from sol to coating is relatively poor, and is an area for future research.

The Ag samples which had demonstrated the best photoactivity were consequently subjected to more rigorous analysis to determine the form of silver present within the films. This could only be determined by combining the results obtained by both the XANES and XPS studies. The results show that the silver in these samples is present as Ag_2O – this is a novel finding, not previously demonstrated by doping.

All synthesised films demonstrated the phenomenon of photoinduced superhydrophilicity (PSH). In terms of PSH, the films were effectively indistinguishable, with very similar water droplet contact angles after UV illumination. As hydrophilic self cleaning surfaces, the materials really have nothing between them in terms of performance. It is in the photocatalytic abilities that differences in performance become apparent. All of the synthesised materials functioned as photocatalysts, but it was the Ag_2O/TiO_2 materials which had superior performance, with an initial rate of destruction of stearic acid of approximately 43 $\times 10^{12}$ molecules cm^{-2} min^{-1}. Evidence was collected for the photocatalytic production of hydroxyl radicals by a fluorescence technique, but further research is required.

In the next chapter the materials will be subjected to antimicrobial testing. The antimicrobial performance of the materials will depend upon their physical and

chemical properties as examined in this chapter, in particular photocatalysis and photoinduced superhydrophilicity. Since all samples demonstrated these properties it is expected that all samples will have some degree of antimicrobial efficacy. However, as has already been demonstrated some samples have more desirable characteristics. The Ag_2O/TiO_2 and photodeposited Ag on TiO_2 samples are likely to be the most interesting antimicrobials as a result.

Chapter 3: Microbicidal Activity Testing

3.1 Introduction

In the previous chapter samples were analysed to determine if they demonstrated the properties of photocatalysis and superhydrophilicity. Samples exhibiting these characteristics make excellent candidates for antimicrobial surfaces, and as such, successful samples were selected for further examination to determine their microbicidal activities. Samples were examined under illumination from a 365 nm black-light blue lamp and from a white light source, with a spectral profile identical to that found in lights used in UK hospitals. Study with the white light source was the predominant method, because it is of significantly greater real world interest. Where time allowed some samples were also investigated under the conditions of ultraviolet illumination. This chapter describes the antimicrobial testing methodology, details the results and discusses them in reference to the material properties.

3.2 Experimental

3.2.1 Microorganism selection

Microorganisms were selected for this study to represent both Gram-positive and Gram-negative types. The distinction between the types is discussed in the introductory chapter. As can be seen from the diagrams on page 30, there is significant difference between the cell wall morphologies, which consequently leads to significant differences in the way the microorganisms behave, especially at their surface. As has been discussed, the proposed microbicidal mechanism for TiO_2 photocatalysts is surface specific (acting upon the cell wall), so one might expect the Gram-positive and Gram-negative organisms to behave in different ways as their walls have different morphologies. Hence both types were tested. Standard laboratory strains from the National Collection of Type Cultures (Health Protection Agency, UK) were selected. *Staphylococcus aureus* (NCTC 6571) (Gram-positive coccus, approx 1 μm in diameter) was selected as a candidate Gram-positive organism, and *Escherichia coli* (NCTC 10418) (Gram-negative rod 1 μm in

diameter by 2 μm in length) was selected as a candidate Gram-negative organism. Both are microbes of clinical importance and are hence relevant to this study. *S. aureus* is perhaps of particular interest because of the much publicised cases of MRSA in UK hospitals. Whilst the NCTC 6571 strain is not methicillin resistant, its behaviour towards photocatalysts should not be expected to be significantly different from a resistant strain. Hence it serves as a useful indicator of the effectiveness of the photocatalyst coatings against potentially resistant microbes.

3.2.2 Viable Colony Counting Technique

In all of the experiments described in this chapter analysis of microbes was performed using serial dilutions and a viable colony counting technique on agar media. This is a very standard technique in microbiology and good descriptions are available in standard texts (notably Brock Biology of Microorganisms[30]), and is used because microbial numbers are so large. An overnight culture may be of the order 10^9 cfu/ml and inoculation of an agar plate with a culture this concentrated will result in confluent growth - that is to say individual colonies are not distinguishable from their neighbours and the plate is uncountable. In order to make it possible to count microbes on an agar plate it is necessary to dilute the inoculum such that fewer microbes are applied and confluent growth is avoided. This is most commonly achieved by carrying out 10 fold serial dilutions of the sample to be counted in a suitable medium (such as PBS or broth), such that each successive dilution is 10 times more dilute than the previous one. These serial dilutions are then plated out onto agar and incubated. After incubation there will be one plate in the dilution series with a countable number of microbes (usually 30 to 300 is considered appropriate). By taking into account the dilution factor upon which the plate count was performed, it is then possible to scale up to the number of microbes present in the original sample. This is the backbone of the antimicrobial testing methodology described throughout this chapter. Figure 3.1, taken from Brock[30], provides an excellent overview of the serial dilution, viable colony counting method. Serial dilution, viable colony counting experiments have a parameter known as the detection limit. This is the smallest inoculum which can be detected on the neat (undiluted) plate. The detection limit is calculated by entering a plate

count of 1 into the calculation for the neat plate and varies from study to study, as a result of differing experimental design. It is important to note therefore that zero organisms on the neat plate means a count below the detection limit. This is not necessarily a zero viable colony count.

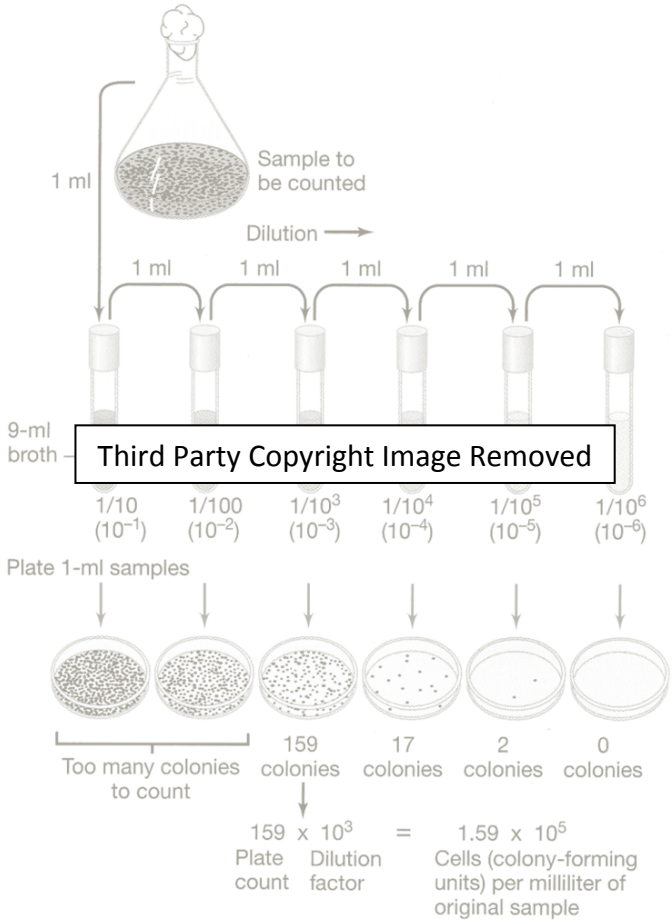

Figure 3.1 Serial dilution and viable colony counting technique. Image from Brock Biology of Microorganisms.[30]

3.2.3 Experimental Design

A significant proportion of the experimental work carried out during this study was in the optimisation of the experimental design, and overcoming significant problems with the methodologies. The various routes taken and results obtained before the development of a reliable methodology will not be examined in great detail, but are presented here, briefly, for the sake of completeness. In previous work carried out by the author[127] 25 µl aliquots of microbial overnight culture in nutrient broth (Oxoid Ltd) were delivered directly onto the coating surface *via*

pipette. The coatings were then placed in individual moisture chambers (constructed from a Petri dish with moist filter paper in the base) before being irradiated by 365 nm BLB lamp (Vilber Lourmat VL-208BLB – VWR Ltd). At the end of the UV irradiation time period the droplets were swabbed up using sterile calcium alginate swabs (TSC Ltd), which were aseptically transferred to a glass bijoux bottle containing 5 to 7 glass beads and 4 ml 'Calgon' Ringer solution (Oxoid Ltd) and vortexed. Serial ten-fold dilutions of this volume were then carried out in phosphate buffered saline [PBS] (Oxoid Ltd). The dilutions were plated out in duplicate onto agar. Inoculated plates were then incubated face down overnight at 37 °C. After colonies had grown sufficiently a viable colony count was carried out and the data processed, taking into account all the dilution factors involved.

When this established and reliable method was applied to the newly produced coatings the droplets of overnight culture did not remain in place. The photoinduced superhydrophilicity of the surface meant that the inoculum behaved differently from before. In some instances the droplet moved across the surface, merging with a neighbouring droplet, or rolled off the edge of the surface completely. In other cases the droplet spread so thinly that it dried out, even when in a saturated moisture chamber. All of these complications led to extremely poor recovery of microorganisms from the surface and to extreme variation in the data. This was clearly an unsuitable situation, so various new methodologies were designed and tested. The approach taken was one to limit the spreading of the inoculum, so that only the photocatalytic properties (and not the hydrophilicity) of the coatings was examined. Glass ring cells and rings of silicone grease were the first to be tried out – with variable success. On many occasions the spreading of the droplet due to the surface superhydrophilicity of the coating was such that leaks occurred – with the grease being lifted from the surface and the inoculum flowing beneath it. Boundaries of waterproof permanent marker pen and of Chinagraph type wax pencil were also examined, but these suffered the same problems as the silicone grease.

The most promising alternative containment method appeared to be the use of a cover glass (VWR 22 × 22 mm, thickness no 1). Although this prevented the

majority of leaks it too was an inconsistent method. Of particular concern was the relatively poor recovery of the inoculum at the end of an experiment. The cover glass and the coating surface both had to be sampled. This involved aseptically transferring the cover glass to a universal bottle containing 5 ml 'Calgon' Ringer solution and vortexing the solution. The sample surface was then swabbed as per usual with an alginate swab. Problems were encountered when the surface superhydrophilicity enabled the cover glasses to move across the sample.

The current and most successful alternative method involved remaking the coatings using a single cavity microscope slide (Jencons PLS 26×76×1.0-1.2 mm) as the substrate. These microscope slides have a cavity 15 mm diameter ground into their surface. Although not very deep (the slides are only 1.0 to 1.2 mm thick) the cavity is more than large enough to hold 25 µl of inoculum. After a six hour exposure to the 365 nm lamp the droplet does not escape the cavity. This enables the study of the microbicidal activity solely due to photocatalysis to be studied whilst minimising any effects due to the surface superhydrophilicity. By minimising the hydrophilic spreading of microbial cells as a result of carrying out the experiment in the cavity, the potential increased exposure both to the coating and to antimicrobials produced by/released from the surface is negated. The cavity slide was thus the substrate of choice throughout unless stated otherwise in the rest of the work discussed in this chapter. In viewing all results one should bear in mind that without the cavity in place the inoculum droplets are able to spread and thin. This results in reducing the microbial overlap and subsequent shielding from both the incident light and the antimicrobial surface. Hence, the coating materials, deployed in real world use, without the restriction on hydrophilicity will most likely have a significantly greater antimicrobial activity than that displayed in the experiments in this study.

One important area for all of the antimicrobial testing was the appropriate and thorough use of control samples. This is essential in experiments where there could be more than one explanation for an observed effect. In the case of this study it principally concerns the potential antimicrobial effect of the illuminating light source (whether it be an ultraviolet source, or a standard fluorescent source). The

impact of this on the experimental design is such that it must allow delineation of observations which might be due to a) the illuminating light source, b) the substrate upon which the experiment is being performed or c) a synergy of the light source coupled with the substrate. For photoactivated materials such as TiO_2, one would expect microbicidal activity to be observed only in the synergistic case – i.e. the best antimicrobial activity is expected to be observed with a photocatalyst substrate, under the appropriate illumination conditions for that material.

3.2.4 Nomenclature

As a result of the number of variables that it is necessary to test in each experiment, it is convenient to devise a system for labelling each sample under test. The reasoning behind this and issues relating to the experimental design were discussed in section 3.2.3, but for the purpose of understanding the experiments and the results obtained, the nomenclature used throughout this work is given in Table 3.1. Where required, any modifications to this basic set of nomenclature will be fully explained - this will become particularly apparent in the study of the TiO_2 films with photodeposited overlayers, since an extra variable has been introduced to the experiments.

Nomenclature	Meaning
L+S+	*Sample in presence of light* (L+) from the chosen light source with *an active substrate* (S+) under test.
L+S-	*Sample in presence of light* (L+) from the chosen light source with *an inactive substrate* (S-) under test.
L-S+	*Sample in absence of light* (L-) from the chosen light source with *an active substrate* (S+) under test.
L-S-	*Sample in absence of light* (L-) from the chosen light source with *an inactive substrate* (S-) under test.

Table 3.1 Standard nomenclature used throughout this study for antimicrobial tests

3.2.5 Decontamination Procedure

Prior to commencing an experimental run, samples, deposited upon cavity microscope slides (Jencons-PLS single cavity), were prepared by firstly being disinfected with a 70% v/v isopropanol/distilled water solution, which was allowed to fully evaporate. This step was tested for any residual microbicidal activity against *Staphylococcus aureus* NCTC 6571 by comparing an inoculated untreated glass control with an inoculated 70% isopropanol treated slide, both left in darkness for a 4 hour period. The experiment was repeated four times. This experiment checks for any potential long term antimicrobial effect exerted by the decontamination procedure. The inocula were recovered aseptically by alginate swab to 'Calgon' Ringers solution (5 ml) in universal bottles, and vortexed. Serial dilutions of the recovered inoculum were performed in PBS, and dilutions were plated out in duplicate on an appropriate growth medium. Viable counts were performed on the dilution with the best countable number of microbes after an overnight incubation at 37 °C. A comparison experiment was also performed, in exactly the same manner, to see if a slide cleaned with commercially available alcohol Azowipes (Vernon Carus/Synergy Health plc, Swindon, UK) demonstrated any residual microbicidal activity.

3.2.6 Microbe Inactivation by Thin Films Under 365 nm Light

The initial decontamination step (detailed in Section 3.2.5) was then followed by a 30 minute pre-activation and decontamination by 254 nm germicidal lamp (Vilber Lourmat VL-208G – VWR Ltd). Microbial suspensions were prepared by overnight culture, aerobically, with shaking for both organisms tested (*S. aureus* NCTC 6571 and *E. coli* NCTC 10418). Overnight cultures were prepared in 10 ml volumes of standard nutrient broth (Oxoid Ltd.). Depending upon the experiment being carried out, the microbial culture was used either neat (this gives an inoculum of ca. 10^9 cfu/ml), or was diluted as appropriate, in further sterile nutrient broth. The test inoculum was then delivered to the cavity on the test sample slides in 25 μl aliquots from a micropipettor. The pipette tip was used to ensure that the droplet of

inoculum was evenly spread in the cavity, and extending to all the extremities. A fresh tip was used for the inoculation of each sample cavity. All samples were examined in duplicate, and each experiment was carried out at least twice, though usually three times. Inoculated samples due to be illuminated for the duration of the experiment were then transferred to a moisture chamber, constructed from a large square Petri dish, with a filter paper saturated in sterile distilled water at its base. The samples were raised above the moist filter paper on swab sticks. The samples were aligned as close together as possible, such that the whole moisture chamber could be positioned directly under the centre of the 365 nm lamp, where its irradiance is most uniform. The lamp-sample distance was maintained at 20 cm. Dark controls were prepared in a similar way, save for the large Petri dish being enveloped in aluminium foil, to prevent the ingress of direct or reflected UV light. Illumination timescales were 4 or 6 hours. After the illumination period had elapsed, the droplets of microbial culture were sampled. The droplet was sampled onto sterile calcium alginate swabs, which were then transferred aseptically to 5 ml of sterile 'Calgon' Ringer's solution, made up from stock tablets (Oxoid Ltd, Basingstoke UK). The swab and Ringer's solution was then vortexed vigorously for the shortest time until the swab tip fully disintegrated into the solution. The solutions were then serially diluted in phosphate buffered saline (PBS) made from stock tablets (Oxoid Ltd, Basingstoke UK). Serial dilutions were then plated out in duplicate (half-plates) onto suitable agar (Mannitol salt agar for *S. aureus* and MacConkey agar for *E. coli*). Agar plates were either made from bulk powder (Oxoid Ltd, Basingstoke UK), or were bought pre-poured (E&O Laboratories Ltd, Bonnybridge, UK). Inoculated plates were incubated aerobically face down at 37 °C overnight. After incubation a viable colony count was carried out, using the serial dilution with the most appropriate countable number of colonies (30 to 300). Calculations were then performed to scale up the viable colony count such that the number recovered from the sample could be determined.

3.2.7 Microbe Inactivation by Thin Films under a Typical Hospital Light

The methodology for this set of experiments was very similar to that carried out with the 365 nm light, the most obvious change being the use of a different light source. The light source chosen for this study was a General Electric 28W Biax™ 2D™ compact fluorescent lamp with a colour temperature of 4000K (cool white). [General Electric part no: F282DT5/840/4P]. This light source was chosen as it has the same characteristics as fluorescent lights used in hospitals in the United Kingdom[95]. The spectral profile of the lamp consists of peaks at approximately 405, 435, 495, 545, 588, and 610 nm. A spectral profile for the lamp (provided by General Electric) is shown in Figure 3.2. The design of the lamp tubes minimises output of ultraviolet radiation, with only a small proportion of UV A radiation being produced by the lamp[152]. The lamp's irradiance at a distance of 20 cm is less than 1×10^{-5} W/cm^2 (1×10^{-2} mW/cm^2) at a wavelength of 365 nm[152]. This is 40 times less than the sun's irradiance measured on a cloudy day which is of the order 0.4 mW/cm^2 (4×10^{-4} W/cm^2). Solar irradiance was measured using a Solarmeter Model 5.0 hand held solar meter, (Solartech Inc, Harrison Township, MI, USA), which has a wavelength response across the total UV region (280 – 400 nm), peaking at 365 nm.

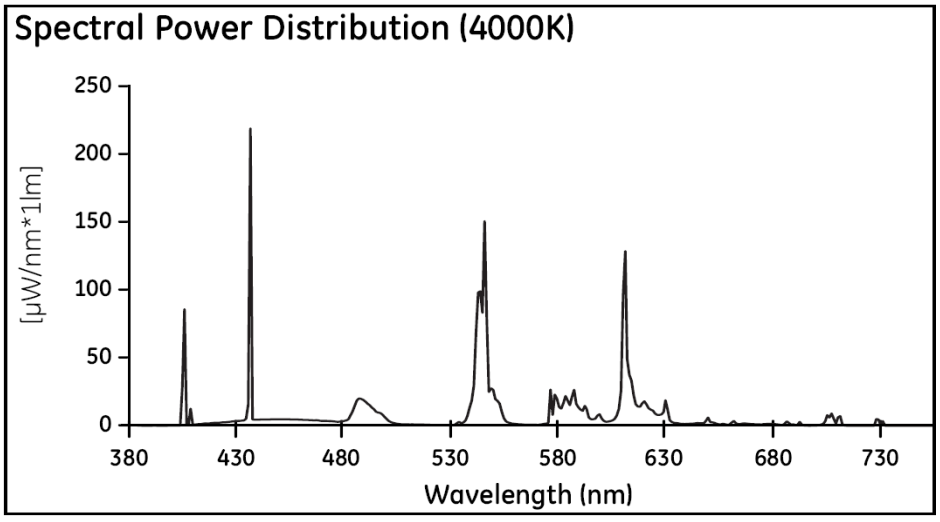

Figure 3.2 Spectral Power Distribution of General Electric 28W Biax™ 2D lamp[152]

Thin film samples were prepared for an experimental run in the same manner as seen previously, by firstly being decontaminated with a 70% v/v isopropanol

solution. Initial experiments showed that the first experiment in a week's run showed significantly lower effect than subsequent experiments carried out with the samples later in the week. This was assigned to the samples not being fully activated for the first experiment. To bypass this effect, a dummy run was performed in the beginning of a week's experiments, with an identical lighting cycle to a real experiment. This was especially important where films had been in the dark and unused over a weekend. A lighting cycle consists of the 30 minute pre-activation stage under the 254 nm light, followed by an 18 hour illumination by the compact fluorescent light source. A secondary experiment was performed in which the UV pre-irradiation step was substituted for a white-light pre-activation step lasting one week – this was intended to demonstrate practicality of the films in a situation where direct UV illumination would not occur.

Samples and controls were inoculated with 25 µl aliquots of a 1 in 1000 dilution of an overnight culture in Nutrient Broth (Oxoid Ltd, Basingstoke UK). Organisms chosen for the fluorescent light experiments were *Staphylococcus aureus* (NCTC 6571) and *Escherichia coli* (NCTC 10418). This dilution gives an initial inoculum of ca. 10^6 cfu/ml. Inoculated samples were then transferred to moisture chambers made from Petri dishes with moist filter paper in the base. For samples being exposed to the light source, a large square Petri dish was used. This enables all samples to be centred under the lamp in a region of more uniform luminosity. Dark controls were placed in an aluminium foil wrapped large square Petri dish, or in individual dark boxes to avoid exposure to light. The experiment was set up in a temperature controlled incubator (LMS Ltd, Sevenoaks UK), maintained at 22 °C. This was done because unlike the short time scale UV 365 nm experiments, some drying out of the inocula droplets was observed in initial experiments. This occurred despite the use of the moisture chambers. Using the temperature controlled incubator this effect was completely negated, plus the experiment was controlled at room temperature – the temperature at which these types of coatings might find widespread use. The distance from the lamp tube to the sample moisture chamber was 20 cm.

At the end of an exposure period, the sample droplets were sampled by sterile calcium alginate swab (Technical Service Consultants Ltd, Heywood UK) and transferred aseptically to 5 ml sterile 'Calgon' Ringers solution (Oxoid Ltd, Basingstoke UK). The solution plus swab tip was then vortexed vigorously to dissolve the swab. The resultant solution was serially diluted in tenfold steps, in sterile PBS solution made from stock tablets (Oxoid Ltd, Basingstoke UK). Serial dilutions were plated in duplicate onto growth media. Mannitol salt agar (Oxoid Ltd, Basingstoke UK) was used for *S. aureus* and MacConkey agar (Oxoid Ltd, Basingstoke UK) was used for *E. coli*. Inoculated plates were incubated face down at least over night at 37 °C. Viable colony counts were then performed using a colony counter on the diluted plate with the best countable number of colonies (between 30 and 300). The viable colony count data was then used to calculate the number of cfu in the original droplet sampled from the slides.

In order to test the materials with a secondary photo-deposited Ag layer, an alteration in experimental procedure was required. The samples were tested in two groups, one which did not have the secondary anneal step (pink looking samples) and one which had been annealed a second time (normal appearance samples). For the photo-deposited materials, a modification in the sample nomenclature is also required; this is described in Table 3.2. The additional samples and complication of the protocol is required because the addition of the $AgNO_3$ derived overlayer effectively adds a third variable to the experimental design, which must be accommodated by the use of further controls. This separates the variables of light, photocatalyst and $AgNO_3$ overlayer. The actual experimental protocol for these samples was unchanged, and the experiment was performed in the same manner as already described in this section. There are simply more samples under test, because of the requirement for further controls.

Nomenclature	Meaning
L+Ti+Ag+	*Sample in presence of light (L+) on a TiO_2 substrate (Ti+) coated with $AgNO_3$ photo-deposited layer (Ag+).*
L+Ti+Ag-	*Sample in presence of light (L+) on a TiO_2 substrate (Ti+) in the absence of an $AgNO_3$ photo-deposited layer (Ag-).*
L+Ti-Ag+	*Sample in presence of light (L+) on a glass substrate (Ti-) coated with $AgNO_3$ photo-deposited layer (Ag+).*
L+Ti-Ag-	*Sample in presence of light (L+) on a glass substrate (Ti-) in the absence of an $AgNO_3$ photo-deposited layer (Ag-).*
L-Ti+Ag+	*Sample in absence of light (L-) on a TiO_2 substrate (Ti+) coated with $AgNO_3$ photo-deposited layer (Ag+).*
L-Ti+Ag-	*Sample in absence of light (L+) on a TiO_2 substrate (Ti+) in the absence of an $AgNO_3$ photo-deposited layer (Ag-).*
L-Ti-Ag+	*Sample in absence of light (L+) on a glass substrate (Ti-) coated with $AgNO_3$ photo-deposited layer (Ag+).*
L-Ti-Ag-	*Sample in absence of light (L+) on a glass substrate (Ti-) in the absence of an $AgNO_3$ photo-deposited layer (Ag-).*

Table 3.2 Modified experimental nomenclature for samples with photo-deposited Ag.

3.3 Statistical Analysis of Data

Where possible to do so, the experimental data was subjected to statistical analysis. This was carried out with assistance from Aviva Petrie (Biostatistican, Eastman Dental Institute). The Mann-Whitney U-test (also known as Wilcoxon Rank Sums Test), was used. This is a non-parametric test, used to test the null hypothesis that the results from two independent samples come from the same population. The test is only valid if a significantly large population of data (more than 3 points) is used, so all experiments had a sufficient number of repeats. The null and alternative hypotheses for this study are outlined below:

The null (H_0) hypothesis: *"There is no difference between the antimicrobial activity of the thin film under test and that of the control material."*

The alternative (H_1) hypothesis: *"The test antimicrobial thin film reduces the viable colony count of microbes compared to the control material."*

The Mann-Whitney U may be calculated by hand by arranging the observations into a ranked series, independent of the sample from which the observations came. The ranks for each sample are then summed to give a sum of ranks for the sample. The U parameter is then calculated:

$$U_1 = R_1 - \frac{n_1(n_1+1)}{2}$$

Equation 3.1 The Mann-Whitney U test. R is the sum of ranks and n is the sample size.

U is then calculated in the same way for the other sample, and whichever yields the smallest value of U is compared to significance tables. It is however more convenient to use a statistical software package. Data was processed utilising SPSS V15.0.1.1 (SPSS Inc., Chicago, Illinois, USA) software. The output from the analysis includes various points of data, but it is the P value that is of interest. The P value of interest is the two tailed one (listed as Asymp. Sig. (2-tailed) in the SPSS output), because the data is two tailed. This is compared to set significance levels to test the null hypothesis:

P Value	Asterisk	Level of Significance
$P < 0.05$	*	Significant (5% level)
$P < 0.01$	**	Very Significant (1% level)
$P < 0.001$	***	Highly Significant (0.1% level)

Table 3.3 Statistical Significance Levels and the Asterisk System

If the P value is less than the significance levels listed above, the null hypothesis is rejected. This means that there is a statistically significant difference between the test material and the control material – i.e. the antimicrobial thin film is exerting an

effect. The asterisk system as outlined in Table 3.3 will be used throughout this chapter to indicate statistical significance of data.

3.4 Results

3.4.1 Residual Effect of the Decontamination Procedure on *S. aureus*

The pre-experimental decontamination procedure, described in Section 3.2.5, involved the use of 70% isopropanol as an antimicrobial and cleaning solvent. It was vital to ensure that this had no residual antimicrobial effect by itself. Consequently an experiment was carried out to assess this factor alone. The residual activity of commercially available alcohol Azowipes (Vernon Carus/Synergy Health plc, Swindon, UK) was also assessed in the same manner. The results from these experiments are shown in Figure 3.3 and Figure 3.4; which are compiled from multiple repeat experiments.

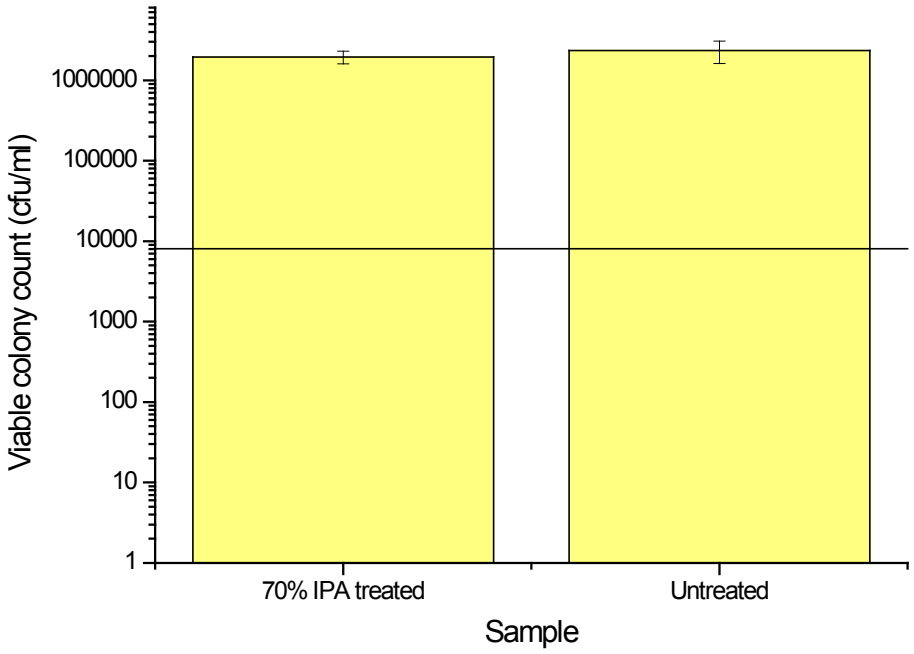

Figure 3.3 Residual microbicidal activity test of 70% IPA solution against a glass control. *S. aureus* NCTC 6571. Detection limit (8.04×10^3 cfu/ml) indicated by horizontal line.

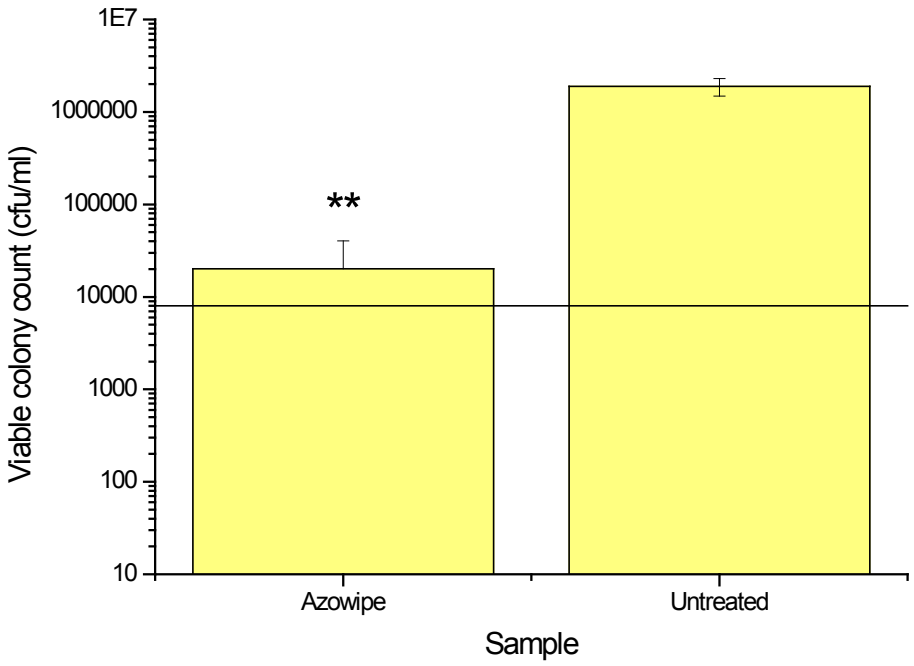

Figure 3.4 Residual microbicidal activity test of Azowipe against a glass control. *S. aureus* NCTC 6571. Detection limit ($8.04x10^3$ cfu/ml) indicated by horizontal line.

It can be seen that there is no statistically relevant residual antimicrobial activity resulting from the treatment of the substrates with 70% isopropanol solution. There is however a very significant (P = 0.01) residual activity when Azowipes are used. Since the alcohol in these wipes swiftly evaporates, the residual effect must be due to residues left behind after wiping (these residues can easily be seen with the naked eye). This is to the author's knowledge the first reported residual antimicrobial activity for Azowipes in the literature.

3.4.2 Ultraviolet Light (365 nm) Results

In this section, the microbicidal activity results obtained under the illumination of a 365 nm black light blue lamp are set out. Results are organised first by organism, then by the experimental conditions. Firstly the Gram positive organism *S. aureus* will be considered, followed by the Gram negative organism *E. coli*.

3.4.2.1 *Staphylococcus aureus* NCTC 6571

3.4.2.1.1 Four Hours Exposure Using a Neat Overnight Culture

This experiment was performed over a four hour illumination period, using a neat overnight culture. This undiluted overnight culture gives an initial inoculum of ca. 10^9 cfu/ml. The coatings tested in these experiments were those derived from a 10% Ag:Ti sol, a 2% W:Ti sol and a TiO_2 control.

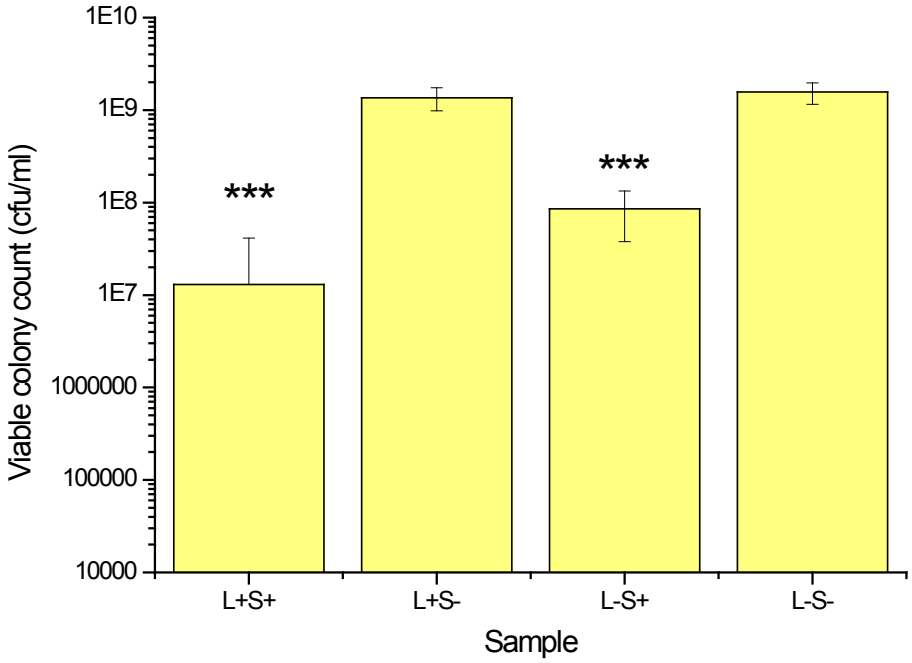

Figure 3.5 Four hour UV microbicidal activity of Ag_2O/TiO_2 sample from 10% Ag:Ti sol against *S. aureus* NCTC 6571 initial inoculum of ca 10^9 cfu/ml. Detection limit 8.04 x10^3 cfu/ml.

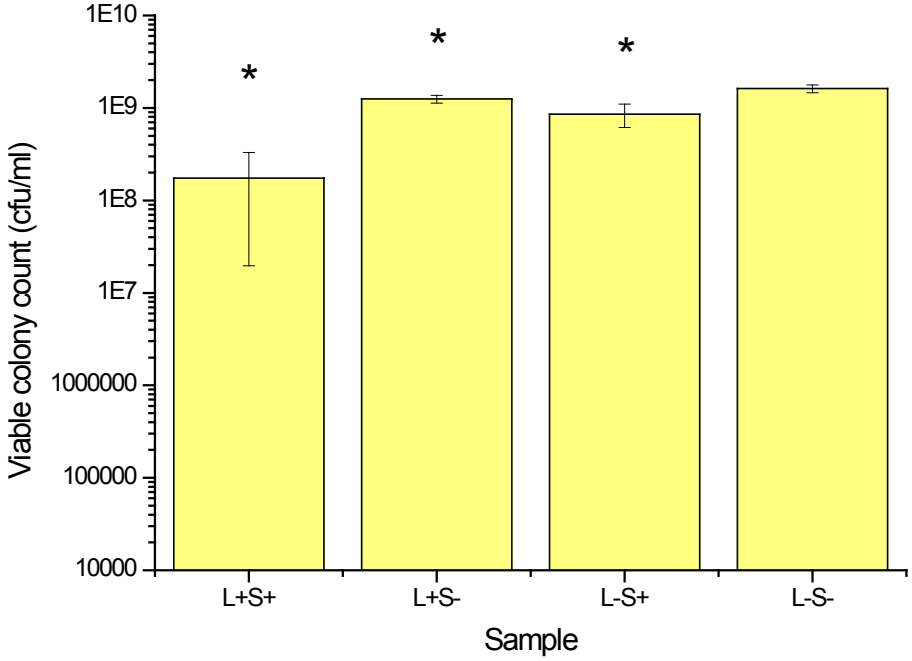

Figure 3.6 Four hour UV microbicidal activity of WO_3/TiO_2 sample from 2% W:Ti sol against *S. aureus* NCTC 6571 initial inoculum of ca 10^9 cfu/ml. Detection limit 8.04 x10^3 cfu/ml.

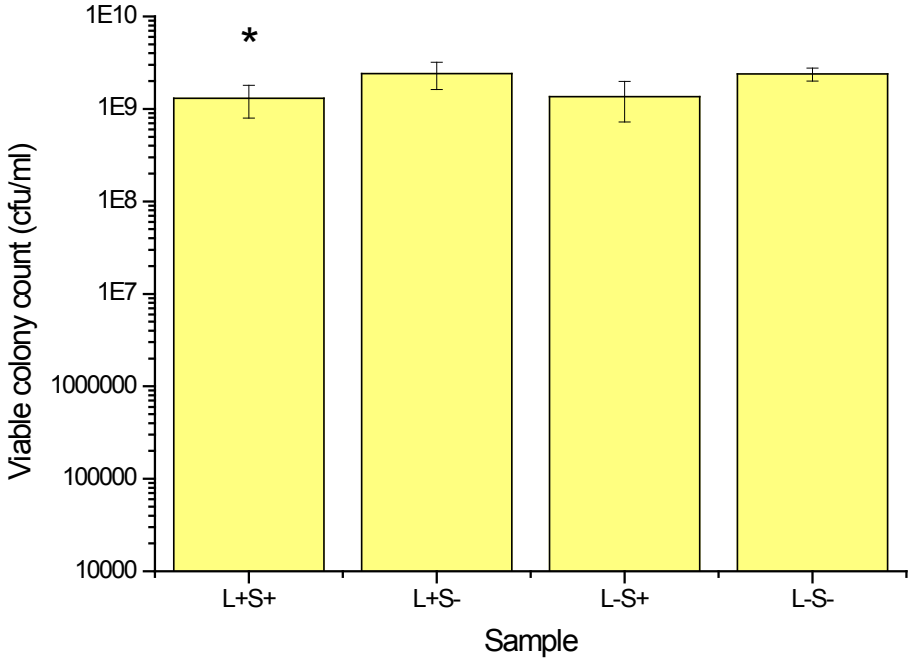

Figure 3.7 Four hour UV microbicidal activity of TiO_2 sample against *S. aureus* NCTC 6571 initial inoculum of ca 10^9 cfu/ml. Detection limit 8.04 x10^3 cfu/ml.

Of the three samples tested under these illumination conditions, the Ag_2O/TiO_2 material (Figure 3.5) demonstrated the greatest efficacy. Highly statistically significant kills were observed in conditions of illumination and darkness, with the greatest activity for an illuminated sample. The UV light by itself not demonstrating a kill. The WO_3/TiO_2 sample (Figure 3.6) showed statistically significant differences for all samples versus the control though the activity of the L+S-, and L-S+ samples is in reality not of consequence in comparison to that of the L+S+ sample. The TiO_2 sample (Figure 3.7) demonstrated the lowest efficacy of the three under test with these conditions, with a statistically significant kill observed for the L+S+ sample only – which is as expected.

3.4.2.1.2 Six Hours Exposure Using a One Hundred Fold Diluted Overnight Culture

This experiment was performed over a six hour illumination period, using an overnight culture which was diluted one hundred fold in sterile broth. This gives an initial inoculum of ca. 10^7 cfu/ml. The coating tested under these conditions was derived from a 10% Ag:Ti sol.

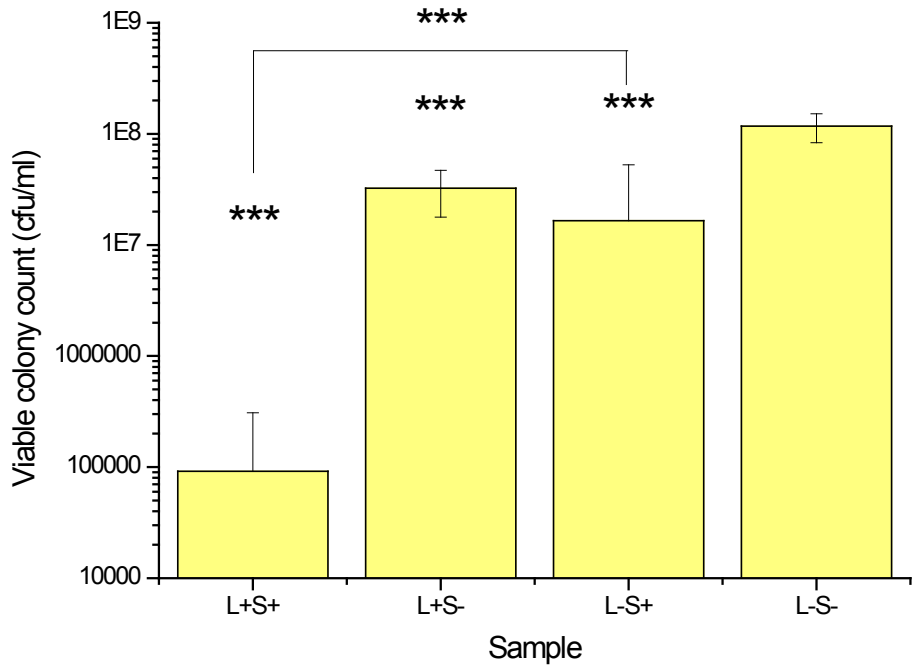

Figure 3.8 Six hour UV microbicidal activity of Ag_2O/TiO_2 sample against *S. aureus* NCTC 6571 initial inoculum of ca 10^7 cfu/ml. Detection limit 8.04 x10^3 cfu/ml.

In Figure 3.8 all samples demonstrated a highly significant difference from the L-S- control. However, in practice, one can see that it is the L+S+ sample which demonstrates a substantially higher activity than all others tested under these conditions. Effects from the light source and possible activity in the dark are apparent in the L+S- and L-S+ samples, this is perhaps observed because of the smaller inoculum size compared to the previous section, but is of less importance than the observed activity of the L+S+ sample. Notably, there is a highly significant statistical difference between the L+S+ and L-S+ samples, which reinforces the notion that the material's antimicrobial action is predominantly light-activated.

3.4.2.1.3 Six Hours Exposure Using a Ten Thousand Fold Diluted Overnight Culture

This experiment was performed over a six hour illumination period, using an overnight culture diluted by a ten thousand fold dilution factor in sterile broth – giving an initial inoculum of ca. 10^4 cfu/ml. The coating tested was derived from a 10% Ag:Ti sol.

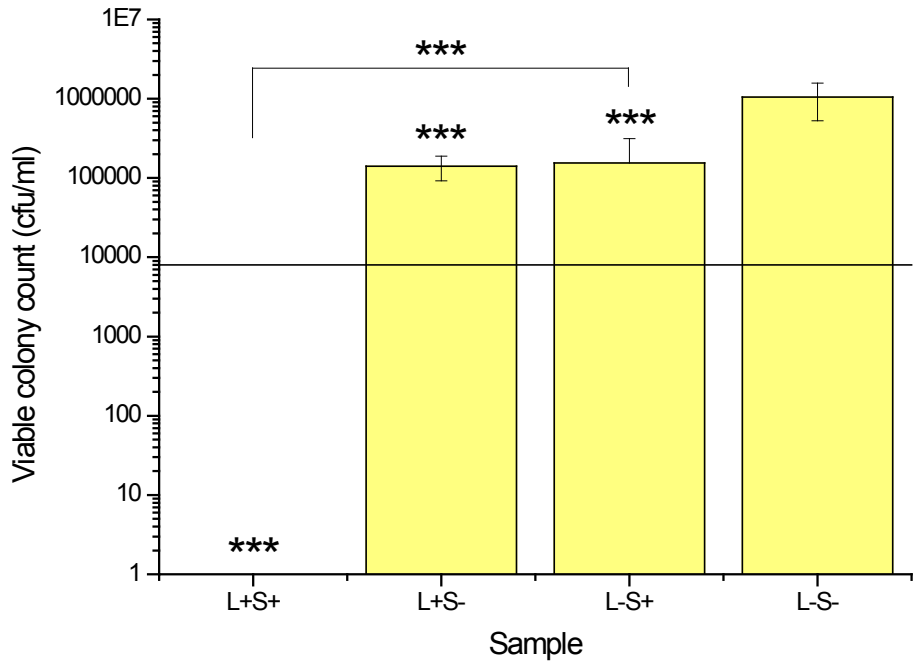

Figure 3.9 Six hour UV microbicidal activity of Ag_2O/TiO_2 sample against *S. aureus* NCTC 6571 initial inoculum of ca 10^4 cfu/ml. Detection limit ($8.04x10^3$ cfu/ml) indicated by horizontal line.

The results in Figure 3.9 bear a similarity to those from the previous experimental conditions (Figure 3.8). There is a highly significant difference for all samples, compared to the control, but the level of kill observed for the L+S- and L-S+ samples is much lower than the L+S+ sample, which has recorded a viable colony count below the experimental detection limit. As with the previously presented data, there is some demonstration of light related killing and dark kill, most probably apparent due to the substantially smaller inoculum. This experiment clearly demonstrates the light-activated nature of these antimicrobial materials, with the light activated L+S+ sample being highly statistically different from the non light-activated (L-S+) one.

3.4.2.2 *Escherichia coli* NCTC 10418

3.4.2.2.1 Six Hours Exposure Using an Undiluted Overnight Culture

This experiment was performed over a six hour illumination period, using an undiluted overnight culture – giving an initial inoculum of ca. 10^9 cfu/ml. The coating tested was derived from a 10% Ag:Ti sol.

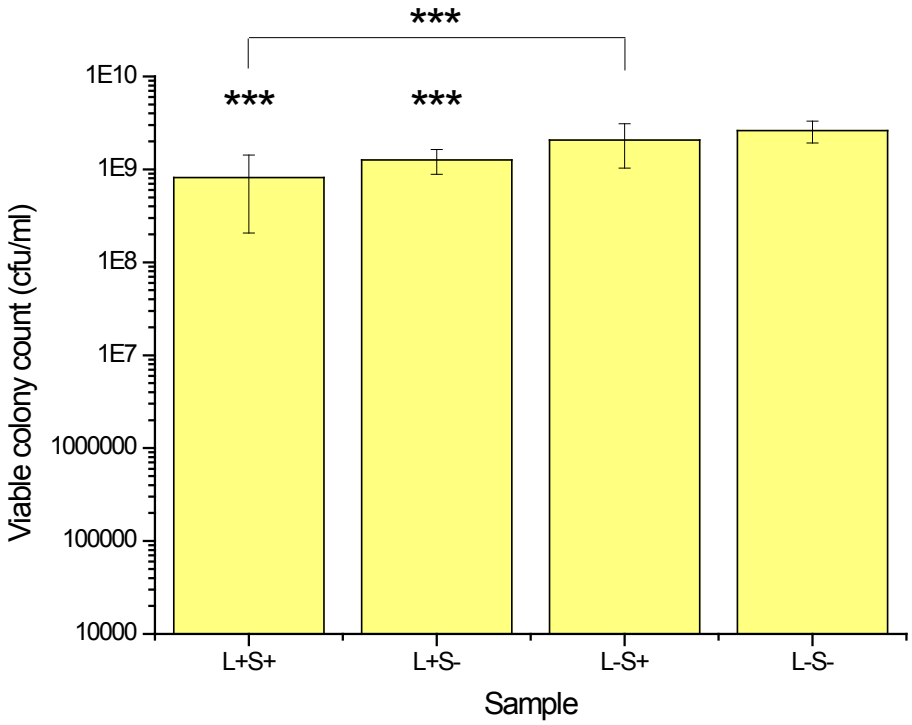

Figure 3.10 Six hour UV microbicidal activity of Ag_2O/TiO_2 sample against *E. coli* NCTC 10418 initial inoculum of ca 10^9 cfu/ml. Detection limit 8.04 x10^3 cfu/ml.

Figure 3.10 demonstrates the relative resilience of a Gram-negative organism to the photocatalyst antimicrobial, compared with that of a Gram-positive. It is essentially the same experiment as the results reported in 3.4.2.1.1 for *S. aureus*, but with a 2 hour longer illumination time, by the same lamp. Whilst highly statistically significant kills are observed for the L+S+ and the L+S- samples, they are significantly lower in magnitude than the kills observed for *S. aureus*. This is a direct result of the differing cell envelope morphologies, and the greater impedance to hydroxyl radicals imposed by the Gram-negative wall, compared to the Gram-positive - as has been observed previously.[127] Whilst not necessarily obvious from the graph, there is a highly significant statistical difference between the L+S+ and L-S+ samples, again reinforcing the constant theme of the light activation of these materials.

3.4.3 Hospital Compact Fluorescent Light Results

In this section, the microbicidal activity results obtained under the illumination of a standard hospital compact fluorescent lamp are set out. Results are organised first by organism, then by the experimental conditions. The organisms tested were

firstly the Gram-positive microbe *S. aureus* NCTC 6571 and secondly, the Gram-negative microbe *E. coli* NCTC 10418.

3.4.3.1 *Staphylococcus aureus* NCTC 6571

3.4.3.1.1 UV 254 nm Pre-activation, 18 hours Compact Fluorescent Illumination

This lighting scheme was examined for the TiO_2 control material, one of the Ag_2O doped materials, prepared from a sol with a 10% Ag:Ti ratio and a WO_3/TiO_2 material prepared form a sol with 2% W:Ti ratio. The initial inoculum was of the order 10^6 cfu/ml.

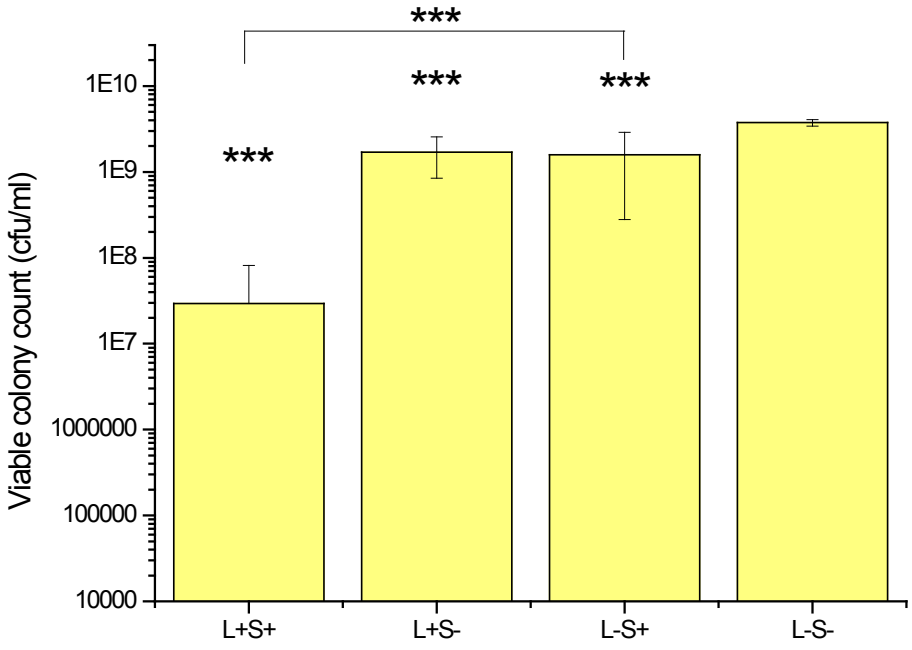

Figure 3.11 Antimicrobial activities against *S. aureus* of TiO_2 thin film coating following a 254 nm pre-activation scheme, followed by 18 hours compact fluorescent illumination. Detection limit 8.04 x10^3 cfu/ml.

Figure 3.11 shows highly statistically significant kills for all samples under the experimental conditions. Notably, the L+S+ sample has the greatest recorded kill. The L+S- and L-S+ samples demonstrate a similar reduction in numbers. In comparing the L+S+ and L-S+ samples, there is statistically a highly significant difference between the samples. This reinforces the light-activated nature of the TiO_2 material as an antimicrobial since the data is shown to come from two different distributions (TiO_2 illuminated and TiO_2 in the dark).

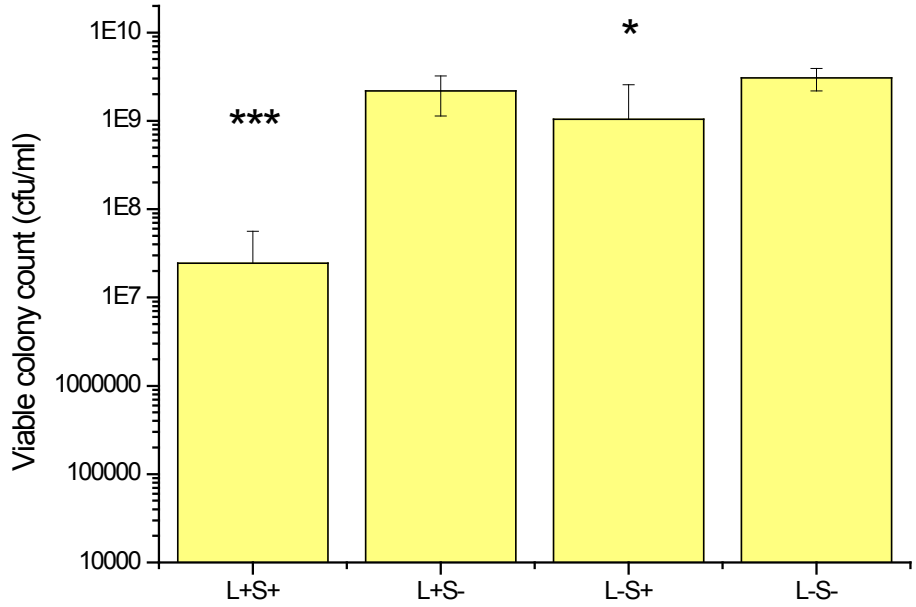

Figure 3.12 Antimicrobial activities against *S. aureus* of Ag_2O/TiO_2 thin film coating following a 254 nm pre-activation scheme, followed by 18 hours compact fluorescent illumination. Detection limit 8.04 x10^3 cfu/ml.

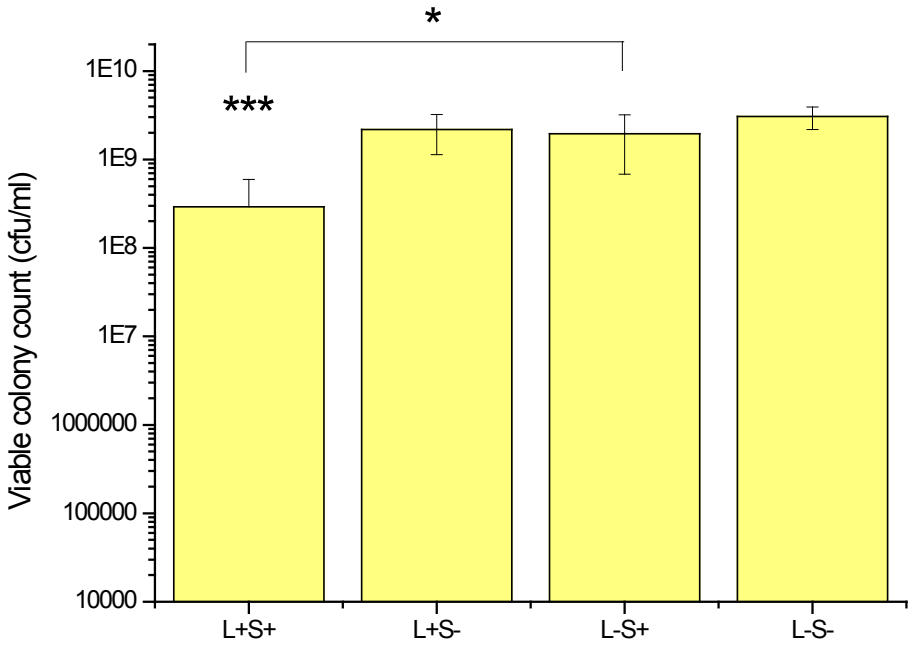

Figure 3.13 Antimicrobial activities against *S. aureus* of WO_3/TiO_2 thin film coating following a 254 nm pre-activation scheme, followed by 18 hours compact fluorescent illumination. Detection limit 8.04 x10^3 cfu/ml.

Figure 3.12 and Figure 3.13 again demonstrate highly statistically significant kills for the L+S+ samples under the experimental conditions. Figure 3.13 reinforces the notion of light-activated antimicrobial behaviour, whilst Figure 3.12 suggests a possible killing mechanism in the dark for the Ag_2O/TiO_2 material, with a small,

albeit statistically significant kill measured. This is supported by the confirmation of the null hypothesis when comparing the Ag_2O/TiO_2 L+S+ and L-S+ data – suggesting they are from the same distribution, and that light-activated behaviour is not being observed under these experimental conditions.

3.4.3.1.2 Compact Fluorescent Pre-activation, Compact Fluorescent Illumination

This lighting scheme was examined for the TiO_2 control material, coupled with one of the Ag_2O doped materials, prepared from a sol with a 10% Ag:Ti ratio. The initial inoculum was of the order 10^6 cfu/ml.

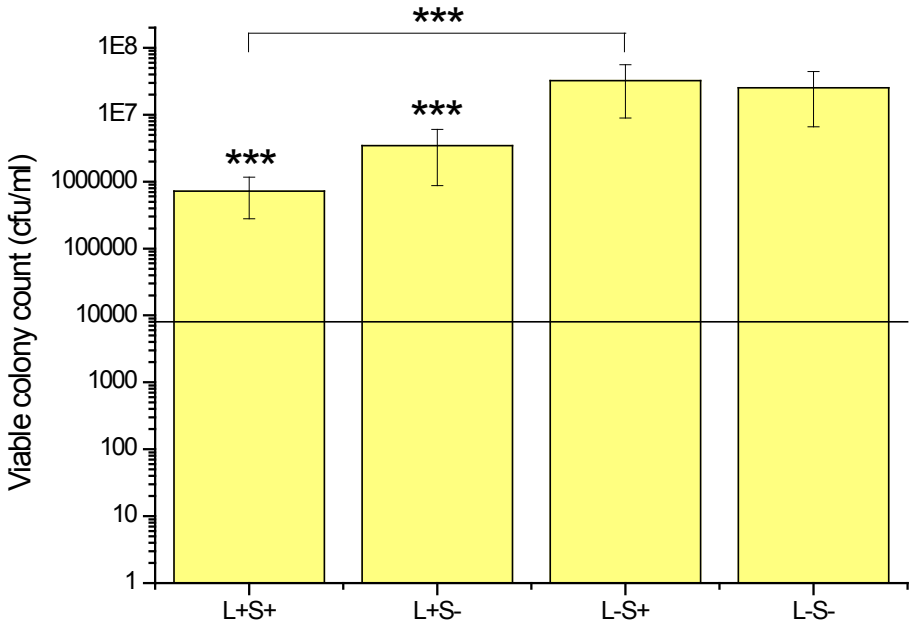

Figure 3.14 Antimicrobial activities against *S. aureus* of TiO_2 thin film coating following a week's compact fluorescent pre-activation scheme, followed by 18 hours compact fluorescent illumination. Detection limit ($8.04x10^3$ cfu/ml) indicated by horizontal line.

The data presented in Figure 3.14 highlights highly statistically significant kills for the TiO_2 L+S+ and L+S- samples, but with the L+S+ having the greater effect. Whilst the light by itself is exerting an effect, the light-activated coating outperforms it. There is a highly significant difference between the L+S+ and L-S+ samples, which demonstrates the light-activated nature of the TiO_2 antimicrobial.

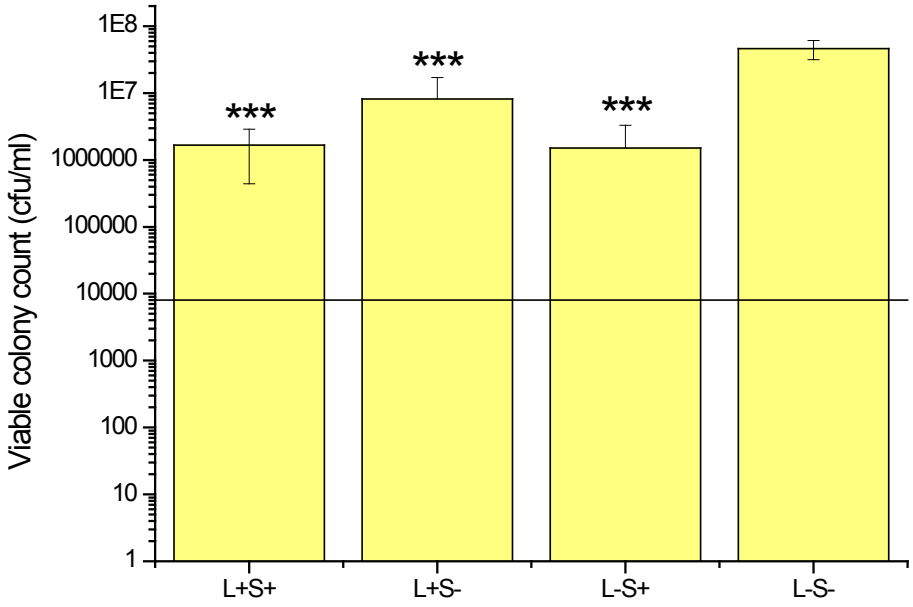

Figure 3.15 Antimicrobial activities against *S. aureus* of Ag_2O/TiO_2 thin film coating following a week's compact fluorescent pre-activation scheme, followed by 18 hours compact fluorescent illumination. Detection limit ($8.04x10^3$ cfu/ml) indicated by horizontal line.

Figure 3.15 presents a highly statistically significant reduction in microbial numbers for the L+S+, L+S- and L-S+ samples. This shows firstly that the light source is having some effect (as it did in Figure 3.14), though this is lower than the effect of the Ag_2O/TiO_2 coating. In common with the data presented in Figure 3.12 the null hypothesis is confirmed for the L+S+ and L-S+ samples, suggesting that the reduction in microbial numbers is due to an effect other than illumination of the sample.

3.4.3.1.3 Survey of Potential Ag-ion Release Mechanism

The results and statistical analysis of the data shown in Figure 3.12 and Figure 3.15 suggest the possibility of a synergistic antimicrobial mechanism, comprising of photocatalysis and a possible Ag ion-release – since the L-S+ sample for the Ag_2O/TiO_2 demonstrates a measured kill, in comparison to the TiO_2 control, which is essentially inert in conditions of darkness. To assess the potential of this, an experiment was carried out with samples which had been kept in the dark since manufacture. One set were then pre-irradiated by the compact fluorescent lamp for a week, and the other set kept in the dark for a week. Samples were then inoculated with a ca 10^6 cfu/ml dilution of *S. aureus* in nutrient broth and placed in

the temperature controlled cabinet for an 18 hour experimental period, with the light source *off*. The results of this experiment are shown in Figure 3.16.

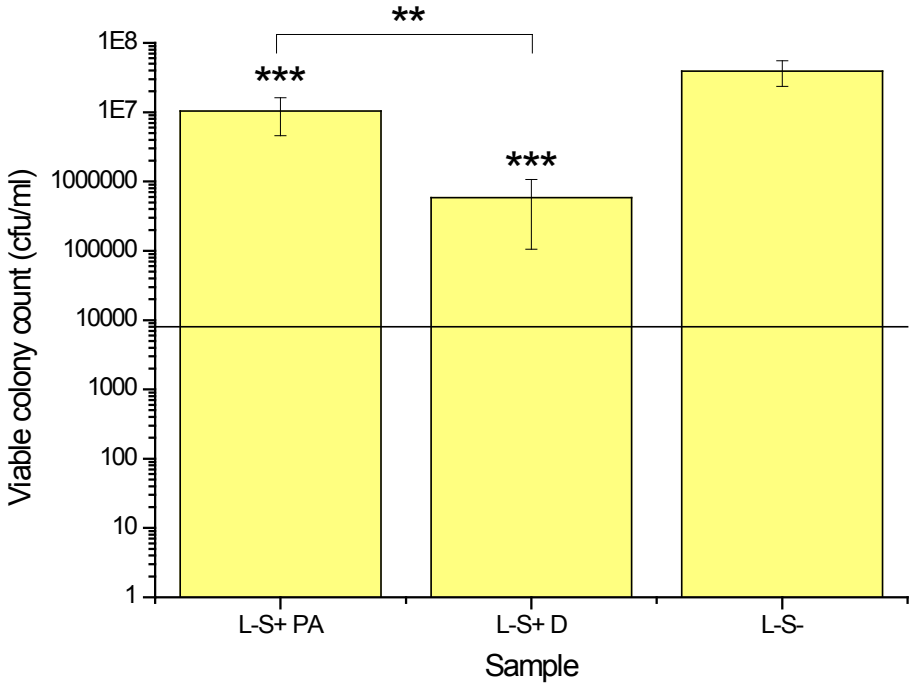

Figure 3.16 Antimicrobial effect of white light pre-activated (PA) and dark (D) Ag_2O/TiO_2 samples against *S. aureus*. Experimental duration 18 hours. Detection limit ($8.04x10^3$ cfu/ml) indicated by horizontal line.

Figure 3.16 demonstrates some interesting findings. A highly significant statistical difference was highlighted between both test materials and the glass control – which shows that killing in the dark can occur for some of the Ag_2O/TiO_2 materials under certain experimental conditions. It should also be noted that there is a moderately significant difference between the test samples themselves. This indicates that the way in which the samples are pre-activated can change their mechanism of performance markedly. By pre-irradiating samples for a prolonged period, their activity in the dark was reduced by a significant amount, in comparison to the "as made" samples.

3.4.3.2 *Escherichia coli* NCTC 10418

3.4.3.2.1 UV 254 nm Pre-activation, 18 hours Compact Fluorescent Illumination

This lighting scheme was examined for the TiO_2 control material, coupled with one of the Ag_2O doped materials, prepared from a sol with a 10% Ag:Ti ratio. The results for this study are shown in Figure 3.17. The study was also extended to the material composed of a TiO_2 baselayer, with a photo-deposited overlayer of Ag, this data is shown in Figure 3.18 to Figure 3.19.

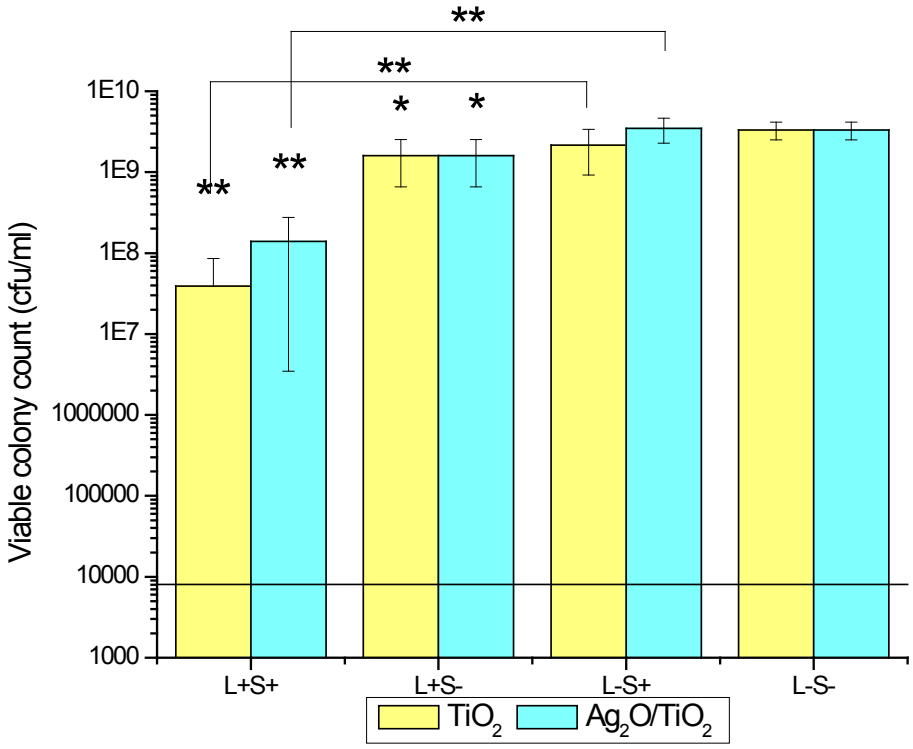

Figure 3.17 Antimicrobial activities against *E. coli* of TiO_2 and Ag_2O/TiO_2 thin film coatings following a 254 nm pre-activation scheme, followed by 18 hours compact fluorescent illumination. Detection limit ($8.04x10^3$ cfu/ml) indicated by horizontal line.

Figure 3.17 demonstrates statistically significant reductions in microbial numbers for both the materials, and also, as previously, shows a small degree of effect due to the light source alone, though this is essentially insignificant compared to the activity of the test materials. There is also a significant difference between the L+S+ and L-S+ samples for both materials, again reinforcing the idea of light-activated antimicrobial behaviour. Unlike the equivalent experiments for *S. aureus* (Figure

3.11 and Figure 3.12) there is no suggestion of antimicrobial activity in the dark for the Ag_2O/TiO_2 material – though it was not particularly high activity in any case and *E. coli* is likely more resilient due to its cell envelope morphology compared to *S. aureus*.

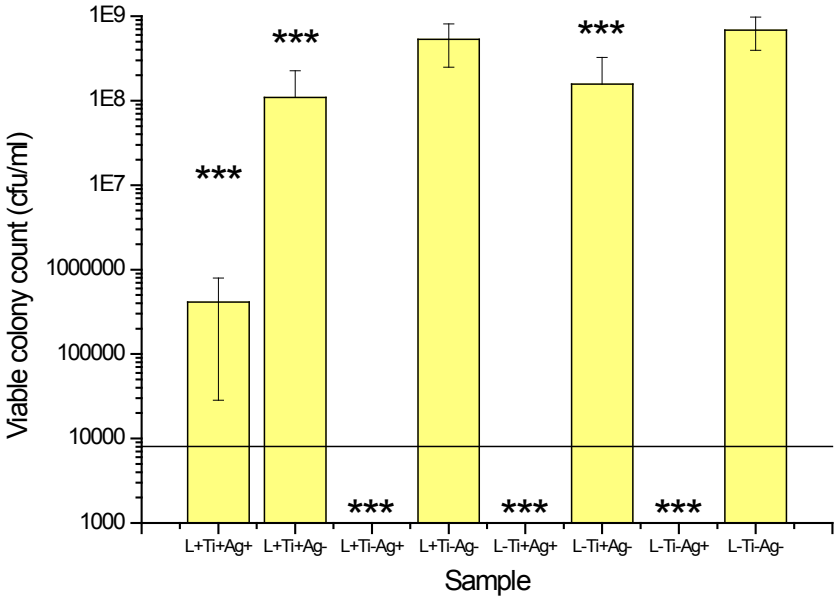

Figure 3.18 Microbicidal activities against *E. coli* of the photo-deposited $AgNO_3$ coatings, which *were not* annealed a second time. Detection limit ($8.04x10^3$ cfu/ml) indicated by horizontal line.

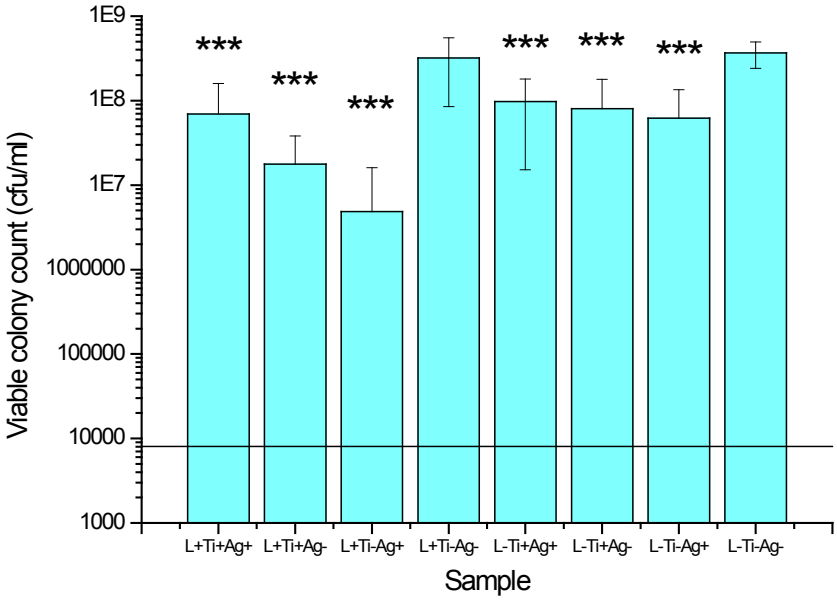

Figure 3.19 Microbicidal activities against *E. coli* of the photo-deposited $AgNO_3$ coatings, which *were* annealed a second time. Detection limit ($8.04x10^3$ cfu/ml) indicated by horizontal line.

Figure 3.18 and Figure 3.19 demonstrate the true effect of the presence of Ag, and the antimicrobial activity of Ag – notably the highly statistically significant antimicrobial efficacy of all samples having the photodeposited Ag overlayer. In particular, the non-secondary annealed samples (Figure 3.18) have a count below the detection limit for all non-irradiated Ag overlayer materials. This is unlike any other result obtained in this study and demonstrates a distinct mechanism from any possible photo-activated behaviour. This will be discussed further in Section 3.5.4.3.

3.4.3.2.2 Compact Fluorescent Pre-activation, Compact Fluorescent Illumination

In order to examine the potential function of the materials in the absence of a direct source of UV light, the coatings were also tested without the use of a UV light source. This compact fluorescent lighting scheme was examined for the TiO_2 control material, coupled with one of the Ag_2O doped materials, prepared from a sol with a 10% Ag:Ti ratio. The results are given in Figure 3.20.

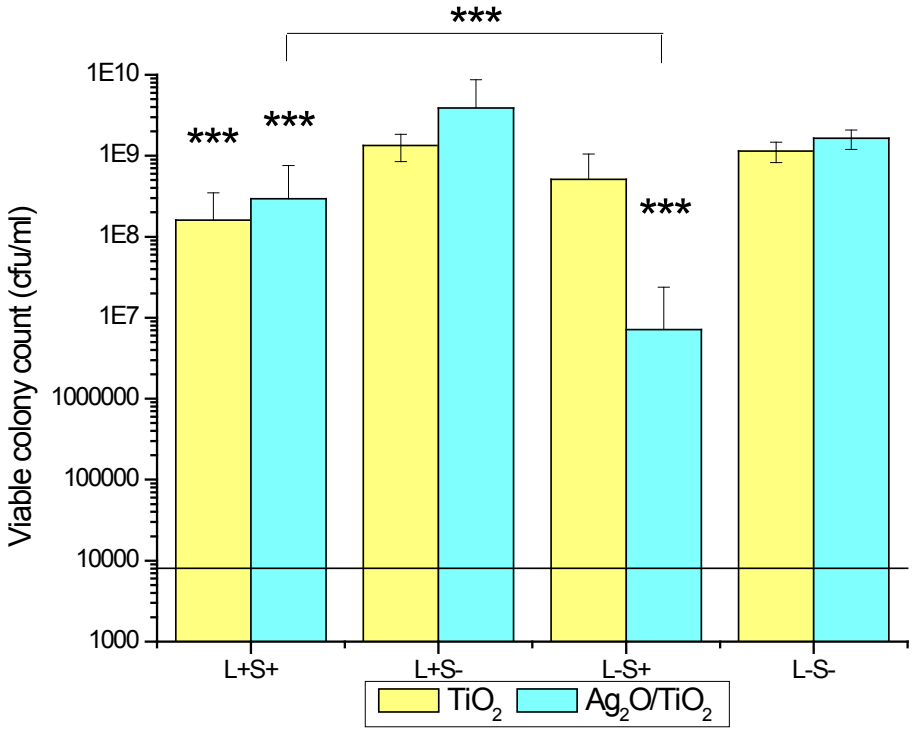

Figure 3.20 Antimicrobial activities against *E. coli* of TiO_2 and Ag_2O/TiO_2 thin film coatings following a week's compact fluorescent pre-activation scheme, followed by 18 hours compact fluorescent illumination. Detection limit ($8.04x10^3$ cfu/ml) indicated by horizontal line.

Figure 3.20 demonstrates highly statistically significant reductions in microbial numbers for both material types under illumination (L+S+). The Ag_2O/TiO_2 material also demonstrates a highly significant kill in the dark – which is shown to be distinct from the activity in the light. This perhaps shows two potential mechanisms at work, light-activated behaviour in L+S+ case and Ag ion release in the L-S+ case.

3.5 Discussion

3.5.1 Sample Re-Use

Throughout the process by which the experimental procedures were refined it was shown that samples could be re-used multiple times. The robustness and the easy clean nature of the materials meant that after repeated uses there was no loss of the activity of the coatings. This suggests the surfaces do not become fouled with debris over prolonged use, and makes the tested materials ideal candidates for real world use, where continued efficacy and robustness are pre-requisite characteristics for an antimicrobial surface coating. Throughout the work care was taken that no sample was given preference for re-use in later experiments. In effect the samples were randomised and at no time was it known what a given sample had been used for in a previous test.

3.5.2 Decontamination Procedure

The pre-experimental decontamination procedure was examined to test for any residual antimicrobial activity resulting from the decontamination step alone. Both a commercially prepared decontamination technique (Azowipes) and a laboratory prepared 70% v/v isopropanol solution in distilled water were tested. It was important to carry this experiment out, so that one can be sure that any observed antimicrobial effect is exerted solely by the material under test, and not by the pre-experiment decontamination. As can be seen in the data (Figure 3.3 and Figure 3.4) this experiment was very worthwhile. The laboratory prepared 70% v/v isopropanol solution demonstrated no significant residual antimicrobial activity. On the other hand, the Azowipe treated samples exhibited a significant residual microbicidal activity. The reduction in the viable colony count when Azowipes were

used was of the order of 2 log units after 4 hours exposure to the treated surface and was statistically very significant (P = 0.01). Whilst the more immediate antimicrobial efficacy of disinfectant wipes (including alcohol based ones) has been reported[153-155], it was not possible to find any mention of this kind of residual antimicrobial activity for alcohol based wipes in the literature. As such this is a novel finding in itself. As a consequence of this finding, for the purposes of the experiments carried out in this study, 70% v/v isopropanol was utilised to decontaminate samples prior to an experiment. The use of Azowipes to decontaminate samples is not advisable for these experiments or any similar studies but the demonstration of their residual efficacy after application is an interesting finding, which provides some positive support for their use in clinical situations.

3.5.3 Microbe Inactivation by Thin Films Under 365 nm Light

Photoactivated thin films are traditionally studied using an ultraviolet light source, because the band gap energies of these materials typically lie within the ultraviolet region of the spectrum. The typical ultraviolet lamps of choice for these studies are the 254 nm (germicidal) and the 365 nm (black light) lamps. The 254 nm lamp is not really suitable to use for antimicrobial testing applications because, as the "germicidal" name suggests, the wavelength of light from these lamps is sufficient to effectively kill microbes. The 365 nm lamp, whilst still having a degree of antimicrobial effectiveness, is less potent to microbes, and so is the lamp of choice when illumination of a photocatalyst with microbes in place is required. Hence, in the ultraviolet light experiments carried out in this study, the pre-activation of the films was carried out using the most energetic light source (the 254 nm lamp), but the part of the experiment with microbes present, was carried out with the less energetic (365 nm) light source. The initial experiments (Figure 3.5 to Figure 3.7 and Figure 3.10) used a 4 hour exposure time (*S. aureus*) and a 6 hour exposure time (*E. coli*) along with an inoculum taken from a neat overnight culture. The different coating materials performed to different levels of effectiveness under these conditions. The most striking result was a kill of approximately 3 log units for

the Ag_2O/TiO_2 material against *S. aureus* (Figure 3.5). All of the other materials demonstrated a limited effectiveness, but did nonetheless exhibit antimicrobial activity, albeit to a much lower degree. Notably, a TiO_2 control film was surprisingly only 49% effective against the undiluted (ca. 10^9 cfu/ml) inoculum (Figure 3.7). As has been observed before[127], *E. coli* was significantly more resilient to the antimicrobial effect of the photocatalyst films than *S. aureus* – most probably a result of the differing cell envelope permeability to the hydroxyl radical.

As a result of the relative performances in these preliminary experiments, the Ag_2O/TiO_2 coating was examined in more detail with further experiments. These experiments, with diluted inocula of 10^7 and 10^4 cfu/ml and a longer, six hour illumination period are shown in Figure 3.8 and Figure 3.9. These experiments show that with a lower inoculum, of a level closer to, but still much greater than typical surface contamination, the material functions more effectively. With the lowest inoculum, the viable colony count recovered was essentially zero (i.e. below the detection limit of the experiment). In the case of the 10^7 cfu/ml inoculum, a 2 log unit reduction in viable colony count was recorded. Whilst one might say that this result is worse than the undiluted case, where a 3 log kill was observed, it must be taken into account the fact that the inoculum was presented in broth, rather than a non culture medium such as PBS. Over the extended time span of the experiment one might expect some re-growth of the culture. This is indeed observed in the L-S- case in both Figure 3.8 and Figure 3.9. However, the active (L+S+) sample has repressed the re-growth, and has reduced microbial numbers, which is more than was observed in the non-diluted case (Figure 3.5), as the culture had reached steady state at 10^9 cfu/ml. The experiment with the 10^4 cfu/ml inoculum (Figure 3.9) also experienced re-growth to approximately 10^6 cfu/ml over the six hours, but notably the active (L+S+) sample inactivated the initial inoculum and completely repressed any re-growth. This clearly demonstrates that the material might be a viable method for disinfection of surfaces, where the level of contamination is much lower than the inoculum tested here. However, this is still dependent upon the UV illumination of the sample, so further experiments using a

typical hospital light source were carried out. The results for these are discussed in the following section.

Statistical analysis of the data revealed some interesting points, not necessarily obvious from direct observation of the graphs plotted. In particular, the light-activated nature of the Ag_2O/TiO_2 material was demonstrated because the null hypothesis could not be accepted, the asymptotic sigma value being greater than the significance levels set out in Section 3.3. The materials do not demonstrate very potent activity in the dark and on the whole, in conjunction with the statistical data it is acceptable to conclude that the materials are principally light-activated with minimal/negligible activity in the dark.

3.5.4 Microbe Inactivation by Thin Films Under a Typical Compact Fluorescent Light as Used in UK Hospitals

Whilst it is relatively simple to demonstrate antimicrobial activity using UV illuminated photocatalyst thin films – as discussed in Section 3.5.3, performing these experiments under typical lighting conditions is carried out far less frequently. Data from these kinds of experiments is far more interesting and relevant to real world applications, because typically these photocatalyst films would not receive a particularly high dose of UV radiation in real world use. Only a very small amount of UV light is emitted by lighting systems – indeed they are typically designed so as not to emit UV radiation in any substantial quantity.[152] By testing the films under a typical light source, as used in UK hospitals, one can begin to assess the potential benefit of these photocatalyst films in a clinical situation. Experiments were performed both with and without pre-irradiation by UV lamp, to demonstrate how the film might function when used in an environment where direct UV illumination would not occur.

3.5.4.1 Inactivation of *S. aureus* Under a Compact Fluorescent Light

The compact fluorescent experiments for *S. aureus* were carried out with 2 different pre-activation types, one using the 254 nm UV lamp to pre-activate and the other using a compact fluorescent lamp to pre-activate. The samples tested

under these conditions were the TiO_2 control, a Ag_2O/TiO_2 thin film and a WO_3/TiO_2 material.

All of the test samples demonstrated antimicrobial activity, in both types of illumination conditions, though to varied degrees. In all cases some re-growth was observed due to the duration of the experiments, coupled with carrying out the experiment in broth, rather than a non-growth medium, such as PBS. Attempts were made to carry out the experiments in PBS, but inconsistent results were obtained. In the UV pre-activated case (Figure 3.11 and Figure 3.12) the antimicrobial activities of both TiO_2 and Ag_2O/TiO_2 appear comparable, with no significant variation between them. In the white light pre-activated case (Figure 3.14 and Figure 3.15) again TiO_2 and Ag_2O/TiO_2 are comparable; the only significant difference between the two arising in the non-illuminated (L-S+) case, where the Ag_2O/TiO_2 sample outperforms the TiO_2 control. Statistical analysis of the data shows the kills recorded were significant. Most interestingly, an analysis of the L+S+ and L-S+ data showed that the TiO_2 and WO_3/TiO_2 materials were light-activated (null hypothesis rejected) and the Ag_2O/TiO_2 material was not. The null hypothesis could not be rejected and the data appears to come from the same distribution. Hence the observed kill must be due to a factor common to the Ag_2O/TiO_2 L+S+ and L-S+ samples – i.e. the coating itself.

Whilst the white light pre-activated samples are not as potent as those pre-activated by UV, these experiments show that even without exposure to a UV light source, the coatings are able to function as antimicrobials. This is a demonstration of their potential for real-world use, where direct illumination by any significant amount of UV light is negligible. Statistical analysis of the data showed that recorded kills were statistically significant. It was shown that the TiO_2 material was light-activated, with no activity in the dark. Once again, for the Ag_2O/TiO_2 material it was not possible to reject the null hypothesis and hence the possibility of a common, non light-activated mechanism must be considered.

The possibility of a non light-activated mechanism for the Ag_2O/TiO_2 materials under compact fluorescent illumination was examined by studying samples which

were not exposed to any light whatsoever, in comparison to samples which underwent the standard illumination cycle. The results for this study, shown in Figure 3.16, highlight a clear difference between the samples which were pre-activated and then kept in the dark for the experiment and those which were kept in the dark the entire time. The samples kept in the dark for the entirety of the study were more antimicrobially active, which suggests that 1) a possible Ag ion-release mechanism is present, since a photocatalyst film cannot be active if it has not been exposed to light at all (as evidenced by numerous TiO_2 L-S+ samples presented here) and 2) pre-activation, whilst preparing the sample for photocatalysis, deactivates to some degree the secondary antimicrobial mechanism, if indeed this is an Ag ion release.

3.5.4.2 Inactivation of *E. coli* Under a Compact Fluorescent Light

Compact fluorescent experiments were also carried out in the same manner as discussed above, for the Gram negative organism, *E. coli*. The results for these parts of the study are given in Figure 3.17 and Figure 3.20. Once again, the test samples of TiO_2 and Ag_2O/TiO_2 demonstrated antimicrobial activity. As was observed in the *S. aureus* experiments, some degree of microbial re-growth occurred over the course of the experiments. This is due to the long experimental duration and carrying out the experiments in a culture medium. In the case of the UV pre-irradiated samples, Figure 3.17, one can see comparable activity (within experimental error limits) for both film types. Statistical analysis of the data showed that recorded kills were significant, and that for both the samples the mechanism of kill was light-activated. This differs from the results with *S. aureus*, in which only the TiO_2 sample demonstrated light-activated behaviour. Exactly why this should be the case is unclear. With the compact fluorescent pre-activation experiment (Figure 3.20), a different pattern emerges – the samples are again comparable, within experimental limits, except for the L-S+ case, where the Ag_2O/TiO_2 sample is far superior to the TiO_2 control (demonstrates a 3 log kill). Statistical analysis shows a significant difference between the L+S+ and the L-S+ samples, with the L-S+ having the greater kill – hence it is material specific. The same trend was observed in the experiments with *S. aureus* (Figure 3.14) though to

a lesser extent. This highlights once again the apparent action of an antimicrobial agent, most probably the Ag ion, in the case of a sample kept in the dark. The illumination of a sample appears to retard this effect, perhaps by providing reducing electrons from the photocatalyst which prevent silver from being present as the antimicrobially active form of Ag+. The difference between the kill observed for *E. coli* and *S. aureus* is most likely due to the differing cell envelope morphology.

3.5.4.3 Compact Fluorescent Illumination of TiO_2 Overlayered with Ag (Tested with *E. coli*)

The results from the photo-deposited coatings are very interesting, and so will be discussed here separately. The materials which have been annealed a second time (Figure 3.19) display very different properties towards the test microbes than their non-annealed counterparts (Figure 3.18). One can clearly see the marked difference in antimicrobial performance – notably the non-annealed samples always outperform the annealed ones when Ag is present (i.e. all Ag+ samples). For samples where Ag is not present, the performance of the samples is comparable. In one case performance is slightly improved by the secondary anneal (sample L+Ti+Ag-). This modest increase in performance is most likely due to improved crystallinity and increased anatase character resulting from the second anneal.

The second pattern to notice in the data is in the non-annealed samples (shown in Figure 3.18). There is a distinct difference between the illuminated and non illuminated samples with the Ag overlayer. The samples without the overlayer perform similarly, regardless of the illumination. The Ag overlayer samples in the dark worked with 100% efficacy (this is effectively a count at or below the experimental detection limit), regardless of the substrate upon which they were deposited. However, their illuminated counterparts were significantly less effective. The L+Ti+Ag+ sample was less effective than the L+Ti-Ag+ sample, which highlights the importance of the photocatalyst in explaining these results. The photocatalyst is providing reducing electrons to the Ag overlayer, and keeping it in a fully reduced Ag^0 oxidation state. In this oxidation state Ag is not microbicidal, however the resultant microbicidal activity is still greater than the L+Ti+Ag- sample,

by a 2 log unit margin. This is nonetheless a significant improvement in the activity of the coating, just by the addition of the secondary layer. With the non-illuminated samples there is no photocatalysis, and no provision of reducing electrons to the Ag overlayer. This means that the Ag present in the overlayer can be present in the microbicidally active oxidation state of Ag^{+}. Hence, for these materials, a 100% kill (within experimental limits) is observed regardless of the substrate upon which the overlayer is deposited. The samples which were annealed a second time were shown to be ineffective in the dark compared to the samples which were not annealed. The rationale for this perhaps being the transformation of the Ag overlayer present to the oxide *via* the high temperature anneal in oxygen. As has been shown with the other experiments in this configuration there is little or no activity in the dark and the material functions primarily as a light-activated antimicrobial. The experiment with the secondary annealed samples behaves very much in the same way as one of the Ag_2O/TiO_2 materials.

These are preliminary results, tested with only one microorganism. *E. coli* is typically more resilient towards the light-activated antimicrobials, than a Gram positive organism (*S. aureus* has been used as the candidate organism throughout this study), due to the cell envelope morphology. The fact that these bifunctional materials have demonstrated significant efficacy with *E. coli* is an encouraging preliminary finding and further investigation with Gram positive organisms, fungi and viruses is obviously required. Despite this, there is clearly a demonstrated proof of concept. The Ag photodeposited on TiO_2 coatings are more active than an identically produced TiO_2 film in conditions of illumination by standard hospital compact fluorescent lamp and are significantly more active in conditions where no illumination is provided at all (other than the 254 nm light used to carry out the initial deposition of the secondary layer). This is an improvement over TiO_2 materials, whose main weakness is the complete lack of antimicrobial activity in the dark. It is postulated that these photodeposited Ag on TiO_2 materials have a synergistic balance between photocatalytic photodisinfection mechanism, enhanced by the presence of Ag^{0} when illuminated, and a microbicidal ion release

mechanism when the material is in darkness, mediated by Ag^+ ions. Also, as an aside, this method can be used to render inert surfaces such as glass antimicrobial in the dark and under conditions of illumination – however it remains to be seen how robust this kind of coating would be to cleaning and the uses and abuses of a real world application.

3.5.5 Potential Antimicrobial Mechanisms

Throughout this work there are essentially two potential mechanisms of antimicrobial activity that one can consider to be of importance. The first mechanism is that of antimicrobial activity *via* the action of the photocatalyst. The second is the action of a film dopant acting as an antimicrobial, such as the Ag^+ ion. Whilst this study has not set out to study explicitly the mechanism of antimicrobial action there is some evidence for the action of both:

3.5.5.1 Light-Activated Antimicrobial Mechanism

The statistical analysis of the experimental data repeatedly gave support to the light-activated antimicrobial mechanism when kill data for L+S+ samples was compared to the L-S+. In particular, the TiO_2 and materials consistently showed light-activated behaviour, regardless of the experiment being carried out. The Ag_2O/TiO_2 material demonstrated light-activated behaviour in all of the 365 nm light experiments with both *S. aureus* and *E. coli*. Of all light-activated kills, the Ag_2O/TiO_2 material demonstrated the greatest antimicrobial potency. In the instances where it is not possible to suggest activity for this sample in the dark, one must attempt to explain the rationale for the greater potency in the light than the TiO_2 control material – action of Ag^+ cannot be used to explain these instances. It is postulated that the presence of the Ag_2O, as confirmed by XANES and XPS in Chapter 2 may act as a charge separator within the bulk of the photocatalyst. Such a centre would be able to prevent electron/hole recombination, and maintain charge separation of these species. In doing so, the reaction of holes and electrons with adsorbates at the catalyst surface will outnumber the recombination of electrons and holes within the bulk or at the surface. This leads to more effective generation of the reactive radical species at the catalyst surface. This line of

thinking is backed up by the greater photocatalytic activities of the Ag_2O doped materials compared with the titania control. Whilst it has not been possible in this study, quantification of the radicals produced would add further weight to the investigation. This has previously been carried out[148] for similar materials *via* EPR measurements and reactive oxygen species, including the hydroxyl radical were detected. Similarly, an investigation of the antimicrobial effect of these radicals would be useful, though plenty of literature studies have already investigated this area successfully – showing breach of the cell wall by the reactive radicals to be the probable mechanism.[116-118] The research into the antimicrobial mechanism of TiO_2 photocatalysis is discussed in the introduction chapter, on Page 52. The mechanism proceeds through three steps: 1) cell wall decomposition, 2) cell membrane breach and finally 3) leakage of intracellular components, resulting in cell death.

3.5.5.2 Diffusible Antimicrobial Mechanism

The other antimicrobial mechanism observed in this study was a non light-activated one. The most significant case of this was in the samples coated with a photodeposited Ag overlayer, which had not been annealed a second time. These samples demonstrated very significant levels of microbial inactivation regardless of the illumination conditions. This was clear evidence for the activity of an Ag antimicrobial. Work on similar films[156] has shown the Ag overlayer to act as an enhancement to the photocatalyst and as an antimicrobial in the dark. This is in direct agreement with the findings of this study.

The non light-activated mechanism was also observed to a much lesser, though statistically relevant extent, for some Ag_2O/TiO_2 materials, most notably in the compact fluorescent light experiments with UV pre-activation. In these cases it is not possible to say definitively if the material is light-activated or not, there is certainly evidence for both mechanisms, perhaps acting synergistically. The materials characterisation in Chapter 2 clearly showed that in these films, the Ag is present as the Ag(I) oxide. Hence if is there is any activity in the dark, it must be due to the presence of the Ag_2O. However, there is very limited support in the literature for the activity of Ag_2O itself as an antimicrobial. In the work of Bellantone and Saravanapavan[157, 158] bioactive glasses containing 3% (wt) Ag_2O

were shown to exhibit bacteriostatic behaviour. That is to say they inhibited the growth of the test microorganism, but the material was not bactericidal. Fan *et al*.[159] studied a commercially available Ag antimicrobial product, and showed the importance of Ag(I) compounds, including Ag_2O, to the overall antimicrobial effect. In particular the dissolution of Ag(I) compounds into solutions was shown - which is of importance in introducing antimicrobial Ag^+ ions.

The work of Bellantone and Saravanapavan[157, 158] is very different from the work carried out in this study. The most significant difference being that the test substance was ground to a powder and used in suspension in a microbial culture. This vastly changes the interaction between the test material and the microbes because the available surface area, compared with that of the thin films is very significantly greater. Despite this and the greater potential for microbicide release from the enhanced surface area, the glasses did not display bactericidal characteristics, even when tested up to a concentration of 40 $mgcm^{-3}$. Due to the nature of the thin films, it is not possible to measure any possible minimum inhibitory concentration (MIC) or minimum bactericidal concentration (MBC) values resulting from possible action of Ag_2O as an antimicrobial. However, in future studies it may be interesting to examine a suspension of annealed sol powder (as examined by powder XRD in Chapter 2). If the Ag_2O/TiO_2 material is acting in the dark *via* a diffusible antimicrobial mechanism, it should be possible to measure the MIC and MBC compared to a reference TiO_2 powder. If the material is truly acting in the dark *via* this mechanism, this experiment should demonstrate an enhancement in the measured MIC/MBC of the Ag_2O doped sample compared to the TiO_2 control. However, it should be noted that by testing powders, effects such as the uptake of TiO_2 particles into microbial cells may become apparent.

As has been discussed in the introductory chapter (Page 35), the antimicrobial mechanism for the silver ion is still poorly understood. It is thought that the Ag^+ ion binds with intracellular thiol (-SH) groups on proteins and enzymes (silver has a high affinity for sulphur). This in turn prevents proper function of these proteins and enzymes, resulting in cell death. However, further research is needed to clarify this mechanism.

3.6 Conclusions

Antimicrobial activity was observed for all of the photoactivated materials under test, though to varying degrees. Films displayed activity under conditions of UV illumination, and conditions of illumination by typical hospital light source. There are two samples of particular interest, because of the contrasting manner in which they function. These are the Ag_2O/TiO_2 and the Ag photodeposited on TiO_2 samples. The Ag_2O/TiO_2 sample functions almost exclusively *via* photocatalysis, with little or no activity observed in the absence of illumination. It is suggested that the enhancement in activity for these samples might be due to a combination of factors. Principally the availability of more active surface area than the TiO_2 control and the prevention of electron-hole recombination by the Ag_2O dopant are offered as explanations for the greater activity of the doped material. There is scant evidence to suggest the action of Ag ions as a diffusible microbicide. In contrast, the photodeposited Ag on TiO_2 samples exhibit antimicrobial activity in both conditions of illumination and conditions of darkness. This is a very useful attribute for an antimicrobial surface, and is a result of the synergy between photocatalyst and Ag overlayer. It is suggested that the photocatalyst maintains reduced Ag upon the surface, such that it is available when there is no illumination of the surface. The material is less effective than the Ag_2O samples under illumination, presumably because some portion of the produced electrons are used up maintaining the Ag in a reduced state and are not available for the production of microbicidal radicals. This should be examined in detail in future studies.

In this chapter it has been demonstrated that photocatalyst thin films can function as antimicrobials under certain conditions. However, a useful antimicrobial surface might also demonstrate the ability to resist microbial fouling, or to self clean. Consequently, the topic of microbial adhesion to the candidate materials will be examined in the next chapter.

Chapter 4: Study of the Adhesion of *Staphylococcus aureus* NCTC 6571 and *Pseudomonas aeruginosa* PA-01 to Coated Glass Substrates.

4.1 Introduction

In the previous chapter, the antimicrobial properties of the TiO_2 based thin films were presented. Aside from the demonstrated antimicrobial properties, a secondary area of interest is whether these superhydrophilic materials are able to prevent initial adhesion of microorganisms. Superhydrophilic surfaces are easy to clean, because water tends to sheet over the surface. Indeed there are some commercial products which utilise this property, for example the "self-cleaning" glasses such as Pilkington Activ™ and Saint-Gobain BIOCLEAN®. It is thought that superhydrophilicity might afford some reduction in microbial adhesion or in the way in which microbes aggregate upon such a surface. Superhydrophobic surfaces on the other hand, are also thought to be suitable for reducing microbial adhesion to surfaces because they encourage water droplets to ball up, roll from the surface, taking dirt and microbes with them. In light of this, a commercially produced superhydrophobic material (Pilkington Hydrotech) was assessed alongside superhydrophilic materials. Studies of the adhesion of microbes to coated glass substrates have received little research attention;[160] in particular sol-gel TiO_2 materials do not appear to have been studied extensively at all and as such all of the work in this chapter is new. Prevention of microbial adhesion would be a useful secondary attribute for an antimicrobial coating in the fight against nosocomial pathogens spread from surface microbial reservoirs – if adhesion is prevented, microbial reservoirs such as biofilms cannot be built up. This chapter will examine the potential anti-adhesive effects of both laboratory produced and commercially available coated glass substrates.

4.2 Experimental

4.2.1 Microbial Adhesion Procedure

Both commercially produced and laboratory produced coatings were prepared for study. The laboratory samples were TiO_2 and Ag_2O/TiO_2 thin films deposited on standard microscope slides, as previously described in Chapter 2. The commercially available materials were uncoated Float Glass, K Glass™ (F-doped SnO_2 coated glass), Hydrotech (hydrophobic coating), Activ™ (25 nm thick TiO_2 coated glass), SnO_2 coated glass and SiO_2 coated glass all from Pilkington Group Ltd and BIOCLEAN® (TiO_2 coated) from Saint-Gobain Glass (SGG) UK Ltd. The Activ™ and BIOCLEAN® samples are the most relevant to the sol-gel materials produced in this study, as they too are photocatalyst thin films. However, the method of deposition is significantly different (CVD and PVD versus sol-gel dip coating).

Samples under test were cut using glass cutters into coupons measuring approximately 12 × 25 mm. This gives the coupons an available surface area of 3 cm^2. The active face of the samples was marked by scratching the surface at the top edge of a coupon with a diamond tipped pencil. Sample coupons were then cleaned using a 70% isopropanol in distilled water solution. This solution washed off the dirt and debris left behind by the cutting process and is also a microbicide, disinfecting the surface prior to the experiment. All coupons were then irradiated by the 254 nm light from a germicidal lamp (BDH/VWR VL208-G) for a period of one hour.

A microbial suspension into which the coupons were to be placed was prepared from an overnight culture of the test organism prepared in nutrient broth (Oxoid Ltd) and grown aerobically with shaking at 37 °C. The organisms tested were *Staphylococcus aureus* NCTC 6571 and *Pseudomonas aeruginosa* PA01. The overnight culture was prepared in 20 ml of nutrient broth, in a Falcon™ tube. This was then spun down to a pellet and re-suspended in an equal volume of sterile PBS (Oxoid Ltd). This re-suspended overnight culture was then serially diluted one

thousand fold in sterile PBS. The diluted microbial suspension was then divided into 5 ml aliquots in sterile screw top universal bottles.

Coupons of test material were dipped into the 5 ml of microbial suspension and left there, vertically for a period of five minutes, before being carefully withdrawn from the suspension. The lower edge of withdrawn coupons was then tapped onto filter paper, and the coupon was placed onto filter paper, inactive side down, so that only the active surface was examined. At no time was the active surface blotted, or in any way touched. Coupons were then transferred aseptically to sterile Petri dishes for an agar overlay. The overlay was carried out with 35 ml of molten agar, made up to 75% of the recommended amount, poured at 42 °C. Mannitol salt agar (Oxoid Ltd) was used for *S. aureus*, and nutrient agar (Oxoid Ltd) was used for *P. aeruginosa*. Coupons were allowed to dry before the overlay was carried out. Overlaid plates were incubated aerobically face up for 24 hours at 37 °C.

4.2.2 Data Acquisition and Analysis

Incubated plates were photographed using a gel imaging system (Alphaimager) which results in monochrome images. The adherent viable colony forming units were counted manually on the digital images using OdoPlus freeware mouse click counter.[161] Where required for the sake of image clarity and ease of counting, images were manipulated using Adobe Photoshop CS3.[162] The results were tabulated and graphed in SPSS V15 statistical software[163] with the assistance of Aviva Petrie (Biostatistician, Eastman Dental Institute).

4.2.3 Imaging

Samples with adherent microbes were also imaged by scanning electron microscopy (SEM) with the assistance of Nicky Mordan (Microscopist technician, Eastman Dental Institute). Microbes were fixed to the surface in glutaraldehyde and the sample sputter coated in gold. Images were obtained on a JEOL instrument with Oxford INCA software. Samples were also kindly analysed by Atomic Force Microscopy (AFM) with assistance from Wojciech Chrzanowski (Biomaterials and Tissue Engineering, Eastman Dental Institute). A Park Systems model XE-100 was

used in non-contact mode with a silicon tip and a scan rate of 1 Hz. Images were collected using the XEP software (Park Systems Inc., CA.), and analysed using XEI (Park Systems Inc., CA.).

4.2.4 Determination of Sample Hydrophilicity and Hydrophobicity

Water droplet contact angles were measured for all samples using the same method as detailed in Section 2.3.2, as a means of quantifying the hydrophilic/hydrophobic nature of the various surfaces. Contact angles were measured on a sessile 5 μl drop of distilled water, placed onto the samples from a 10 μl micro pipettor. The droplet diameter was measured optically using a ×20 Measuring Microscope (Peak Optics). The diameter and volume data were then used to calculate a contact angle for the droplet using a suitable computer program. Contact angle data was obtained on both UV irradiated (1 hour, 254 nm) and non-irradiated samples, to demonstrate the photoinduced superhydrophilicity (PSH) of the titania materials as compared with the remainder of the samples.

4.3 Results

4.3.1 Experimental

The adopted methodology provided a simple and relatively rapid method for the study of microbial adhesion to the test substrates. Sterility of the samples prior to experiment was ensured by the utilisation of an isopropanol wash and UV irradiation. This UV irradiation process further disinfects the surface of the coupons in addition to the 70% isopropanol wash. It also provides the UV pre-activation required for the photocatalytic materials (TiO_2, Ag_2O/TiO_2, Pilkington Activ™ and SGG BIOCLEAN®). Image capture by gel imaging camera produced good quality, monochrome images, with microbial colonies clearly visible. In earlier experiments, full colour photos were taken with a digital camera through the eyepiece of a plate counting microscope, however this awkward and unsatisfactory technique was replaced with the monochrome image from the gel imaging system due to the higher quality and contrast in these images.

4.3.2 Adhesion of *S. aureus* NCTC 6571

Some representative images of adherent *S. aureus* on all test substrates are shown in Figure 4.1 to Figure 4.9. The images show black dots attached to the substrate coupon, and in some cases embedded in the surrounding agar overlay. The black dots are individual microbial colonies. Figure 4.8 and Figure 4.9 were recorded using a different image capture technique, but importantly the experimental method prior to image capture was the same. This means that despite the images looking different, the data from them can be included with the other data from the superior imaging technique. Again, in Figure 4.8 and Figure 4.9 the black dots represent one microbial colony, arising from one adherent microbe initially.

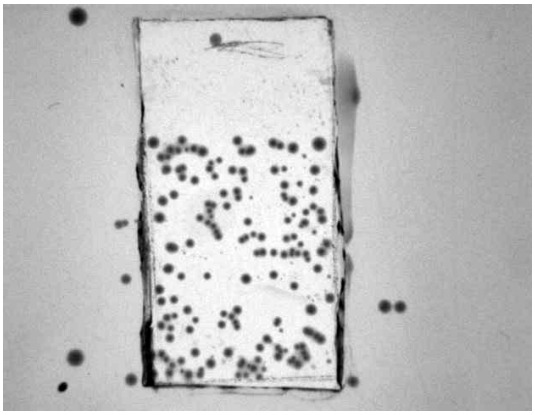

Figure 4.1 Adhesion of *S. aureus* (black dots) to Float Glass coupon (12 × 25 mm)

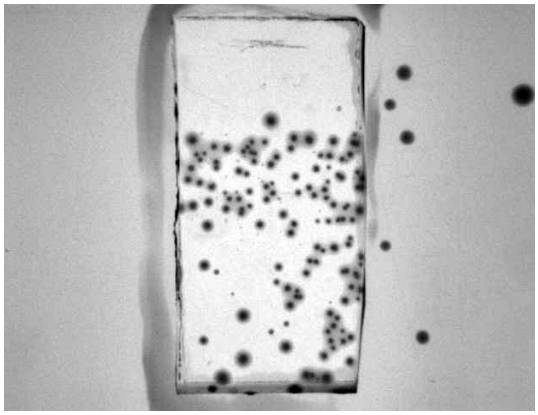

Figure 4.2 Adhesion of *S. aureus* (black dots) to SiO_2 coupon (12 × 25 mm)

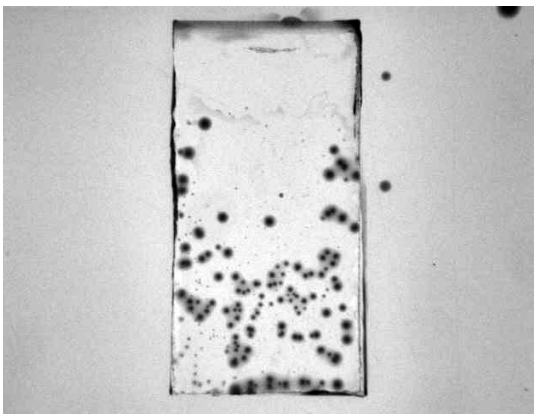

Figure 4.3 Adhesion of *S. aureus* (black dots) to SnO_2 coupon (12 × 25 mm)

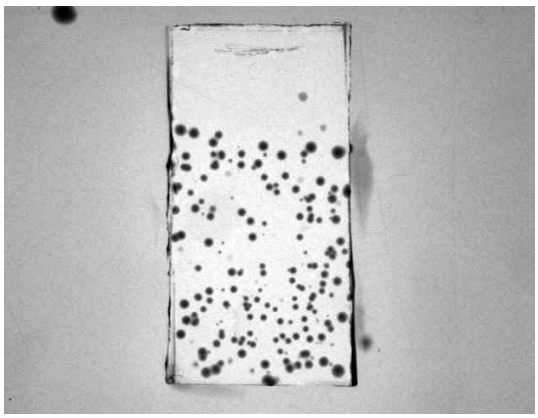

Figure 4.4 Adhesion of *S. aureus* (black dots) to Activ™ coupon (12 × 25 mm)

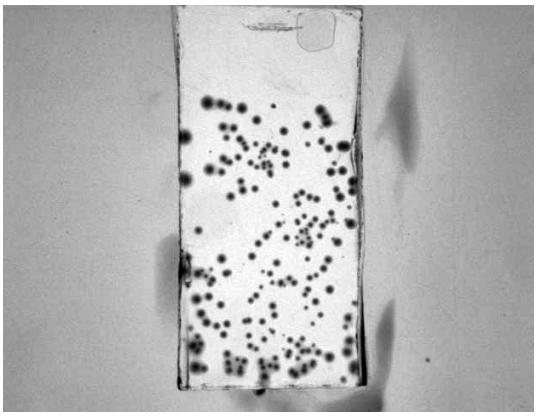

Figure 4.5 Adhesion of *S. aureus* (black dots) to BIOCLEAN® coupon (12 × 25 mm)

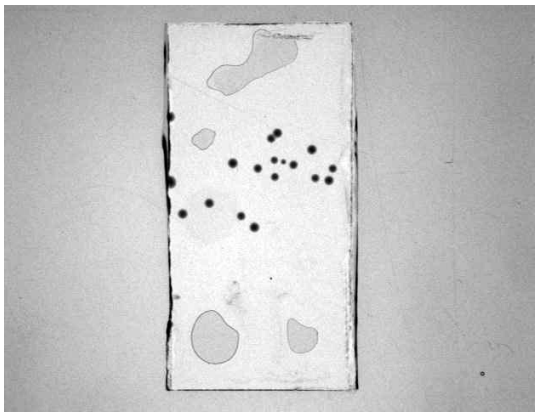

Figure 4.6 Adhesion of *S. aureus* (black dots) to K-Glass™ coupon (12 × 25 mm)

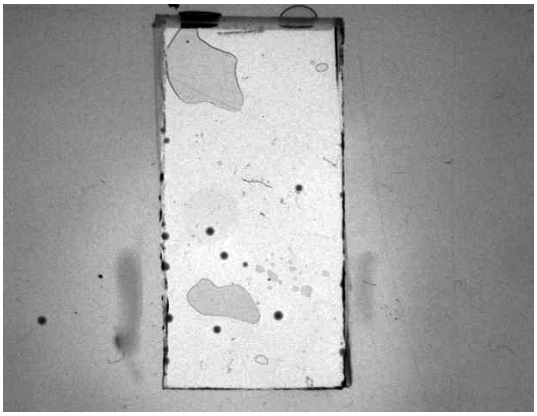

Figure 4.7 Adhesion of *S. aureus* (black dots) to Hydrotech coupon (12 × 25 mm)

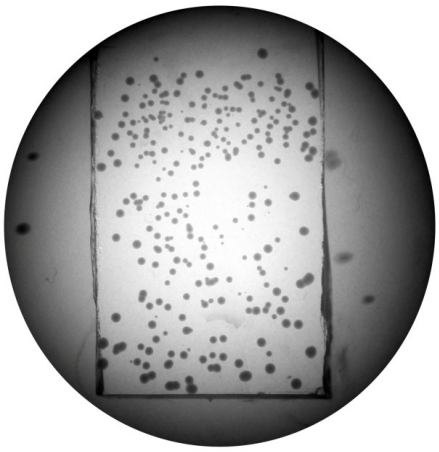

Figure 4.8 Adhesion of *S. aureus* to sol-gel TiO_2 coupon (12 × 25 mm). [Note image taken through microscope eyepiece]

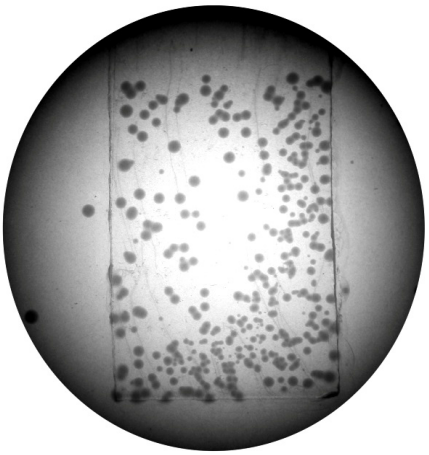

Figure 4.9 Adhesion of *S. aureus* to sol-gel Ag_2O/TiO_2 coupon (12 × 25 mm). [Note image taken through microscope eyepiece]

Sample	Mean adherent microbes cfu/coupon	Mean adherent microbes cfu/cm^2
Float Glass	196 (68)	65 (23)
SiO_2	74 (43)	25 (14)
SnO_2	127 (45)	42 (15)
Activ™	228 (110)	76 (37)
BIOCLEAN®	161 (180)*	54 (60)*
K-Glass™	16 (7)	5 (2)
Hydrotech	9 (8)	3 (3)
Sol GelTiO_2	125 (110)	42 (37)
Sol Gel Ag_2O/TiO_2	283 (99)	94 (33)

Table 4.1 Adhesion data for *S. aureus* on various substrates (standard deviations in brackets)

Table 4.1 shows the adhesion data in tabular form. It is clear that microbial adhesion is variable across the sample set, and there is also significant variation within each sample's repeat measurements (data not shown). The data in Table 4.1 marked with an asterisk has such a wide spread of the data that the standard deviation calculation yields a result larger than the mean value. This is an indicator of the limitation of the experimental technique.

4.3.3 Adhesion of *P. aeruginosa* PA01

Some representative images for the experiments with *P. aeruginosa* are given in Figure 4.10 to Figure 4.14. These images were recorded in the same fashion, but the behaviour of the microbes in the agar was different. The agar overlay washed the microbes from the surface, hence images of the whole Petri dish are presented in these figures. Consequently the whole plate was counted for data acquisition and analysis. The grey/black spots represent individual microbial colonies and arise from one microbe initially adherent upon the coupon. Table 4.2 lists the mean adherent colony forming units per unit area for a selection of the coated glass substrates.

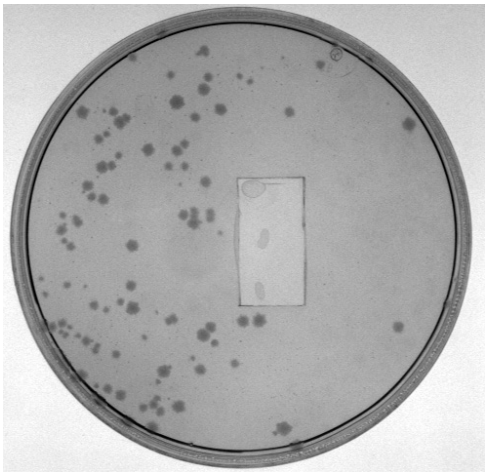

Figure 4.10 Adhesion of *P. aeruginosa* (grey spots) to Float Glass coupon (12 × 25 mm)

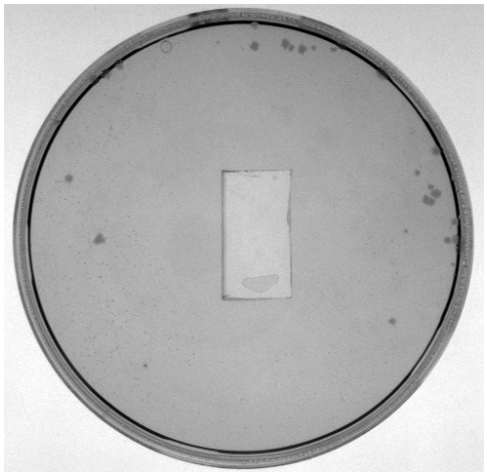

Figure 4.11 Adhesion of *P. aeruginosa* (grey spots) to SiO_2 coupon (12 × 25 mm)

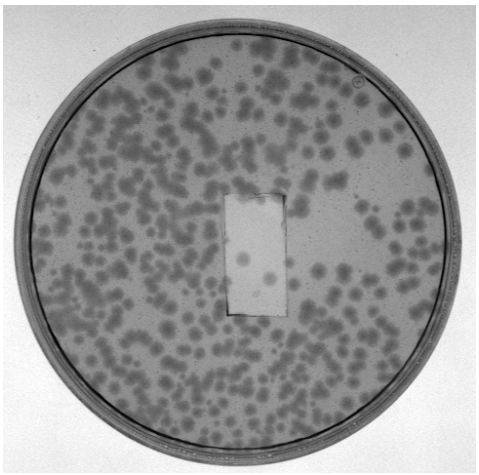

Figure 4.12 Adhesion of *P. aeruginosa* (grey spots) to Activ™ coupon (12 × 25 mm)

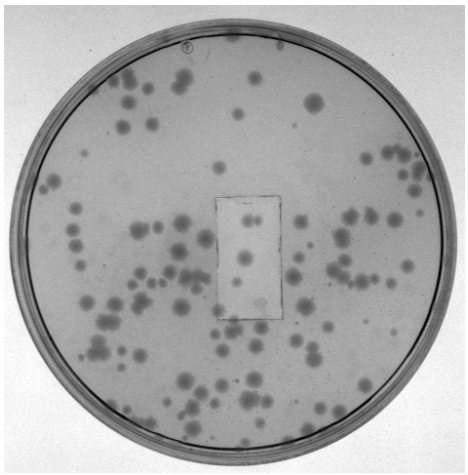

Figure 4.13 Adhesion of *P. aeruginosa* (grey spots) to K-Glass™ coupon (12 × 25 mm)

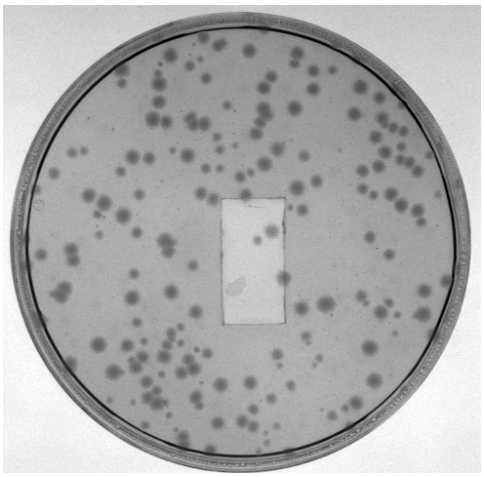

Figure 4.14 Adhesion of *P. aeruginosa* (grey spots) to Hydrotech coupon (12 × 25 mm)

Sample	Mean adherent microbes cfu/coupon		Mean adherent microbes cfu/cm^2	
Float Glass	72	(27)	24	(9)
SiO_2	75	(33)	25	(11)
Activ™	74	(72)	25	(24)
K-Glass™	73	(48)	24	(16)
Hydrotech	125	(62)	42	(21)

Table 4.2 Adhesion data for *P. aeruginosa* on various substrates (standard deviations in brackets)

Adherence of microorganisms to the test surfaces varied widely. In common with the data from *S. aureus*, there is considerable variation and spread in the data. This is clearly visible in Table 4.2. In future experiments, a more reliable and consistent methodology would have to be considered to alleviate this effect.

4.3.4 Scanning Electron Microscopy

Scanning electron microscopy was carried out on *S. aureus* adhered to a glass substrate and to sol-gel TiO_2 materials. Substrates were exposed to UV light before the inoculum was added, and subsequently divided into two sets of samples. The first set was kept in the dark for six hours, the second set illuminated by 254 nm light for six hours. Images of these are shown together, for ease of comparison, on the following page in Figure 4.15 to Figure 4.20.

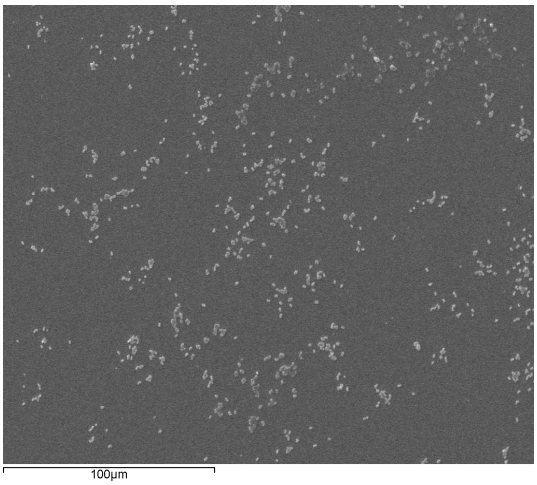

Figure 4.15 SEM image of *S. aureus* on glass L-

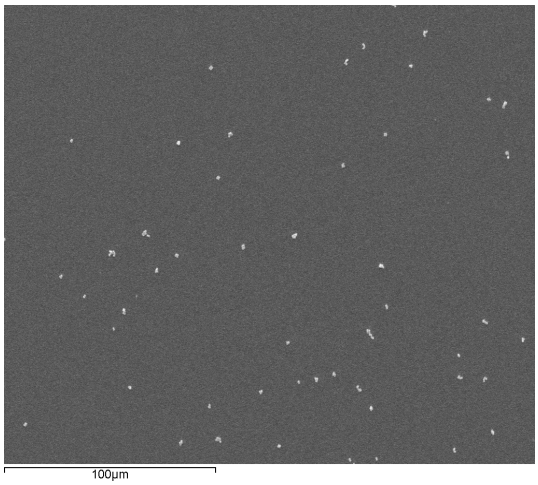

Figure 4.16 SEM image of *S. aureus* on glass L+

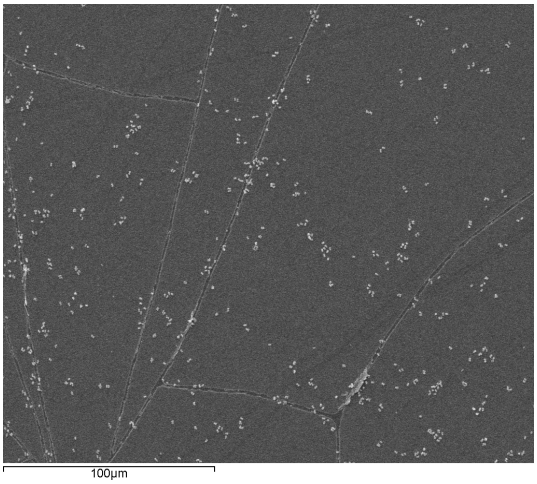

Figure 4.17 SEM image of *S. aureus* on TiO_2 L-

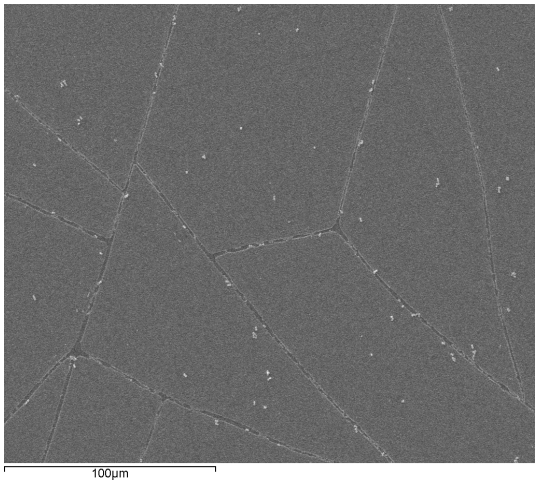

Figure 4.18 SEM image of *S. aureus* on TiO_2 L+

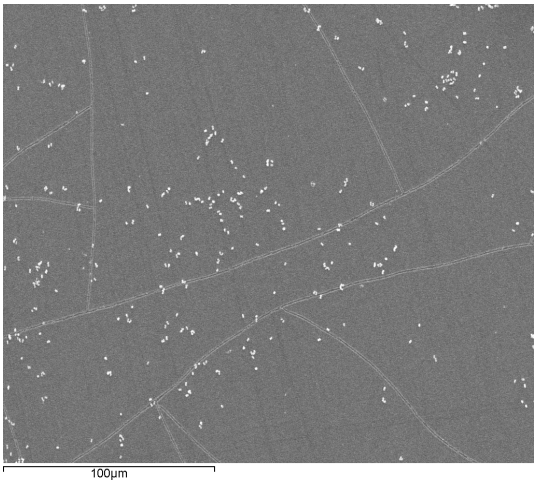

Figure 4.19 SEM image of *S. aureus* on Ag_2O/TiO_2 L-

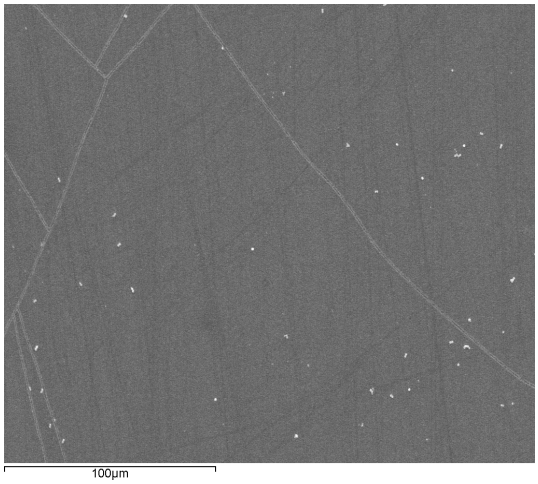

Figure 4.20 SEM image of *S. aureus* on Ag_2O/TiO_2 L+

In these figures the bright white dots are individual microbes adherent to the substrate material below. Clear differences are observed between the samples which have been left in the dark and samples which have been UV illuminated, and there is also a difference between the glass control and the sol-gel materials. Notably, the UV illuminated substrates have fewer adherent microbes – this is most likely due to the antimicrobial effect of UV light itself. Secondly, it can be seen in the non illuminated samples that there is a clear difference in the way in which the microbes are dispersed across the surface. It appears as though the microbes adherent upon the hydrophilic materials are in smaller groups than on the glass control and are more evenly dispersed. The microbes on the glass surface are collected together in larger groups and are unevenly dispersed, with large areas of un-colonised space. Higher magnification images, with a larger inoculum were collected to further examine this and compare a TiO_2 sample with a glass control. This is shown in Figure 4.21 and Figure 4.22.

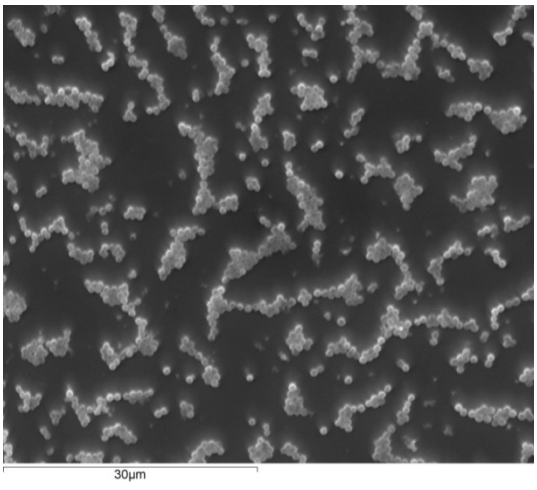

Figure 4.21 SEM image of *S. aureus* on glass substrate. Scale bar 30 µm.

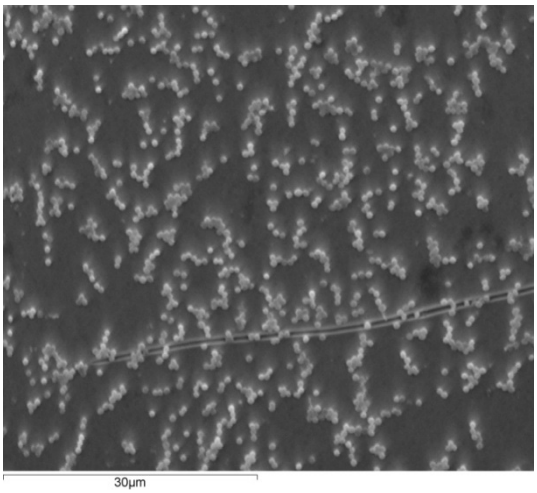

Figure 4.22 SEM image of *S. aureus* on a sol-gel TiO_2 coating. Scale bar 30 µm

The nature of the surface greatly affected the morphology of the adherent colonies. On the glass (Figure 4.21), the microbes tended to adhere in micro-colonies, with some degree of separation between them. There are few individual microbes that are adherent on the surface. In contrast, the adherent microbes on the sol-gel TiO_2 material (Figure 4.22) were more dispersed. Although there was some aggregation into micro-colonies, the adherent microbes tended to be in smaller groups, or as

single cells. This may be a reflection of the comparative hydrophilicities of the materials. The TiO_2 is more hydrophilic, and demonstrates photoinduced superhydrophilicity, when compared to the glass substrate. This may prevent the adhesion of microbes in large micro-colonies and encourage them to form only small adherent colonies – which would be more easily destroyed by the photocatalyst.

4.3.5 Atomic Force Microscopy

Atomic Force Microscopy (AFM) studies were performed on all of the samples. The intention was to observe the typical morphology of the surfaces and to calculate surface roughness (R_a) values as a means to explain the adhesion of microorganisms to the various substrates. R_a values were calculated in the software across multiple profiles of the surface, and the data points averaged. Table 4.3 shows the calculated average surface roughness (R_a) of the samples.

Sample	Average Surface Roughness R_a /nm	
Float Glass	3.11	(0.75)
SiO_2	0.72	(0.30)
SnO_2	17.18	(14.63)
Activ™	4.92	(1.07)
BIOCLEAN®	5.17	(0.29)
K-Glass™	5.67	(0.82)
Hydrotech™	1.36	(1.75)
Sol Gel TiO_2	25.10	(8.84)
Sol Gel Ag_2O/TiO_2	18.88	(11.93)

Table 4.3 Average surface roughness (R_a) of samples. Bracketed figures show standard deviations.

The different levels of roughness and surface morphologies can be clearly seen in the three dimensional AFM images in Figure 4.23 to Figure 4.31. Shrink cracks, resulting from the anneal process can be seen in the sol-gel TiO_2 examples (Figure 4.30 and Figure 4.31), these are quite unusual, in that some are raised from the surface by approximately 100 nm – this leads to the high roughness measurements.

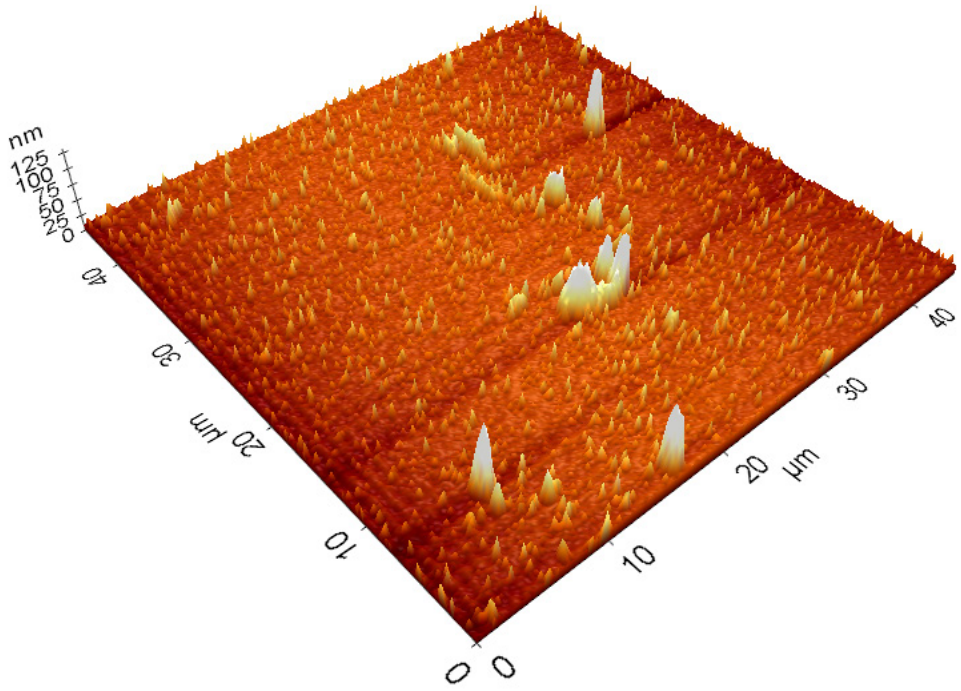

Figure 4.23 Three dimensional AFM of float glass, 45 µm square.

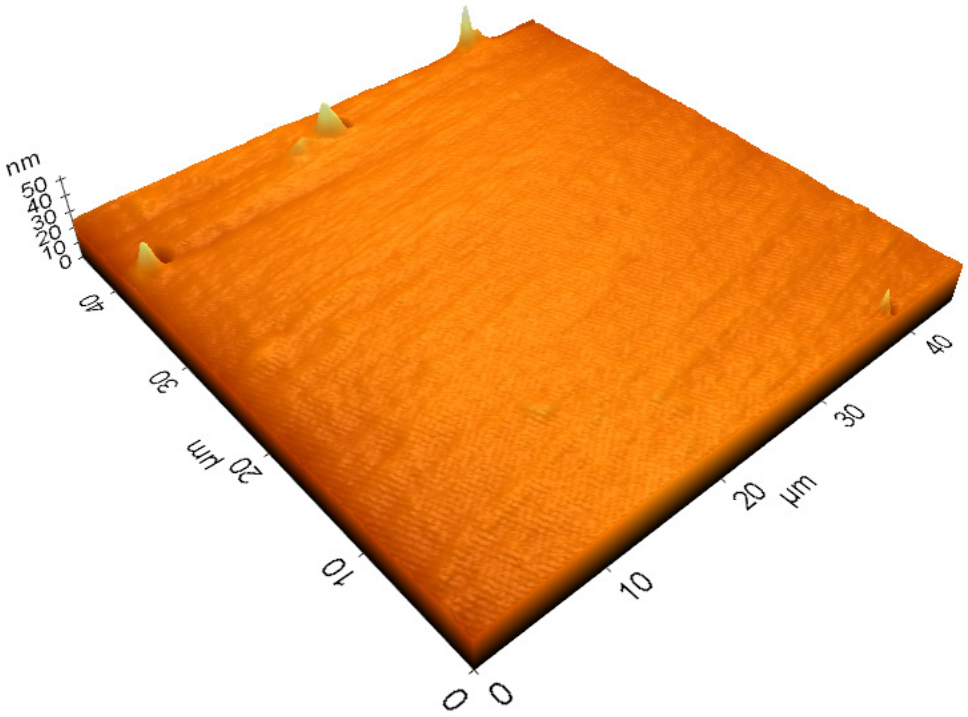

Figure 4.24 Three dimensional AFM of SiO_2 Coated glass, 45 µm square.

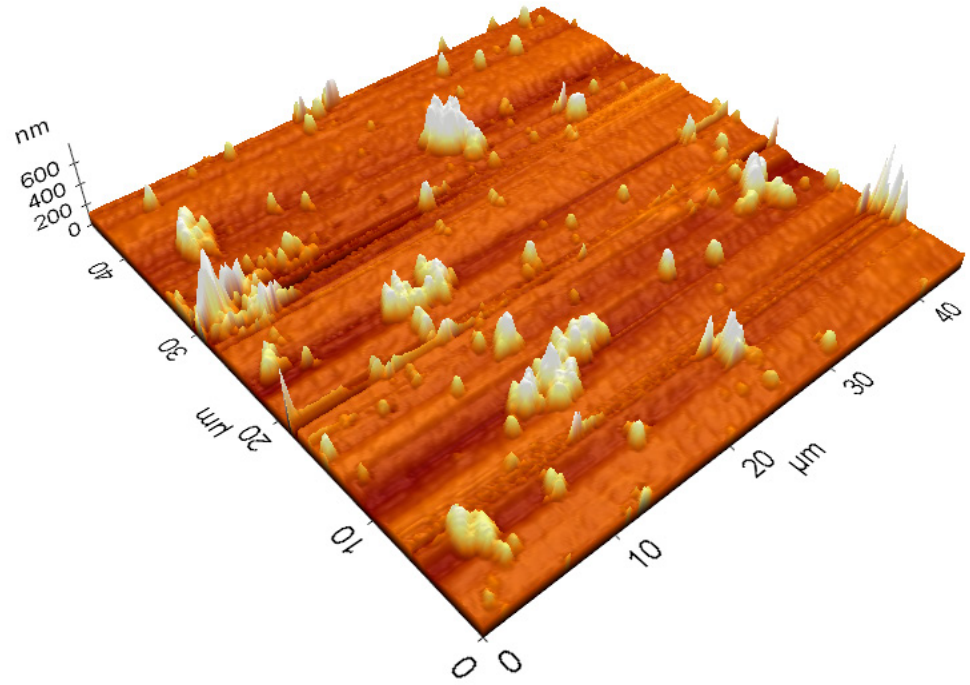

Figure 4.25 Three dimensional AFM of SnO_2 Coated glass, 45 µm square.

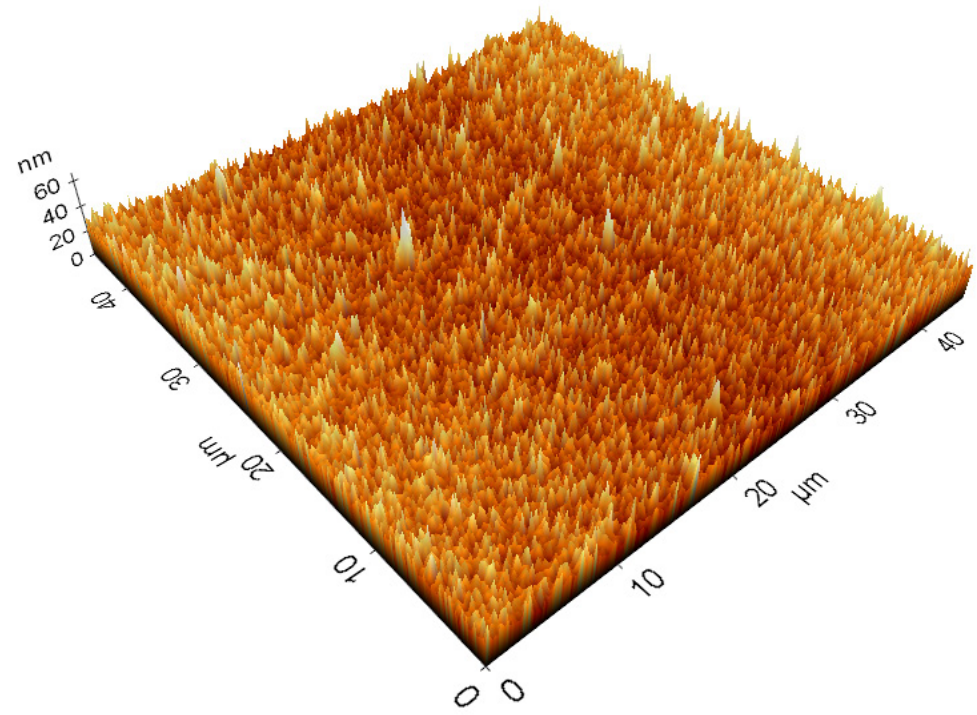

Figure 4.26 Three dimensional AFM of Pilkington Activ™, 45 µm square.

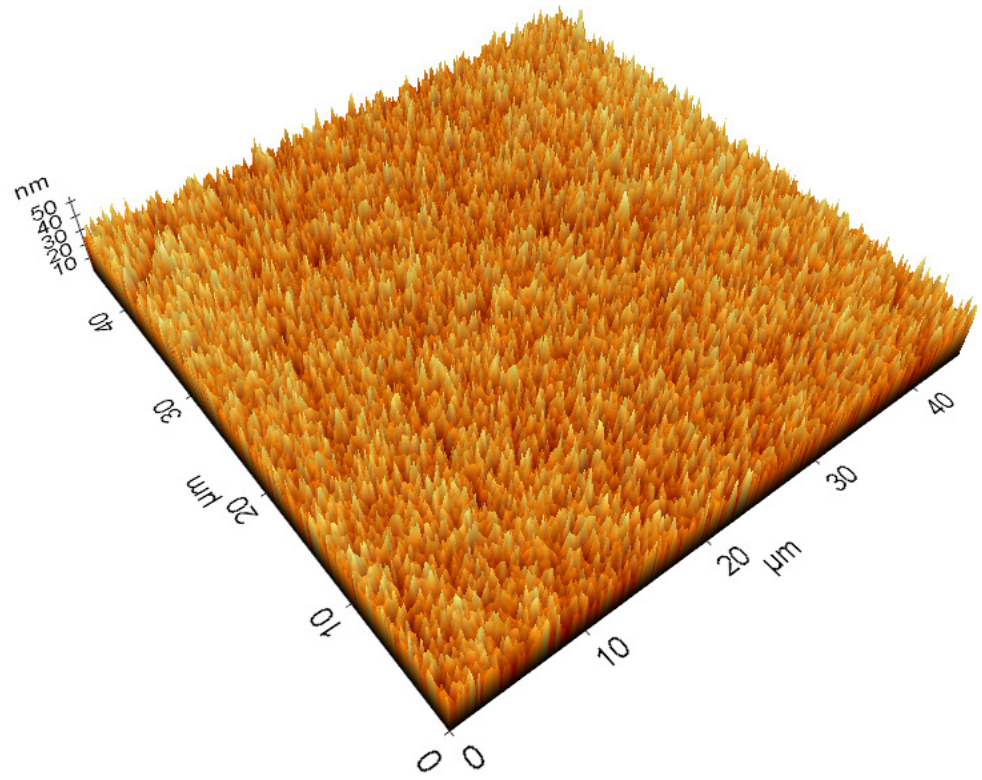

Figure 4.27 Three dimensional AFM of Saint Gobain BIOCLEAN®, 45 µm square.

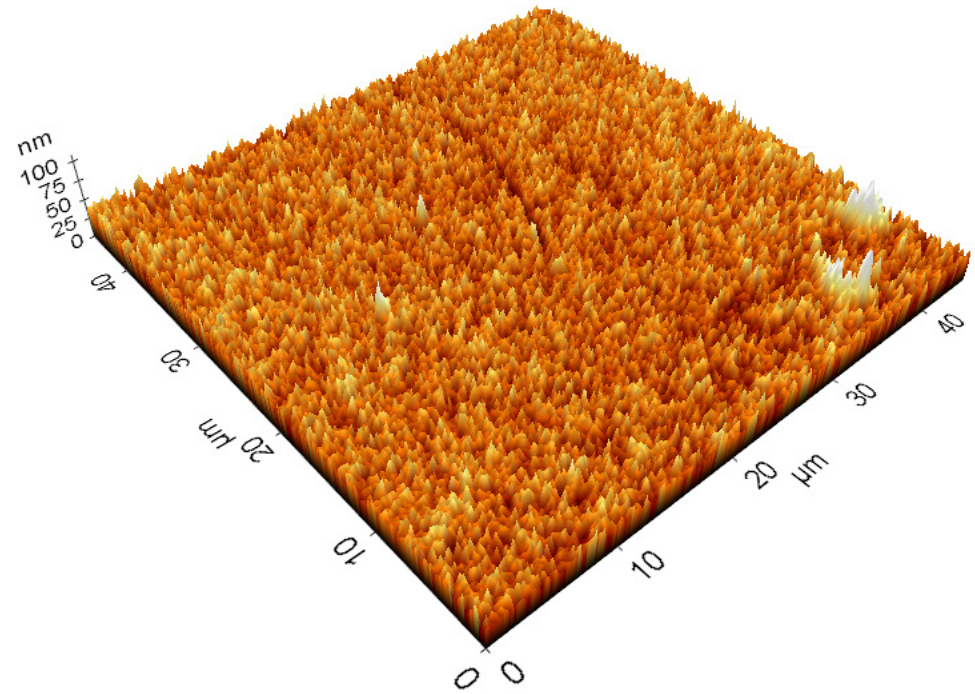

Figure 4.28 Three dimensional AFM of Pilkington K Glass™, 45 µm square.

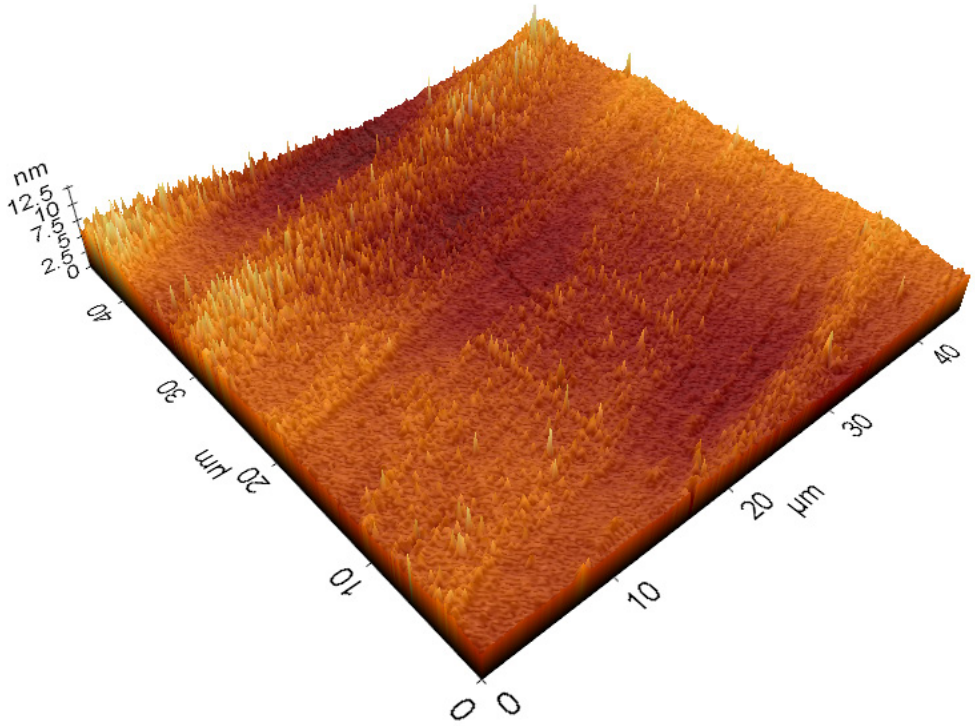

Figure 4.29 Three dimensional AFM of Pilkington Hydrotech, 45 µm square.

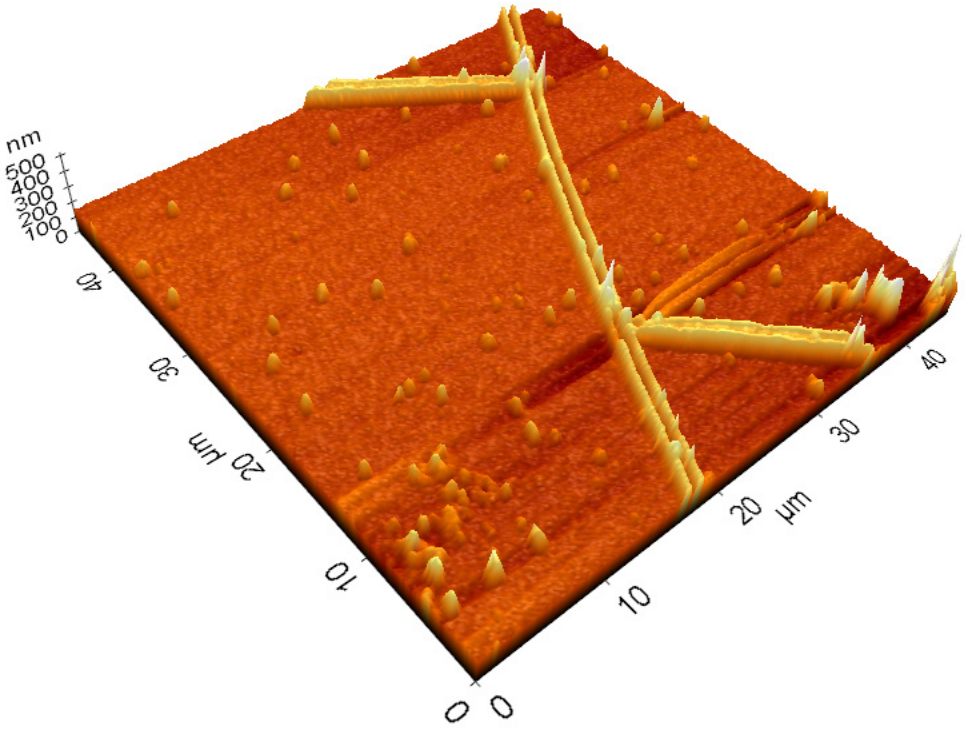

Figure 4.30 Three dimensional AFM of Sol-gel TiO_2 coated glass, 45 µm square.

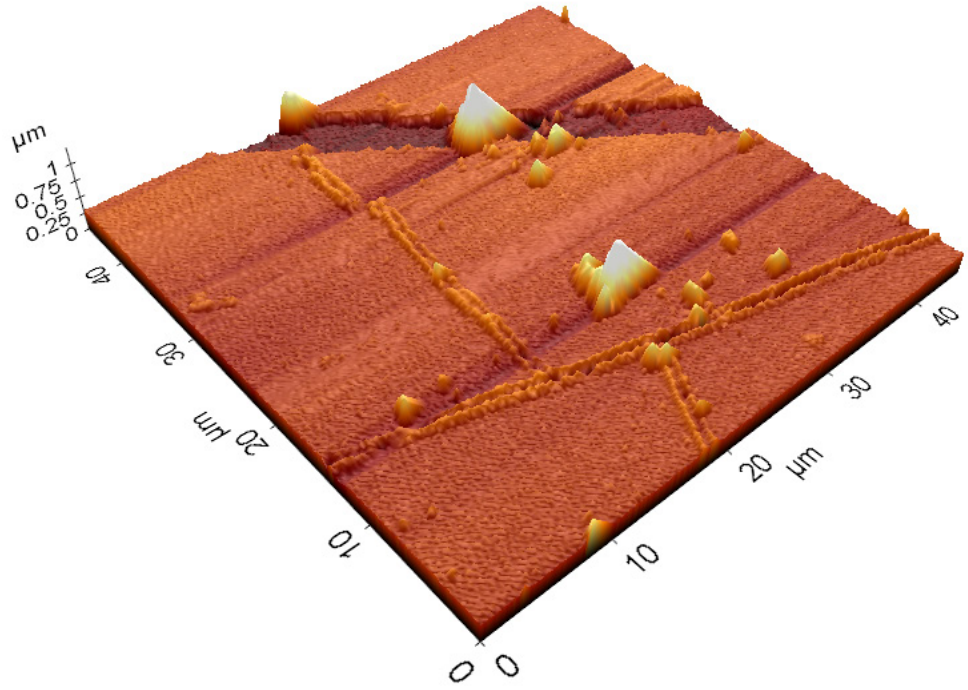

Figure 4.31 Three dimensional AFM of Sol-gel Ag_2O/TiO_2 coated glass, 45 µm square.

4.3.6 Water Droplet Contact Angle

The comparative hydrophilic/hydrophobic properties of the materials were assessed by measurement of the contact angle of a water droplet on the surface. Low contact angles arise from the spreading of the water droplet, demonstrating the affinity of the surface for water. Conversely a high contact angle arises from the tendency of a droplet to not spread, and to remain stationary. Contact angles can be influenced by both the chemistry and the morphology of the surface. For example, a rough surface, with cracks and channels can allow water to spread more easily than on a smooth surface of the same chemical composition. Also the chemistry of the surface, for example hydroxylation, resulting from photoactivity of a material can cause hydrophilicity, and the enhanced tendency for a droplet of water to spread. This is known as photoinduced hydrophilicity. To see if any of the samples demonstrated photoinduced hydrophilicity, contact angles were recorded before and after a period of 254 nm UV irradiation. The results are shown in Table 4.4.

	Water Droplet Contact Angle /degrees			
Sample	**Before Irradiation**		**After Irradiation**	
Float Glass	57	(5)	62	(4)
SiO_2	46	(3)	51	(8)
SnO_2	68	(0)	66	(2)
Activ™	79	(2)	11	(3)
BIOCLEAN®	67	(2)	7	(2)
K-Glass™	64	(2)	56	(7)
Hydrotech™	133	(7)	128	(8)
Sol Gel TiO_2	55	(10)	15	(2)
Sol Gel Ag_2O/TiO_2	42	(3)	15	(3)

Table 4.4 Contact angle measurements to the nearest degree taken before and after UV irradiation (254 nm). Bracketed figures show standard deviations.

The data clearly shows that most samples do not demonstrate photoinduced hydrophilicity, since the before and after measurements were not significantly different. This study showed that Pilkington Activ™, sol gel TiO_2, sol gel Ag_2O/TiO_2 and SGG BIOCLEAN® were the only samples to exhibit significant photoinduced hydrophilicity. The sol gel materials tended towards superhydrophilic behaviour with contact angles of ca 15° and the commercial materials performed slightly better around 10°. The other sample of particular interest was the Pilkington Hydrotech, which was very hydrophobic, with a contact angle of ca. 130°. This is a value approaching that of a superhydrophobic surface. It should be noted that the contact angles for this part of the study were obtained independently of those in Section 2.4.3 and hence the measured angles are not identical. The larger contact angles here may be a result of less well cleaned surfaces, or insufficient UV irradiation time. This is however not too much of a concern as the trends observed are still the same.

4.4 Discussion

It has previously been observed that surface roughness can directly affect the level of microbial adhesion on a surface. This has been studied in particular with regard to dental acrylics. It was shown in one study[164] that there was a clear positive

correlation between the surface roughness and the level of microbial adhesion to the surface. Rougher surfaces harboured more microbes on them and hence adhesion to the surface was greater than for smoother surfaces. However, in the work presented in this chapter one can see that there is no direct correlation between the roughness of the surfaces and the level of microbial adhesion. Whilst this may appear in contradiction to published work, the level of roughness recorded in this study and those published in the literature are of a different order of magnitude. In the published work[164], the roughness of the materials was analysed by laser profilometry, and was on a micrometre scale of magnitude. In this work, measurement of roughness was initially attempted by laser profilometry, but the surfaces were too smooth to be studied by this technique. It was only by utilising AFM methods that surface roughness could be calculated, and it was found to be on a nanometre scale. This has important implications, and can perhaps provide a rationale for the observed discrepancy between the findings in this work and the published literature. The typical size of a rod shaped prokaryote is 1-5 μm long by 1 μm wide – *E. coli* cells for example measure 1 x 2 μm.[30] This means that the roughness "experienced" by a microbe in the published literature case, is of the same order of magnitude as the microbe's own size. However, in the case of the results from this study, the roughness is three orders of magnitude smaller than the typical dimensions of a prokaryotic cell. In other words, the level of roughness in the materials studied here is too small to have an effect upon the adhesion of microbes. A microbe approaching the surfaces examined here is considerably larger than the dimensions of the surface roughness, so it is of little consequence in determining if a microbe sticks to the surface or not. It is without doubt, the surface chemistry and the physico-chemical interactions between the surface and the microbe which are of greatest importance.

The principle physico-chemical interaction which has been examined in this study is the relative hydrophilic/hydrophobic natures of the surfaces. The photocatalytic materials all demonstrated photoinduced superhydrophilicity (PSH), with contact angles in the region of 10 – 15° after UV illumination. The Pilkington Hydrotech sample, with a near-superhydrophobic contact angle of ca. 130° was unaffected by

UV illumination, neither were all other samples – which is as expected. When one compares the data for contact angle, versus the number of adherent cfu on a sample, it is particularly difficult to extract any meaningful correlations. Figure 4.32 shows a plot of these parameters. What is clear, is that the near-superhydrophobic surface has the lowest level of adherent microbes, and also, some of the superhydrophilic materials have the highest number of adherent microbes. In the central region, of contact angles around 60° there is great variation in the number of adherent microbes, this clearly shows that in a material which is neither hydrophilic, nor hydrophobic, there are other factors in play which determine the level of microbial adhesion. Incidentally, this reason is not surface roughness, as if only the materials with intermediate contact angles are considered, there is still no correlation between their roughness and the level of microbial adhesion. It is probable that the reason for the differences in microbial adhesion displayed by the samples studied is due to other physico-chemical interactions, such as Van-der-Waal's and electrostatic forces between the surface and approaching microbes.

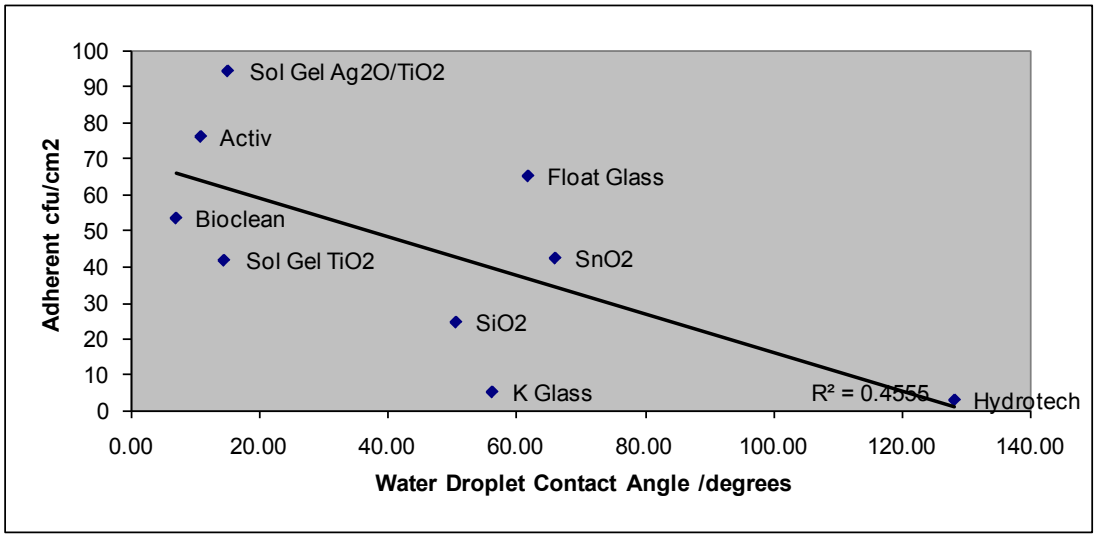

Figure 4.32 Comparison of adherent *S. aureus* per cm^2 versus water droplet contact angle

The SEM study of the hydrophilic materials has also shown one other aspect, which may assist in their function as useful antimicrobial surfaces, despite their apparent tendency to permit adhesion of more microbes than other surfaces. Specifically, the tendency of the superhydrophilic surface to spread the microbes out across its surface, rather than allow their aggregation in larger clumps, is beneficial to the

photocatalytic function of the coatings. By spreading across the surface, shielding of the photocatalyst is reduced, and the thickness of the microbial overlayer is reduced. This allows the photocatalyst to function more effectively, and ultimately allows the material to act as a more effective antimicrobial surface. In other words, the synergy between the photocatalysis and the PSH, works in the favour of a better antimicrobial surface, despite the slightly higher tendency of these surfaces to adsorb microbes.

The results clearly show that there are two strategies for an antifouling surface, both having their own merits. If a surface which cannot be easily fouled is desired, then from the results of this study, a hydrophobic or superhydrophobic surface is required. These surfaces prevent the spread of water droplets and self clean of dirt and microbes using the Lotus effect. However, the drawback is that if microbes are readily sloughed from such a surface, they will be transferred somewhere else, and may continue to pose a risk there. With the superhydrophilic surfaces, we see that the level of microbial adhesion is greater than for the hydrophobic surfaces. However, the adherent microbes are well dispersed on these surfaces, and because all of the superhydrophilic materials tested here are also photocatalysts, this is beneficial to their function. A thinner, more spread out overlayer of microbes will not shield the photocatalyst from atmospheric oxygen and incident light as much as a thick layer and so photodisinfection will be more efficacious. If a surface which actively disinfects is required, then a hydrophilic photocatalyst surface is required. In certain situations it could conceivably be possible to design products incorporating both kinds of surface into their design, such that for example microbes are physically removed from one area of a device by the hydrophobic surface, and collect in a region treated with photocatalyst, such that the microbes that are transferred there are killed. Such a device would be a fusion of the two methodologies and incorporates the good points of both technologies.

Adhesion of microbes to TiO_2 photocatalyst surfaces has only been examined sparingly in the literature. Some studies[165-167] which appear to discuss microbial adhesion to TiO_2, are really focussing on the antimicrobial properties. In these studies it was however suggested that TiO_2 surfaces under UV illumination reduced

microbial adhesion. Perhaps the best study of microbial adhesion to oxide thin films, which includes many of the materials examined in this work is that of Li and Logan.[160] In the Li and Logan study, it was shown that adhesion of *P. aeruginosa* to thin films increased in the order float glass (Sn side) < float glass (air side) < TiO_2 (Activ™ equivalent) < SnO_2 <SnO_2:F (K-Glass™ equivalent). The work in this study correlates well with the findings from the Li and Logan study, in that TiO_2 materials appear to increase microbial adhesion compared to a glass control. However, in the literature study, the TiO_2 films were not UV irradiated, and so PSH and its potential impact on microbial adhesion was not really investigated. Whilst this was carried out in this work it does not appear to have had a significant impact and has not really altered the results from those seen in the Li and Logan study. Designing a more elaborate experimental procedure to adequately assess this area is undoubtedly required. However, it will be challenging to create an experiment in which the necessary UV irradiation, required to generate PSH, does not result in observation of the already demonstrated antimicrobial characteristics of TiO_2 based thin films. Perhaps the samples could be irradiated for an extended time period (substantially longer than used in this study) by 254 nm lamp, to generate the hydrophilic surface, and then microbial adhesion characteristics be examined as swiftly as possible in the absence of further UV illumination. Microbial adhesion could be examined under conditions of flow (by flow cell techniques), by microscopy or by AFM. Flow cell techniques are commonly used for microbial adhesion studies, but may not be appropriate for these materials as conditions of microbial flow across the surface in a fluid medium may not be routinely encountered by these materials in real world use. Direct microscopic analysis, could also be used, in conjunction with a revised experimental method in which the samples were perhaps washed in a uniform manner to leave only adherent organisms which could be stained and observed directly. This is however not an ideal experimental technique either – due to the sample washing step. AFM would perhaps be the most interesting route as the tip could be used to measure the attractive and repulsive forces between a microbe of choice immobilised on the AFM cantilever and the surface. This would also not require the sample to be away

from UV illumination for an extended period whilst measurements are taken. AFM measurement would result in quantitative analysis of the microbial adhesion to the surface, independent of fluid flow conditions or washing from the substrate. Such investigations by AFM have already been carried out for other substrates,[168] but not on TiO_2 thin films, to the authors knowledge.

4.5 Conclusion

In this chapter we have seen how the adhesion of microbes to surfaces can be affected by numerous physico-chemical factors, and the complexity of microbial adhesion has been demonstrated. There is no one clear explanation for the behaviour of all of the materials with regard to adhesion of microbes to their surface. What has been demonstrated is that at a magnitude smaller than microbial size, surface roughness is no longer of any consequence to adhesion. Similarly, water droplet contact angles do not provide an accurate indicator of the tendency of microbes to adhere to a surface either. However one can broadly say that a hydrophobic surface such as Hydrotech is fouled less easily, whereas a superhydrophilic surface such as the sol-gel materials is fouled more easily. When the contact angle is neither hydrophilic nor hydrophobic there is great variation in adhesion. This can only be explained by other physico-chemical factors not determined in this study. What is clear though is that both superhydrophilic and superhydrophobic surfaces can have their place in a antimicrobial coatings strategy – provided that the functional properties are considered in relation to the requirements of a coating in a particular setting, i.e. the fine line between self cleaning and self disinfecting must be considered.

Chapter 5: Conclusions and Future Work

Initially this study reviewed the role of inanimate surfaces in the epidemiology of hospital acquired infections (HAIs). It was demonstrated how surfaces play a key role in the epidemiology of HAIs and it was shown how the introduction of an antimicrobial surface, an antifouling surface, or a combined approach could be used to control HAIs linked with surfaces. A number of strategies were reviewed, but it was the light-activated materials which demonstrated some of the greatest promise because of their non-selective mode of action and the low probability of initiating resistance in microbes. For hard surface applications, the TiO_2 based photocatalyst films are obvious candidates, and it was for this reason that they became the focus of this study.

Materials produced during this study were characterised by numerous techniques. In all cases an anatase TiO_2 base material was present, having an optical band gap in the region of 3.2 eV. Characterisation of dopants was difficult due to the relatively poor efficiency in transfer from sol to coating. Specialised techniques including XPS and XANES were required to show the presence of Ag_2O as a dopant in the Ag/TiO_2 films. In future work, full study of the efficiency of doping, and its characterisation by XANES in particular, would be a useful enhancement to the study as it may enable production of materials with higher photoactivity to be produced. All samples demonstrated photocatalytic activity and photoinduced superhydrophilicity. The doped materials were superior in performance to the TiO_2 control.

All of the photocatalyst samples demonstrated antimicrobial activity towards the test microorganisms. It was shown that the photocatalysts could utilise 365 nm UV light and also the light from a standard compact fluorescent lamp, of the same spectral profile as those used in UK hospitals. This demonstrates the potential worth of these materials in a clinical setting, where they might work to reduce microbial loads on surfaces. Of all the materials tested, it was the Ag_2O/TiO_2 and the photodeposited Ag on TiO_2 samples that were the most interesting. These functioned in different ways, but were both particularly potent. The former was

potent as a photocatalytic antimicrobial, the latter working in the dark too, as a microbicide release antimicrobial.

Some materials were also compared to commercially available materials in terms of their potential antifouling and anti-adhesive properties. The superhydrophilic materials, including the sol-gel TiO_2 type materials were shown not to inhibit adhesion. However, under SEM it was possible to observe the spreading of microcolonies on the TiO_2 materials, compared to a glass control. This is in fact beneficial, as a contaminant layer of microbes is spread more thinly, exposed to a greater surface area of the photocatalyst, and hence destroyed more effectively. If one requires a true antifouling, self cleaning surface, the hydrophobic Pilkington Hydrotech sample was quite spectacular. Microbe attachment to this sample was markedly reduced, and water beads up and rolls off easily. It would therefore appear that perhaps an anti-adhesive and antimicrobial surface made from photocatalyst might not be possible. However, this should not detract from the argument, since the microbial inocula used in this study are many orders of magnitude greater than real-world contamination. The materials produced here would therefore likely function very well, even under room lighting and any anti-adhesive property might not necessarily bring significant extra benefit. Experiments to study these materials in a clinical environment are presently being carried out.

Although not extensively examined in this study, the mechanism for the destruction of stearic acid and of microbes is accepted to be by the production of radical species, the hydroxyl radical in particular. Attempts were made during the course of this study to measure the production of hydroxyl radicals using a hydroxyl radical specific fluorescent probe. Hydroxyl radical production from a TiO_2 powder was confirmed, but analysis of the thin films proved fruitless. This is possibly due to the much smaller surface area of the film compared with a powder, resulting in lower hydroxyl radical production. In future incarnations of this work, quantification and analysis of radicals produced, perhaps *via* EPR measurements would be useful. This has been carried out before on similar films by previous members of the research group, and so was not attempted for this study. It would also be of interest to

study the mechanism by which microbes are killed. Whilst this has been demonstrated for TiO_2, doped materials haven't been studied. It is logical to assume that the films made in this study, functioning as photocatalysts will kill microbes in this way also.

Publications Arising From This Work

1) K. Page, R.G. Palgrave, I.P. Parkin, M. Wilson, S.L.P. Savin, and A.V. Chadwick, *Titania and silver-titania composite films on glass-potent antimicrobial coatings.* ***Journal of Materials Chemistry***, 2007, 17(1), p. 95-104.
2) Wilson, M., Parkin, I.P. and Page, K., Patent PCT/GB2006/004036, *Antimicrobial Films*
3) K. Page, I. P. Parkin and M. Wilson, *2007 NSTI Nanotechnology Conference and Trade Show - NSTI Nanotech 2007, Technical Proceedings*, 2007, pp. 356-359.
4) K. Page, M. Wilson and I.P. Parkin, *Antimicrobial surfaces and their potential in reducing the role of the inanimate environment in the incidence of hospital-acquired infections*, ***Journal of Materials Chemistry***, 2009, 19(23), p3819-3831.

References

1. Sanborn, W.R., *The Relation of Surface Contamination to the Transmission of Disease.* American Journal Of Public Health, 1963. **53**(8): p. 1278-1283.

2. Dancer, S.J., *Importance of the environment in meticillin-resistant Staphylococcus aureus acquisition: the case for hospital cleaning.* Lancet Infectious Diseases, 2008. **8**(2): p. 101-113.

3. NHS. *NHS Health A-Z: MRSA*. 2008 16/02/2009]; Available from: http://www.nhs.uk/Conditions/MRSA/Pages/Introduction.aspx?url=Pages/What-is-it.aspx&r=1&rtitle=MRSA+-+Introduction.

4. Dancer, S.J., *How do we assess hospital cleaning? A proposal for microbiological standards for surface hygiene in hospitals.* Journal of Hospital Infection, 2004. **56**(1): p. 10-15.

5. Hota, B., *Contamination, disinfection, and cross-colonization: Are hospital surfaces reservoirs for nosocomial infection?* Clinical Infectious Diseases, 2004. **39**(8): p. 1182-1189.

6. Oie, S., Hosokawa, I., and Kamiya, A., *Contamination of room door handles by methicillin-sensitive/methicillin-resistant Staphylococcus aureus.* Journal of Hospital Infection, 2002. **51**(2): p. 140-143.

7. Talon, D., *The role of the hospital environment in the epidemiology of multi-resistant bacteria.* Journal of Hospital Infection, 1999. **43**(1): p. 13-17.

8. Dietze, B., Rath, A., Wendt, C., and Martiny, H., *Survival of MRSA on sterile goods packaging.* Journal of Hospital Infection, 2001. **49**(4): p. 255-261.

9. Oie, S. and Kamiya, A., *Survival of methicillin-resistant Staphylococcus aureus (MRSA) on naturally contaminated dry mops.* Journal of Hospital Infection, 1996. **34**(2): p. 145-149.

10. Neely, A.N. and Maley, M.P., *Survival of enterococci and staphylococci on hospital fabrics and plastic.* Journal of Clinical Microbiology, 2000. **38**(2): p. 724-726.

11. Banerjee, D., Fraise, A., and Chana, K., *Writing pens are an unlikely vector of cross-infection with methicillin resistant Staphylococcus aureus (MRSA).* Journal of Hospital Infection, 1999. **43**(1): p. 73-75.

12. Bures, S., Fishbain, J.T., Uyehara, C.F.T., Parker, J.M., and Berg, B.W., *Computer keyboards and faucet handles as reservoirs of nosocomial pathogens in the intensive care unit.* American Journal of Infection Control, 2000. **28**(6): p. 465-471.

13. Cohen, H.A., Amir, J., Matalon, A., Mayan, R., Beni, S., and Barzilai, A., *Stethoscopes and otoscopes - a potential vector of infection?* Family Practice, 1997. **14**(6): p. 446-449.

14. Ciragil, P., Gul, M., and Aral, M., *Bacterial contamination of computers and telephones in a university hospital in Turkey.* Journal of Hospital Infection, 2006. **62**(2): p. 247-248.

15. Boyce, J.M., Potter-Bynoe, G., Chenevert, C., and King, T., *Environmental contamination due to methicillin-resistant Staphylococcus aureus: Possible infection control implications.* Infection Control and Hospital Epidemiology, 1997. **18**(9): p. 622-627.

16. Bhalla, A., Pultz, N.J., Gries, D.M., Ray, A.J., Eckstein, E.C., Aron, D.C., and Donskey, C.J., *Acquisition of nosocomial pathogens on hands after contact*

with environmental surfaces near hospitalized patients. Infection Control and Hospital Epidemiology, 2004. **25**(2): p. 164-167.

17. Rountree, P.M., *Effect of desiccation on viability of Staphylococcus aureus.* Journal of Hygiene, 1963. **61**(3): p. 265.

18. White, L.F., Dancer, S.J., and Robertson, C., *A microbiological evaluation of hospital cleaning methods.* International Journal of Environmental Health Research, 2007. **17**(4): p. 285-295.

19. Griffith, C.J., Cooper, R.A., Gilmore, J., Davies, C., and Lewis, M., *An evaluation of hospital cleaning regimes and standards.* Journal of Hospital Infection, 2000. **45**(1): p. 19-28.

20. Rutala, W.A., Katz, E.B.S., Sherertz, R.J., and Sarubbi, F.A., *Environmental-Study of a Methicillin-Resistant Staphylococcus-Aureus Epidemic in a Burn Unit.* Journal of Clinical Microbiology, 1983. **18**(3): p. 683-688.

21. Bernard, L., Kereveur, A., Durand, D., Gonot, J., Goldstein, F., Mainardi, J.L., Acar, J., and Carlet, J., *Bacterial Contamination of Hospital Physicians' Stethoscopes.* Infection Control and Hospital Epidemiology, 1999. **20**(9): p. 626-628.DOI: doi:10.1086/501686.

22. Aycicek, H., Oguz, U., and Karci, K., *Comparison of results of ATP bioluminescence and traditional hygiene swabbing methods for the determination of surface cleanliness at a hospital kitchen.* International Journal of Hygiene and Environmental Health, 2006. **209**(2): p. 203-206.

23. Hardy, K.J., Gossain, S., Henderson, N., Drugan, C., Oppenheim, B.A., Gao, F., and Hawkey, P.M., *Rapid recontamination with MRSA of the environment of an intensive care unit after decontamination with hydrogen peroxide vapour.* Journal of Hospital Infection, 2007. **66**(4): p. 360-368.

24. Upmann, M. and Reuter, G., *The surface count on equipment and premises and the handling of hygiene in a meat cutting plant for pork - Part 2.* Fleischwirtschaft, 1998. **78**(9): p. 971-974.

25. Kaneko, K.I., Hayashidani, H., Takahashi, K., Shiraki, Y., Limawongpranee, S., and Ogawa, M., *Bacterial contamination in the environment of food factories processing ready-to-eat fresh vegetables.* Journal of Food Protection, 1999. **62**(7): p. 800-804.

26. Grosspietsch, R., Einschutz, K., Jaeger, D., and Fries, R., *Survey on the hygienic status of plastic doors of a pig abattoir.* Journal of Food Protection, 2006. **69**(11): p. 2738-2741.

27. Jackson, V., Blair, I.S., McDowell, D.A., Kennedy, J., and Bolton, D.J., *The incidence of significant foodborne pathogens in domestic refrigerators.* Food Control, 2007. **18**(4): p. 346-351.DOI: 10.1016/j.foodcont.2005.10.018.

28. Gounadaki, A.S., Skandamis, P.N., Drosinos, E.H., and Nychas, G.J.E., *Microbial ecology of food contact surfaces and products of small-scale facilities producing traditional sausages.* Food Microbiology, 2008. **25**(2): p. 313-323.DOI: 10.1016/j.fm.2007.10.001.

29. French, G.L., Otter, J.A., Shannon, K.P., Adams, N.M.T., Watling, D., and Parks, M.J., *Tackling contamination of the hospital environment by methicillin-resistant Staphylococcus aureus (MRSA): a comparison between conventional terminal cleaning and hydrogen peroxide vapour decontamination.* Journal of Hospital Infection, 2004. **57**(1): p. 31-37.

30. Madigan, M.T. and Martinko, J., *Brock Biology of Microorganisms*. 11 ed. 2006: Pearson Prentice Hall.

31. Costerton, J.W., Lewandowski, Z., Caldwell, D.E., Korber, D.R., and Lappinscott, H.M., *Microbial Biofilms.* Annual Review of Microbiology, 1995. **49**: p. 711-745.

32. Donlan, R.M. and Costerton, J.W., *Biofilms: Survival mechanisms of clinically relevant microorganisms.* Clinical Microbiology Reviews, 2002. **15**(2): p. 167-193.DOI: 10.1128/cmr.15.2.167-193.2002.

33. Costerton, J.W., Stewart, P.S., and Greenberg, E.P., *Bacterial biofilms: A common cause of persistent infections.* Science, 1999. **284**(5418): p. 1318-1322.

34. Leewenhoeck, A., *An Abstract of a Letter from Mr. Anthony Leewenhoeck at Delft, Dated Sep. 17. 1683. Containing Some Microscopical Observations, about Animals in the Scurf of the Teeth, the Substance Call'd Worms in the Nose, the Cuticula Consisting of Scales.* Philosophical Transactions of The Royal Society (1683-1775), 1684. **14**: p. 568-574.

35. Davey, M.E. and O'Toole, G.A., *Microbial biofilms: from ecology to molecular genetics.* Microbiology and Molecular Biology Reviews, 2000. **64**(4): p. 847-867.

36. Gilbert, P., Das, J., and Foley, I., *Biofilm susceptibility to antimicrobials.* Advances In Dental Research, 1997. **11**(1): p. 160-167.

37. Flemming, H.C., *Biofilms and Environmental-Protection.* Water Science and Technology, 1993. **27**(7-8): p. 1-10.

38. Roberts, A.P., Pratten, J., Wilson, M., and Mullany, P., *Transfer of a conjugative transposon, Tn5397 in a model oral biofilm.* Fems Microbiology Letters, 1999. **177**(1): p. 63-66.

39. Center for Biofilm Engineering. *Biofilms Online - A Biofilms Primer*. [Online Textbook] 2008 [cited 2008 13/10/2008]; Available from: http://www.biofilmsonline.com/cgi-bin/biofilmsonline/ed_intro_primer.html.

40. Strevett, K.A. and Chen, G., *Microbial surface thermodynamics and applications.* Research in Microbiology, 2003. **154**(5): p. 329-335.

41. Geoghegan, M., Andrews, J.S., Biggs, C.A., Eboigbodin, K.E., Elliott, D.R., Rolfe, S., Scholes, J., Ojeda, J.J., Romero-Gonzalez, M.E., Edyvean, R.G.J., Swanson, L., Rutkaite, R., Fernando, R., Pen, Y., Zhang, Z.Y., and Banwart, S.A., *The polymer physics and chemistry of microbial cell attachment and adhesion.* Faraday Discussions, 2008. **139**: p. 85-103.DOI: 10.1039/b717046g.

42. Beveridge, T.J., Makin, S.A., Kadurugamuwa, J.L., and Li, Z.S., *Interactions between biofilms and the environment.* FEMS Microbiology Reviews, 1997. **20**(3-4): p. 291-303.

43. Prescott, L.M., Harley, J.P., and Klein, D.A., *Microbiology*. 6 ed. 2002, Boston, London: Mc Graw-Hill.

44. Park, K.D., Kim, Y.S., Han, D.K., Kim, Y.H., Lee, E.H.B., Suh, H., and Choi, K.S., *Bacterial adhesion on PEG modified polyurethane surfaces.* Biomaterials, 1998. **19**(7-9): p. 851-859.

45. Chapman, R.G., Ostuni, E., Liang, M.N., Meluleni, G., Kim, E., Yan, L., Pier, G., Warren, H.S., and Whitesides, G.M., *Polymeric thin films that resist the adsorption of proteins and the adhesion of bacteria.* Langmuir, 2001. **17**(4): p. 1225-1233.

46. Ostuni, E., Chapman, R.G., Liang, M.N., Meluleni, G., Pier, G., Ingber, D.E., and Whitesides, G.M., *Self-Assembled Monolayers That Resist the Adsorption of Proteins and the Adhesion of Bacterial and Mammalian Cells.* Langmuir, 2001. **17**(20): p. 6336-6343.DOI: doi:10.1021/la010552a.

47. Hou, S., Burton, E.A., Simon, K.A., Blodgett, D., Luk, Y.-Y., and Ren, D., *Inhibition of Escherichia coli Biofilm Formation by Self-Assembled Monolayers of Functional Alkanethiols on Gold.* Appl. Environ. Microbiol., 2007. **73**(13): p. 4300-4307.DOI: 10.1128/aem.02633-06.

48. Grill, A., *Review Of The Tribology Of Diamond-Like Carbon.* Wear, 1993. **168**(1-2): p. 143-153.

49. Robertson, J., *Diamond-like amorphous carbon.* Materials Science & Engineering R-Reports, 2002. **37**(4-6): p. 129-281.

50. Hauert, R., *A review of modified DLC coatings for biological applications.* Diamond and Related Materials, 2003. **12**(3-7): p. 583-589.DOI: 10.1016/s0925-9635(03)00081-5.

51. Aisenberg, S. and Chabot, R., *Ion-Beam Deposition Of Thin Films Of Diamondlike Carbon.* Journal of Applied Physics, 1971. **42**(7): p. 2953-2958.

52. Greenwood, N.N. and Earnshaw, A., *Chemistry of the Elements*. 1 ed. 1995, Oxford: Butterworth-Heinemann.

53. Liu, C., Zhao, Q., Liu, Y., Wang, S., and Abel, E.W., *Reduction of bacterial adhesion on modified DLC coatings.* Colloids and Surfaces B: Biointerfaces, 2008. **61**(2): p. 182-187.

54. Kwok, S.C.H., Zhang, W., Wan, G.J., McKenzie, D.R., Bilek, M.M.M., and Chu, P.K., *Hemocompatibility and anti-bacterial properties of silver doped*

diamond-like carbon prepared by pulsed filtered cathodic vacuum arc deposition. Diamond and Related Materials, 2007. **16**(4-7): p. 1353-1360.DOI: 10.1016/j.diamond.2006.11.001.

55. Bourn, J., *The Management and Control of Hospital Acquired Infection in Acute NHS Trusts in England*. 2000: National Audit Office.

56. Hockenhull, J.C., Dwan, K., Boland, A., Smith, G., Bagust, A., Dündar, Y., Gamble, C., McLeod, C., Walley, T., and Dickson, R., *The clinical effectiveness and cost-effectiveness of central venous catheters treated with anti-infective agents in preventing bloodstream infections: a systematic review and economic evaluation.* Health Technology Assessment, 2008. **12**(12).

57. Lewis, A.L., *Phosphorylcholine-based polymers and their use in the prevention of biofouling.* Colloids and Surfaces B-Biointerfaces, 2000. **18**(3-4): p. 261-275.

58. Rose, S.F., Okere, S., Hanlon, G.W., Lloyd, A.W., and Lewis, A.L., *Bacterial adhesion to phosphorylcholine-based polymers with varying cationic charge and the effect of heparin pre-adsorption.* Journal of Materials Science-Materials in Medicine, 2005. **16**(11): p. 1003-1015.

59. Hirota, K., Murakami, K., Nemoto, K., and Miyake, Y., *Coating of a surface with 2-methacryloyloxyethyl phosphorylcholine (MPC) co-polymer significantly reduces retention of human pathogenic microorganisms.* FEMS Microbiology Letters, 2005. **248**(1): p. 37-45.

60. Cheng, G., Zhang, Z., Chen, S.F., Bryers, J.D., and Jiang, S.Y., *Inhibition of bacterial adhesion and biofilm formation on zwitterionic surfaces.* Biomaterials, 2007. **28**(29): p. 4192-4199.DOI: 10.1016/j.biomaterials.2007.05.041.

61. Okada, A., Nikaido, T., Ikeda, M., Okada, K., Yamauchi, J., Foxton, R.M., Sawada, H., Tagami, J., and Matin, K., *Inhibition of Biofilm Formation using Newly Developed Coating Materials with Self-cleaning Properties.* Dental Materials Journal, 2008. **27**: p. 256-272.

62. Barthlott, W. and Neinhuis, C., *Purity of the sacred lotus, or escape from contamination in biological surfaces.* Planta, 1997. **202**(1): p. 1-8.

63. Parkin, I.P. and Palgrave, R.G., *Self-cleaning coatings.* Journal of Materials Chemistry, 2005. **15**(17): p. 1689-1695.

64. Bico, J., Marzolin, C., and Quere, D., *Pearl drops.* Europhysics Letters, 1999. **47**(2): p. 220-226.

65. Hosono, E., Fujihara, S., Honma, I., and Zhou, H., *Superhydrophobic Perpendicular Nanopin Film by the Bottom-Up Process.* Journal of the American Chemical Society, 2005. **127**(39): p. 13458-13459.

66. Microban International Ltd. [cited 2008 27/11/08]; Available from: http://www.microban.com/europe/?lang=en.

67. What's New In Building. *John Radcliffe Hospital Embraces Technology in the Fight against Hospital Acquired Infections*
[cited 2008 27/11/08]; Available from: http://www.wnibi.com/Building/Articles.aspx/488.

68. Latch, D.E., Packer, J.L., Arnold, W.A., and McNeill, K., *Photochemical conversion of triclosan to 2,8-dichlorodibenzo-p-dioxin in aqueous solution.* Journal of Photochemistry and Photobiology a-Chemistry, 2003. **158**(1): p. 63-66.DOI: 10.1016/s1010-6030(03)00103-5.

69. Mezcua, M., Gómez, M.J., Ferrer, I., Aguera, A., Hernando, M.D., and Fernández-Alba, A.R., *Evidence of 2,7/2,8-dibenzodichloro-p-dioxin as a photodegradation product of triclosan in water and wastewater samples.* Analytica Chimica Acta, 2004. **524**(1-2): p. 241-247.

70. AcryMed Inc. *SilvaGard™ Technology Summary*. [Technology Summary Document] 2005 16/02/2009]; Available from: http://www.acrymed.com/pdf/SilvaGard%20Technical%20Summary.pdf.

71. Lansdown, A.B.G., *Silver in Healthcare: an Enigma and Pathological Fascination.* The Bulletin of The Royal College of Pathologists, 2006. **133**: p. 36-38.

72. Silver, S., *Bacterial silver resistance: molecular biology and uses and misuses of silver compounds.* Fems Microbiology Reviews, 2003. **27**(2-3): p. 341-353.

73. AgION Technologies Inc. *AgION™ Technology*. 2005 10/01/2006]; Available from: http://www.agion-tech.com.

74. Domek, M.J., LeChevallier, M.W., Cameron, S.C., and McFeters, G.A., *Evidence for the role of copper in the injury process of coliform bacteria in drinking water.* Applied and Environmental Microbiology, 1984. **48**(2): p. 289-293.

75. Kuhn, P.J., *Doorknobs: a source of nosocomial infection?* Diagnostic Medicine, 1983. **6**(8): p. 62-63.

76. Wilks, S.A., Michels, H., and Keevil, C.W., *The survival of Escherichia coli O157 on a range of metal surfaces.* International Journal of Food Microbiology, 2005. **105**(3): p. 445-454.

77. Noyce, J.O., Michels, H., and Keevil, C.W., *Potential use of copper surfaces to reduce survival of epidemic meticillin-resistant Staphylococcus aureus in the healthcare environment.* Journal of Hospital Infection, 2006. **63**(3): p. 289-297.

78. Wilks, S.A., MichelS, H.T., and Keevil, C.W., *Survival of Listeria monocytogenes Scott a on metal surfaces: Implications for cross-contamination.* International Journal of Food Microbiology, 2006. **111**(2): p. 93-98.

79. Noyce, J.O., Michels, H., and Keevil, C.W., *Inactivation of influenza A virus on copper versus stainless steel surfaces.* Applied and Environmental Microbiology, 2007. **73**(8): p. 2748-2750.

80. Weaver, L., Michels, H.T., and Keevil, C.W., *Survival of Clostridium difficile on copper and steel: futuristic options for hospital hygiene.* Journal of Hospital Infection, 2008. **68**(2): p. 145-151.

81. Copper Development Association. *Antimicrobial Copper Clinical Trial*. 2008 08/06/2008]; Available from: http://www.copperinfo.co.uk/antimicrobial/clinical-trial.shtml.

82. Sulakvelidze, A., Alavidze, Z., and Morris, J.G., *Bacteriophage therapy.* Antimicrobial Agents and Chemotherapy, 2001. **45**(3): p. 649-659.

83. Stone, R., *Bacteriophage therapy: Stalin's forgotten cure.* Science, 2002. **298**(5594): p. 728-731.

84. Markoishvili, K., Tsitlanadze, G., Katsarava, R., Morris, J.G., and Sulakvelidze, A., *A novel sustained-release matrix based on biodegradable poly(ester amide)s and impregnated with bacteriophages and an antibiotic shows promise in management of infected venous stasis ulcers and other poorly*

healing wounds. International Journal of Dermatology, 2002. **41**(7): p. 453-458.

85. Jikia, D., Chkhaidze, N., Imedashvili, E., Mgaloblishvili, I., Tsitlanadze, G., Katsarava, R., Morris, G.J., and Sulakvelidze, A., *The use of a novel biodegradable preparation capable of the sustained release of bacteriophages and ciprofloxacin, in the complex treatment of multidrug-resistant Staphylococcus aureus-infected local radiation injuries caused by exposure to Sr90.* Clinical and Experimental Dermatology, 2005. **30**(1): p. 23-26.

86. Curtin, J.J. and Donlan, R.M., *Using bacteriophages to reduce formation of catheter-associated biofilms by Staphylococcus epidermidis.* Antimicrobial Agents and Chemotherapy, 2006. **50**(4): p. 1268-1275.

87. Speier, J.L. and Malek, J.R., *Destruction of microorganisms by contact with solid surfaces.* Journal of Colloid and Interface Science, 1982. **89**(1): p. 68-76.

88. Klibanov, A.M., *Permanently microbicidal materials coatings.* Journal of Materials Chemistry, 2007. **17**(24): p. 2479-2482.DOI: 10.1039/b702079a.

89. Haldar, J., An, D.Q., de Cienfuegos, L.A., Chen, J.Z., and Klibanov, A.M., *Polymeric coatings that inactivate both influenza virus and pathogenic bacteria.* Proceedings of the National Academy of Sciences of the United States of America, 2006. **103**(47): p. 17667-17671.

90. Mukherjee, K., Rivera, J., and Klibanov, A., *Practical Aspects of Hydrophobic Polycationic Bactericidal "Paints".* Applied Biochemistry and Biotechnology, 2008. **151**(1): p. 61-70.

91. Park, D., Wang, J., and Klibanov, A.M., *One-step, painting-like coating procedures to make surfaces highly and permanently bactericidal.* Biotechnology Progress, 2006. **22**(2): p. 584-589.

92. Wilson, M., *Light-activated antimicrobial coating for the continuous disinfection of surfaces.* Infection Control and Hospital Epidemiology, 2003. **24**(10): p. 782-784.

93. Ireland, J.C., Klostermann, P., Rice, E.W., and Clark, R.M., *Inactivation of Escherichia coli by Titanium-Dioxide Photocatalytic Oxidation.* Applied and Environmental Microbiology, 1993. **59**(5): p. 1668-1670.

94. Bonnett, R., *Photosensitizers of the Porphyrin and Phthalocyanine Series for Photodynamic Therapy.* Chemical Society Reviews, 1995. **24**(1): p. 19-33.

95. Decraene, V., Pratten, J., and Wilson, M., *Cellulose acetate containing toluidine blue and rose bengal is an effective antimicrobial coating when exposed to white light.* Applied and Environmental Microbiology, 2006. **72**(6): p. 4436-4439.

96. Decraene, V., Pratten, J., and Wilson, M., *Assessment of the Activity of a Novel Light-Activated Antimicrobial Coating in a Clinical Environment.* Infection Control and Hospital Epidemiology, 2008. **29**(12): p. 1181-1184.DOI: 10.1086/592413.

97. Decraene, V., Pratten, J., and Wilson, M., *Novel light-activated antimicrobial coatings are effective against surface-deposited Staphylococcus aureus.* Current Microbiology, 2008. **57**(4): p. 269-273.DOI: 10.1007/s00284-008-9188-7.

98. Perni, S., Piccirillo, C., Pratten, J., Prokopovich, P., Chrzanowski, W., Parkin, I.P., and Wilson, M., *The antimicrobial properties of light-activated polymers*

containing methylene blue and gold nanoparticles. Biomaterials, 2009. **30**(1): p. 89-93.DOI: 10.1016/j.biomaterials.2008.09.020.

99. Perni, S., Prokopovich, P., Piccirillo, C., Pratten, J., Parkin, I.P., and Wilson, M., *Toluidine blue-containing polymers exhibit potent bactericidal activity when irradiated with red laser light.* Journal of Materials Chemistry, 2009. **19**(18): p. 2715-2723.DOI: 10.1039/b820561b.

100. Matsunaga, T., Tomoda, R., Nakajima, T., and Wake, H., *Photoelectrochemical Sterilization of Microbial-Cells by Semiconductor Powders.* FEMS Microbiology Letters, 1985. **29**(1-2): p. 211-214.

101. Jacoby, W.A., Maness, P.C., Wolfrum, E.J., Blake, D.M., and Fennell, J.A., *Mineralization of bacterial cell mass on a photocatalytic surface in air.* Environmental Science & Technology, 1998. **32**(17): p. 2650-2653.

102. Ibanez, J.A., Litter, M.I., and Pizarro, R.A., *Photocatalytic bactericidal effect of TiO_2 on Enterobacter cloacae. Comparative study with other Gram (-) bacteria.* Journal of Photochemistry and Photobiology A: Chemistry, 2003. **157**(1): p. 81-85.

103. Vohra, A., Goswami, D.Y., Deshpande, D.A., and Block, S.S., *Enhanced photocatalytic inactivation of bacterial spores on surfaces in air.* Journal of Industrial Microbiology & Biotechnology, 2005. **32**(8): p. 364-370.

104. Keleher, J., Bashant, J., Heldt, N., Johnson, L., and Li, Y.Z., *Photo-catalytic preparation of silver-coated TiO_2 particles for antibacterial applications.* World Journal of Microbiology & Biotechnology, 2002. **18**(2): p. 133-139.

105. Rincon, A.G. and Pulgarin, C., *Photocatalytical inactivation of E. coli: effect of (continuous-intermittent) light intensity and of (suspended-fixed) TiO_2 concentration.* Applied Catalysis B-Environmental, 2003. **44**(3): p. 263-284.

106. Rincon, A.G. and Pulgarin, C., *Bactericidal action of illuminated TiO_2 on pure Escherichia coli and natural bacterial consortia: post-irradiation events in the dark and assessment of the effective disinfection time.* Applied Catalysis B-Environmental, 2004. **49**(2): p. 99-112.

107. Rincon, A.G. and Pulgarin, C., *Field solar E. coli inactivation in the absence and presence of TiO_2: is UV solar dose an appropriate parameter for standardization of water solar disinfection?* Solar Energy, 2004. **77**(5): p. 635-648.

108. Zhang, L.Z., Yu, J.C., Yip, H.Y., Li, Q., Kwong, K.W., Xu, A.W., and Wong, P.K., *Ambient light reduction strategy to synthesize silver nanoparticles and silver-coated TiO_2 with enhanced photocatalytic and bactericidal activities.* Langmuir, 2003. **19**(24): p. 10372-10380.DOI: 10.1021/la035330m.

109. Ertl, G., Knözinger, H., and Weitkamp, J., eds. *Preparation of Solid Catalysts*. Illustrated ed. 1999, Wiley VCH.

110. Mills, A. and LeHunte, S., *An overview of semiconductor photocatalysis.* Journal of Photochemistry and Photobiology A: Chemistry, 1997. **108**(1): p. 1-35.

111. Matsunaga, T., Tomoda, R., Nakajima, T., Nakamura, N., and Komine, T., *Continuous-Sterilization System That Uses Photosemiconductor Powders.* Applied and Environmental Microbiology, 1988. **54**(6): p. 1330-1333.

112. Evonik Industries AG. *AEROSIL® Fumed Silica - Product Groups (Hydrophilic Fumed Metal Oxides)*. 2008 25/08/2008]; Available from: http://www.aerosil.com/aerosil/en/solutions/productgroups/fumedmetaloxides/default.

113. Evonik Industries AG, *Product Information: AEROXIDE® TiO_2 P 25 Hydrophilic Fumed Titanium Dioxide*. 2007.

114. Evans, P. and Sheel, D.W., *Photoactive and antibacterial TiO_2 thin films on stainless steel.* Surface & Coatings Technology, 2007. **201**(22-23): p. 9319-9324.DOI: 10.1016/j.surfcoat.2007.04.013.

115. Rampaul, A., Parkin, I.P., O'Neill, S.A., DeSouza, J., Mills, A., and Elliott, N., *Titania and tungsten doped titania thin films on glass; active photocatalysts.* Polyhedron, 2003. **22**(1): p. 35-44.

116. Watts, R.J., Kong, S.H., Orr, M.P., Miller, G.C., and Henry, B.E., *Photocatalytic Inactivation of Coliform Bacteria and Viruses in Secondary Waste-Water Effluent.* Water Research, 1995. **29**(1): p. 95-100.

117. Huang, Z., Maness, P.C., Blake, D.M., Wolfrum, E.J., Smolinski, S.L., and Jacoby, W.A., *Bactericidal mode of titanium dioxide photocatalysis.* Journal of Photochemistry and Photobiology A: Chemistry, 2000. **130**(2-3): p. 163-170.

118. Lu, Z.X., Zhou, L., Zhang, Z.L., Shi, W.L., Xie, Z.X., Xie, H.Y., Pang, D.W., and Shen, P., *Cell damage induced by photocatalysis of TiO_2 thin films.* Langmuir, 2003. **19**(21): p. 8765-8768.

119. Asahi, R., Morikawa, T., Ohwaki, T., Aoki, K., and Taga, Y., *Visible-light photocatalysis in nitrogen-doped titanium oxides.* Science, 2001. **293**(5528): p. 269-271.

120. Kisch, H. and Macyk, W., *Visible-light photocatalysis by modified titania.* ChemPhysChem, 2002. **3**(5): p. 399-400.

121. Justicia, I., Ordejon, P., Canto, G., Mozos, J.L., Fraxedas, J., Battiston, G.A., Gerbasi, R., and Figueras, A., *Designed self-doped titanium oxide thin films for efficient visible-light photocatalysis.* Advanced Materials, 2002. **14**(19): p. 1399-1402.

122. Epifani, M., Giannini, C., Tapfer, L., and Vasanelli, L., *Sol-gel synthesis and characterization of Ag and Au nanoparticles in SiO_2, TiO_2, and ZrO_2 thin films.* Journal of the American Ceramic Society, 2000. **83**(10): p. 2385-2393.

123. Mills, A., Elliott, N., Parkin, I.P., O'Neill, S.A., and Clark, R.J.H., *Novel TiO_2 CVD films for semiconductor photocatalysis.* Journal of Photochemistry and Photobiology a-Chemistry, 2002. **151**(1-3): p. 171-179.

124. Binions, R., Carmalt, C.J., and Parkin, I.P., *Germanium phosphide coatings from the atmospheric pressure chemical vapour deposition of GeX_4 (X=Cl or Br) and $PCyc^{hex}H_2$.* Polyhedron, 2003. **22**(13): p. 1683-1688.

125. Mills, A., Lepre, A., Elliott, N., Bhopal, S., Parkin, I.P., and O'Neill, S.A., *Characterisation of the photocatalyst Pilkington Activ (TM): a reference film photocatalyst?* Journal of Photochemistry and Photobiology A: Chemistry, 2003. **160**(3): p. 213-224.

126. Blackman, C., Carmalt, C.J., Parkin, I.P., Apostolico, L., Molloy, K.C., and Rushworth, S., *Titanium Phosphide Coatings from the Atmospheric Pressure Chemical Vapor Deposition of $TiCl_4$ and RPH_2 (R = t-Bu, Ph, CyHex).* Chemistry of materials, 2002. **14**(7): p. 3167-3173.

127. Page, K., Palgrave, R.G., Parkin, I.P., Wilson, M., Savin, S.L.P., and Chadwick, A.V., *Titania and silver-titania composite films on glass-potent antimicrobial coatings.* Journal of Materials Chemistry, 2007. **17**(1): p. 95-104.

128. Tauc, J., Grigorov.R, and Vancu, A., *Optical Properties And Electronic Structure Of Amorphous Germanium.* Physica Status Solidi, 1966. **15**(2): p. 627.

129. Tauc, J., *Absorption edge and internal electric fields in amorphous semiconductors.* Materials Research Bulletin, 1970. **5**(8): p. 721-729.

130. Sharma, S.K., Vishwas, M., Rao, K.N., Mohan, S., Reddy, D.S., and Gowda, K.V.A., *Structural and optical investigations of TiO_2 films deposited on transparent substrates by sol-gel technique.* Journal of Alloys and Compounds, 2009. **471**(1-2): p. 244-247.

131. Binsted, N., (1998), EXCURV98: CCLRC Daresbury Laboratory computer program [computer software],

132. Binsted, N., Campbell, J.W., Gurman, S.J., and Stephenson, P.C., (1992), SERC Daresbury Program Library [computer software],

133. Mills, A. and Crow, M., *A study of factors that change the wettability of titania films.* International Journal of Photoenergy, 2008.DOI: 10.1155/2008/470670.

134. Takeuchi, M., Sakamoto, K., Martra, G., Coluccia, S., and Anpo, M., *Mechanism of photoinduced superhydrophilicity on the TiO_2 photocatalyst surface.* Journal of Physical Chemistry B, 2005. **109**(32): p. 15422-15428.DOI: 10.1021/jp058075i.

135. Kume, S. and Nozu, T., *Difficult stainable glass product*, J.P.P. Office, Editor. 1988.

136. Wang, R., Hashimoto, K., Fujishima, A., Chikuni, M., Kojima, E., Kitamura, A., Shimohigoshi, M., and Watanabe, T., *Light-induced amphiphilic surfaces.* Nature, 1997. **388**(6641): p. 431-432.

137. Fujishima, A., Rao, T.N., and Tryk, D.A., *Titanium dioxide photocatalysis.* Journal of Photochemistry and Photobiology C: Photochemistry Reviews, 2000. **1**(1): p. 1-21.

138. Fujishima, A. and Zhang, X., *Titanium dioxide photocatalysis: present situation and future applications.* Comptes Rendus Chimie, 2006. **9**: p. 750-760.

139. Mills, A. and Wang, J.S., *Simultaneous monitoring of the destruction of stearic acid and generation of carbon dioxide by self-cleaning semiconductor photocatalytic films.* Journal of Photochemistry and Photobiology A: Chemistry, 2006. **182**(2): p. 181-186.DOI: 10.1016/j.jphotochem.2006.02.010.

140. Mills, A., Elliott, N., Hill, G., Fallis, D., Durrant, J.R., and Willis, R.L., *Preparation and characterisation of novel thick sol-gel titania film photocatalysts.* Photochemical & Photobiological Sciences, 2003. **2**(5): p. 591-596.DOI: 10.1039/b212865a.

141. Fang, X.W., Mark, G., and vonSonntag, C., *OH radical formation by ultrasound in aqueous solutions .1. The chemistry underlying the terephthalate dosimeter.* Ultrasonics Sonochemistry, 1996. **3**(1): p. 57-63.

142. Qu, X.H., Kirschenbaum, L.J., and Borish, E.T., *Hydroxyterephthalate as a fluorescent probe for hydroxyl radicals: Application to hair melanin.* Photochemistry and Photobiology, 2000. **71**(3): p. 307-313.

143. Saran, M. and Summer, K.H., *Assaying for hydroxyl radicals: Hydroxylated terephthalate is a superior fluorescence marker than hydroxylated benzoate.* Free Radical Research, 1999. **31**(5): p. 429-436.

144. Soh, N., *Recent advances in fluorescent probes for the detection of reactive oxygen species.* Analytical and Bioanalytical Chemistry, 2006. **386**(3): p. 532-543.

145. Hirakawa, T., Yawata, K., and Nosaka, Y., *Photocatalytic reactivity for $O_2^{\bullet-}$ and $OH^{\bullet}$ radical formation in anatase and rutile TiO_2 suspension as the effect of H_2O_2 addition.* Applied Catalysis A-General, 2007. **325**(1): p. 105-111.

146. Ishibashi, K., Fujishima, A., Watanabe, T., and Hashimoto, K., *Detection of active oxidative species in TiO_2 photocatalysis using the fluorescence technique.* Electrochemistry Communications, 2000. **2**(3): p. 207-210.

147. Ishibashi, K., Fujishima, A., Watanabe, T., and Hashimoto, K., *Quantum yields of active oxidative species formed on TiO_2 photocatalyst.* Journal of Photochemistry and Photobiology a-Chemistry, 2000. **134**(1-2): p. 139-142.

148. Rampaul, A., *The photocatalytic and cytotoxic effects of titanium dioxide particles used in sunscreen*. UCL Department of Chemistry. PhD. 2006: University of London. 251 pages.

149. Hyett, G., 2009, Personal Communication

150. NIST. *X-ray Photoelectron Spectroscopy Database*. 2000 10/01/2006]; Available from: http://srdata.nist.gov/xps/.

151. Li, W.X., Stampfl, C., and Scheffler, M., *Insights into the function of silver as an oxidation catalyst by ab initio atomistic thermodynamics.* Physical Review B, 2003. **68**(16): p. 165412-1 - 165412-15.

152. General Electric Company, *Biax™ 2D™ Lamps Technical Datasheet v1.6*. 2005.

153. Lee, S.Y., Hillers, V., McCurdy, S.M., and Kang, D.H., *Comparison of cleaning methods for reduction of attached microorganisms from consumer-style thermometers.* Journal of Rapid Methods and Automation in Microbiology, 2004. **12**(4): p. 225-233.

154. Menyhay, S.Z. and Maki, D.G., *Disinfection of needleless catheter connectors and access ports with alcohol may not prevent microbial entry: The promise of a novel antiseptic-barrier cap.* Infection Control and Hospital Epidemiology, 2006. **27**(1): p. 23-27.

155. Williams, G.J., Denyer, S.P., Hosein, I.K., Hill, D.W., and Maillard, J.Y., *The development of a new three-step protocol to determine the efficacy of disinfectant wipes on surfaces contaminated with Staphylococcus aureus.* Journal of Hospital Infection, 2007. **67**(4): p. 329-335.

156. Liu, Y., Wang, X.L., Yang, F., and Yang, X.R., *Excellent antimicrobial properties of mesoporous anatase TiO_2 and Ag/TiO_2 composite films.* Microporous and Mesoporous Materials, 2008. **114**(1-3): p. 431-439.DOI: 10.1016/j.micromeso.2008.01.032.

157. Bellantone, M., Coleman, N.J., and Hench, L.L., *Bacteriostatic action of a novel four-component bioactive glass.* Journal of Biomedical Materials Research, 2000. **51**(3): p. 484-490.

158. Saravanapavan, P., Patel, M.H., and Hench, L.L. *Effect of particle size on the concentration and rate of Ag^+ release from antimicrobial SiO_2-CaO-P_2O_5-Ag_2O gel-glasses*. 2002. Sydney, Australia.

159. Fan, F.R.F. and Bard, A.J., *Chemical, electrochemical, gravimetric, and microscopic studies on antimicrobial silver films.* Journal of Physical Chemistry B, 2002. **106**(2): p. 279-287.DOI: 10.1021/jp012548d.

160. Li, B.K. and Logan, B.E., *Bacterial adhesion to glass and metal-oxide surfaces.* Colloids and Surfaces B-Biointerfaces, 2004. **36**(2): p. 81-90.DOI: 10.1016/j.colsurfb.2004.05.006.

161. Lellmann, J., (2001), OdoPlus (Version 1.6 Build 281) [computer software], Fridgesoft.

162. Adobe Systems Inc., (2007), Photoshop CS3 Extended (Version 10.0.1) [computer software], San Jose, CA., USA.: Adobe Systems Inc.

163. SPSS Inc., (2007), SPSS for Windows (Release 15.0.1.1) [computer software], Chicago: SPSS Inc.

164. Morgan, T.D. and Wilson, M., *The effects of surface roughness and type of denture acrylic on biofilm formation by Streptococcus oralis in a constant depth film fermentor.* Journal of Applied Microbiology, 2001. **91**(1): p. 47-53.

165. Gopal, J., George, R.P., Muraleedharan, P., Kalavathi, S., Banerjee, S., Dayal, R.K., and Khatak, H.S., *Photocatalytic inhibition of microbial fouling by anodized Ti6Al4V alloy.* Journal of Materials Science, 2007. **42**(13): p. 5152-5158.DOI: 10.1007/s10853-006-1286-y.

166. Gopal, J., George, R.P., Muraleedharan, P., Kalavathi, S., Mangamma, G., and Khatak, H.S., *Heat treated anodised titanium surfaces showing enhanced photocatalytic inhibition of microbial fouling.* Surface Engineering, 2007. **23**(3): p. 194-200.DOI: 10.1179/174329407x174425.

167. Gopal, J., George, R.P., Muraleedharan, P., and Khatak, H.S., *Photocatalytic inhibition of microbial adhesion by anodized titanium.* Biofouling, 2004. **20**(3): p. 167-175.DOI: 10.1080/08927010400008563.

168. Emerson, R.J. and Camesano, T.A., *Nanoscale investigation of pathogenic microbial adhesion to a biomaterial.* Applied and Environmental Microbiology, 2004. **70**(10): p. 6012-6022.DOI: 10.1128/aem.70.10.6012-6022.2004.